This dissertation has been microfilmed exactly as received

65–3148

GORDON, Stuart Albert, 1924–
FLOW OF LOW DENSITY AIR OVER A HEATED FLAT PLATE AT MACH NO. 0.5.

University of Toronto, Ph.D., 1964
Engineering, aeronautical

University Microfilms, Inc., Ann Arbor, Michigan

Reproduced with permission of the copyright owner. Further reproduction prohibited without permission.

FLOW OF LOW DENSITY AIR OVER A HEATED FLAT PLATE AT MACH NO. 0.5

by

Stuart Albert Gordon

A thesis submitted in conformity with the requirements for the degree of Doctor of Philosophy in the University of Toronto

1964

Reproduced with permission of the copyright owner. Further reproduction prohibited without permission.

UNIVERSITY OF TORONTO

SCHOOL OF GRADUATE STUDIES

PROGRAMME OF THE FINAL ORAL EXAMINATION

FOR THE DEGREE OF DOCTOR OF PHILOSOPHY

OF

STUART ALBERT GORDON

2:00 p.m., Thursday, May 7th, 1964

School of Graduate Studies

FLOW OF LOW-DENSITY AIR OVER A HEATED FLAT PLATE AT MACH NUMBER 0.5

Committee in Charge:

Professor J. W. Scott, Chairman
Professor I. I. Glass
Professor J. B. French
Professor J. C. Stryland
Professor O. Trass
Professor W. D. Baines
Professor B. Bernholtz
Professor P. P. Biringer
Professor G. B. Craig
Professor J. H. de Leeuw
Professor G. N. Patterson

Reproduced with permission of the copyright owner. Further reproduction prohibited without permission.

THESIS

FLOW OF LOW-DENSITY AIR OVER A HEATED FLAT PLATE AT MACH NUMBER 0.5

Experimental tests have been performed on flat plates at a nominal Mach number of 0.5, for the cases of an essentially adiabatic plate, and for plates with nominal surface temperatures of 100°C and 200°C. By using a new design of the free-molecule pressure probe it has been possible to get accurate measurements of molecular speed ratio in the flow field near the plate. By using this probe in consort with an equilibrium temperature probe it has proved possible to determine both speed-ratio and static temperature at all points in the flow. By suitable calculations it is then possible to determine all other flow parameters as desired. It has been shown that the equilibrium temperature probe response is very sensitive to slight departures from adiabatic flow and is therefore unreliable in boundary layers when used to determine speed-ratio. Errors in the measurements have been carefully considered.

The "two-stream" type distribution function has been considered and its effect on probe response near a wall investigated, making certain simple assumptions about molecular interactions with a wall. It has been shown that for accommodation coefficients and flow conditions present in these experiments, the effect of a two-stream response on probe measurements is not significantly different from that of a simple Maxwellian distribution with the same average properties for T and S.

A theoretical solution for flow around the leading edge of a flat plate has been developed which agrees with the experimental data. In this solution, the "Rayleigh problem" has been solved explicitly for the "modified" or "single-relaxation-time" form of the Boltzmann equation. It has been shown that this solution can apply only in a somewhat restriced way, but that within these limits the solution should be meaningful. Expressions for slip-velocity and temperature-jump have been obtained. It has been shown that the Maxwell slip-conditions are incompatible with this solution.

An analysis has been made of the flow around the leading edge of the flat plate, with and without heat addition. It has been possible to show that:

1) The boundary-layer begins to form well ahead of the leading edge, with a measurable effect as much as ten mean-free paths ahead. This is a true boundary-layer effect and propagates forward by a diffusion of the disturbance.

2) The Maxwell slip conditions probably do not hold near the leading edge.

3) To the same degree, the temperature-jump conditions to not hold near the leading edge.

Reproduced with permission of the copyright owner. Further reproduction prohibited without permission.

4) Slip velocity and molecular speed-ratio decrease exponentially with distance along the plate.

5) Temperature-jump decreases exponentially with distance along the plate.

6) Measured accommodation coefficients are lower than most values quoted in the literature. Values of accommodation obtained tend to agree with values quoted in the literature for "clean" surfaces rather than for normal "engineering" surface.

A detailed investigation has been made of the use of constant temperature thermocouple vacuum gauges in low-density wind tunnels. Several designs have been tried, the most successful being an all-metal design with an extremely small internal volume and a high sensitivity. The high precision and small internal volume of this gauge has been applied to free-molecule pressure probes. The small size of these probes allows them to be used in higher density flows than heretofore possible, thus extending the range of usefulness of the free-molecule pressure probe. Details of a technique to allow construction of even finer probes have been described. Another application of these gauges has been described in which the sensing element is embedded in a glass plate less than 1/8" thick.

Reproduced with permission of the copyright owner. Further reproduction prohibited without permission.

BIOGRAPHY

1924 -	Born Limerick, Saskatchewan
1946 -	B.A. University of Saskatchewan
1948 -	M.A. (Physics) University of Saskatchewan
1957 - 1961	Research Assistant, Institute of Aerophysics, University of Toronto
(1957 - 1958	School of Graduate Studies,
(1958 - 1959	University of Toronto
(1963 - 1964	

GRADUATE STUDIES

Major Subject:

Molecular Flow of Gases — Professor G. N. Patterson

Minor Subjects:

Advanced Applied Aerodynamics — Professor G. N. Patterson

Viscous Fluids — Professor J. A. Steketee

PUBLICATIONS

"Construction of Small Leaks of Predictable Throughput", Rev. Sci. Inst. 29, 501 (1958)

"Thickness and Conduction Correction to the Thin-Wall Calorimeter", AeroChem TP-69, July, 1963.

"High Sensitivity Pressure Probes for Use in the Millitorr Region", Transactions of the Tenth National Vacuum Symposium, ed. by George H. Bancroft (MacMillan Co., New York, 1963).

"On the Limits on Wall Thickness in the 'Thin Wall' Calorimeter Heat Flux Gauge", AeroChem TP-70, August, 1963; J. of Heat Transfer (to be published, May 1964).

"Flow of Low Density Air Over a Heated Flat Plate at Mach No. 0.5", submitted for presentation at the Fourth International Symposium on Rarefied Gas Dynamics, University of Toronto, July 14-17, 1964.

PATENT

"Fluid Testing Columns", Patent 3,005,514, October 24, 1961 (with Cole, L.G.).

Reproduced with permission of the copyright owner. Further reproduction prohibited without permission.

ACKNOWLEDGEMENT

The insight and attention to detail of many people has helped to make this work more complete and comprehensive in a great many respects, and it is the author's earnest desire to acknowledge this indebtedness at this time. He wishes to express his gratitude to the Staff of the Institute for Aerospace Studies for their assistance and encouragement in this undertaking. In particular, he wishes to thank Dr. G. N. Patterson, whose patience and inspiration as supervisor is deeply appreciated. The advice of,and the many helpful discussions with Dr. J. H. deLeeuw have also contributed in large measure to this research.

This work was supported in part by Grumman Aircraft Engineering Corporation of Bethpage, Long Island, New York. The original request for this study came from Dr. Richard Omann of that company and was suggested in part by the work of Dr. E. L. Harris at this Institute. These many contributions and the financial support of the Defence Research Board of Canada are gratefully acknowledged.

Reproduced with permission of the copyright owner. Further reproduction prohibited without permission.

SUMMARY

Experimental tests have been performed on flat plates at a nominal Mach number of 0.5, for the cases of an essentially adiabatic plate, and for plates with nominal surface temperatures of 100°C and 200°C. By using a new design of the free-molecule pressure probe it has been possible to get accurate measurements of molecular speed ratio in the flow field near the plate. By using this probe in consort with an equilibrium temperature probe it has proved possible to determine both speed-ratio and static temperature at all points in the flow. By suitable calculations it is then possible to determine all other flow parameters as desired. It has been shown that the equilibrium temperature probe response is very sensitive to slight departures from adiabatic flow and is therefore unreliable in boundary layers when used to determine speed-ratio. Errors in the measurements have been carefully considered.

The "two-stream" type distribution function has been considered and its effect on probe response near a wall investigated, making certain simple assumptions about molecular interactions with a wall. It has been shown that for accommodation coefficients and flow conditions present in these experiments, the effect of a two-stream response on probe measurements is not significantly different from that of a simple Maxwellian distribution with the same average properties for T and S.

A theoretical solution for flow around the leading edge of a flat plate has been developed which agrees with the experimental data. In this solution, the "Rayleigh problem" has been solved explicitly for the "modified" or "single-relaxation-time" form of the Boltzmann equation. It has been shown that this solution can apply only in a somewhat restricted way, but that within these limits the solution should be meaningful. Expressions for slip-velocity and temperature-jump have been obtained. It has been shown that the Maxwell slip conditions are incompatible with this solution.

An analysis has been made of the flow around the leading edge of the flat plate, with and without heat addition. It has been possible to show that:

1) The boundary-layer begins to form well ahead of the leading edge, with a measurable effect as much as ten mean-free paths ahead. This is a true boundary-layer effect and propagates forward by a diffusion of the disturbance.

2) The Maxwell slip conditions probably do not hold near the leading edge.

3) To the same degree, the temperature-jump conditions do not hold near the leading edge.

Reproduced with permission of the copyright owner. Further reproduction prohibited without permission.

4) Slip velocity and molecular speed-ratio decrease exponentially with distance along the plate.

5) Temperature-jump decreases exponentially with distance along the plate.

6) Measured accommodation coefficients are lower than most values quoted in the literature. Values of accommodation obtained tend to agree with values quoted in the literature for "clean" surfaces rather than for normal "engineering" surface.

A detailed investigation has been made of the use of constant-temperature thermocouple vacuum gauges in low-density wind tunnels. Several designs have been tried, the most successful being an all-metal design with an extremely small internal volume and a high sensitivity. The high precision and small internal volume of this gauge has been applied to free-molecule pressure probes. The small size of these probes allows them to be used in higher density flows than heretofore possible, thus extending the range of usefulness of the free-molecule pressure probe. Details of a technique to allow construction of even finer probes have been described. Another application of these gauges has been described in which the sensing element is embedded in a glass plate less than 1/8" thick.

Reproduced with permission of the copyright owner. Further reproduction prohibited without permission.

TABLE OF CONTENTS

		Page
	NOTATION	vii
1.	INTRODUCTION	1
	1.1 Definitions	2
	1.2 Previous Work	3
	1.3 Object	3
2.	THEORY	4
	2.1 Interaction Between Gas Molecules and a Wall	4
	2.2 Experimental Data on Accommodation Coefficient	5
	2.3 Maxwell Slip Conditions	6
	2.4 Calculations Using Two-Stream Distribution Functions	8
	2.4.1 Average Values in a Two-Stream Distribution	10
	2.4.2 Response of an Orifice Probe	12
	2.4.3 Response of an Equilibrium Temperature Probe	13
	2.4.4 Effect of Accommodation on a Two-Stream Response	14
3.	APPARATUS	16
	3.1 Equilibrium Temperature Probe	17
	3.1.1 Design of Equilibrium Temperature Probe	18
	3.1.2 Use of Equilibrium Temperature Probe	20
	3.1.3 Equilibrium Temperature Probe Data Reduction	22
	3.1.4 Radiative Heat Transfer	23
	3.1.5 Non-Uniform Flow Corrections	24
	3.1.6. Knudsen Number Effect	25
	3.2 Pressure Probe	25
	3.2.1 Pressure Pair Probe	27
	3.2.2 Temperature Corrections	29
	3.2.3 Knudsen Number Effects	30
	3.2.4 Corrections for Non-Uniform Flow	30

Reproduced with permission of the copyright owner. Further reproduction prohibited without permission.

3.3 Flat Plate Model 31

3.3.1 Heaters 32
3.3.2 Instrumentation 33
3.3.3 Performance 34

4. PROCEDURE 34

4.1 Setting up Model and Apparatus 34
4.2 Preliminary Steps 36

4.2.1 Speed Ratio 36
4.2.2 Tunnel Performance 37

4.3 Setting Flat Plate Conditions 37
4.4 Experimental Runs 38

5. RESULTS 40

5.1 Fixed Point Data 40
5.2 Traverses 40
5.3 Other Data 41

6. DISCUSSION 41

6.1 Initial Observations 41
6.2 Estimate of Errors 42

6.2.1 Molecular Speed Ratio 43
6.2.2 Uniformity of Jet 43
6.2.3 Heater Surfaces 44
6.2.4 Overall Error 44

6.3 Discussion of Results 45

6.3.1 Room Temperature Plate: Discrepancy Between Probe Readings 45
6.3.2 Flow Ahead of the Leading Edge 47
6.3.3 Maxwell Slip Conditions 49
6.3.4 Temperature Jump Conditions 52
6.3.5 Exponential Decay of Slip Velocity and Temperature Jump 52
6.3.6 Accommodation Coefficients 53

7. CONCLUSIONS 57

REFERENCES 58

TABLES

APPENDIX A and B

Reproduced with permission of the copyright owner. Further reproduction prohibited without permission.

NOTATION

A	effective area of radiating body
dA	an infinitesimal area
C_i	$\frac{c_i}{c_m}$
c_i	random molecular velocity along X_i coordinate axis
c_m	most probable speed of molecule = $\sqrt{2RT}$
d	diameter of probe
E	energy transported across dA in unit time
ΔE	thermocouple output of the equilibrium temperature gauge
E_o	voltage equivalent to 273/s
erf X	error function = $\frac{2}{\sqrt{\pi}} \int_0^x e^{-y^2} dy$
f	symbol for the distribution function at a point (x, y, z)
f	$(S^2 + 3) Z_1 + (S^2 + \frac{7}{2}) Z_2$
g	$3(Z_1 + Z_2)$
h	distance above plate in experiments
I_o	modified Bessel function of zero order
I_1	modified Bessel function of first order
Kn	Knudsen Number (mean free path divided by a characteristic length = λ / L)
k	Boltzmann's constant
L	characteristic length of a body
M	Mach number(mass velocity divided by the speed of sound $\frac{U}{\sqrt{\gamma RT}}$)
m	mass of molecule
n	number density of molecules in the gas (number/unit volume)
dN	number of molecules crossing an area dA in unit time

Reproduced with permission of the copyright owner. Further reproduction prohibited without permission.

p	pressure, in particular, static pressure
p_o	total pressure
R	gas constant (per unit mass)
Re	Reynold number $\frac{\rho UL}{\mu}$
s	thermocouple sensitivity (degrees/mv.)
S	molecular speed ratio - $S = \frac{U}{cm}$ -(mass velocity divided by the most probable speed of the molecules)
T	absolute temperature, in particular, static temperature
T_{wire}	equilibrium temperature of a wire transverse to the flow
T_o	total temperature of the gas
T_{av}	average static temperature for a two-stream distribution function
ΔT	temperature jump at the wall $T_{in(y=0)} - T_{wall}$
ΔT	$T_{wire} - T_o$ in the equilibrium probe
δT	elevation of cold junction temperature of equilibrium temperature probe due to flow
U	free stream velocity - parallel to the wall
u_i	generalized velocity mass components corresponding to directions x_i
V	velocity normal to the wall (y axis)
$W = W(s)$	function relating long-tube probe response to S
x, y, z	cartesian coordinates (with x_1, x_2, x_3 as alternative designation)
Z_1	$e^{-\frac{S^2}{2}} I_o\left(\frac{S^2}{2}\right)$
Z_2	$\pi S^2 e^{-\frac{S^2}{2}} \left[I_o\left(\frac{S^2}{2}\right) + I_1\left(\frac{S^2}{2}\right) \right]$

Reproduced with permission of the copyright owner. Further reproduction prohibited without permission.

α	thermal accommodation coefficient = $\frac{T_{in} - T_{out}}{T_{in} - T_{wall}}$
α_s	accommodation coefficient for speed ratio = $\frac{S_{in} - S_{out}}{S_{in}}$
γ	ratio of specific heat = $\frac{c_p}{c_v}$
ϵ	emmissivity of wall
ϵ	voltage reading on thermocouple corresponding to the correction for flow at the cold junction of the equilibrium temperature probe
λ	mean free path of a molecule
Λ_i	c_i/cm
ρ	density = nm
μ	viscosity of the gas
σ	Maxwell's slip coefficient = $\frac{U_{in} - U_{out}}{U_{in}}$
σ	Stefan-Boltzmann constant
$\chi_{(s)}$	the function $e^{-s^2} + S\sqrt{\pi}(1 + \text{erf } S)$
$\psi_{(s)}$	$\frac{f(s)}{g(s)} - 1$ difference between equilibrium temperature and static temperature divided by static temperature
$\phi_{(s)}$	$\frac{f(s)}{g(s)} \cdot \frac{1}{1 + \frac{\gamma-1}{2}S^2} - 1$ difference between stagnation temperature and equilibrium temperature divided by stagnation temperature
ξ_i	$c_i + u_i$ molecular velocity component along the x_i axis
ζ	$= \zeta(s)$ a function relating equilibrium temperature, static temperature and speed ratio

Subscripts

in	referred to the incoming stream of a two-stream distribution of molecules
out	referred to the outgoing stream of a two-stream distribution of molecules

Reproduced with permission of the copyright owner. Further reproduction prohibited without permission.

wall	referred to wall conditions, usually a Maxwellian distribution at wall temperature
wire	referred to conditions on a transverse cylinder in the flow
TS	referred to a two-stream distribution function
obs	observed conditions that one calculates for an ideal probe in a given flow
∞	referred to free stream conditions
(x, y)	referred to the point (x, y) in the stream
i, 1, 2, 3	referred to the coordinate axis where x_1 is equivalent to x, x_2 to y, and x_3 to z, x_i is a general coordinate
(av.)	single average value of a parameter corresponding to net effect of a two-stream distribution

Reproduced with permission of the copyright owner. Further reproduction prohibited without permission.

1. INTRODUCTION

The advancement of any field of science is intimately connected with the performance of accurate measurements in that field. In the field of low density flows there has been all too little progress in the last fifty years, and there has been little experimental work. However, in recent years the development of low-density wind tunnels, operating at pressures as low as one-millionth of an atmosphere, has enlarged the field of research and hastened the pace of discovery. In general, such measurements as have been made have had somewhat limited application, because not all of the significant parameters of the flow have been measured. Typically, the flow has been assumed adiabatic and the molecular speed-ratio measured, or perhaps the static temperature has been assumed constant and pressures measured. The technique reported here, however, allows both the speed-ratio and temperature of a non-adiabatic flow to be measured with some precision.

The determination of flow parameters over a flat plate at low densities has interesting aspects that make this project one of considerable importance. In the first place it allows one to explore the flow field at the leading edge of a flat plate in that region where the Blasius solution does not apply and so helps to close the gap in our knowledge of the mechanism of boundary layer growth. Secondly, it should add to our meager knowledge of the nature of the interaction of gas molecules with solid boundaries, for the important case where the molecules have a large mass velocity with respect to the wall. Finally, it ought to provide engineering data of importance in extremely high altitude flight where, although forces on rockets and satellites are small, the long-term integrated effects of these on the vehicle surfaces makes their consideration necessary in some cases.

Any flight at high altitude is necessarily very high Mach number flight, with resultant high stagnation temperature. In any practical case there would therefore be a large temperature difference between the relatively cool vehicle wall and the high enthalpy gas flowing over it. Since these conditions are difficult to attain in the wind tunnel, the inverse problem, i.e. hot wall and a relatively low stagnation temperature was studied, because of the great simplification in experimental technique it involved. Experimental methods for high Mach number, high enthalpy flows at low density are not sufficiently developed to allow any great degree of accuracy, and it was hoped that by means of these modifications it might be possible to obtain relatively accurate data which would still be closely enough related to the central problem so that they could further its understanding. It was felt that the flow field must be completely specified by the measured parameters if no ambiguity of interpretation was to result, but, as will be shown, this is difficult to do even for the simplified model chosen. The results of these investigations, therefore, cannot be considered as a direct simulation of high altitude flight, yet they are related and applicable to the problem. For this reason, in reducing the data, particular attention

Reproduced with permission of the copyright owner. Further reproduction prohibited without permission.

has been given to comparing them λ to those λ predicted by current fluid-mechanical models.

1.1 Definitions

Since, in this work the problem is considered from a kinetic theory point of view rather than in terms of continuum theory a few definitions must be given (Ref. 1).

An important parameter is the Knudsen number of a body, Kn, the ratio of a mean-free-path of a gas particle to the characteristic dimension of the body, (i.e. λ /L.) The mean free path itself can be related to the more familiar continuum quantities of pressure p, viscosity μ, density ρ, the gas constant R and temperature T by the formula:

$$\lambda = \frac{16}{5\sqrt{2\pi}} \frac{\mu}{\rho} \frac{1}{\sqrt{RT}} \qquad \text{(Ref. 3)} \qquad (1.1)$$

The mass motion is described by the molecular speed ratio S, which is the ratio of the average directed motion of the individual particles to the most probable molecular speed i.e., $S = U/cm = U/\sqrt{2RT}$. S is related to the Mach number M, as used in continuum theory by the expression $S = \sqrt{\gamma}/2\ M$. The Reynolds number $Re = \rho UL/\mu$ can also be expressed in terms of Kn and S, i.e., $Re = 1.772\ S/Kn = 1.253\ \gamma^{\frac{1}{2}}\ M/Kn$.

The Knudsen number is used to define the different domains of fluid mechanics. If Kn is very small, continuum theory applies, while if Kn is very large kinetic theory solutions will apply. For low Mach number it is somewhat arbitrarily assumed that for $Kn < 0.01$ the flow is continuum. For $0.01 < Kn < 0.1$ the slip-flow region occurs. In this latter region, the usual continuum theory applies, except that the no-slip boundary conditions must be abandoned in favour of the assumption that some relative motion does occur between the bounding wall and the gas in contact with it. The regime $0.1 < Kn < 10$ is often called the transition region, and although it is at present under intensive study, the mathematics has not yet been advanced which will handle this flow in a general way. The regime for which $Kn > 10$ is called the free-molecule-flow regime and in this region the pure kinetic-theory concepts of individual collisions apply.

Continuum theory is relatively advanced and well verified by experiment. There is little doubt that the free-molecular flow theory also applies quite well in its designated region, and a considerable body of experimental evidence supports the limited number of theoretical solution that have been obtained. It seems well established that continuum theory can be extended into the slip-flow regime by proper observance of boundary conditions, although the exact limits of this method are not clearly delineated. In an analogous way, free-molecular solutions are presently being extended into the transition regime by a variety of mathematical tricks. However, it is important to realize that in general, experimental evidence is very

Reproduced with permission of the copyright owner. Further reproduction prohibited without permission.

scarce once one leaves the safe bounds of the continuum regime.

At any density, the idealization of flow over an infinite flat plate must encompass something closely resembling all four flow regimes. Using a strict definition of free-molecule flow as being a flow in which the largest dimension of the body is always less than one tenth of a mean free path, it is manifestly impossible to ever have an infinite flat plate in anything but continuum flow. However, if one accepts a looser definition of free-molecule flow as being a region in which kinetic theory solutions must be applied, one can usefully think of the leading edge of any flat plate as being in free-molecule flow, while further back, transition flow, then slip flow and finally continuum flow occurs. This is a concept which is usually accepted implicitly or explicitly when considering flow near the leading edge of a flat plate, and which allows one to understand the use of a low density wind tunnel in this problem. In effect increasing the mean-free path of a flow changes the scaling factor, so that one is able to examine the flow with reasonable sized instruments in greater and greater detail around the leading edge of the plate as one lowers the pressure.

1.2 Previous Work

Because of experimental difficulties and lack of facilities very little previous experimental data are available on this problem, and those which are available are of a somewhat qualitative character. Laurmann has obtained some data at Mach 2 using an equilibrium-temperature probe (to be described later) in what was presumably an almost adiabatic flow (Ref. 2). In fact his data have features that he could not explain by any simple assumptions, so that the results were largely qualitative. A few tentative effects were suggested, but in general the data were not conclusive.

More recently Harris has investigated adiabatic flow around the leading edge of a flat plate in subsonic flow using an orifice pressure-probe (Ref. 3). Due to a peculiarity of low density flows, his impact pressure readings do not allow the determination of either S or T, so that his data too, are somewhat indeterminate. Since this work was completed a few scattered references have appeared using somewhat similar approaches to low density measurements (Ref. 4).

1.3 Object

The object of these experiments was first to develop a technique of measurement that would allow the important flow parameters to be completely specified, next to check the accuracy of this technique and finally to use this technique to obtain the flow parameters for adiabatic and non-adiabatic flow over a flat plate.

Reproduced with permission of the copyright owner. Further reproduction prohibited without permission.

2. THEORY

In the following section, the theory necessary to the consideration of these experiments will be developed. Because the probes were operated near a heated wall, attention is given to the problem of interpreting probe response in that region where the distribution function cannot a priori be considered to be Maxwellian and where the more usual formulae do not necessarily hold.

2.1 Interaction Between Gas Molecules and a Wall

The question of how gas molecules interact with a wall has been the subject of much speculation for very many years (Ref. 5, 6, and 7). A detailed consideration of this problem is beyond the scope of this work, even though it has an important bearing on any attempt to interpret the data collected here. For stationary gases, the thermal accommodation coefficient α, is usually defined as

$$\alpha = \frac{T_{in} - T_{out}}{T_{in} - T_w} \tag{2.1}$$

where T_{in} is the temperature of the incoming gas molecules, and T_{out} is the temperature of the reflected stream, while T_w is the temperature of the wall with which the streams are interacting. For the special case of a thin heated wire in partial vacuum in which no mass flow occurs, these quantities can be rather well defined and measured with some precision (Ref. 6, 8, and 9). However, near the leading edge of an infinite flat plate in a flowing gas this definition is most unsatisfactory from an experimental standpoint, since neither T_{out} nor T_{in} is at all clearly defined. Some modification of the definition is needed in non-stationary gases.

The detailed microscopic picture of a flowing gas interacting with a wall is so complex that there is little theoretical justification for assuming, without experimental verification, that a single coefficient (or even several) can adequately describe the process. To date, the little experimental evidence that exists does not seem to clarify the problem (Ref. 10).

A typical approach to the problem is to define several different accommodation coefficients, in a manner analogous to the thermal accommodation coefficient, and to use these coefficients in discussing the interaction phenomena (Ref. 11). Thus, one can talk of the coefficient of accommodation of tangential momentum (or the Maxwell slip coefficient σ).

$$\sigma = \frac{U_{in} - U_{out}}{U_{in}} \tag{2.2}$$

Reproduced with permission of the copyright owner. Further reproduction prohibited without permission.

where U_{in} refers to the average incoming tangential velocity and U_{out} to the average outgoing velocity. Accommodation coefficients for normal velocity, rotational energy, vibrational energy, and many other quantities can also be defined, although they will not be considered here. The various accommodation coefficients used in this work have usually been picked for computational convenience. Thus α is defined as in Eq. 2.1 while α_s has been defined as

$$\alpha_s = \frac{S_{in} - S_{out}}{S_{in}} \tag{2.2a}$$

where S_{in} and S_{out} are the molecular speed ratios corresponding to U_{in} and U_{out} respectively. At Mach 0.5 they do not differ sufficiently from more orthodox coefficients to warrant the extra labor of determining the latter. Whether they have any greater significance must be judged by the final results.

2.2 Experimental Data on Accommodation Coefficient

Recent refinements in measurements of the thermal accommodation coefficient have proven it to be a fairly meaningful number in non-flowing systems, and have demonstrated that it is extremely sensitive to surface contamination (Ref. 9). Even mono-molecular layers of almost any substance will greatly increase α, apparently by as much as a factor of ten in some instances. Since monomolecular layers occur almost instantaneously, except at extremely low pressures ($< 10^{-6}$ mm) it is usually assumed that ordinary engineering surfaces have a coefficient of almost 1, as the earlier data showed (Ref. 11).

Since pressures in these experiments are of the order of 10^{-2} mm, any measured accommodation coefficients that depart significantly from unity would be considered surprising. The apparatus used in these experiments was designed under the assumption that the inevitable monomolecular films would result in accommodation coefficients of unity or very close to unity irrespective of the procedure followed or the material used. However, since the data obtained was quite sufficient to give a crude measure of the relevant accommodation coefficients, these values were calculated, with quite surprising results.

Basically, in this experiment one measures only the average value of temperature and molecular speed ratio at any given point in the flow. Unfortunately there is no unambiguous way to relate these quantities to the quantities called for in the original definitions (Eq. 2.1 etc.).

In subsequent calculations it will be assumed that :

(1) $$T_{av} = \frac{T_{in} + T_{out}}{2} \tag{2.3}$$

(2) $$S_{av} = \frac{S_{in} + S_{out}}{2} \tag{2.4}$$

Reproduced with permission of the copyright owner. Further reproduction prohibited without permission.

2.3 Maxwell Slip Conditions

A very early expression for the interaction of a gas molecule with a wall was given by Maxwell, assuming a uniform gas moving past an infinite wall so that only the velocity gradients normal to the wall were important (Ref. 5). Because of its simplicity and lack of ambiguity, it is a model still much used in theoretical calculations even today although usually it is given with a modern, less elaborate treatment such as used here.

Assume that for an incoming stream of molecules, the molecules rebound as two distinct groups, on striking a wall. One group is reflected specularly with no change in the average tangential velocity and with only a change in sign for the normal velocity. The other group is reflected diffusely, that is it is fully "accommodated" and is reflected with an average tangential velocity equal to the wall velocity (i. e. zero). The fraction of molecules in the diffusely reflected group is thus σ (from Eq. 2. 2) and $(1 - \sigma)$ in the specularly reflected group. Maxwell postulated that the tangential velocity of the incoming molecules would be the same as the average tangential velocity of all molecules one mean-free-path away from the wall. Thus if U_0 is the tangential velocity at wall and U_{in} the average tangential velocity of the incoming molecules

$$U_{in} = U_0 + \lambda \left(\frac{\partial U}{\partial y}\right)_0 \qquad (2.5)$$

$$U_0 = \frac{U_{in} + U_{out}}{2}$$

(where U_{out} is the average tangential velocity of the reflected molecule).

$$U_0 = \frac{(1-\sigma) U_{in} + U_{in}}{2}$$

$$= \frac{2-\sigma}{\sigma} \lambda \left(\frac{\partial U}{\partial y}\right)_0 \qquad (2.6)$$

$$= U_s \quad \text{(the slip velocity at the wall)}$$

This model is obviously rather crude, in that it seems unreasonable to expect such a neat division into truly specular and truly diffuse reflection, but it does illustrate that slip will occur even when all molecules are diffusely reflected ($\sigma = 1$).

A similar theory may be propounded for the effect of a wall on gas temperature (Ref. 7). Once again there will be a discontinuity at the wall, usually called the temperature jump, so that if one defines

$$\Delta T = T_{av(y=0)} - T_{wall} \qquad (2.7)$$

Reproduced with permission of the copyright owner. Further reproduction prohibited without permission.

then

$$\Delta T \propto \frac{2-\alpha}{\alpha} \lambda \left(\frac{\partial T}{\partial y}\right)_0 \qquad (2.8)$$

In this theory however, one does not divide the reflected molecules into the two groups of specular and diffuse reflections but rather one assumes that on the average the molecules change their random energies so that the temperature of the outgoing stream is partially accommodated to the wall temperature. The degree of accommodation is given by the thermal accommodation coefficient α, which has already been defined (Eq. 2.1).

Thus one may arrive at two separate empirical constants for any flow. While the two models used in deriving these expressions are not really compatible, Maxwell's derivation might be considered a mathematical trick to give an average accommodation coefficient for tangential velocity.

The assumptions used to derive Maxwell slip conditions (Eq. 2.8) were applied to permit calculations of the accommodation coefficients from the experimental data using Eqs. 2.3 and 2.4. It was assumed that the temperature of the incoming stream of molecules was the gas temperature that obtained exactly one mean free path away from the point on the wall in question. As a matter of convenience it was further assumed that, of all the points on the hemisphere one mean-free-path from the point in question, the point with the temperature nearest the free-stream temperature would be chosen. In effect, this tended to make the coefficient as large as possible, since one is measuring in the direction of greatest change. Similar assumptions were used to determine the tangential velocity accommodation coefficient (Maxwell's slip coefficient). ($S_{tangential}$ was determined rather than U, but for the speed ratios involved the numerical difference was not significant). Because of the lack of rigour in the assumptions, the final determination of coefficients by this method is less accurate than the actual data used.

These same data may be used in a different way to check the validity of the Maxwell slip conditions and the temperature jump conditions themselves. This check is of considerable importance since much use has been made of these assumptions in theoretical calculations of flow near the leading edge of a flat plate. Inspection of Eqs. 2.6 and 2.8 shows that a plot of $(\partial U/\partial y)_0$ vs. $(U)_0$ along the plate should give a straight line of positive slope through the origin. Since these numbers can be determined experimentally, the accuracy of the theory can be checked. However, one ambiguity remains. Maxwell's development really applies in an established boundary layer where the only changes in conditions are perpendicular to the plate. Near the leading edge, conditions change with position along the plate as well. It might therefore be more in keeping with the spirit of Maxwell's development to plot $(\partial U/\partial n)_0$ vs. U_0 instead of $(\partial U/\partial y)_0$ vs. U_0 where n is a vector pointing in the direction of maximum rate of change of U. In fact, plots were tried for both assumptions, with no significant difference.

Reproduced with permission of the copyright owner. Further reproduction prohibited without permission.

The temperature jump assumptions can be checked with the same degree of accuracy in a similar manner by plotting $(\partial T/\partial n)$ vs. ΔT.

2.4 Calculations Using Two-Stream Distribution Functions

It has been implicit in the preceding discussion that, at the wall, the general distribution function can be written as the sum of two partial distribution functions, one of which deals with those molecules approaching the wall, the other relating to molecules reflecting off the wall. This is a purely mathematical manipulation and is quite proper. It is customary to go further and assume that the incoming and reflected distribution functions are Maxwellian in form, (that is, that the random velocities are distributed in the same way as they would be in a gas in equilibrium, except that the incoming stream has no velocity components away from the wall while the reflected stream has no components directed toward the wall). This assumption of Maxwellian form is partly a matter of convenience and should be backed by experimental proof. Since no such proof seems to have been advanced, it is a matter of fundamental doubt just how flow near a wall is to be treated.

On the other hand, it seems definitely proved that well away from the wall a slightly non-Maxwellian flow distribution containing first-order correction terms given by velocity and temperature gradients is equivalent to a Navier-Stokes solution and applies quite accurately, except possibly inside higher Mach number shock fronts (Ref. 1, and 12). Now, if a two-stream distribution does hold at the wall, it is obvious that random collisions must soon cause it to approach the slightly-non-Maxwellian form. This process will start at the wall and build up until, after an uncertain number of collisions, the distribution has assumed its more degenerate form.

Just how many mean-free-paths (or fractions of mean-free-paths) will be required for this process to complete itself is a matter of conjecture, but since in a shock wave, where there is a really strong discontinuity, the shock thickness is of the order of a few mean-free-paths it seems likely the process will occur quite rapidly.

It is quite possible that in certain situations the two formulations will lead to practically the same results and can be used interchangeably. When this is the case, it will then be possible to calculate probe response by formulae already available. It will be shown later that, for the flows involved here, the difference between probe response to Maxwellian and slightly non-Maxwellian flows is negligible if average values are used for T and S. It is therefore assumed in these experiments that for the particular measurements made, a two-stream distribution functi is equivalent to a Maxwellian flow with average S and T as far as probe response is concerned, and sufficient numerical calculations will be made to justify this assumption.

Reproduced with permission of the copyright owner. Further reproduction prohibited without permission.

The following paragraphs will develop the theory necessary to make these calculations.

The Maxwell distribution function can be written:

$$f = \frac{n\, e^{-\zeta_c^2}}{c_m^3\, \pi^{3/2}}\, d\xi_1\, d\xi_2\, d\xi_3\, dx\, dy\, dz \qquad (2.9)$$

where n is the number of molecules per unit volume; ξ_i are the velocity components in some frame of reference; where c_i are the components of random velocity; c_m is the most probable velocity = $\sqrt{2RT}$; so that:

$$\xi_i = u_i + c_i \text{ where}$$

u_i = directed component of velocity

$$S_i = \frac{u_i}{c_m}, \qquad C_i = \frac{c_i}{c_m}$$

$$\Lambda_i = \xi_i / c_m$$

For a two-stream distribution $f = f_1 + f_2$

where $f_1 = \frac{n_1 e^{-\zeta_1'^2}}{c_{m_1}^3\, \pi^{3/2}}\, d\xi_1\, d\xi_2\, d\xi_3\, dx\, dy\, dz$ (2.10)

for all values of ξ_1 & ξ_3 and for $-\infty \le \xi_2 \le 0$

$$f_2 = \frac{n_2 e^{-\zeta_i''^2}}{c_m^3\, \pi^{3/2}}\, d\xi_1\, d\xi_2\, d\xi_3\, dx\, dy\, dz$$

for $0 \le \xi_2 \le \infty$ (2.11)

$= 0$ for $-\infty \le \xi_2 \le 0$

The unprimed coordinates refer to a frame of reference fixed with respect to the wall; primed coordinates refer to a coordinate system moving at the mass velocity of the incoming stream; double-primed coordinates refer to a coordinate system moving at the mass velocity of the reflected stream.

Reproduced with permission of the copyright owner. Further reproduction prohibited without permission.

It is assumed that the incoming stream has a mass velocity U_{in} in the x direction parallel to the plate* and a most probable speed $c_{m_{in}} = \sqrt{2RT_i}$. Similarly the reflected stream has a mass velocity of U_{out} parallel to the wall and most probable speed of $c_{m_{out}}$. The number of molecules striking the plate is assumed equal to the number leaving the plate so that $n_{in}\, c_{m_{in}} = n_{out}\, c_{m_{out}}$. Because of the geometry of the plate and probes in this experiment it is always possible to assume that the response to the half distribution will be exactly one-half of that which one would get for a corresponding full-Maxwell distribution, on grounds of symmetry alone.

2.4.1 Average Values in a Two Stream Distribution

With these preliminaries and using standard definitions of kinetic theory (Ref. 1) it is possible to write:

$$n_{av} = \frac{n_{in} + n_{out}}{2} = \frac{n_{in}}{2}\left(1 + \frac{c_{m_{in}}}{c_{m_{out}}}\right) \tag{2.12}$$

$$\xi_1 = u_{in} + c_1' = u_{out} + c_1'' = u_{av} + c_1$$

$$\therefore c_1 = u_{in} - u_{av} + c_1' = \Delta u_{in} + c_1'$$

$$= u_{out} - u_{av} + c_1'' = \Delta u_{out} + c_1'' \tag{2.13}$$

$$U_{av} = \frac{1}{n_{av}} \int_{-\infty}^{\infty}\int_{-\infty}^{\infty}\int_{-\infty}^{\infty} f\, \xi_1\, d\xi_1\, d\xi_2\, d\xi_3 \tag{2.14}$$

$$= \frac{1}{n_{av}} \int_{-\infty}^{\infty}\int_{-\infty}^{\infty}\int_{-\infty}^{\infty} f_1\, \xi_1\, d\xi_1\, d\xi_2\, d\xi_3 + \frac{1}{n_{av}} \int_{-\infty}^{\infty}\int_{-\infty}^{\infty}\int_{-\infty}^{\infty} f_2\, \xi_1\, d\xi_1\, d\xi_2\, d\xi_3$$

which eventually yields

$$U_{av} = \frac{1}{2n_{av}}\left(n_{in}\, c_{m_{in}}\, S_{in} + n_{out}\, c_{m_{out}}\, S_{out}\right) \tag{2.15}$$

---

* This is not quite accurate. What is really assumed is that the equivalent full Maxwell distribution would have a mass velocity U_{in} parallel to the plate. It is obvious that the incoming stream has an additional mass velocity toward the wall which would be exactly cancelled by the discarded outgoing half of the distribution. Because of the way the mathematics is handled in subsequent calculations this does not cause difficulty.

Reproduced with permission of the copyright owner. Further reproduction prohibited without permission.

$$\therefore U_{av} = (S_{in} + S_{out}) \frac{c_{m_{in}} \cdot c_{m_{out}}}{c_{m_{in}} + c_{m_{out}}} \tag{2.16}$$

Assume the definition $3RT_{av} = \overline{c^2}$ (Ref. 13)

$$\therefore 3RT_{av} n_{av} = \frac{1}{2} \int_{-\infty}^{\infty}\int_{-\infty}^{\infty}\int_{-\infty}^{\infty} \frac{n_{in} e^{-\zeta_1^{\prime 2}}}{c_{m_{in}}^3 \pi^{3/2}} \left[\Delta U_{in}^2 + 2\Delta U_{in} c_1' + c_1'^2 + c_2'^2 + c_3'^2\right] \times d\xi_1 d\xi_2 d\xi_3 + \frac{1}{2} \int_{-\infty}^{\infty}\int_{-\infty}^{\infty}\int_{-\infty}^{\infty} \frac{n_{out} e^{-\zeta_1^{\prime\prime 2}}}{c_{m_{out}}^3 \pi^{3/2}} \left[\Delta U_{out}^2 + 2\Delta U_{out} c_1'' + c_1''^2 + c_2''^2 + c_3''^2\right] d\xi_1 d\xi_2 d\xi_3 \tag{2.17}$$

$$= \frac{1}{2} n_{in} \left[\Delta U_{in}^2 + \frac{3}{2} c_{m_{in}}^2\right] + \frac{1}{2} n_{out} \left[\Delta U_{out}^2 + \frac{3}{2} c_{m_{out}}^2\right]$$

This will reduce to:

$$T_{av} = \frac{c_{m_{out}}}{c_{m_{in}} + c_{m_{out}}} \frac{\left[\Delta U_{in}^2 + \frac{3}{2} c_{m_{in}}^2\right]}{3R} + \frac{c_{m_{in}}}{c_{m_{in}} + c_{m_{out}}} \frac{\left[\Delta U_{out}^2 + \frac{3}{2} c_{m_{out}}^2\right]}{3R}$$

$$= \sqrt{T_{in} \cdot T_{out}} + \frac{c_{m_{in}} c_{m_{out}}}{3R} \frac{\Delta S_{in}^2 c_{m_{in}} + \Delta S_{out}^2 c_{m_{out}}}{c_{m_{in}} + c_{m_{out}}}$$

$$= \sqrt{T_{in} \cdot T_{out}} \left[1 + \frac{2}{3} \frac{\sqrt{T_{in}} \cdot \Delta S_{in}^2 + \sqrt{T_{out}} \cdot \Delta S_{out}^2}{\sqrt{T_{in}} + \sqrt{T_{out}}}\right] \tag{2.18}$$

In this, ΔS is defined so that:

$$\Delta S_{in} = \frac{\Delta U_{in}}{c_{m_{in}}} = \frac{U_{in} - U_{av}}{c_{m_{in}}} \tag{2.19}$$

It is also apparent from Eq. 2.16 that:

$$\Delta S_{out} = \frac{U_{out} - U_{av}}{c_{m_{out}}} = -\Delta S_{in} \tag{2.20}$$

So that Eq. (2.18) yields:

$$T_{av} = \sqrt{T_{in} \cdot T_{out}} \left[1 + \frac{2}{3} \left(\frac{S_{in}\sqrt{T_{in}} - S_{out}\sqrt{T_{out}}}{\sqrt{T_{in}} + \sqrt{T_{out}}}\right)^2\right] \tag{2.21}$$

Reproduced with permission of the copyright owner. Further reproduction prohibited without permission.

If one defines

$$c_{m_{av}} = \sqrt{2RT_{av}} \tag{2.22}$$

$$\therefore S_{av} = \frac{U_{av}}{c_{m_{av}}} = \frac{S_{in}+S_{out}}{c_{m_{in}}+c_{m_{out}}} \sqrt{\frac{c_{m_{in}} \cdot c_{m_{out}}}{1+\frac{2}{3}\left(\frac{S_{in}\sqrt{T_{in}}-S_{out}\sqrt{T_{out}}}{\sqrt{T_{in}}+\sqrt{T_{out}}}\right)^2}} \tag{2.23}$$

$$= \frac{S_{in}+S_{out}}{\sqrt{T_{in}}+\sqrt{T_{out}}} \sqrt{\frac{\sqrt{T_{in}} \cdot \sqrt{T_{out}}}{1+\frac{1}{3R}\left(\frac{U_{in}-U_{out}}{\sqrt{T_{in}}+\sqrt{T_{out}}}\right)^2}}$$

2.4.2 Response of an Orifice Probe

It has been shown that if dN is the number of molecules crossing a surface dA per unit time, in a Maxwellian flow (Ref. 1).

$$dN = \frac{n\,c_m}{2\sqrt{\pi}}\left[e^{-S^2} + S\sqrt{\pi}\,(1+\operatorname{erf} S)\right] \tag{2.24}$$

$$= \frac{n\,c_m}{2\sqrt{\pi}}\,\chi$$

For a two-stream distribution as previously postulated

$$dN_{TS} = \frac{n_{in}\,c_{m_{in}}}{4\sqrt{\pi}}\left(\chi_{in}+\chi_{out}\right) \tag{2.25}$$

Consider a probe with an opening dA. Assume the pressure inside is p_1 and temperature T_1.

In the steady state, the number of molecules entering dA = number leaving:

$$\frac{n_{in}\,c_{m_{in}}}{4\sqrt{\pi}}\left(\chi_{in}+\chi_{out}\right) = \frac{n_1\,c_{m_1}}{2\sqrt{\pi}} \tag{2.26}$$

since $c_{m_1} = \sqrt{2RT_1}$

and $p_1 = n_1 m R T_1$

$$\therefore n_1 c_{m_1} = \frac{p_1}{\sqrt{T_1}}\frac{\sqrt{2}}{m\sqrt{R}}$$

$$\therefore \frac{p_1}{p_{in}}\sqrt{\frac{T_{in}}{T_1}} = \frac{\chi_{in}+\chi_{out}}{2} \quad \text{for a two-stream function} \tag{2.27}$$

Reproduced with permission of the copyright owner. Further reproduction prohibited without permission.

2.4.3 Response of an Equilibrium Temperature Probe

Using Stalder's solution for the energy transported to a cylinder by diatomic molecules (Ref. 8):

$$\frac{E_{in}}{2\pi r \ell} = \frac{n_\infty c_m}{2\sqrt{\pi}} kT \left\{ (s^2+3)\, e^{-\frac{s^2}{2}} \cdot I_0\left(\frac{s^2}{2}\right) + \left(s^2+\frac{7}{2}\right)\pi s^2 e^{-\frac{s^2}{2}} (I_0+I_1) \right\}$$

$$\equiv \frac{n_\infty c_m}{2\sqrt{\pi}} kT \left\{ (s^2+3) Z_1 + \left(s^2+\frac{7}{2}\right) Z_2 \right\} \qquad (2.28)$$

(I_0 and I_1 are modified Bessel functions of the first and second kind.) and remembering the property of symmetry we get the expression for a two-stream function.

$$\frac{E_{in}}{A} = \frac{n_{in} c_{m_{in}}}{4\sqrt{\pi}} k \left\{ T_{in} \left[(s_{in}^2+3) Z_1\left(\frac{s_{in}^2}{2}\right) + \left(s_{in}^2+\frac{7}{2}\right) Z_2\left(\frac{s_{in}^2}{2}\right) \right] \right. \qquad (2.29)$$

$$\left. + T_{out} \left[(s_{out}^2+3) Z_1\left(\frac{s_{out}^2}{2}\right) + \left(s_{out}^2+\frac{7}{2}\right) Z_2\left(\frac{s_{out}^2}{2}\right) \right] \right\}$$

In the ideal case (i. e. heat is transferred only by convection) the energy transported away from the cylinder depends on the number of molecules striking (and subsequently leaving) the surface, and on the wall temperature. In Stalders' notation, (Ref. 8)

$$\frac{E_{out}}{A} = \frac{n_\infty c_m}{2\sqrt{\pi}} 3k T_{wire} \left\{ Z_1\left(\frac{s}{2}\right)^2 + Z_2\left(\frac{s}{2}\right)^2 \right\} \qquad (2.30)$$

so that finally:

$$\frac{T_{wire}}{T} = \frac{(s^2+3) Z_1 + \left(s^2+\frac{7}{2}\right) Z_2}{3\,(Z_1+Z_2)} - \frac{\text{error terms}}{\alpha} \qquad (2.31)$$

where the error terms are proportional to the relative magnitudes of the non-convective heat transport mechanisms compared to convective transport.

In the case of a two-stream function let us assume α is the same for the incident and reflected stream. From considerations of symmetry we can write down:

$$T_{wire} \left\{ \frac{3}{2} \left[Z_1\left(\frac{s_{in}^2}{2}\right) + Z_2\left(\frac{s_{in}^2}{2}\right) \right] + \frac{3}{2} \left[Z_1\left(\frac{s_{out}^2}{2}\right) + Z_2\left(\frac{s_{out}^2}{2}\right) \right] \right\}$$

$$= \frac{T_{in}}{2} \left\{ \left[s_{in}^2+3 \right] Z_1\left(\frac{s_{in}^2}{2}\right) + \left[s_{in}^2+\frac{7}{2} \right] Z_2\left(\frac{s_{in}^2}{2}\right) \right\} \qquad (2.32)$$

$$+ \frac{T_{out}}{2} \left\{ \left[s_{out}^2+3 \right] Z_1\left(\frac{s_{out}^2}{2}\right) + \left[s_{out}^2+\frac{7}{2} \right] Z_2\left(\frac{s_{out}^2}{2}\right) \right\} - \frac{\text{error terms}}{\alpha}$$

Reproduced with permission of the copyright owner. Further reproduction prohibited without permission.

$$T_{wire} = \frac{T_{in}\left\{\left[S_{in}^2+3\right]Z_1\left(\frac{S_{in}^2}{2}\right)+\left[S_{in}^2+\frac{7}{2}\right]Z_2\left(\frac{S_{in}^2}{2}\right)\right\}+ T_{out}\left\{\left[S_{out}^2+3\right]Z_1\left(\frac{S_{out}^2}{2}\right)+\left[S_{out}^2+\frac{7}{2}\right]Z_2\left(\frac{S_{out}^2}{2}\right)\right\}}{\left\{\left[Z_1\left(\frac{S_{in}^2}{2}\right)+Z_2\left(\frac{S_{in}^2}{2}\right)\right]+\left[Z_1\left(\frac{S_{out}^2}{2}\right)+Z_2\left(\frac{S_{out}^2}{2}\right)\right]\right\}} - \frac{\text{error terms}}{\alpha} \quad (2.33)$$

using Stalders notation for f(s) and g(s)

$$T_{wire} = \frac{T_{in}\cdot f(S_{in}) + T_{out}\cdot f(S_{out})}{g(S_{in}) + g(S_{out})} - \frac{\text{error terms}}{\alpha}$$

2.4.4 Effect of Accommodation on Two-Stream Response

When α_s and $\alpha = 0$, $S_{in} = S_{out}$ and $T_{in} = T_{out}$, the two-stream and Maxwellian expression are identical as one would expect. From physical reasoning, one would expect the maximum difference in response to occur where α_s and $\alpha = 1$, that is when $S_{out} = 0$ and $T_{out} = T_w$.

In this case $$\frac{\chi_{in}+\chi_{out}}{2} = \frac{1+e^{-S_{in}^2}+S_{in}\sqrt{\pi}\left(1+\operatorname{erf}S_{in}\right)}{2} \quad (2.34)$$

$$S_{av} = \frac{S_{in}}{\lambda_{m\,in}+\lambda_{m\,out}}\cdot\sqrt{\lambda_{m\,in}\cdot\lambda_{m\,out}} \quad (2.35)$$

and

$$\frac{T_{wire}}{T_{av}} = \frac{T_{in}\,f(S_{in}) + T_w\,f(0)}{\sqrt{T_{in}\cdot T_w}\,\left[g(S_{in})+g(0)\right]} \quad (2.36)$$

In general for any α_s and α for flow parallel to the plate one can write (according to Eqs. 2.1 and 2.2(a))

$$S_{out} = (1-\alpha_s)\,S_{in}$$

$$T_{out} = \frac{(1-\alpha)\left(S_{in}^2+3\right)T_{in} + 3\alpha T_w}{(1-\alpha_s)^2 S_{in}^2 + 3} \quad (2.37)$$

For the long tube probe it is easily shown that, just as the orifice-probe two-stream response is given by $p_1/p_2 = (\chi_{in}+\chi_{out})/2$, so the long-tube response is $p_1/p_2 = (W_{(in)} + W_{(out)})/2$ where W is Harris and Patterson's long-tube parameter (Ref. 14).

Reproduced with permission of the copyright owner. Further reproduction prohibited without permission.

For the case of a long tube parallel to the flow, and a short tube perpendicular to the flow, such as described in Sec. 3.2,

$$\frac{p_1}{p_2} = \frac{W(S_{in}) + W(S_{out})}{2} \tag{2.38}$$

Using these equations it is possible to calculate probe response in a two-stream distribution and compare this to the response in a simple Maxwellian flow having the same average parameters. The values of the parameters in the following representative calculation have been chosen to approximate the experimentally observed values in the 100°C experiments described later. The probe response was calculated for assumed values of $\alpha = \alpha_S = 1$, 0.5 and 0.25. For the pressure-pair probe of Section 3.2, the error of the probe reading was determined from the ratio of $S_{observed}/S_{av}$ where $S_{observed}$ is that average value of S needed to give the pressure ratio identical to the two-stream ratio of Eq. (2.38) and S_{av} as given by Eq. (2.35). The error in determining temperature with the equilibrium-temperature gauge and pressure-pair gauge used in consort was calculated in the following fashion: The experimentally determined values of temperature contains two possible errors, one due to the assumption that the equilibrium temperature probe has the identical response for a two-stream distribution and a simple Maxwellian flow having the same average values of T and U, and the second due to the assumption that the pressure probe responds identically as well. For a simple Maxwellian flow we have from Stalder's development that,

$$T_{wire} = T \cdot \varphi(S)$$

If primed quantities represent erroneous values obtained because of the difference in response to Maxwellian and two-stream values

$$\frac{T'}{T} = \frac{T'_{wire} \cdot \varphi(S)}{T_{wire} \cdot \varphi(S')} = \frac{T'_{wire} \cdot \varphi(S)}{T \cdot \varphi(S) \cdot \varphi(S')} = \frac{T'_{wire}}{T \cdot \varphi(S')} \tag{2.39}$$

Using the two-stream value for S as calculated for the pressure pair probe (Eq. 2.38) one can determine $\varphi(S')$. Similarly using the two-stream assumptions one can calculate T_{wire}/T_{av} for the equilibrium temperature probe (Eq. 2.33). The ratio of these two quantities is a measure of the error introduced by the two-stream effect in using these probes to get T.

Table I indicates that the error in measuring temperature and speed-ratio is small, even in the presence of a two-stream distribution function. Thus, for the case investigated here, and with the values of α determined by the experiments ($\alpha \gtrsim 0.5$ or less) the errors are no greater than the experimental scatter and would not affect any of the conclusions reached later.

Reproduced with permission of the copyright owner. Further reproduction prohibited without permission.

3. APPARATUS

The instrumentation of continuum-flow wind tunnels has been well developed over the years so that at present many powerful and accurate means of measurement exist. By use of pressure probes, drag balances, optical methods such as schlieren, optical interferometers and shadowgraphs, and various types of temperature probes it is possible to determine flow parameters accurately and unambiguously. However, no comparable developments oftechnique and probes exist for low-density wind tunnels.

The U. T. I. A.S. wind tunnel (plate 1 and Ref. 15) is an open-jet non-return type which, when equipped with its subsonic nozzle, can have test-section static pressures which vary over a wide range. In various experiments these pressures have been as low as 2 microns (0. 002 mm Hg. or 2.66×10^{-6} atmospheres) and as high as 40 microns (. 04 mm, or 5.3×10^{-5} atmospheres) with the possibility of further extension if desired To date, measurements have usually utilized pressure probes of one type or another. While these probes are the most important single source of information in the tunnel, they suffer from several severe limitations not found at ordinary pressures. In the first place, a static pressure probe small enough to be in free-molecular flow does not measure pressure itself, but rather the ratio $p/\sqrt{T}$ (Ref. 16). Since the same probe in continuum flow would measure p one must always be certain of the regime in which it is operating under the given conditions and make the appropriate allowance.

In small probes at low density the speed of response of a probe can be very slow. Since at these low pressures large volumes of gases (such as water vapour) can be released inside the gauge volume by a slight drop in pressure (i. e. outgassing), the effective speed of response can be orders of magnitude less than indicated by geometry alone. For a practical probe it is thus desirable to keep the internal volume of the probe head, probe tip and connecting line to minimum. For this reason many otherwise satisfactory probes and gauges cannot be used.

At the low pressures involved, the total forces available to operate a sensing element are extremely small. For this reason, ordinary pressure gauges of the bellows or pressure-cell type are of diminishing utility as the pressure goes below, say, one millimeter. As a result it is rarely practical to measure true pressure in the low density wind tunnel. Instead, one usually measures some other phenomenon, (such as change in thermal conductivity), and calibrates this in terms of pressure. The calibration will be sensitive to other factors such as gas composition or temperature so that considerable care must be exercised in interpreting the readings.

Optical methods, being sensitive to absolute changes in density rather than relative changes, lack sensitivity in this tunnel, so that this elaborate and powerful technique is of limited value. The conse-

Reproduced with permission of the copyright owner. Further reproduction prohibited without permission.

quent loss of these reliable methods of flow visualization complicates experimental work enormously.

On the other hand, measurement of flow temperatures is rather more satisfactory. Using methods described here, it seems that one can determine temperatures at least as accurately and simply as in continuum flow. Less complicated mathematical relationships exist between thermometer temperature and flow parameters in free-molecular flow as compared to continuum flow.

Drag-balance measurements can be obtained in a low-density wind tunnel (Ref. 17) but are not considered here. In addition, the special properties of low density atmospheres make possible entirely new methods of probing the flows. Electron beams, glow discharge flow-visualization, electron lens interferometery and other techniques are being developed by various laboratories, but none of these more unusual schemes is reported here.

Various people have considered the problem of determining the local molecular-speed ratios in a general fashion. Patterson has indicated that by using free-molecular orifice-probes one can determine speed-ratios unambiguously by making three simultaneous local pressure measurements (Ref. 16). Sherman (Ref. 12) and Laurmann (Ref. 2) have mentioned similar schemes to determine S using an equilibrium temperature probe. However there seems to have been no previous practical suggestion for determining flow temperatures as well.

A problem that probes seem to have in common in all regimes is the degree to which their physical presence will disturb the flow itself. In most cases this problem can be overcome in continuum flow and one might reasonably hope for similar success for probes in free-molecule flow. However, each case must be considered individually.

3.1 The Equilibrium Temperature Probe

In free-molecular flow, an adiabatic cylinder placed transverse to the flow will assume an equilibrium temperature which is a function of local static temperature and the molecular speed-ratio. The relationship has been given by Stalder et al. (Ref. 18) for uniform (Maxwellian) flow and by Bell and Schaff (Ref. 19) for a non-uniform flow.

For any flow the local static temperature can be written in terms of the local total temperature and local Mach number. When this total temperature is constant (i. e. adiabatic flow), the equilibrium temperature will vary only as the Mach Number (or molecular speed ratio) varies. If the stagnation temperature is known, such a device can then be used to measure speed ratio. Since the cylinder can be in the form of a very small diameter wire it is rather simple to make a probe with relatively high Knudsen number. As a result the free-molecular equilibrium

Reproduced with permission of the copyright owner. Further reproduction prohibited without permission.

temperature probe can be a very useful instrument for determining molecular speed ratio.

In non-adiabatic flows this approach is useless since T_o is not known. Even for adiabatic flows this simple picture is complicated by several factors, one of the chief being non-uniformity of the flow field. Bell and Schaaf have shown that for a slightly non-Maxwellian flow, it is possible to write down the equilibrium temperature in terms of the Maxwellian flow plus heat-conduction and viscosity terms. Since most flows can be expressed in terms of a slightly-non-Maxwellian distribution function, the method is usually adequate and the correction terms are small. Calculations will be made to show that in these experiments the corrections are in fact negligible (Sec. 3.1.5). Since, moreover, the response to a two-stream distribution has been shown to be numerically equivalent to an average Maxwellian distribution, in these experiments the probe may in fact be used anywhere in the flow field with some certainty as to the meaning of its response.

3.1.1 Design of the Equilibrium Temperature Probe

The equilibrium temperature probe, as used by Sherman (Ref. 12) was made of 0.00025 inch tungsten wire, the temperature being determined by the resistance of the $\frac{1}{2}$" central length of this wire. While this probe combined reasonable strength with a large Knudsen number it did not give a point-measurement of temperature, but only the average over $\frac{1}{2}$". The small current needed to make a resistance measurement acted as a small source of energy input, upsetting the adiabatic assumption slightly.

Because the U T. I. A. S. tunnel operates at a significantly lower pressure, convective heat transfer is less, so that this latter fault would tend to be more of a problem in our case. However, the larger mean-free-paths of the U. T. I. A. S. tunnel allowed the use of a more attractive method of temperature measurement, the thermocouple. After some experimentation it proved possible to successfully weld together high-tensile-strength thermocouples of diameters as low as 0.0005 inches. The advantages of using a thermocouple are many:

1. Temperature can be measured very easily with much increased precision.

2. No significant power input is required so that the probe is more essentially adiabatic.

3. Truer point measurements of temperature can be made so that more precise location of data-points are possible.

4. Mechanically, the probe is simple and easier to use.

Reproduced with permission of the copyright owner. Further reproduction prohibited without permission.

5. End conduction losses are much less serious because lower conductivity wires may be used.

By using chromel-alumel materials, which have about one-third the strength of tunsten one may construct a somewhat stronger probe then a given tungsten hot-wire probe by using thermocouples that are twice the diameter of the tungsten. In the U. T. I. A. S. tunnel it is a reasonable compromise to halve the maximum Knudsen number to obtain the advantages of a thermocouple probe.

The design of the U. T. I. A. S. equilibrium temperature probe is shown in Figure 1 and Plate II. Two dissimilar metal wires are joined so that the hot-junction of the thermocouple pair is strung in tension midway between two spreader arms. These spreader arms are insulated from the thermocouple wires and form part of a bracket which is mounted on the traversing mechanism of the test section. In this way the hot junction may be moved anywhere in the flow-field of the tunnel. The thermocouple wires are carried through flexible leads and hermetic seals into the stagnation chamber where a cold-junction of similar materials is permanently mounted on the nozzle axis about 2 inches upstream of the nozzle entrance. One of the flexible leads is cut at a convenient point in the test section so that leads may be brought off from these two ends, through hermetic seals to a terminal board and eventually to a high precision self-balancing potentiometer. *

A second junction at the same position in the stagnation chamber as the previously mentioned cold-junction was used in conjunction with a reference junction in an ice bath, to establish T_o .

The reading of this equilibrium temperature probe is given by the difference in temperature between the hot-junction on the traversing mechanism and the cold-junction in the stagnation chamber. This reading is thus extremely sensitive to velocity of the gas and relatively insensitive to normal changes in stagnation temperature. As a result the problems of stagnation temperature fluctuation that plagued Laurmann (Ref. 2) were avoided without the necessity of regulating the stagnation temperature. This design feature is an important improvement over current "hot wire" designs.

Several diameters of thermocouple wire were tried for manufacturing of the probe junctions, with complete success for wires as small as 0.0005 inches. However, for reasons of ruggedness and ease of fabrication, 1 mil wires were used. The thermocouple wires were carefully lap-welded** and then trimmed under a microscope to produce a strong junction substantially circular in cross-section and of the same

---

* Brown-Rubicon Model No. 156 x 15-VH-0-70 MV in 1.0 MV steps

** Welding Head Model W. H. D 5A Ewald Instruments, Kent, Connecticut

Reproduced with permission of the copyright owner. Further reproduction prohibited without permission.

diameter as the wire. The junction was centered between the spreader arms and the wires soft-soldered to insulated pins mounted at the tips of these two arms. The arms were cantilever springs about 3" x $\frac{1}{4}$" made from 0.0008" and 0.012" feeler gauge stock. One arm was made much stiffer than the other to eliminate any uncertainty in the junction position.

Since the overall distance between the spreader arms was twelve inches, Sherman's data indicates that end conduction through the wires could be neglected (Ref. 12).

For the cold junction a pair of wires were crossed to form an elongated "X" and spot-welded at the point of cross-over. This "X" was mounted in the stagnation chamber perpendicular to the nozzle axis with the junction on the centerline of the nozzle. This formed a single junction with two separate sets of leads. One set was used to form the cold-junction of the equilibrium temperature probe, the other was used to measure T_o in conjunction with an external junction in an ice bath.

The temperature calibration of these thermocouples was checked at room temperature by comparison with a mercury-in-glass thermometer calibrated to 0.1°C. Since no significant error could be observed, standard chromel-alumel thermocouple tables were used in subsequent measurements.

3.1.2 Use of the Equilibrium-Temperature Probe

The technique for using the equilibrium-temperature probe was as follows:

1. T_o was determined using the cold-junction thermocouple. This value was normally checked against a second stagnation temperature gauge further upstream.

2. The probe junction was moved into the lee of the nozzle wall where no mass flow would be expected and the voltage difference between the two junctions, ($\epsilon = \Delta T_o \beta$ where β is the reciprocal of the thermoelectric power), noted. Because the air was not truly stationary at the stagnation chamber "cold" junction, whereas it was at the "hot" junction, (for this particular position), the voltage difference was negative and represented a correction that had to be subtracted from the observed stagnation temperature reading to get true stagnation temperature.* In speed-ratio measurements this same correction had to be added to the observed ΔT (the difference between the probe junction (hot junction) and the cold junction) to give the true difference for a cold junction at the true stagnation temperature. Since this correction was constant for any given free-stream Mach number, it need only be determined once in a run.

---

* The correctness of this procedure was confirmed by various bits of internal evidence.

Reproduced with permission of the copyright owner. Further reproduction prohibited without permission.

(footnote continued)

1. The results always gave reasonable values for the speed ratio at the nozzle exit.

2. The calculated T_o using the correction agreed well with room temperature and the other stagnation-temperature probe.

3. The configuration of the nozzle at this point made flows very difficult to imagine on physical grounds.

4. In any case, any error that might have arisen using this assumption would be too small to have a significant effect except at the very lowest flow rates where the total temperature difference ΔT would be quite small.

5. A careful probing of the whole space that could be reached by the traversing mechanism never produced a lower reading. If $d\epsilon$ is the error in ϵ, the error in $\Delta T/T_o$ then introduced would be $\simeq \Delta\, d\epsilon/(\Delta\epsilon + T_o)$ and would be negligible except at very low speed ratios. Since the probe is most susceptible to heat-transfer error in the region near the wall (i.e. where S is low) the probe is unreliable in this region in any case. It must be concluded that the error in ϵ is unimportant.

---

3. The probe was then used to measure flow conditions. ΔT was determined at each measurement location, allowing ample time for the probe to come to equilibrium. T_o was checked at regular intervals. Because T_o changed only slowly and since these changes did not affect the results particularly, it was not necessary to determine it at every point.

4. From these measurements it was possible to obtain the ratio $\Delta T/T_o$. This ratio could then be located on the appropriate theoretical curve (Fig. 2) to give molecular speed ratio S.

This technique applied only if T_o could be assumed to be constant throughout the flow. In non-adiabatic flows where the probe was not used to measure S, only the value $\Delta T + T_o = T_{wire}$ is required, so that the zero-flow correction is not needed.

When used in a low-density flow, the instrument was found to give very reproducible results. Because of other uncertainties in the use of this probe no attempt was made to obtain readings closer than the nearest 0.1°C although a least-count of 0.01°C was possible. It is felt that the thermocouple itself had an absolute accuracy of at least 0.1°C.

At twenty microns pressure the probe had a response time of a few seconds so at least twenty seconds were allowed for equilibration of reading. At a pressure two orders-of-magnitude lower the probe was noticeably more sluggish but still showed no measureable hysteresis. This indicates that the power supplied to the thermocouple by heat transfer is still greater than the minimum power required to operate the potentiometer

Reproduced with permission of the copyright owner. Further reproduction prohibited without permission.

and that power fed back to the thermocouple by a poor potentiometer balance can be safely ignored. The general conclusion is that the measuring system as a whole placed no limitation on the utility or accuracy of the probe. Any limitations that did appear were inherent in the probe itself.

3.1.3 Equilibrium Temperature Probe Data Reduction

For the special case in which the flow is adiabatic, so that the stagnation temperature is uniform, the equilibrium temperature probe can be used to determine S directly. In fact it is not even necessary to determine temperatures explicitly. As indicated previously it is necessary to determine

(1) a correction for the effect of the mass flow past the stagnation chamber cold-junction (let us assume this correction to be ϵ_{mv} equivalent to δT_o),

(2) the stagnation cold-junction reading (E_o equivalent to $T_o + \delta T_o$) and

(3) the difference reading, (ΔE equivalent to $\Delta T - \delta T_o$).

We wish to know

$$\frac{\Delta T}{T_o} = \frac{T_{wire}}{T_o} - 1 \qquad (3.1)$$

If $\mathcal{A}$ is the thermocouple sensitivity in (C^o/mv), we have

$$\frac{\Delta T}{T_o} = \frac{(\Delta E + \epsilon)\mathcal{A}}{(E_o - \epsilon)\mathcal{A} + 273^o} \qquad (3.2)$$

since E_o is referred to a cold junction at 0^oC.

$$\frac{\Delta T}{T_o} = \frac{\Delta E + \epsilon}{E_o - E + \frac{273}{\mathcal{A}}} \qquad (3.3)$$

Since $\mathcal{A}$ = 25 degrees/mv for a chromel-alumel thermocouple $\Delta T/T_o$ is quickly calculated.

Reproduced with permission of the copyright owner. Further reproduction prohibited without permission.

Using the relationship

$$\frac{T_o}{T} = 1 + \frac{\gamma - 1}{\gamma} S^2 \qquad (3.4)$$

a curve for $\Delta T/T$ vs S (Fig. 3) is readily calculated from the theory of Ref. 18.* A similar curve for $\Delta T/T_o$ vs S is also given (Fig. 2). When the jet flows over a heated plate, T_o is no longer constant so that S may not be determined by this probe. Since S may be determined by the pressure probe data, it is possible to use the inverse procedure to determine local values of T_o and T. We have $T_{wire}/T_o = 1 + \psi(S)$ (Fig. 3) and $T_{wire}/T = 1 + \phi(S)$ (Fig. 2), so that $T_o = \frac{T_{wire}}{1 + \psi(S)}$ and $T = \frac{T_{wire}}{1 + \phi(S)}$

where

$$T_{wire} = \frac{\Delta E + E_o}{.040} + 273^oK \qquad (3.5)$$

for the particular thermocouple used.

3.1.4 Radiative Heat Transfer

Because T_{wire} could be higher than the wall temperature and lower than the flat-plate temperature it was not certain what the magnitude (or even the direction) of the radiative heat transfer would be. Still-air runs (Figs. 4, 5, 6, and 7) were undertaken to estimate the nature of this effect.

At low pressures it can be assumed that gaseous heat conduction is small compared to radiative transfer. For a given plate temperature and probe position this radiative transfer is independent of pressure. If the probe temperature is T_1 the heat radiated from the probe to the surroundings is $A\epsilon\sigma T_1^4$ where A is the effective area, ϵ is emissivity and σ is the Stefan-Boltzmann constant. This is equal in magnitude to the incoming radiation heat-load, which will not change with pressure or probe temperature. At some other pressure the probe temperature will be, say, T_2 and the difference in radiative heat transfer will be

$$A\epsilon\sigma (T_1^4 - T_2^4) \qquad (3.6)$$

As calculated for our experimental conditions, the magnitude of the error term due to radiative heat transfer according to Stalder's

* It is useful to note than an approximate value for $\Delta T/T$ for small values of S is given by $\Delta T/T = \log (1 + S^2/2) + 0.3 (S^2/2)^3 +$ error term where the error term is of the order of $(S^2/2)^4$. This is readily seen by developing the terms of the exact expression as infinite series and manipulating. At S = 0.5 the error is about 0.025%.

Reproduced with permission of the copyright owner. Further reproduction prohibited without permission.

development (Ref. 8) will therefore be

$$\frac{\epsilon \sigma (T_1^4 - T_2^4)}{p \cdot c_m \cdot \alpha \cdot g(S)} \qquad (3.7)$$

where

$$g(S) \approx 10$$

$$\sigma = 5.672 \times 10^{-5} \text{ ergs/sec cm}^2 \text{ deg. c}^4$$

$$c_m \simeq 3 \times 10^4 \text{ cm.}$$

$$p = 26.5 \text{ dynes/cm}^2$$

$$\epsilon = \text{emmissivity of wire} = 0.36$$

The error term $\simeq \frac{3 \times 10^{-12}}{\alpha} (T_1^4 - T_2^4)$ (3.8)

one can make the approximation $T_1^4 - T_2^4 = \Delta T. \ T^3$

where

$$\Delta T = T_1 - T_2 \text{ and } T = \frac{T_1 + T_2}{2}$$

Taking a pessimistic estimate for the 200°C plate

$$T = 380^\circ K \qquad \Delta T = 20^\circ K$$

the error term becomes $\simeq \frac{0.2^\circ C}{\alpha}$

That is, the error term will always be small, normally less than the error introduced by other considerations.

3.1.5 Non-Uniform Flow Corrections

The theory of Bell and Schaaf (Ref. 19) allows an estimate to be made of the size of the correction terms for the effects of non-uniform flow on the temperature response of the equilibrium temperature probe. As will be seen (Fig. 8) these terms are of the order

1. $5 \times 10^{-6} \ \frac{\partial U}{\partial y} \ A$ (3.9)

where A is of the order of 0.15, or

2. $\frac{1.5 \times 10^{-2}}{U} \ \frac{\partial T}{\partial x} \ B$ where B is $\simeq 0.1$ (3.10)

Reproduced with permission of the copyright owner. Further reproduction prohibited without permission.

If the magnitude of the gradients are measured from the appropriate curves it turns out that the corrections will be small, always less than 0.04% of the uniform flow case i.e. $.04/100 \times T_{wire}/T < 0.1^{o}C$. This represents a negligible correction.

3.1.6 Knudsen Number Effect

Sherman (Ref. 7) has shown that for a Knudsen number greater than 10 the equilibrium temperature probe assumed the values for free-molecular flow. From considerations of energy it is apparent that the flow cannot be disturbed significantly by a probe whose Knudsen number is 100, as was the case for these experiments, so that it is assumed here that the probe is truly in free-molecular flow.

3.2 Pressure Probe

Patterson has shown that for an orifice probe in free-molecular flow the gauge-head pressure is related to the static pressure as a function of the speed ratio and the ratio of absolute temperature of the gas in the gauge head and at the orifice (Ref. 11). He has further shown that in non-uniform flows certain additional terms proportional to the flow gradients must be added. If these measurements are made at any one locality, with the orifice facing in three specific directions he has indicated that it is possible to determine the molecular speed-ratio even in the presence of gradients. It might therefore be expected that two measurements would be sufficient to determine S in a uniform flow. This is true, as will be shown, and in addition it turns out that the magnitudes of the correction terms that must be added are not significant in the sort of non-uniform flow fields obtained in this experiment. Two pressure readings therefore suffice to determine S, with sufficient accuracy for these experiments.

The orifice probe as normally constructed (Ref. 3 and 15) is a simple closed tube in which one section of the wall has been cut away and replaced by a thin foil containing a single small orifice. Such a probe tends to be rather bulky and the exact orientation of the orifice is somewhat in doubt. As a result it is not always a simple instrument to use. For a long-tube impact probe the orientation of the opening is rather accurately known while the diameter of the probe is as small as possible in any construction. Since Harris and Patterson (Ref. 14) have developed an expression for the response of a long-tube impact probe in uniform flow it is possible to use such a construction to give meaningful measurements. The further fact that, short tubes and orifice probes give almost identical readings* when used as static probes (i.e. with the opening perpendicular

* There is in fact a small dependence on speed-ratio, with the difference being about 2% at the highest speed ratio used here.

Reproduced with permission of the copyright owner. Further reproduction prohibited without permission.

to the flow so that the effective speed ratio is zero) makes it possible to construct a probe which will provide an accurate and simple means of determining S directly.

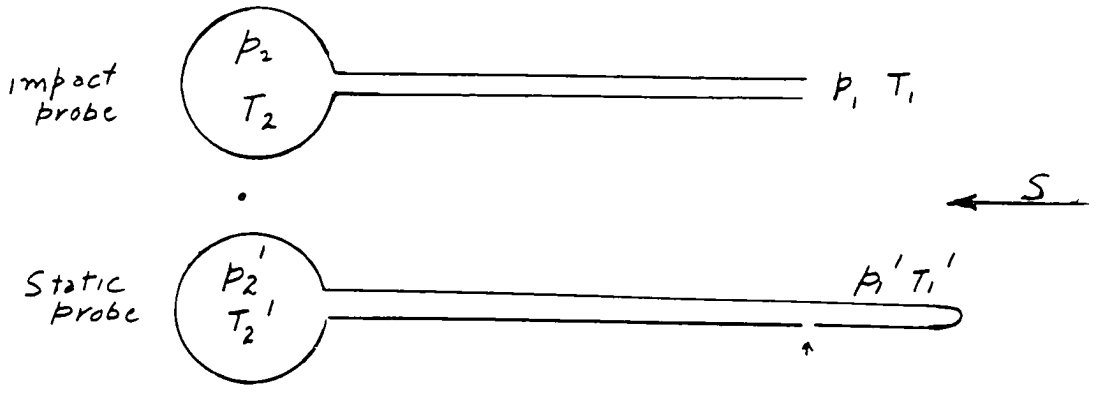

Consider a long-tube impact probe with its long axis in the direction of the flow and its opening perpendicular to the flow. If p_2 and T_2 refer to pressures and temperatures in the gauge head and p_1 and T_1 to the gas static pressure and temperature at the probe opening, Harris has shown that

$$\frac{p_2}{p_1}\sqrt{\frac{T_1}{T_2}} = W(s) \qquad (3.11)$$

For a static probe

$$\frac{p_1'}{p_2'}\sqrt{\frac{T_1'}{T_2'}} = 1 \qquad (3.12)$$

where primed quantities are for conditions referred to the static probe. If both probes are placed in the same region then $p_1' = p_1$ $T_1' = T_1$. If both gauge heads are held at the same temperature then $T_2' = T_2$

$$\therefore \frac{p_2}{p_2'} = W(s) \qquad (3.13)$$

It is a simple matter to drill a small hole in the wall of a metal tube perpendicular to the long axis on the side remote from the impact probe, to close off the upstream end and to use this as the static probe.

Reproduced with permission of the copyright owner. Further reproduction prohibited without permission.

The advantages of this type of construction are:

1. The tube diameter can be kept to an absolute minimum.

2. Orientation of the probe relative to the flow can be accurately determined.

3.2.1 Pressure Pair Probe

These considerations led to the development of a probe for measuring molecular-speed ratios which will be called here a pressure-pair probe (Fig. 9). In this probe, two essentially identical sensing heads are built into a single block of metal and set to operate with identical wire temperatures. The excellent thermal contact assures that the wall temperature will be identical in both gauges so that a pair of gauges satisfies the condition $T_2 = T_2'$ (cf Appendix A).

Small diameter hypodermic tubing connects each gauge head to its respective probe tip. These probe tips are accurately aligned so that they are parallel, with the open end of the impact probe exactly opposite the hole in the static probe. The end of the static probe is plugged with soft-solder. The whole assembly is rigidly braced and mounted with the long axis of the probes pointing directly into the flow and with the probe tips lying in a plane parallel to the flat plate (Fig. 10). If the flow is essentially two-dimensional the probe satisfies the other requirement, $p_1 = p_1'$ $T_1 = T_1'$ (otherwise the probe must be displaced sideways during measurement so that impact and static measurements are made at exactly the same spot). The ratio of the two gauge-head pressures is now W(s) where W(s) is the expression for the long-tube pressure ratio as developed by Harris (Ref. 3, Fig. 11). This probe is particularly suited to the flat plate experiment where flow is essentially two-dimensional and parallel to the plate.

The probes will have some effect on the flow and therefore on each other. By a highly simplified argument it is possible to show that this interference effect might reasonably be expected to be small. *

---

* Let us consider the effect of the impact probe on the static probe if the two probes are separated by a distance of one mean-free-path as they were in this particular experiment. Suppose the probe tip diameter is d, and probe separation is λ (see sketch)

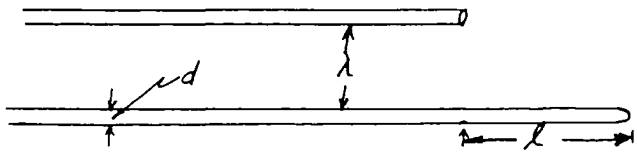

Because of the geometry, no molecule will deflect directly from the impact probe to the hole of the static probe. The static probe should affect the

Reproduced with permission of the copyright owner. Further reproduction prohibited without permission.

impact probe however. If one assumes no intermolecular collisions, the fraction of molecules striking the impact tube which have been reflected from the static probe will bear a relationship to the solid angle subtended by the static probe at the impact probe. This ratio is

$$R = d\ell / 2\pi\lambda^2$$

where ℓ is the distance the static probe extends beyond the impact probe for $\ell = \lambda$ this gives $R = (2\pi Kn)^{-1}$

Making the pessimistic assumption that all regions of the hemispherical cap of radius λ (solid angle 2π) give equal contributions to the response of the probe, the ratio of the actual probe response to the ideal probe response (no interference) is $1-R(1 - 1/W(s))$ for a long tube impact probe, assuming diffuse reflection at the static probe. (W(s) is the previously mentioned long tube response factor of Ref. 3). W has a maximum value of 2 in these experiments and a minimum value of 1, so that the pressure ratio error,is not greater than a fraction R/2.

Since collisions do occur, on the average $\frac{1}{2}$ the molecules from the static probe are deflected from the impact probe so that the disturbance will be less than R/4. For Kn = 4 (this case) the error will be at most 2%. Since the assumption that all elements of the spherical cap contribute equally to probe response is least valid at higher speed ratios (where the error is larger) it seems safe to assume a maximum error of no more than 1% even for perfectly diffuse reflection.

The particular pressure-pair gauge-head used in these experiments was made of stainless steel pieces cemented together with an epoxy resin. The sensing elements were high precision thermocouple gauges with constant filament temperature. The total internal volume of each gauge was less than 1.0 cc. The probe tips were 0.025 inch O.D. hypodermic tubing (0.022 inch I.D.) and were placed 0.100 inches apart. The static probe had a 0.012 inch hole.

The pressure-pair probe was somewhat slower to use than the equilibrium temperature probe. Having determined individual gauge calibrations one could then measure impact and static pressures at any given point by positioning first one and then the other probe in that position. The two probes were spaced 0.100 inches apart, but because the flow was essentially two-dimensional, no observable error was introduced by neglecting the offset of the static pressure probe. The long-tube formula developed by Harris (Ref. 3) could then be used to determine local values of S as indicated by the ratios of the pressures.

Reproduced with permission of the copyright owner. Further reproduction prohibited without permission.

3.2.2 Temperature Corrections

During the course of the 100°C plate run (Section 4.4) it became apparent that the pressure readings were showing small departures from the expected pattern in a way which was not physically reasonable. Careful examination of these discrepancies made it apparent that they correlated with certain probe positions which could be expected to cause large changes in gauge-head temperature. Because of the low thermal conductivity of the gas, quite small changes in radiative heat transfer could result in large changes in gauge-head temperature. This in turn could cause small zero shifts in the gauge calibration which, because of the high gauge sensitivity, would show up in the final results.

In preliminary experiments using a room temperature plate, it was observed that, within the limits of the accuracy of observation, the static pressure was constant over the plate, so that it was possible to devise a systematic correction to the observations which reduced the internal inconsistency of the data to negligible proportions. The static pressure was assumed to be constant over the plate. Because there were two separate gauges measuring this pressure; (the static pressure member of the pressure-pair and the gauge embedded in the plate wall)(cf. 3.3.2), it was possible to relate the change in calibration of the static pressure member of the pair with the change in calibration of the impact probe. This was done through the calibration of the two gauges at various temperatures and 20 microns (Fig. 12). Since this temperature effect was a true zero-shift which did not affect the gauge sensitivity, it was possible to draw a family of calibration curves for each gauge head in which each member of the family represented a different zero shift. Through the data of Fig. 12 it was possible to relate the zero shifts in the two gauges so that each member of the static pressure gauge family of curves had a corresponding member in the impact pressure calibration family*.

---

* For the gauges used, the power input to the gauge varied linearly with pressure. The gauges had a sensitivity $A^{microns}/(mv^2)$, where mv is a voltage proportional to the current applied to the gauge, so that $(mv)^2$ is proportional to power.

Thus $$\Delta p = A\left[(mv)^2 - (mv_o)^2\right]$$

$$p - po = A\,\Delta mv\,(mv + mv_o)$$

where mv_o is the voltage at pressure p_o. If p_o and mv_o are taken to be, say, 20 microns and its corresponding gauge reading, then it is possible to draw a calibration curve through this point, knowing the value of A. By assuming the gauge head temperature has changed by an unspecified amount sufficient to change mv_o by a convenient increment, a second member of the family of calibration can also be drawn. This process is repeated to obtain the entire family.

If we now consider Fig. 12 it is possible to construct a second family of calibration curves, this time for the impact gauge, each member of which corresponds in gauge head temperature to a similar member in the static gauge calibration family.

Reproduced with permission of the copyright owner. Further reproduction prohibited without permission.

The two families of calibration curves are given in Fig. 13 and 14. Knowing the static pressure and the static pressure gauge reading it was possible to determine which member of the calibration-curve family was to be used. Using the corresponding member of the impact-pressure family, the true impact pressure could readily be determined.

The main justification for this method is that it produced self-consistent data. Near the trailing edge of the plate and near the nozzle wall the molecular speed ratio dropped to a low value so that the ratio of static and impact pressures was very close to unity and as a result very sensitive to errors in pressure measurement. Before correction, the observed ratios were frequently less than one, which would be physically impossible. After correction this never happened. Since these two probe positions would represent the two extremes in gauge-head temperature it seems impossible that the corrections made here could give a reasonable answer in both cases unless the methods of manipulation were substantially correct.

Fortunately, it happens that errors due to departures from the assumption of constant pressure would tend to be cancelled out. An error in the static pressure assumed in fact produces a temperature correction in such a direction as to partially correct for the original error. Thus small changes in the static pressure over the plate are not as serious as might be thought as first. For these reasons, it is felt that the corrections are justified.

As a final argument it might be pointed out that, except when the speed ratio was very low, the corrections made less than a 5% difference in S. As will be seen, none of the conclusions reached in this experiment would be changed by this sort of variation.

3.2.3 Knudsen Number Effects

The Knudsen number for these probes, based on probe diameter, is at the lower limit of free molecule-flow, being $\approx$ 4, but the end-on position of the impact probe tends to minimize the Knudsen number effect, compared to orifice probes. Experimental evidence suggests that impact pressures will read 2% below the free-molecule value at this Knudsen number (Ref. 20).

3.2.4 Corrections for Non-Uniform Flow

It is possible to calculate corrections for the orifice probe in the same way as for the equilibrium temperature probe (Ref. 14). Making the reasonable assumption that the corrections for a long-tube impact probe will be of the same order of magnitude as for the orifice probe, the results can be extended to the pressure-pair probe. The magnitude of these terms is given by the data of Fig. 15 and when checked against flow parameters, the results appear once more to be corrections of negligible size.

Reproduced with permission of the copyright owner. Further reproduction prohibited without permission.

3.3 Flat Plate Model

It was decided that the model to be used in these experiments should have low heat-conductivity, a uniform heat input per unit area, a sharp leading edge, a flat, smooth upper surface and sufficient instrumentation to determine unambiguously T_{wall}, p_{wall}, and local heat input.

The proper size of the plate to be used was not at all obvious. It was desired that the leading edge effect should merge into that predicted by established boundary-layer theory. From the standpoint of wing theory it was desirable to get some idea of trailing-edge effect. The plate should be wide enough to make the flow two-dimensional and as thin as possible, consistent with good rigidity and sufficient thickness to mount a pressure gauge. Finally it should be mounted securely, in the proper position and attitude, but in such a way that the mount would give a minimum interference with the flow.

Since previous work (Ref. 2 and 3) had suggested that the boundary layer becomes fully established about ten mean-free-paths downstream from the leading edge, it was felt that this was the absolute minimum length that could be used. Investigation of the free jet of the UTIAS subsonic nozzle indicated that it spread rather rapidly with a consequent slowing down and change in free-stream conditions. It seemed unlikely that one could consider the jet as being uniform for much more than three inches downstream of the nozzle. Preliminary investigation and general background information suggested that the flow should be investigated well ahead of the leading edge. It was thus impossible to get both a long plate and a meaningful trailing edge effect measurement at the same time without some compromise. It was eventually decided to use a chord of two inches (twenty mean-free-paths) with the leading edge set back one inch (ten mean-free-paths) from the nozzle exit. Final analysis of the data suggests that it might have been better to use a very long chord, neglecting any attempt to obtain a trailing edge effect and to use only the data from the first two inches of the chord. Even this conclusion could be disputed however, since the two-inch chord seems to have been just adequate to separate the trailing-edge effect from the leading-edge effect.

Preliminary data also indicated the necessity of a span of about six inches. In practice this proved quite adequate to give two-dimensional flow.

The final model was built up of three glass plates, each 2 inches by 2 inches by a trifle under 1/8 inch thick. These plates were set side by side on a holder to give a model with a six inch span and a two inch chord (Figs. 16 and 17). The leading edge of each plate was sharpened to approximately a 30° bevel by hand grinding.* To eliminate chipping the

* The grinding was done on the flat side of an ordinary grinding wheel immersed in a pan of water, and went quite rapidly. A final dry dressing was performed on ordinary fine carborundum paper mounted on a flat surface. It is felt that commercial lens-grinders would make a much better job,

Reproduced with permission of the copyright owner. Further reproduction prohibited without permission.

(footnote continued)
but, at the time, the method of construction and design of the plate was still being worked out. The hand grinding method was simple enough and quite adequate.

---

leading edge was ground down to about 0.020 inches at this angle and the remaining flat removed by grinding at a 45° angle. Occasional chipping still occurred, giving flats never greater than 0.005". It was felt that this edge could be considered ideally sharp since the mean-free-path was 0.10 inches.

3.3.1 Heaters

Since it was desired to supply a known quantity of heat to the surface of the plate it seemed best to use thin-film metallic coatings as a resistance element to heat the plate. Such films are used commerically and as heat gauges in shock-tube work. Some time was spent trying to adapt this technique to the flat plate model and eventually a rather effective method was developed. Unfortunately, failure to take into account the dangers of using too high a voltage at a pressure of 20 microns led to the construction of thin film heater elements whose resistance was high enough to be operated at 50 - 120 volts. During the initial runs a disastrous glow discharge occurred which severely damaged the model. As a result make-shift repairs had to be made. If the heater voltages had been kept to a few volts this sparking would not have occurred.

The films were made by firing on one of several kinds of precious-metal-bearing paints which are commercially available for the purpose, and which, when fired, leave a conductive metal surface securely bonded to the glass surface. *

In attempting to get a high resistance it was found that only one coat was necessary. Repeated application and firing would give a lower resistance and a better coating. The technique as finally developed was to wash the plate thoroughly in soap and water, rinse well with distilled water and finally with alcohol. A crude silk-screening method was used to apply the paint evenly. Material from an ordinary nylon stocking was streched uniformly in an embroidery hoop and set on top of the surface to be coated. Paint was dropped onto the nylon mesh and spread over the entire surface by a lucite squeegee sharpened to a "V" edge. The mesh of the cloth gave a uniform coating of paint whose thickness was controlled by the thread diameter. This coated plate was then fired according to manufacturer's instructions in a small muffle furnace (i.e. brought to 600°C in 1/2 hour and then let cool in the furnace).

---

* Hanovia Bright Gold No. 6853
Engelhard Industries Inc., Hanovia Liquid Gold Div.,
1 West Central Ave., East Newark, Harrison P.O., N.J.

Reproduced with permission of the copyright owner. Further reproduction prohibited without permission.

A grid pattern was next scribed on the coated surface with a carbide point to provide a long conductive path approximately 8" by $\frac{1}{4}$" (Fig. 17). This ensured a uniform heat input over the whole plate. A hole was drilled completely through the plate at each end of this resistance path, using a 2 mm diamond-chip-impregnated dentist's burr. Nickel wire power-leads were securely anchored with Sauer-eisen cement to the underside of the plate close to each hole. Connection was made between these wires and the ends of the heater grid by coating the inside of the hole, the cemented ends of the wires, and the upper surface of the grid surrounding the hole with a generous application of flexible silver circuit-paint.* When used in a vacuum this paint remained conductive at temperatures well above the melting point of soft-solder and appeared to suffer no deterioration. It is felt that the plastic binder evaporated off early in the run without charring, leaving a coating which was substantially pure silver. This technique of making power connections left a smooth upper surface on the plate that did not snag the equilibrium temperature probe.

3.3.2 Instrumentation

Using a diamond burr, several holes were drilled in the underside of the plate to accommodate the various gauges. These holes were spaced along the chord-wise center-line of the central plate 1/4", 13/32", 1", 1-1/2" and 1-3/4" back from the leading edge. The holes were stopped some 0.010 to 0.020 inches short of the upper surface. The second and fourth holes were enlarged somewhat to a rough cruciform shape (each arm about 2 mm long and 1.5 mm deep) to take the four arms of a small thermocouple pressure gauge.

At this point the plate was turned over and small (0.012") holes were drilled down from the upper surface to break through into the 2 mm holes previously drilled in the underside. Jeweller's pivot-drills were used for this purpose and, when sharp and operated at a very low speed, they worked very well, making a neat hole with no chipping at the edges.

Chromel-alumel thermocouples were made by lap-welding a pair of 0.005" wires and trimming off the free ends. These were cemented into the first, third, and fifth holes so that the weld protruded slightly above the upper surface of the plate. When the cement had hardened this projection was carefully ground off under a microscope to leave the weld exactly flush with the heater surface.

Two small thermocouple pressure-gauge elements (similar to those described in Appendix A) were cemented in the third and fourth holes. These elements consisted of chromel-alumel spirals spot-welded to nickel wires. The nickel wires were cemented in place with Sauer-

---

* Hanovia Flexible Silver Coating No. 16.

Reproduced with permission of the copyright owner. Further reproduction prohibited without permission.

eisen cement and the whole assembly covered with a flake of microscope-slide cover-glass, which was also cemented in place by Sauer-eisen (detail Fig. 17). The fourteen wires comprising the leads for these five gauges were carefully anchored to the underside of the plate with spots of Sauer-eisen and led off to the side.

The two side-plates were constructed in exactly the same way as the center plate, except that no holes were drilled for gauges. Instead, to monitor its temperature, a single thermocouple was cemented to the trailing edge of each plate, flush with the top surface.

The three plates were carefully aligned and mounted on an adjustable holder. Two 0.020" piano wires were mounted in tension between the spreader arms of the holder and the plates were cemented onto these wires with Sauer-eisen cement (Fig. 16). The final assembly was quite rigid and completely adjustable in six degrees of freedom.

After the leads had been carefully dressed to the spreader bars (twenty leads in all) the whole bottom surface of the assembly was coated with a layer of Silicone cement.* This effectively sealed any possible leaks in the pressure gauges, anchored, insulated the numerous leads and gave a smooth surface to the underside of the plate. In addition it filled the cracks between the plates to form an unbroken upper surface.

3.3.3 Performance

In operation the assembly worked quite well until an attempt was made to go to a high plate temperature. A disastrous sparking occurred which cut the power leads to the side plates and broke the forward pressure-gauge. It was impossible to completely repair the damage, but sufficient repairs were made to allow it to operate without power to the side-plate heaters. The chief change necessary was to lower the resistance of the center heater. Since the plate could no longer be fired, it was necessary to use a coating of the flexible silver paint rather than the gold.

The heater was run off the A.C. mains through a Variac and a filament transformer. Power was measured by an AC ammeter and voltmeter. In practice the plates proved to be subject to temperature drifts because of changing line voltage, so that frequent readjustment of the Variac was necessary.

4. PROCEDURE

4.1 Setting up Model and Apparatus

All experiments described here were conducted in the

* Dow-Corning A-4000 Silicone Cement

Reproduced with permission of the copyright owner. Further reproduction prohibited without permission.

U. T. I. A. S. Low Density Wind Tunnel using the subsonic nozzle (Ref. 15). The flat plate model was set up in its holder and carefully adjusted so that the leading edge of the plate was exactly 1.00 inches from the nozzle exit plane and parallel to it, and symmetrically positioned about the nozzle centre line. The plane of the plate was made horizontal, intersecting the nozzle centreline, with the mid-line of the model, (on which the various pressure orifices and thermocouples were located) exactly along it. The arms of the holder itself lay outside the jet boundaries to minimize interference.

The equilibrium-temperature probe and the pressure-pair-probe was mounted on the traversing mechanism of the tunnel and positioned above the model as shown in plate 2. (The flat plate shown is an earlier model, without instruments or side plates.) The sensing wire of the equilibrium-temperature probe was very carefully adjusted to be parallel with the leading edge of the plate and the position of the temperature-sensing point located with respect to the nozzle axis and leading edge.

The pressure-pair probe was mounted with the impact probe tip 0.293 inches back of the equilibrium-temperature wire and some four inches away from its hot junction in the transverse direction. The plane defined by the two probe tips intersected the line of the equilibrium-temperature probe and was parallel to the flat plate surface. The probe tips were carefully aligned parallel to the nozzle axis.

With this arrangement either probe could explore the region above the plate and ahead of it as far as the nozzle exit. Since the span of the equilibrium temperature probe was greater than the nozzle diameter, no readings could be taken upstream of the nozzle exit plane. The pressure-pair probe was displaced far enough sideways from the equilibrium temperature probe junction (40 mean-free-paths) so that there was no likelihood of mutual interference. The plane of the flat plate was measured to be parallel to the horizontal plane of the traversing mechanism to within 0.005 inches in 2 inches of plate length. The position of the probe tips relative to the thermojunction and thus to the rest of the apparatus was determined as accurately as possible, to about 0.010 inches. Relative positions were determined by revolution counters on the traversing mechanism lead-screws (Ref. 15). The least-count of these was 0.001 inches and the absolute accuracy for the worst case (vertical traverse) was no worse than 0.004 inches.

In addition to the two pressure gauges and three thermocouples on the instrumented section of the model, there were high-sensitivity thermal-conductivity gauges mounted in the walls of the test section and stagnation chamber. A high precision McLeod gauge* was also mounted in the test section while a McLeod gauge with a range of 2 mm was connected to the stagnation chamber.** A separate thermocouple

* 0 - 50μ - 400 cc volume McLeod Gauge, Edwards High Vacuum Limited, Crawley, Sussex, England.

** UTIAS No. 1 -- 0-2 mm: 100$\frac{cc}{}$ cutoff Vol. (Ref. 4)

Reproduced with permission of the copyright owner. Further reproduction prohibited without permission.

served to measure stagnation-chamber temperature independently of the equilibrium-temperature cold-junction arrangement. Commercial vacuum gauges were used in the pump manifold to monitor pump performance.

4.2 Preliminary Steps

The tunnel and instruments were held at a low pressure (10^{-4}mm) with pumps throttled back by their isolation valves until such time as the gauge-heads all indicated no significant outgassing. A slight flow of air was arranged to avoid gauge contamination by pump vapours and to ensure that the gas in the tunnel was truly air.

When a satisfactory steady-state had been achieved, the gauges were all calibrated against the precision McLeod, many determinations being taken over the whole range of interest in the experiment. The output voltages of the thermal-conductivity gauges were squared and plotted against p. A very good straight line was obtained, as theory predicts, and calibration data were obtained from the slope and intercept. Care was taken to ensure that all measurements were taken in still air to avoid spurious pressure readings due to dynamic head. The flow valve was then opened and the flow set to the desired value.

4.2.1 Speed Ratio

Of the various methods tried for determing molecular speed ratio it was found that the ratio of stagnation to test section pressures was by far the least reliable for at least two reasons.

1. Mach number is a very sensitive function of this pressure ratio at Mach number 0.5 so that slight errors in pressure ratio gave much larger errors in estimated Mach numbers. *

2. It soon became apparent that systematic errors in these pressure readings also occurred. There appeared to be a small but significant drop in stagnation-chamber pressure itself, from one end to the other. Since the pressure tap was placed about its midpoint these pressures probably read too high. Similarly, the test-section pressure readings appeared to be too low. Apparently the jet acted as an ejector in the test-section so that the pressure at the test-section walls was lower than in the jet itself. The combined result of these errors was to give an estimate of S that was much higher than that given by other methods.

---

* It was calculated that under ideal conditions the probable random error in pressure ratio as determined by two McLeod gauge readings (UTIAS No. 1 and Edwards 0-50μ) would be about 5%. This would represent an error of about 18% in Mach number!

Reproduced with permission of the copyright owner. Further reproduction prohibited without permission.

Determinations made by the equilibrium-temperature probe method and by the pressure-pair probe method agreed quite well in the free stream and in the absence of a better method of calibration this agreement was taken as a mutual calibration of the two probes. Because of its greater ease of manipulation, the equilibrium temperature probe was used to set free-stream flow conditions in all adiabatic flows. When a heated plate was used, the pressure-pair probe was utilized to get S.

4.2.2 Tunnel Performance

A preliminary investigation of the undisturbed flow in the jet revealed that the tunnel was operating in two distinct stable modes which differed from each other slightly in speed-ratio. The pressure would shift occasionally and randomly by about 1/2% between the two relatively stable values as an attempt was made to regulate the molecular speed-ratio. Corresponding random shifts occurred in speed ratio as the pressure changed. Since these changes were less than the expected experimental accuracy this was not a matter of great concern. The reasons for this type of performance was never completely determined, although a similar, though much larger fluctuation was found to be due to malfunctioning booster pumps.

4.3 Setting Flat Plate Conditions

Considerable drift was found in the setting of the plate temperature with most of it being due to fluctuating line voltage. Heater current and voltage as well as temperature (at all three locations) were measured at frequent time intervals. Voltage was adjusted by hand in an attempt to keep the temperature constant. Because the rate of heat loss was low, temperatures changed rather slowly, so that the temperature could be held within one or two degrees for the most part.

Total power to the plate was obtained by measuring current and voltage applied to the external leads of the plate. No attempt was made to determine power lost in the leads. It was felt that these particular measurements would not be particularly accurate or useful but they were recorded as a matter of routine.

Because of the failure of the side-plate heaters at the start of the experiment only the center plate could be heated so there were rather large spanwise gradients in temperature above the plate. Transverse temperature and speed ratio sweeps were made for all runs so that these gradients could be checked (Figs. 18, 19, and 20). The data show that at the higher plate temperatures, the temperature dropped off rather rapidly a short distance away from the center line. Viewed as a percentage of total temperature these changes are still rather small however, and in the final result do not particularly alter the picture presented by the adiabatic plate data. The existence of these transverse temperature gradients is, in fact, one of the less satisfactory aspects of the experimental setup, but apparently, as far as the final conclusions are concerned, their effects were not too large (cf. Sec. 6.3).

Reproduced with permission of the copyright owner. Further reproduction prohibited without permission.

In order to measure the true static pressure in the jet the flat-plate pressure gauge was calibrated at 20 microns and at various plate temperatures with no flow over the plate in order to determine zero shifts. This information together with the usual calibration curve enabled a measurement to be made of the jet static pressure during all runs. It was this measurement which showed that the jet static pressure was higher than the rest of the test-section when the flow was on . In continuum boundary layer theory it is assumed that no change in static pressure occurs across the boundary layer. There is no particularly valid argument that indicates the same result should hold in relatively thick boundary layers produced in a low density wind tunnel. In fact however, careful preliminary measurements failed to show any measurable change in static pressure near the plate at room temperature although it had been anticipated that boundary layer displacement effects might have produced a detectable effect.

4.4 Experimental Runs

After thorough outgassing and calibration of pressure gauges the tunnel conditions were set as closely as tunnel characteristics would allow to give a Mach 0.5 flow (S = 0.425) with a jet static pressure of 20 microns. For the first run the plate was unheated, so that a run, under what were presumed to be adiabatic conditions, could be made. Traverses were made first with the equilibrium-temperature probe and then with the pressure-pair probe at sufficient points to give a reasonable measurement-grid pattern. A fairly detailed survey was made with the equilibrium-temperature probe to get an overall picture of the flow pattern.

Because of the large number of measurements needed to get a complete mapping, it was impossible to complete the survey in a single day. This raised the problem of drift in tunnel conditions during the run. It was felt that with care the long-term drifts could be kept to a size comparable with short-term drifts, so that it was permissible to extend the runs over several days. On the other hand, tunnel outgassing times and calibration times were so long that it was felt that all three proposed runs should be made consecutively without letting the tunnel up to atmosphere between runs. It was apparent that the runs could not extend much more than a week without considerable risk of a tunnel breakdown which would end the run. As a compromise between the amount of data collected and the chance of breakdown, measurements were made at five longitudinal stations; at the nozzle exit, 1/2 inch downstream, at the leading edge of the plate, at the mid-point of the plate and at the trailing edge. Vertical traverses were made at these locations to give points about 0.2 inches apart, extending from the plate to the edge of the jet. Plate temperatures at three positions on the plate surface were recorded at suitable time intervals, as were the plate pressure gauge reading, the stagnation temperature at two points in the stagnation chamber, test section and stagnation chamber pressure and room temperature.

Reproduced with permission of the copyright owner. Further reproduction prohibited without permission.

When the equilibrium temperature probe data had been collected a few key measurements were repeated using the pressure-pair probe. Because of the longer time taken to make each measurement, it was decided to compromise on fewer points.

When this run was completed, power was applied to the heater and the plate temperature raised to a convenient temperature close to 100°C. (In fact a somewhat lower temperature was chosen to avoid too-frequent range-switching on the potentiometer used to measure temperatures.)

Flow conditions were checked, reset and traverses and measurements similar to those already described were repeated. In this case power, voltage and current to the plate were also recorded. Because both probe readings were needed at each point to determine the flow properties in non-adiabatic flows, the number of pressure-pair probe readings was increased to equal the equilibrium temperature probe readings.

When this so-called 100°C run was completed the plate temperature was raised to approximately 200°C and the measurements repeated at the new temperature.

At the end of each day's run, the flow was shut down, except for a very small bleed, the pumps were throttled to reduce back-streaming of oil vapour and the plate temperature was reduced somewhat to what was felt to be a safe level. Tunnel pressure was held to about 1×10^{-4} mm overnight. At the start of the day's run the plate temperature was raised to the working level and the flow started. By the time flow conditions had been re-established and necessary spot-check calibrations completed (usually two hours) the tunnel would be in complete equilibrium once more.

For purposes of comparison and to get an estimate of radiative heat transfer and still-air heat transfer, equilibrium temperature traverses were taken for nominal 100°C and 200°C plates in still air at pressures of 20 microns and of 2×10^{-4} mm.

Next, because it was noticed that the pressure-pair probe readings were showing a definite amount of zero shift due to changes in gauge-head temperature, further calibrations were performed at 20 microns in still air. With the plate heated as in previous runs the pressure-pair probe was shifted to various positions to change heat load and gauge-head temperature. Since both gauges now were experiencing the same pressure (20 microns) it was possible to determine temperature effects on the gauge readings and to correct previous readings for changes in gauge-head temperature as indicated in Sec. 3.2.2.

Finally the plate was cooled down, the tunnel let up to atmosphere and the apparatus examined. Some evidence was observed of

Reproduced with permission of the copyright owner. Further reproduction prohibited without permission.

the formation of local hot-spots at the trailing edge, but these spots did not seem too severe. This was confirmed by the relatively slight rise in plate temperature at the most rearward thermocouple, which indicated that the temperature in the hot-spots could not have been excessive. Fortunately none of these spots occurred near the center line of the plate where measurements were taken.

5. RESULTS

5.1 Fixed Point Data

Because heater power was being continually adjusted to maintain plate temperature constant, the fixed point data, plate temperature, power, etc.were taken at irregular intervals. These data were averaged over the whole run and are presented in Table II.

5.2 Traverses

As previously mentioned, the bulk of the data were obtained as vertical traverses at fixed longitudinal stations along the nozzle center line. Some transverse traverses were made and these data as given in Figs. 18, 19 and 20 indicate the degree to which two-dimensional flow was established in the three runs.

Figure 21 gives vertical traverses at Mach 0.5 obtained by the equilibrium temperature probe at 20 microns for the adiabatic plate. These data have been reduced by the method described in Sec. 3.2.2 to give S.

Figure 22 gives equilibrium temperature probe vertical traverses for the 100°C plate for Mach 0.5 flow at 20 microns.

Figure 23 repeats these data for the 200°C plate.

In Fig. 24, 25 and 26 are presented the similar pressure-pair probe data. The longitudinal stations are not always exactly the same as for the previous graphs since this probe was 0.293 inches back of the equilibrium-temperature probe. The data have been corrected for temperature effects, as explained in Sec. 3.2.2 and reduced to give S.

Tables of data used to obtain these curves are presented in Tables IV, V, VI, VII, VIII, and IX.

The vertical traverses of Figs.25 and 26 give the experimental data for S, but in an inconvenient form. These results were therefore crossplotted in Figs. 27 and 28 to give S vs longitudinal position at various heights above the plate. Using these two sets of curves the data were then replotted over again to give lines of constant S in the flow field above the plate, in the plane of symmetry (i.e. above the center line of the plate). The process was tedious and time consuming, but because all

Reproduced with permission of the copyright owner. Further reproduction prohibited without permission.

three plots had to agree and because one could safely assume relatively uniform variation with position, it was possible to obtain curves which were relatively accurate and free from error.

These "contour maps"of the flow-field contain all the information available for the whole field, displayed in a form that is relatively easy to digest. (Figs. 29, 30 and 31). In the case of the adiabatic plate (Fig. 29), not enough pressure-pair probe points were obtained to completely map the field, but the field close to the wall is given. For purposes of comparison, the more extensive "map" as obtained from the equilibrium temperature probe data is given in Fig. 32. As will be shown in Sec. 6.3.1, this figure should be in error near the wall.

Using the data for equilibrium temperature and speed ratio at each point it was possible to reduce the data to give T and T_o as well, as indicated in Sec. 3.1.3. From the data, values were calculated for T_o and T at various longitudinal stations. By cross-plotting, "contour maps" for T_o and T were obtained for the flow field (Figs. 33, 34, 35 and 36). Because of the lack of enough points, temperature data for the room temperature plate are presented in a slightly different form in Fig. 37.

5.3 Other Data

As explained in Sec. 3.1.4, plots of T_{wire} vs h for the no-flow traverses (Figs. 4, 5, 6, and 7) were used to infer the magnitude of radiative heat loss correction for the equilibrium temperature probe (since S = 0, $T_{wire} = T_o = T$ for these data).

Using the average readings of the thermocouples embedded in the flat plate model, one can plot plate wall temperature vs position in the three flow cases, (Figs. 38, 39 and 40). The thermocouple positions were 1/4", 1", 1-3/4" downstream from the leading edges. The dotted line in Fig. 38 represents a reasonable extrapolation to the leading edge of the plate.

6. DISCUSSION

The data as presented in maps of constant S, T and T_o specify the parameters of the flow about the leading edge of a flat plate. Though obtained at low densities they can be taken to represent what actually would occur very near the leading edge of an ideally flat plate at atmospheric pressures. A casual glance reveals that both slip-flow and temperature-jump occur as expected.

6.1 Initial Observations

1. An interesting result is that the boundary layer appears to start about ten mean-free-paths ahead of the leading edge. This is a constant feature in all the maps for both speed-ratio and temperature

Reproduced with permission of the copyright owner. Further reproduction prohibited without permission.

2. Examination of the temperature maps indicates that the trailing edge effect seems to extend almost to the mid-point of the plate, since there seems no other way to explain the observeddecreases in temperature that begin to appear about that point.

3. The boundary-layer of the nozzle is nicely delineated in the S maps. It is quite thick and merges rapidly with the flat-plate boundary layer.

4. These same maps also show the spreading of the jet as it travels downstream.

5. The spreading of the jet and the merging of the boundary layer indicate that it will be difficult to obtain absolute valuesof slip, heat transfer and other such engineering quantities with any great precision and suggest that efforts might better be spent checking general theoretical questions to which these data relate.

6. **Figures 39 and 40 are of real engineering interest. Since heat input per unit area is essentially constant over the whole plate, the fact that temperature rises linearly along the plate indicates that the inverse of the heat transfer coefficient (i.e., the thermal boundary layer) increases linearly with distance back from the leading edge. This contrasts with continuum theory where the dependence is on the square root of the distance.**

7. The temperature rise at the leading edge in Fig. 38 is the sort of rise one would expect in the free-molecule limit, where the equilibrium temperature is greater than T_o.

8. A further observation is that the values for S and T at the leading edge are higher than one would expect from free-molecule theory, assuming $\alpha = 1$. For that case S should be about one-half of the incoming stream (i.e. one mean free path away) and ΔT should be one-half of the difference between wall and incoming temperature. This indicates that α was much less than the generally accepted values for normal engineering surfaces (Ref. 11).

9. In order to compare the many theories that have been developed for flow near the leading edge of a flat plate, various theoretical solutions (Refs. 21, 22, 23, 24 and 25) have been compared with actual results (Figs. 41 and 42). These curves are of considerable practical interest.

6.2 Estimate of Errors

Since most of the methods used to collect these data are new and untried, and since as will be seen, there is some disagreement with generally accepted theory, it is necessary to examine the range of

Reproduced with permission of the copyright owner. Further reproduction prohibited without permission.

validity of these observations with care. It should be stated here that the disagreements observed are disagreements in functional dependence and are not simply a question of magnitude. It is difficult to imagine any reasonable source of error so large that these discrepancies can be explained away.

6.2.1 Molecular Speed Ratio

As pointed out in Section 4.2.1, there are several methods of measuring molecular speed ratio, of which the pressure-pair probe used in this work is the most general. If the pressure-heads were to be accurately temperature-compensated, (a relatively simple procedure,) the method would be potentially very accurate. Even using the rather crude method for temperature correction applied in these experiments the results agreed with the equilibrium temperature probe data in free-stream (i.e. at the nozzle exit on the center line) to within 2%. Individual error in pressure measurement in a properly operated gauge-head seemed to be less than 1/2% so that the error in the pressure-ratio could probably be held to no more than 1% in a temperature-regulated gauge, and possibly to much less. Except at the lower values of S this would represent an error in S of 1% or less.

It would seem that the absolute error in determining S is less than 5% for S greater than 0.25. The relative error between two such readings is probably about 2%. When the absolute values of S are used in determining flow temperatures this represents an error of at most $0.5^{o}C$ in these experiments.

It will be shown in a later section that the equilibrium temperature gauge is extremely sensitive to very small changes in total temperature. Except in the free-stream or where one is completely satisfied that the flow is adiabatic this gauge cannot be used to determine S. If these conditions are fulfilled however, the gauge is an extremely precise instrument. In practice, tunnel stability itself limited the reproducibility of this gauge. With the circuit used in these experiments, the limitations on its accuracy are those imposed by such uncertainties in the theory as the value of the accommodation coefficient and the size of the radiation correction.

6.2.2 Uniformity of Jet

The greatest unavoidable limitation on accuracy seemed to be in the jet itself. The observed bi-stable operation of the jet may be due to malfunction of the pumps and therefore be susceptible to improvement, but the non-uniformities within the jet seem to be inherent in any low density wind tunnel and are probably unavoidable. The thick boundary layer in the nozzle can be avoided only at great expense. The ejector action of the jet has been very clearly demonstrated and seems unavoidable. It is

Reproduced with permission of the copyright owner. Further reproduction prohibited without permission.

presumed that the spreading and slowing of the jet is the result of this dilution of the high-speed flow with entrained air, so that this deficiency seems inherent too.

Because of the profound effect of the insertion of the flat plate on the whole jet structure, it was impossible to assess the contributions of these defects in jet uniformity to any particular measurement, but near the trailing edge the non-uniformity was probably already sizeable. For the free jet, at any rate, the speed-ratio, as measured at the centerline, had dropped by 12% at this position (3 inches downstream). Preliminary experiments showed that insertion of a flat plate effected the flow so much that it could not be considered simply as a small perturbation. For instance, it was not possible to decide how much of the change was due to boundary layer effects on the plate and how much was due to spreading of the jet.

6.2.3 Heater Surfaces

Construction of the heaters of flexible silver conducting paint, (Sec. 3.3.2), introduced an unexpected variable into the experiment. It has been the consensus of opinion in the literature that, for all engineering surfaces, α is always close to 1 (Ref. 11). For this reason it was felt originally that the heater material was quite unimportant. Since it turned out that α was much less than 1, this assumption has proved unjustified. Because of the presence of a binder which is volatile at high temperatures in a vacuum, it is not even certain that the nature of the surface was constant from run to run. The net result is that the determinations of α contain an extra imponderable that would not have existed if a gold film resistance element could have been used. On the other hand, there is no concrete evidence that the binder caused any trouble.

6.2.4 Overall Error

Examination of the curves for gas temperature vs. height at various longitudinal stations gives a good picture of the overall reliability of the data (Figures 43, 44, 45 and 46). For instance, it will be observed that the total temperature across the nozzle exit is essentially constant, to a few tenths of a degree. Since in calculating this curve the speed-ratio has run the complete gamut of values from free-stream to practically zero, it is apparent that:

1. The nozzle flow is essentially adiabatic in that total temperature does not vary appreciably across the jet. Particularly in the subsonic nozzle with its peculiar reaction to models inserted too near the exit plane, there has been serious questioning of this fact.

2. The method of temperature correction used for the pressure-pair probe is adequate.

Reproduced with permission of the copyright owner. Further reproduction prohibited without permission.

3. Even in the 200°C plate runs, there is a region of essentially undisturbed flow at the nozzle exit.

4. The random error in temperature measurement by this method is only a few tenths of a degree. Systematic error, as exemplified by the slight change in measured T_o with h (presumably due to radiation heat flux) is of about the same magnitude.

The static temperature curves are as theory would suggest. Because the speed ratio corrections are larger in this case than for total temperature, the random errors might be expected to be larger. The flat portion of these curves near the nozzle exit plane centerline indicates the extent of the isentropic core.

In each curve these data were assembled over at least two days running time. The good agreement observed among the data taken on different days indicated that tunnel drift was small. Short term drifts or shifts have been averaged out in getting speed-ratio and T_{wire} data, but the small random error shown here indicates that the averaging method is fairly good.

It should be observed that a Mach 0.5 the difference between T_{wire} and T is only about 8%, in all, say about 20°C. An error of 0.4°C would represent about 1% error in S. At lower S a proportionately larger error in S can be tolerated for the same error in T. It might be reasonable to claim a random error of less than $\pm$ 0.005 or $\pm$ 2% in speed ratio (which ever is larger). To get the same precision in temperature measurement at higher Mach numbers, one would need more accurate values of S because of the proportionately larger difference between T_{wire} and T.

6.3 Discussion of Results

6.3 1 Room Temperature Plate: Discrepancy between Probe Readings

For the adiabatic plate it is possible to obtain the value of S by means of either probe. This provides a method of checking the accuracy of one probe against the other. At present there seems to be no way of checking the absolute accuracy of either gauge, and one must assume that mutual agreement of the two gauges is equivalent to both gauges reading correctly. Since the gauges are quite different devices, this assumption does not seem too unreasonable.

In Fig. 47 the data obtained from the adiabatic run is given as S vs. longitudinal distance, at different heights above the plate, for both probes. At free-stream conditions (near the nozzle exit) the two measurements agree quite well, but near the wall the values differ by a factor of 2! It might be possible to explain this discrepancy by one of the following effects:

Reproduced with permission of the copyright owner. Further reproduction prohibited without permission.

a. Contributions due to non-uniform flows.

b. Peculiarities of the two-stream distribution function.

c. Neglect of the radiation term in the equilibrium-temperature probe.

d. Incorrect temperature correction in the pressure-pair probe.

e. Violation of the adiabatic assumption, due to heat transfer from the wall, with a consequent change to T_o.

It has been shown that contribution from non-uniform flow corrections is negligible and that the radiation term is negligible. All indications are that the temperature correction is reasonably good.* As the data of Table I indicate, the two-stream effect is negligible even for a wall at 100°C at Mach 0.5. For the room temperature wall at lower Mach numbers the effect would be even smaller, so that this explanation is not possible.

The only remaining explanation, that the flow is non-adiabatic is easily able to explain the discrepancy. It is readily calculated that one need only increase the total temperature of the gas by 1.2°C at the wall to explain the discrepancy between equilibrium temperature probe and pressure-pair probe data. An examination of the data reveals that the average plate temperature was 1.4°C above the measured stagnation temperature of the incoming flow. When one makes allowance for the fact that the gas would not have quite attained wall temperature at the trailing edge, it seems reasonable to assume that convective heat transfer from the plate was changing the total temperature of the flow sufficiently to explain the whole discrepancy. This leads to the following observations:

1. This indicates how extremely sensitive the equilibrium temperature is to small changes in total temperature in the boundary layer.

2. It appears that magnitudes of the errors estimated for the equilibrium temperature probe are substantially correct and that the error in temperature measurement is small.

3. The pressure-pair probe and equilibrium temperature probe, on this hypothesis appear to check very well throughout the flow, so that one can place considerable confidence in their readings.

---

* At the low pressure ratios that obtain at these low Mach numbers very small errors in correction are quite noticeable. However, no obvious discrepancies in pressure ratio occurred even in the high temperature runs where the temperature corrections were the highest. In the adiabatic run the temperature corrections themselves are small so that errors should be even less important. For these reasons this explanation was abandoned.

Reproduced with permission of the copyright owner. Further reproduction prohibited without permission.

4. The extra heat which appeared on the plate seems to have been developed by the pressure-gauge embedded in the plate. Power consumption of this gauge is of the order of a few milliwatts. A power input of roughly 10 watts raises the plate temperature about 150°C, which turns out to be about 70 milliwatts per degree. Making allowance for the expected non-linearity of transfer with temperature difference due to the importance of radiative heat transfer at higher temperatures this seems to be about the right order-of-magnitude.

5. Since we have measured a difference between plate temperature and stagnation temperature which must result in the performance we observed, the data seems to indicate that the temperature corrections made to the pressure gauge readings were right and that the two-stream effect was negligible. The agreement is complete and well-rounded.

6. This discussion emphasizes the fallacy of using an equilibrium temperature probe near a wall where even slight heat flow can occur and probably goes a long way toward accounting for some of the strange results obtained by Laurmann (Ref. 2).

7. The final problem that remains is one of checking the absolute accuracy of one or the other of the gauges by an independent method. This has been done for the single long-tube probe by Muntz (Ref. 33). He obtained good agreement between experiment and theory, so that it would appear that considerable confidence can be placed in the measurement of S by the pressure-pair probe.

6.3.2 Flow Ahead of the Leading Edge

One feature common to all these flows is a pronounced influence on the flow field which starts well ahead of the leading edge. This type of behaviour might be attributed to the following mechanism:

1. Stagnation flow as around a blunt body.

2. A type of wedge flow due to the displacement thickness of the boundary layer.

3 A true boundary-layer flow with dissipation.

As far as the first two suggestions are concerned, these both represent potential-flow solutions and must be accompanied by very significant static pressure changes. In the room-temperature runs the temperature corrections that were made were quite small. The uncorrected data showed no indication of a significant pressure rise or fall along the plate. After pressure corrections had been made (on the assumption that static pressure did not change) the agreement between the two different probes measuring S was exactly as it should be, (making allowance for change in total temperature). Thus all the evidence points to the static pressure being

Reproduced with permission of the copyright owner. Further reproduction prohibited without permission.

essentially constant, and to the absence of potential flow effects. For a wedge-type flow, or for a stagnation-point type flow, speed ratio should first decrease ahead of the leading edge (with a corresponding increase in static pressure) and then increase again over the plate. In fact, no evidence for either type of performance was found.

It would seem likely that boundary layer displacement thickness would cause a change in static pressure, due to a wedge-type flow. Although there is rapid thickening of the boundary layer at the leading edge, there does not seem to be a commensurate effect on the static pressure. Although a pressure effect had been anticipated, none was observed. No explanation for this result is offered.

The only obvious objection to the boundary-layer interpretation is that it begins far ahead of the leading edge, whereas it is customary to think of the boundary-layer as starting at the leading edge. In fact, however, kinetic theory would lead one to predict this behaviour. If a molecule strikes the leading edge there is a certain finite probability that it will be reflected back in an upstream direction. But Maxwell's work on "persistence of molecular velocity" following collision predicts that molecules reflecting in that direction will continue for several mean-free paths. Since these molecules will have an average velocity different from the free stream values, there will be a net transfer of momentum several mean-free paths upstream. This is what is observed, in that the average velocity of the molecules begins to decrease well ahead of the leading edge.

This is a random-walk phenomenon and it should therefore exhibit a typical diffusion pattern, with an error-function type distribution of velocity differences. To check this, the relevant data were plotted in such a fashion that a true Gaussian distribution would plot as a straight line. *

---

* For a Gaussian Error Curve

$$\phi = \phi_o e^{-\frac{t^2}{2}} \quad \text{where } \phi_o = .3989 \text{ and}$$

t is the running variable.

$$\text{Set } \frac{Q - Q_o}{Q_1 - Q_o} = t$$

where $Q_1 - Q_o$ is the maximum variation of the variable to be tested and $Q - Q_o$ is its variation at any given point x. If the variable has a Gaussian response, plotting ϕ / ϕ_o vs. X should give a straight line. (ϕ / ϕ_o is most easily determined for various values of t from a table of ordinates of the normal error curve.)

Reproduced with permission of the copyright owner. Further reproduction prohibited without permission.

This has been done in Figs. 48 and 49 for both S and T. Up to the leading edge the lines are reasonably straight. This has been taken to indicate that the flow ahead of the leading edge is produced by dissipative mechanisms and is a true boundary-layer flow.

The possibility that the boundary layer would start well ahead of the plates does not seem to have been seriously considered before and requires some consideration. At first glance, it appears to conflict with the findings of Nagamatsu (Ref. 27) who finds evidence of slip-flow in his hypersonic shock-tunnel data. In this case he is able to get a schlieren photograph showing a shock wave starting several mean-free paths down-stream of the leading edge. In fact, there need not be any disagreement between these two findings, since, in his data no information is available for the region upstream of the shock. Shock formation may well occur some distance downstream of the point of formation of the boundary layer. Since the mean-free path does not change very much going through a shock, it may be expected that the leading-edge flow for supersonic and hypersonic flight is qualitatively similar to that determined here for Mach 0.5.

This upstream influence of the leading edge explains some of the puzzling behaviour that Harris observed in his flat plate experiments (Ref. 3). He found that when he inserted a plate in the flow of a subsonic jet there was a radical change in the whole flow pattern of the nozzle, which made interpretation most difficult. Since he was operating with a mean-free-path of about 1 inch, the upstream influence must have extended through the nozzle, well into the stagnation chamber, with a consequent radical effect on mass flow, Mach number and so on. The addition of the plate was equivalent to changing the whole shape of the nozzle

6.3.3 Maxwell Slip Conditions

The experimental data can be used to check the usual Maxwell slip conditions by determining slip velocity and velocity gradients at the wall and checking them against the formula

$$U_s = \frac{2-\sigma}{\sigma}\lambda\left(\frac{\partial U}{\partial y}\right)_0 + \frac{0.6\lambda}{T}\left(\frac{\partial T}{\partial x}\right)_0$$

Within the expected accuracy of these results it is possible to neglect the relatively small temperature term in this equation. In the same way, the variation of c_m along the plate may be ignored, so that the equation may be written:

$$S_s = \frac{2-\sigma}{\sigma}\lambda\left(\frac{\partial S}{\partial y}\right)_0 \qquad (3.45)$$

The values for S_s on the centerline of the plate (nozzle axis) are shown in Fig. 50 for all three plate temperatures.

Reproduced with permission of the copyright owner. Further reproduction prohibited without permission.

It was argued in Section 2.3 that possibly the value $\left(\frac{\partial S}{\partial n}\right)_0$ would be more representative of slip conditions than $(\partial S/\partial y)_0$. Consequently, the values of $(\partial S/\partial n)_0$ as a function of distance along the plate are plotted in Fig. 51 for the three experimental plate temperatures. The values of $(\partial S/\partial n)_0$ vs. S_s' are given in Fig. 52. In both figures it is apparent that the 200°C plate data are rather different from the other cases. Since the 200°C data were the least satisfactory from the experimental standpoint on several counts (as previously discussed) it is not clear that any significance can be attached to this difference in the shape of 200°C curves. Therefore, in subsequent discussions most weight will be accorded to the room temperature and 100°C plate data.

It is quite apparent that the data ahead of the leading edge cannot be reconciled with the Maxwell slip theory by any means, and that a rather abrupt change in mechanism seems to occur near the leading edge as indicated by the cusps.* This fact is not particularly surprising when it is remembered that the expressions were developed for the case of an infinite plane, but it does emphasize that the slip conditions cannot safely be applied where the leading-edge effects are a significant fraction of the total response of the plate. On the other hand, the Maxwell conditions have been used extensively for flows further from the leading edge, apparently with good results, so that their validity appears to be established for regions a considerably distance from the leading edge. Certainly Fig. 52 shows such a region back of the maximum. This fact can be demonstrated more clearly by tabulating the speed-ratio data from Fig. 24 for the room temperature plate and those from Fig. 27 for the 100°C plate. The value of the gradient $(\partial S/\partial y)_0$ is approximated by dividing the difference in the values of S at the wall and at a distance 0.2" above the plate by the difference in height. If Maxwell's slip conditions apply, then the ratio

$$A \equiv \frac{S_s}{\left(\frac{dS}{dy}\right)_0}$$

should be constant.

---

* Note should be made here of the presence of the apparent cusps which appear ahead of the plate in the various "maps" of constants S and T. It is obvious from theory that these lines must cross the x-axis at 90 degrees. However, the measurements showed them approaching the axis at an acute angle. The resolution of the measurements was not sufficient to indicate the point at which the break occurred, although it was apparently rather close to the axis. The lines were therefore drawn to agree with the experimental points, with the mental reservation that they were not quite right on the axis. In fact, this does not affect the results to any significant degree since $(\partial S/\partial n)_0$ rather than $(\partial S/\partial y)_0$ was used in the subsequent treatment. The cusps of Figs. 50, 51, etc. are physically acceptable, on the other hand, since it is the derivative of a physical quantity which is being plotted, with the discontinuity representing an abrupt change in mechanism.

Reproduced with permission of the copyright owner. Further reproduction prohibited without permission.

In the room temperature case the mean free path is $\lambda = 0.10''$, since the static pressure is 20 micron Hg. For the case of 100°C plate, the mean free path was calculated on the basis of an average static for temperature of 334°K as obtained from Fig. 34. This gave a value of $\lambda = 0.11''$.

ROOM TEMPERATURE PLATE

Distance from L.E. (inches)	S_s	S (y = 0.2)	$\frac{\Delta S}{\Delta y}$	$\frac{S}{\lambda \left(\frac{\Delta s}{\Delta y}\right)_0}$
0.0	.25	.376	.63	3.96
0.2	.178	.346	.85	2.09
0.4	.147	.305	.82	1.72
0.6	.117	.265	.74	1.58
0.8	.101	.218	.58	1.74
1.0	.090	.291	.50	1.79
1.2	.082	.170	.44	1.86
1.4	.075	.157	.41	1.83
1.6	.069	.144	.37	1.86
1.8	.065	.135	.35	1.86

100°C PLATE

0.0	.250	.370	.60	3.7
0.2	.175	.330	.77	1.92
0.4	.130	.285	.76	1.53
0.6	.100	.265	.82	1.08
0.8	.078	.196	.59	1.19
1.0	.065	.165	.50	1.16
1.2	.055	.140	.42	1.16
1.4	.050	.122	.36	1.24
1.6	.045	.110	.32	1.20
1.8	.040	.105	.32	1.12

These results show that except very near the leading edge, the quantity A is reasonably constant. While this is gratifying, it must not be overlooked that there is evidence of a trailing edge effect which appears to set in about 1 inch downstream of the leading edge (e.g., Figs. 55 and 56). Just how this would effect these data is not clear, but it could be obscuring the point at which the Maxwell conditions begin to apply. Neglecting this difficulty, the data seems to indicate that the slip speed-ratio is proportional to the gradient of the speed-ratio for regions more than five mean-free-paths downstream of the leading edge.

Reproduced with permission of the copyright owner. Further reproduction prohibited without permission.

The significance of these findings is that they cast doubt on the basic assumptions of a fairly large body of theoretical solutions for flow near the leading edge of various bodies (Ref. 21, 22, 23, 24 and 25). It has been the practice for some time to insert Maxwell's conditions, sometimes with elaborate second-order terms, for flows near the leading edge. Such a practice appears to be valid in the slip-flow regime, farther back from the leading edge, but it does not seem to agree with the experimental evidence close to the leading edge.

6.3.4 Temperature Jump Conditions

The experimental data for the static temperatures near the plate were used to make an analysis of the observed temperature jump in terms of the vertical temperature gradient at the plate. The gradients along the plate are shown in Fig. 53 for the two heated plate flows. The graph of Fig. 54 shows the temperature jump as a function of the temperature gradient. Observations similar to the speed-ratio case apply here. The cusp in the curve represents the change from the flow ahead of the plate, where temperature jump is not defined, to flow over the plate, so that again only the part of the curve to the left of the cusp can be handled by the temperature-jump theory.

It may be noted that the curve for the 100°C plate is reasonably well behaved, as was the case for the velocity slip. However, the data for the 200°C plate are anomalous as before. Again downstream of the leading edge, it is not possible to interpret the behavior unambiguously, although the trend is toward agreement with the "jump" theory. In general, the observations made in the previous section apply equally well here.

6.3.5 Exponential Decay of Slip Velocity and Temperature Jump

An approximate theoretical investigation of leading edge flows using the "Rayleigh problem" analogy and a modified form of the Maxwell-Boltzmann equation (Appendix B) leads to the conclusion that, downstream of the leading edge, the slip velocity and temperature jump should decrease exponentially with distance along the plate. For this reason the data, normalized in terms of free-stream plate-wall differences, were plotted against longitudinal position, on semi-logarithmic paper (Figs. 55 and 56). The results for the slip velocity clearly delineate three distinct regions; a section ahead of the leading edge, a linear region between the leading edge and mid-point of the plate and a trailing edge region back of the midpoint. The linear region from the temperature jump has a somewhat smaller range of validity than that for the slip velocity.

Reproduced with permission of the copyright owner. Further reproduction prohibited without permission.

As pointed out in Appendix B

$$S(x, o) \quad \frac{S_\infty}{2} e^{-\frac{\beta k x}{U}}$$

$$T_w - T_{x,o} = \frac{T_w - \sqrt{T_o \cdot T_w}}{2} e^{-\frac{\beta k x}{U}} \cdot Q$$

where Q is a slowly changing function of x. In general, the theory should not hold at the leading edge or ahead of it, but might be expected hold, in a functional way, for some distance back of the leading edge. The straight line in the central region indicates that the results of the theory of Appendix B describe the behavior of the slip velocity and temperature jump immediately back of the leading edge and that the quantities in question change exponentially with distance.

The general conclusions from these considerations are that for subsonic flows:

1. There is a region ahead of the leading edge where parameters change by diffusion processes, resulting in a definite boundary-layer up to about ten mean-free-paths ahead of the plate.

2. There is a second region back of the leading edge where flow parameters change exponentially with distance down the plate.

3. The second region blends into a region where the effects of the trailing edge are quite noticeable. It seems probable from the data of Sec. 6.3.3 and Sec. 6.3.4 that "slip" and "jump" conditions apply in this region.

6.3.6 Accommodation Coefficients

The calculations of Section 6.3.4 can be used to make an estimate of the accommodation coefficients. In particular, the tangential velocity accommodation coefficients can be determined from the values of the quantity

$$A = S_s / \left[\lambda \left(\frac{\Delta s}{\Delta y} \right)_o \right]$$

since clearly from Eq. (3.4.5)

$$\sigma = \frac{2}{1 + A}$$

Reproduced with permission of the copyright owner. Further reproduction prohibited without permission.

For the room temperature plate A has an average value of 1.8, leading to $\sigma = 0.715$. The result for the 100°C plate, using an average value for A of 1.2 is $\sigma = 0.91$.

Similar calculations for the 200°C plate vary widely along the plate but at all points the apparent values of the accommodation coefficient are quite low, for instance at the mid-point of the plate a value of $\sigma = 0.36$ was obtained. Since the results for this last case were seriously at variance with Maxwell's slip conditions there is some uncertainty about this value. However, the difference in the apparent values of σ for the room temperature and 100°C plates seems difficult to explain.

Values for the temperature accommodation coefficient can be calculated in a similar fashion. Here, the values are presented as calculated from the data on Figs. 40, 44 and 46 for the mid-point of the two heated plates. The mean-free-path for the 100°C plate is taken as 0.11" and for the 200°C plate the value of $\lambda = 0.126$" is used, which corresponds to a mean gas temperature of 376°K. In addition, the jump conditions are used in the form given in Ref. 28.

$$\Delta T = \frac{2-\alpha}{\alpha} \frac{2\gamma}{\gamma+1} \frac{1}{Pr} \lambda \left(\frac{\partial T}{\partial y}\right)_0$$

Using the values of $\gamma = 1.4$ and $Pr = 0.72$, the numerical factor $\frac{2\gamma}{\gamma+1} \cdot \frac{1}{Pr} = 1.62$. From Fig. 44 it is found that $T_0 = 334$°K, and $(\Delta T/\Delta y)_0 = 51$°K/inch. Figure 40 indicates a wall temperature at the mid-point of $T_w = 362$°K so that

$$\Delta T = \frac{2-\alpha}{\alpha} \times 1.62 \times 0.11 \times 51$$

Hence, $\alpha = 0.49$

The results for the 200°C plate are $T_0 = 380$°K, $T_w = 466$°K and $(\partial T/\partial y)_0 = 86$°K/inch. This leads to a value $\alpha = 0.34$. These calculations suffer from the shortcoming that one must accept the validity of the Maxwell slip conditions and the temperature jump conditions in order to perform them. Using the assumptions of Section 2.2 (Eqs. 2.3 and 2.4) it is possible to perform an alternative calculation which goes back to more basic mechanisms. Because it is obviously excluded from the preceding calculations and because flow conditions are most clearly defined there, these calculations have been carried out for the leading edge only, using data of the "contour maps" of Figs. 29, 30, 31, 33, 34, 35 and 36. For the sake of simplicity it was assumed that one mean-free-path was exactly 0.100 inches in all experiments. This assumption is acceptable in view of the other uncertainties in the treatment of the data.

Reproduced with permission of the copyright owner. Further reproduction prohibited without permission.

TABLE III

Room Temperature Plate	S			U	T_o			T		
	S_{av} .25	S_{in} .36	α_S .61	u .61	$T_{o\,av.}$	$T_{o\,in}$	α_{T_o}	T_{av}	T_{in}	α_T
100°C plate	.25	.34	.53	.51	318.8	310.5	0.34	313	302	0.38
200°C plate	.325	.35	.14	.10	346.0	332.0	0.22	334	318	0.23

It is apparent from these values that the accommodation coefficients are significantly less than unity in all cases, contrary to the usually accepted values. No reasonable manipulation of the various assumptions can alter this conclusion. In addition, there is not too much correspondence between the results as determined by the two different methods.

While in general it is usually considered that accommodation coefficients are close to unity for engineering surfaces, the most reliable values, for scrupulously clean surfaces, are very much lower. Wachmann for instance (Ref. 9) gets values from as low as 0.02 to about 0.6 depending on the surface and impinging gas. The distinction between the low values and the high values seems to be associated with the difference between "clean" and "dirty" surfaces. The question arises therefore whether the low values we obtain could indicate a "clean" surface. Since the model was exposed to a blast of dried air while being heated, it seems possible that the oil film, or adsorbed layer of water-vapour (which seems to constitute a "dirty" surface) could have been removed to given an effectively "clean" surface.

It may also be possible that some peculiar characteristic of the plastic binder used in the heater material may have produced a low accommodation coefficient. It seems very likely that the binder would have evaporated during preliminary tests, but it is possible that a change in the surface may have occurred between the start of the room temperature run and the end of the 200°C run. As will be observed, accommodation coefficients decreased from the room temperature run to the 200°C run but there is no way of knowing whether the observed changes in this quantity were true temperature effects or not.

It would also be instructive to compare these data with other available results. The previously mentioned experiments by Laurmann on Mach 2 flow over a flat plate (Ref. 2) can be treated to yield tentative data to support these findings. He has investigated what was presumed to be an adiabatic flow over a flat plate with an equilibrium temperature probe. In fact this data shows rather large discrepancies of the type that were observed in our slightly non-adiabatic flow, except that in Laurmann's case

Reproduced with permission of the copyright owner. Further reproduction prohibited without permission.

there seems to be heat subtracted from the flow by the plate. Keeping this in mind, one can determine the accommodation coefficient at the leading edge from the assumptions of Sec. 2.2 as before. In this case the values are quite comparable to those obtained in these studies, (i.e. $\sigma = 0.33$). Experimentally, any errors introduced by heat loss to the plate would tend to make T_{wire} lower and therefore make the accommodation coefficients seem higher than the true value. It may be that determining accommodation coefficients in a wind tunnel will give values in the same range as those obtained by Thomas and his students even when no particular precautions are taken to obtain "clean" surfaces.*

These results suggest that testing in a high-speed air-jet gives an effectively "clean" surface; one covered say, with a monolayer of nitrogen and oxygen. Alternatively it may be that the coefficient, even for a "dirty" surface, becomes lower in a high-speed flow. This is equivalent to saying that the degree of accommodation decreases as the amount of energy to be accommodated per collision increases. This is not an unreasonable assumption and qualitatively at least, would fit the data of Table III.

On the other hand, these results may merely be a comment on an inadequacy of the entire concept of surface accommodation. The whole problem is complex and may not yield to the rather simple treatment by which these data were obtained. The fact that the values for σ obtained by these experiments and by Laurmann in an essentially similar experiment agree amongst themselves at the leading edge and disagree with other results might be considered to indicate that some unanticipated mechanism is at work and even to cast doubts on the theory itself.

In summing up this section it seems correct to say that the values of accommodation coefficient as determined by this experiment, though subject to considerable systematic error, are significantly lower than most of the comparable values in the literature and approach the values obtained for "clean" surfaces. The method, though subject to large systematic errors, has much lower random errors and might be a useful tool for investigating relative changes in accommodation coefficient produced by manipulation of the various parameters. It might well represent a new tool in a field where there is at present a great need for reproducible data.

---

* As an interesting aside, it appears from Laurmann's data as though the shock front does not form at the leading edge of the plate, but downstream of it. Unfortunately the data is somewhat distorted by changes in total temperature so that only a general overall impression can be gained from the published data.

Reproduced with permission of the copyright owner. Further reproduction prohibited without permission.

7. CONCLUSIONS

1. The flow characteristics for a Mach 0.5 flow field around the leading edge of a flat plate have been measured for plate temperatures close to room temperature, 100°C and 200°C. The mean-free-path was 0.1 inch corresponding to a Knudsen number, based on plate length, of 0.05, so that the measurements extended well down into the slip-flow region. These measurements have been compared to the predictions of existing theories for flow over a flat plate.

2. The pressure-pair probe and the equilibrium temperature probe, as described here, are sensitive and potentially very accurate methods of investigating low-density flows. Used in consort they provide a method for completely determing the flow parameters by direct measurement. Measurement of flow temperature seems to be at least as direct and accurate in free-molecule flow as in continuum flow.

3. Flow about the leading edge of a flat plate is characterized by an upstream boundary-layer extending almost ten mean-free-paths ahead of the leading edge. This region of the boundary layer shows a rate of change of parameters characteristic of diffusion. Downstream of the leading edge the parameters decrease exponentially with distance, into what is normally considered the slip-flow region.

4. The Maxwell slip-flow conditions and the related temperature-jump conditions are not adequate to describe the interaction of a moving gas with a flat plate near the leading edge since they do not include the effect of the upstream boundary layer. Immediately downstream of the leading edge the fit to the slip-flow theory is not as good as it is to an exponential decay, as predicted by a modified Boltzman type distribution.

5. Values for the accommodation coefficients for both energy and tangential momentum lower than normally predicted for engineering surfaces were found. It has not been possible to decide whether the discrepancy is due to the relatively high tangential velocity involved, peculiarities in the particular surface tested, or inadequacies in the theoretical model itself.

6. The heat transfer coefficient varies almost inversely with distance down the flat plate.

7. A new type of pressure gauge circuit has been developed which has improved features compared to presently available ones.

8. An approximate theoretical solution of the Rayleigh problem has been found which solves the modified Boltzman equation and gives explicitly the dependence of flow-field near the leading edge of a flat plate.

Reproduced with permission of the copyright owner. Further reproduction prohibited without permission.

REFERENCES

1. Patterson G. N. — Molecular Flow of Gases, J. Wiley and Sons, 1956.

2. Laurmann, J. A. — Experimental Investigation of the Flow About the Leading Edge of a Flat Plate, California University Insitute of Engineering Research, HE-150-156, Oct. 15, 1954.

3. Harris, E. L. — Investigation of Free Molecule and Transition Flows near the Leading Edge of a Flat Plate, UTIA Report No. 53, Nov. 1958.

4. Dewey, C. F., Jr. — Hot Wire Measurements in Low Reynolds Number Hypersonic Flows, ARS Journal 31, 1709 (1961).

5. Maxwell, J. C. — On Stresses in Rarefied Gases, Phil, Trans. Roy. Soc. Part 1, 1879; The Scientific Papers of James Clerk Maxwell, Vol. 2, Dover Publications Inc., N. Y.

6. Knudsen, M. — The Kinetic Theory of Gases, Methuen and Co., Ltd., London, 1934.

7. Street, R. E. — Problem of Slip Flow in Aerodynamics, NACA RM 57A30, March 1957.

8. Brown, R. E. — The Thermal Accommodation of Helium and Neon on Beryllium PhD Dissertation University of Missouri, Columbia, Mo., 1957.

9. Wachmann, H. Y. — The Thermal Accommodation Coefficient: A Critical Survey, ARS Journal 32, 2 (1962).

10. Hartnett, J. P. — A Survey of Thermal Accommodation Coefficients, Rarefied Gas Dynamics, Proceedings of the Second International Symposium (1960), Talbot-Ed.

11. Patterson, G. N. — Recent Trends in the Mechanics of Highly Rarefied Gases, UTIA Review No. 16, 1960.

12. Sherman, F. S. — A Low Density Wind Tunnel Study of Shock Wave Structure and Relaxation Phenomena in Gases, University of California Institute of Research Engineering, HE-150-122, May 1954 (also NACA TN 3298, July 1955)

Reproduced with permission of the copyright owner. Further reproduction prohibited without permission.

13. Grad, H. — On the Kinetic Theory of Rarefied Gases, Comm. Pure Appl. Math Vol. 2, No. 4, p. 331, 1949.

14. Harris, E.L. Patterson, G.N. — Properties of Impact Probes in Free Molecule Flow, UTIA Report No. 52, April 1958.

15. Enkenhus, K.R. — The Design, Instrumentation and Operation of the UTIA Low Density Wind Tunnel, UTIA Report No. 44, June 1957.

16 Patterson, G.N. — Theory of Free-Molecule Orifice-Type Pressure Probes in Isentropic and Non-Isentropic Flows, UTIA Report No. 41, Nov. 1956.

17. Sreekanth, A.K — Drag Measurements on Circular Cylinders and Spheres in the Transition Regime at a Mach Number of 2, UTIA Report No. 74, April 1961.

18. Stalder, J.R. Goodwin, G., Creager, M.O. — A Comparison of Theory and Experiment for High Speed Free Molecule Flow, NACA Report 1032, also NACA TN 2244, Dec. 1950.

19. Schaaf, S.A. Bell, S. — Aerodynamic Forces on a Cylinder for the Free-Molecule Flow of a Non-uniform Gas, ARS Journal 23, 314 (1953).

20. LaFrance, J.C. — Pressure Measurement in Transition and Free Molecular Flows Using Orifice Probes, UTIA Technical Note No. 67, June 1963.

21. Laurmann, J.A. — Slip Flow over a Short Flat Plate, Rarefield Gas Dynamics, Proceedings F.M. Devienne Ed., Pergamon Press, 1960.

22. Maslen, S.H. — Second Approximation to Laminar Compressible Boundary Layer on a Flat Plate in Slip Flow, NACA TN 2818, Nov. 1952.

23. Mirels, H. — Estimate of Slip Effect on Compressible Laminar Boundary Layer Skin Friction, NACA TN 2609, Jan. 1952.

24. Yang, H.T. Lees, L. — Rayleighs Problem at Low Mach Number According to the Kinetic Theory of Gases, J. Math and Phys. 35, No. 3 (Oct. 1956).

Reproduced with permission of the copyright owner. Further reproduction prohibited without permission.

25. Yang , H T. Lees, L. — Rayleighs Problem at Low Reynolds Number According to the Kinetic Theory of Gases, Rarefied Gas Dynamics, Proceedings F. M. Devienne, Ed., Pergamon Press, 1960.

26. Muntz, E. P. — Pressure Measurements in Free Molecule Flow with a Rotating Arm Apparatus, UTIA TN 22, May, 1958.

27. Nagamatsu, H. T Sheer, R. E. Schmidt, J. R. — High Temperature Rarefied Hypersonic Flow over a Flat Plate, ARS Journal 31, 902 (1961).

28 — Fundamentals of Gas Dynamics, p. 719, Ed. H. W. Emmons, Princeton University Press, Princeton (1958).

REFERENCES IN APPENDIX A

1. Leck, J. H. — Pressure Measurements in Vacuum Systems, Institute of Physics, London, 1957.

2. Laurmann, J.A. Ipsen, D. C. — Use of a Free Molecule Probe in High Speed Rarefied Gas Flow Studies, Oct. 1957, WADC Tech. Rep. 57-440.

REFERENCES IN APPENDIX B

1. Gross, E. P. Jackson, A. E. — Kinetic Theory of the Impulsive Motion of an Infinite Plane, Phys. of Fluids 1, No. 4, p. 318, (1958).

2. Yang, H. T. Lees, L. — Rayleighs Problem at Low Mach Number According to the Kinetic Theory of Gases, J. Math and Phys. 35, No. 3, (Oct. 1956).

3. Yang , H. T. Lees, L. — Rayleighs Problem at Low Reynolds Number According to the Kinetic Theory of Gases, Rarefied Gas Dynamics, Proceedings F. M. Devienne, Ed., Pergamon Press, 1960.

4. Grad, H. — On the Kinetic Theory of Rarefied Gases, Comm. Pure Appl. Math Vol. 2, No. 4, p. 331, 1949.

5. Gross, E. P. Jackson, A. E. Ziering, S. — Boundary Value Problems in Kinetic Theory of Gases, Am. Phys. 1, (1957).

Reproduced with permission of the copyright owner. Further reproduction prohibited without permission.

6. Krook, M. Dynamics of Rarefied Gases, Phys. Rev. 99, 1896 (1955).

7. Patterson, G.N. Molecular Flow of Gases, J. Wiley and Sons, 1956.

8. Churchill, R. Modern Operational Mathematics in Engineering, McGraw-Hill, 1944.

Reproduced with permission of the copyright owner. Further reproduction prohibited without permission.

TABLE I

Effect of a Two-Stream Distribution Function on Probe Response

parameter	$\alpha = 1$	$\alpha = 0.5$	$\alpha = 0.25$
T_w	470	470	470
T_{in}	310	310	310
α_s	1	0.5	0.25
α	1	0.5	0.25
S_{in}	.37	.37	.37
T_{out}	470	392.5	351.5
S_{out}	0	.185	.278
S_{av}	.182	.2765	.3235
T_{av}	388.3	350.3	330.5
χ_{in}	1.787	1.787	1.787
χ_{out}	1.0	1.362	1.567
χ_{av}	1.362	1.567	1.676
$f(S_{in})$	10.727041	10.727041	10.727041
$g(S_{in})$	10.05953	10.05953	10.05953
$f(S_{out})$	9.424779	9.75427	10.15572
$g(S_{out})$	9.424779	9.58839	9.77124
$\frac{T_{wire}}{T_{av}}$ (two stream)	1.03652	1.0392	1.0522
S' (measured by probe)	.200	.281	.324
$\frac{S'}{S}$	1.09	1.015	1.000
$\varphi(S')$	1.0195	1.0380	1.0508
$\frac{T'}{T}$	1.017	1.001	1.001

Reproduced with permission of the copyright owner. Further reproduction prohibited without permission.

TABLE II

Fixed Point Data

p = 20.0 μ | $\lambda_\infty \simeq$ 0.096" | S_∞ = 0.430 | M_∞ = 0.515

Run	Quantity Measured		Temperature °K	Power (watts)
Room Temperature	Room Temperature		297.9	
Mach 0.5	To Nozzle		296.3	
20 μ	Plate Temperatures			
	1/4" back of L.E.	A	298.2	
	1" back of L.E.	B	297.9	
	1-3/4" back of L.E.	C	297.9	
100°C	Room Temperature		297.3	
Mach 0.5	To Nozzle		298.6	
20 μ		A	360.0	
		B	361.8	
		C	363.2	
	Power			2.73
200°C	Room Temperature		300.3	
Mach 0.5	To Nozzle		302.5	
20 μ		A	460.7	
		B	466.5	
		C	473.4	
	Power			9.95
200°C	Room Temperature		301.0	
Mach 0.0		A	464.7	
10^{-4}mm		B	464.4	
		C	476.7	
200°C		A	464.7	
Mach 0.0		B	465.3	
20 μ		C	477.7	
	Power			9.76
100°C		A	364.2	
Mach 0.0		B	364.2	
10^{-4} mm		C	368.4	
	Power			2.50
100°C		A	363.8	
Mach 0.0		B	364.3	
20 μ		C	367.2	
	Power			2.85

Reproduced with permission of the copyright owner. Further reproduction prohibited without permission.

Received without Table III.

Filmed as received.

University Microfilms, Inc.

Reproduced with permission of the copyright owner. Further reproduction prohibited without permission.

TABLE IV

ROOM TEMPERATURE PLATE DATA USING THE EQUILIBRIUM TEMPERATURE PROBE

Distance downstream of nozzle exit plane (inches	Distance above nozzle centerline (inches)	E (mv)	E_o mv	S
0.00"	0.000	.320		.421
	.200	.320		.423
	.400	.325	1.018	.424
	.700	.330		.425
	..900	.328		.425
	1.200	.309		.412
	1.400	.271		.389
	1.900	.180		.327
	2.300	.065		.235
minimum reading		-0.077 = $-\ell$		
0.50"	0.000	.275		.391
	0.200	.290		.401
	0.400	.310		.415
	0.700	.328	1.022	.425
	0.900	.327		.425
	1.200	.312		.416
	1.500	.274		.390
	1.900	.180		.327
1.00"	0.000	.184		.330
	0.200	.257		.378
	.400	.326		.425
	.700	.351	1.022	.440
	.900	.348		.437
	1.200	.327		.425
	1.500	.278		.393
	1.900	.187		.331
2.00"	0.000	.000		.174
	.100	.036		.213
	.300	.118		.282
	.500	.202	1.022	.341
	..700	.270		.387
	1.050	.333		.429
	1.200	.332		.428
	1.700	.256		.378
	2.200	.144		.303
3.00"	.100	.000		.173
	.200	.022		.198
	.300	.044		.220
	.500	.096	1.022	.266
	.700	.154		.310
	1.200	.247		.372
	1.500	.264		.383
	1.700	.252		.376
	2.200	.175		.324

Reproduced with permission of the copyright owner. Further reproduction prohibited without permission.

TABLE V

ROOM TEMPERATURE PLATE PRESSURE-PAIR PROBE DATA

Distance from nozzle exit plane (inches)	Distance above nozzle center-line (inches)	Impact Probe mv.	Static Probe mv.	Plate Static Pressure	S
.315	0.00	12.534	10.018	19.6	.430
.743		12.346	10.064		.391
1.243		11.254	9.946		.170
1.743		10.924	9.894		.107
2.243		10.802	9.856		.080
2.743		10.730	9.842		.067
1.743		11.446	9.840		.228
2.243		11.148	9.838		.167
2.743		11.026	9.838		.138

Reproduced with permission of the copyright owner. Further reproduction prohibited without permission.

TABLE IV

TEMPERATURE PLATE DATA USING THE EQUILIBRIUM TEMPERATURE PROBE

e downstream of exit plane (inches	Distance above nozzle centerline (inches)	E (mv)	E_o mv	S
0.00"	0.000	.320		.421
	.200	.320		.423
	.400	.325	1.018	.424
	.700	.330		.425
	.900	.328		.425
	1.200	.309		.412
	1.400	.271		.389
	1.900	180		.327
	2.300	.065		.235
minimum reading		-0.077 = $-\ell$		
0.50"	0.000	.275		.391
	0.200	.290		.401
	0.400	.310		.415
	0.700	.328	1.022	.425
	0.900	.327		.425
	1.200	.312		.416
	1.500	.274		.390
	1.900	.180		.327
1.00"	0.000	.184		.330
	0.200	.257		.378
	.400	.326		.425
	.700	.351	1.022	.440
	.900	.348		.437
	1.200	.327		.425
	1.500	.278		.393
	1.900	.187		.331
2.00"	0.000	.000		.174
	.100	.036		.213
	.300	.118		.282
	.500	.202	1.022	.341
	.700	.270		.387
	1.050	.333		.429
	1.200	.332		.428
	1.700	.256		.378
	2.200	.144		.303
3.00"	.100	.000		.173
	.200	.022		.198
	.300	.044		.220
	.500	.096	1.022	.266
	.700	.154		.310
	1.200	.247		.372
	1.500	.264		.383
	1.700	.252		.376
	2.200	.175		.324

Reproduced with permission of the copyright owner. Further reproduction prohibited without permission.

TABLE V

ROOM TEMPERATURE PLATE PRESSURE-PAIR PROBE DATA

Distance from nozzle exit plane (inches)	Distance above nozzle center-line (inches)	Impact Probe mv.	Static Probe mv.	Plate Static Pressure	S
.315	0.00	12.534	10.018	19.6	.430
.743		12.346	10.064		.391
1.243		11.254	9.946		.170
1.743		10.924	9.894		.107
2.243		10.802	9.856		.080
2.743		10.730	9.842		.067
1.743		11.446	9.840		.228
2.243		11.148	9.838		.167
2.743		11.026	9.838		.138

Reproduced with permission of the copyright owner. Further reproduction prohibited without permission.

TABLE VI

100°C PLATE EQUILIBRIUM TEMPERATURE PROBE DATA

Distance from nozzle exit (inches)	Distance above nozzle centerline (inches)	T_{wire} °K
0.00	0.000	306.5
	0.200	306.5
	0.400	306.7
	0.600	306.8
	0.800	306.9
	1.000	306.8
	1.500	305.5
	2.000	302.7
	2.500	299.2
0.50	0.00	306.5
	0.200	306.8
	0.400	307.2
	0.600	307.5
	0.800	307.6
	1.000	307.5
	1.500	306.0
	2.000	303.0
	2.500	299.8
1.00	0.000	322.8
	0.100	317.1
	0.200	315.0
	0.400	312.8
	0.600	311.2
	0.800	310.1
	1.000	309.5
	1.500	306.9
	2.000	303.6
	2.500	300.4
2.00	.200	328.4
	.400	324.2
	.600	320.8
	.800	318.3
	1.000	315.9
	1.500	310.6
	2.000	306.2
	2.500	302.4
3.00	0.000	324.4
	0.100	323.8
	0.200	322.5
	0.400	319.9
	0.600	318.4
	0.800	316.9
	1.000	315.6
	1.500	312.2
	2.000	308.4
	2.500	304.6

Reproduced with permission of the copyright owner. Further reproduction prohibited without permission.

TABLE VII

100°C PLATE PRESSURE-PAIR PROBE DATA

Distance downstream of nozzle exit (inches)	Distance above nozzle centerline (inches)	Impact Probe mv.	Static Probe mv.	Plate Static Pressure	S
0.315"	0.020	12.446	10.075	19.2	.421
	0.200	12.449	10.038	19.2	.425
	0.500	12.451	10.016	19.2	.427
	0.800	12.416	9.972	19.2	.425
	1.100	12.360	9.888	19.2	.418
	1.400	12.203	9.830	19.2	.397
1.300"	0.000	11.150	10.002	19.5	.151
	0.200	11.850	9.918	19.5	.310
	0.400	12.055	9.772	19.7	.358
	0.700	12.236	9.716	19.7	.394
	1.000	12.257	9.701	19.7	.398
	1.500	12.076	9.656	19.7	.366
	2.000	11.675	9.652	19.7	.290
2.300"	0.000	10.607	9.680	19.9	.048
	0.200	10.944	9.684	19.7	.131
	0.400	11.292	9.705	19.7	.206
	0.700	11.710	9.696	19.7	.293
	1.000	11.945	9.678	19.7	.342
	1.500	11.965	9.672	19.7	.345
	2.000	11.690	9.650	19.7	.298

Reproduced with permission of the copyright owner. Further reproduction prohibited without permission.

TABLE VIII

200°C PLATE EQUILIBRIUM TEMPERATURE PROBE DATA

Distance Downstream of Nozzle Exit (inches)	Distance above Nozzle Centerline (inches)	T_{wire} °K
0.00	0.020	311.2
	0.200	311.4
	0.450	311.8
	0.700	312.0
	1.200	311.7
	1.700	309.8
	2.200	306.3
	2.700	303.2
0.50"	0.020	313.5
	0.200	313.5
	0.400	314.0
	0.600	314.3
	0.800	314.3
	1.200	313.3
	1.700	310.7
1.00"	0.020	350.9
	0.100	342.6
	0.200	338.0
	0.450	327.9
	0.700	322.6
	0.950	319.5
	1.200	317.0
	1.300	316.4
	1.700	312.4
2.00"	0.100	374.7
	0.200	368.2
	0.450	354.9
	0.700	344.0
	0.950	335.1
	1.200	328.0
3.00"	0.020	359.7
	0.100	357.7
	0.200	354.5
	0.450	346.5
	0.700	339.9
	0.950	334.6
	1.200	329.8

Reproduced with permission of the copyright owner. Further reproduction prohibited without permission.

TABLE IX

200°C PLATE PRESSURE-PAIR PROBE DATA

Distance Downstream of Nozzle Exit (inches)	Distance above Nozzle Centerline (inches)	Impact Probe mv.	Static Probe mv	Plate Static Pressure	S
0.320	0.100	12.487	10.108	19.4	.415
	0.400	12.446	9.900	19.7	.425
	0.600	12.434	9.826	19.7	.427
	0.800	12.397	9.762	20.4	.403
	1.000	12.365	9.725	20.1	.409
	1.200	12.328	9.725	20.1	.403
	1.700	12.153	9.728	19.9	.373
1.000	0.400	12.166	9.748	19.2	.391
	0.600	12.252	9.752	19.3	.406
	0.800	12.280	9.684	19.1	.425
	1.200	12.227	9.661	19.2	.415
	1.700	11.947	9.560	19.1	.363
	2.200	11.441	9.545	19.2	.260
	2.700	10.931	9.534	19.3	.139
3.000	0.100	10.521	9.511	19.3	.052
	0.200	10.639	9.520	18.9	.079
	0.400	10.896	9.514	19.3	.143
	0.600	11.114	9.521	19.1	.187
	0.800	11.319	9.528	19.1	.238
	1.200	11.609	9.510	19.1	.304
	1.700	11.696	9.486	19.2	.316
	2.200	11.524	9.501	19.4	.277
	2.700	11.261	9.502	19.3	.225

Reproduced with permission of the copyright owner. Further reproduction prohibited without permission.

TABLE OF CONTENTS

APPENDIX A

		Page
A1.	INTRODUCTION	A1
A2.	THEORY OF HEAT TRANSFER GAUGES	A2
	A2.1 Effect of Wall Temperature Variations on Gauge Readings	A4
A3.	DESIGN CONSIDERATIONS	A6
A4	EXPERIMENTAL TESTS	A7
	A4.1 O-Ring Thermocouple Gauge	A7
	A4.2 Coiled-Wire Thermocouple Gauge	A8
	A4.3 All-Metal Gauges	A8
A5.	POWER SUPPLY	A9
A6.	SENSING ELEMENTS	A11
A7.	CONSTRUCTION OF PROBES	A11
	A7.1 Analysis of Relative Gauge Discussion	A11
	A7.2 Pressure-Pair Probe	A12
	A7.2.1 Glass Probe Tips	A13
A8.	CALIBRATION OF GAUGES	A14
	A8.1 McLeod Gauge	A14
	A8.2 Calibration of Thermocouple Gauge	A15
A9.	PERFORMANCE	A16
A10.	RESULTS	A17
A11.	CONCLUSIONS	A18
	REFERENCES	A19

Reproduced with permission of the copyright owner. Further reproduction prohibited without permission.

LIST OF SYMBOLS

APPENDIX A

A	internal area of gauge
d	diameter of tubing
K_n	$\frac{\lambda}{L}$ Knudsen number, ratio of mean free path to a characteristic dimension
k_c	constant for thermal conductivity
k_r	constant for radiative heat transfer
p	gas pressure
p'	the pressure in the gauge head at which radiative heat transfer equals conductive heat transfer
E	quantity of heat transfer
ΔT	$T_{wire} - T_{wall} = T - T_o$ difference in temperature
λ	mean free path of a gas molecule

Reproduced with permission of the copyright owner. Further reproduction prohibited without permission.

APPENDIX A

Thermocouple Pressure Gauge and Power Supply for Use in Low Density Wind Tunnels

A. 1 INTRODUCTION

In a low-density wind tunnel, pressure gauges are the most important single source of information available and the demands made upon these gauges are quite exacting. A satisfactory instrument should be small, precise and reliable, with a fast continuous response and low power consumption. Since these demands tend to be self-contradictory a satisfactory compromise must be sought. There are many instruments available, each with its own characteristics.

1. The McLeod Gauge has for years been the laboratory standard for low pressure measurements, but, in general, is unsuitable for routine measurements in a low-density wind tunnel. It is extremely bulky and slow to operate and does not provide a continuous reading. High precision and large internal volume are inescapably linked, and if it is not used properly the gauge is susceptible to many unsuspected errors.

2. Bellows, Diaphragm and Bourdon Gauges perform so well at atmospheric pressure that many attempts have been made to use them at low pressures. At pressures below 1 mm Hg this sort of gauge becomes rapidly more and more unsatisfactory. To increase sensitivity, internal volumes are increased but in the neighbourhood of a few microns Hg., hysteresis in the bellow material and temperature effects introduce relatively large uncertainties.

3. Liquid Manometers are extremely useful at higher pressures but in the micron region they too suffer from many defects. In particular, surface tension effects make them very vulnerable to contamination and temperature variation. Increasing the bore decreases the problem but increases the internal volume. In addition, relatively high vapour-pressure and large outgassing rates are sources of much trouble.

4. The Ionization Gauge is most satisfactory at pressures below 1 micron. Though it can be made to operate above this region its performance is liable to be erratic and the sensitivity low.

5. A variety of more exotic types of gauges such as viscosity, molecular drag, Knudsen, glow-discharge and so on have been described in the literature, but none has proved particulary successful in this application.

6. Heat transfer gauges of various types are the most successful gauges in this pressure range. Their useful range generally extends

Reproduced with permission of the copyright owner. Further reproduction prohibited without permission.

from 1 micron to 1 mm, but can be extended about two orders of magnitude in either direction by a variety of devices.

The familiar Pirani gauge and the rather similar thermocouple gauge are the most common examples of this type and have been commercially available for years in many different forms. These commercial gauges are not satisfactory for wind tunnel use on several counts, but held enough promise so that some time was devoted to their further development.

A2. THEORY OF HEAT-TRANSFER GAUGES

The general theory of heat transfer gauges is rather well understood and, to name one source, has been presented by Leck (Ref. A1) in a work which describes most types of vacuum gauges rather fully. In a gas at reduced pressure such that the mean-free-path is of the order of the container dimensions, the amount of heat transfer becomes dependent on gas pressure, among other things, and, if the pressure is low enough, can be written as

$$E = k_c \cdot p \cdot \Delta T + \text{Radiative transfer} + \text{End conduction losses} \qquad \text{(A2. 1)}$$

If one thinks of a heated wire, E will represent the heat transferred to the walls, k_c a constant depending on geometry, accommodation coefficient and gas composition, p the pressure while ΔT is $T_{wire} - T_{wall} \cong T - T_o$.

The radiation and end-conduction terms represent other parallel modes of heat transport. In general, if they are kept small the sensitivity of the gauge is increased, whereas if they are large there is a faster speed of response and proportionately greater sensitivity at the higher pressures.

Such gauges are heated electrically and can be operated in two basic ways. In one case the voltage, or possibly the current or power input, is kept constant so that the wire temperature varies with pressure; in the other the power input is varied so as to keep the wire temperature constant. The first type is much simpler and cheaper to construct and operate and can be quite sensitive but it is essentially non-linear in response. The mathematics is quite complicated and the gauge requires point-by-point calibration over its whole range.

For the other method, the operation is more laborious and equipment more expensive, but the theoretical prediction of response is much simpler. End-conduction and radiation losses are essentially constant so that there is a linear relationship between power and pressure over a wide range. In addition the gauge retains good sensitivity to much higher pressures.

Reproduced with permission of the copyright owner. Further reproduction prohibited without permission.

The Pirani gauge is a common example of the first type of gauge. Temperature is determined by an unbalanced Wheatstone bridge arrangement with the heated wire also acting as a temperature-sensitive resistance-element. Commercial gauges are also available in which an automatic feed-back circuit changes the power supplied to some temperature-sensitive resistance element so as to keep the temperature constant. The power input is thus a measure of pressure.

The so-called "Thermistor" gauge is basically similar to the Pirani gauge. It uses a thermistor, (a sintered metal-oxide composition), rather than a metallic wire as its sensing element and has a somewhat higher resistance and temperature sensitivity than the tungsten wires normally used in the Pirani gauge. It is otherwise very similar. The thermistor gauge has been used for this type of work with some success, but because of difficulties in obtaining matched thermistors and several other small but valid objections, its use was rejected. *

In the thermocouple gauge, the temperature-sensing device is not a resistance element but rather a thermocouple. Aside from that, the operation is basically similar to that of the Pirani and thermistor gauge. The thermocouple signal output is less than that of the corresponding Pirani gauge, but the commerically available models have the reputation of being rugged and reliable gauges. Since this design represented fewer construction problems to a small laboratory than a resistance-element gauge, it was given serious consideration.

Apparently no attempt has ever been made to operate a thermocouple as a constant-temperature gauge, yet it has several important advantages which recommend it. A peculiarity of the thermocouple arrangement, as normally connected, is that the temperature it measures is the difference between wall temperature and wire temperature. This happens because the cold-junction of the pair is almost invariable at the lead-through in the gauge casing rather than at the power supply.

A glance at Eq. A2. 1 shows that it is just this difference which enters into the heat-conductivity term. For this reason a thermocouple gauge is less sensitive to ambient temperature variations at the

---

* In particular, it was felt that the porous nature of the bead would make it extremely susceptible to outgassing errors compared to a dense smooth surfaced wire. Since the material is in the form of a sphere, it tends to have a low area to-volume ratio, so that its sensitivity at low pressures tends to be small. Its relatively high resistance makes it difficult to match to low-impedance electronic circuits.

Reproduced with permission of the copyright owner. Further reproduction prohibited without permission.

gauge wall. Even if one uses a Pirani-type element as a constant temperature device it will still be susceptible to wall temperature variation. For this reason a constant-temperature thermocouple gauge should be superior to a constant-temperature Pirani gauge, other things being equal.

A2.1 Effect of Wall Temperature Variations on Gauge Readings

1. In a constant-temperature thermocouple gauge $\Delta T \equiv T - T_o$ is a constant. For a given change in wall temperature, dT_o, $dT = dT_o$

and
$$d(\Delta T) = 0 \qquad \text{(A2.2)}$$

2. On the other hand, for a constant-temperature resistance element gauge,
$$dT = 0 \text{ and } d(\Delta T) = dT_o \qquad \text{(A2.3)}$$

3. Let us define relative temperature sensitivity as the change in pressure needed to exactly cancel the effect of a change in wall temperature, dT_o.

4. Neglect thermal conductivity along the leads.

5. Assume energy input = Energy lost to walls
= Radiative losses + gaseous conduction

$$E_t = k_r (T^4 - T_o^4) + k_c\, p\, (T - T_o) \qquad \text{(A2.4)}$$

Taking the derivative with respect to T, for constant E_t one gets:

$$0 = 4k_r (T^3\, dT - T_o^3\, dT) + k_c (T - T_o)\, dp$$

For a thermocouple gauge ($dT = dT_o$)

$$\therefore \frac{dp}{dT_o} = -4 \frac{k_r}{k_c} \frac{T^3 - T_o^3}{T - T_o} = 4 \frac{k_r}{k_c} (T^2 + TT_o + T_o^2) \qquad \text{(A2.5)}$$

k_r/k_c can be evaluated experimentally be determing the pressure, p', at which $E_{radiative} = E_{conductive}$

$$\therefore \frac{k_r}{k_c} = p' \frac{T - T_o}{T^4 - T_o^4} \qquad \text{(A2.6)}$$

so that
$$\frac{dp}{p} \Big/ \frac{dT_o}{T_o} = 4 \frac{p'}{p} \frac{T_o (T - T_o)(T^2 + TT_o + T_o^2)}{T^4 - T_o^4}$$

$$\therefore \frac{dp}{p} \simeq -3 \frac{p'}{p} \left\{1 - \frac{\Delta T}{T_o} + 2\left(\frac{\Delta T}{T_o}\right)^2 + \cdots\cdots\right\} \frac{dT_o}{dT_o} \qquad \text{(A2.7)}$$

Reproduced with permission of the copyright owner. Further reproduction prohibited without permission.

Similarly for the Pirani gauge:

$$-4k_r T_0^{\,3} dT_0 - k_c p\, dT_0 + k_c (T - T_0)\, dp = 0$$

Therefore $$\frac{dp}{dT_0} = \frac{k_c p + 4k_r T_0^{\,3}}{k_c (T - T_0)}$$

$$= \frac{p}{\Delta T} + \frac{4p'}{T_0^4 + 4T_0^3\Delta T + 6T_0^2\Delta T^2 + 4T_0\Delta T^3 + \Delta T^4 - T_0^4}$$

Expressed as relative change in pressure and relative change in wall temperature

$$\therefore \frac{dp}{p} = \frac{T_0}{\Delta T}\left\{1 + \frac{p'}{p}\left[1 - \frac{3}{2}\frac{\Delta T}{T_0} + \frac{5}{4}\left(\frac{\Delta T}{T_0}\right)^2 + \cdots\right]\right\}\frac{dT_0}{T_0} \qquad \text{(A2.8)}$$

$$\therefore \frac{\left(\frac{dp}{p}\right)_{Pirani}}{\left(\frac{dp}{p}\right)_{T.C}} = -\frac{T_0}{\Delta T}\;\frac{1 + \frac{p'_{Pirani}}{p}\left[1 - \frac{3}{2}\frac{\Delta T}{T_0} + \cdots\right]}{3\frac{p_{T.C}}{p}\left[1 - \frac{\Delta T}{T_0} + \cdots\right]} \qquad \text{(A2.9)}$$

if $\frac{\Delta T}{T}$ is small

and $p'_{Pirani} = p'_{T.C.}$

$$\therefore \frac{\left(\frac{dp}{p}\right)_{Pirani}}{\left(\frac{dp}{p}\right)_{T.C}} \simeq -\frac{1}{3}\left[1 + \frac{T_0}{\Delta T} + \frac{p}{p_1}\left(-\frac{1}{2} + \frac{T_0}{\Delta T} - \frac{3}{2}\frac{\Delta T}{T_0}\right)\right]$$

$$\simeq -\frac{1}{3}\left\{1 + \frac{T_0}{\Delta T}\left[1 + \frac{1}{2}\frac{p}{p_1}\left(2 - \frac{\Delta T}{T_0}\right)\right]\right\}$$

$$\simeq -\frac{1}{3}\frac{T_0}{\Delta T}\left(1 + \frac{p}{p_1}\right) \qquad \text{(A2.10)}$$

$$\frac{\Delta T}{T_0} \ll 1$$

Reproduced with permission of the copyright owner. Further reproduction prohibited without permission.

thus for small $\Delta T/T_o$ the Pirani gauge is much less satisfactory. The higher the pressure, the less satisfactory the Pirani gauge becomes. If $\Delta T/T_o$ were say 1/3, (the highest value desirable for practical reasons), and $p''_P = p'_{TC}$

$$\frac{\left(\frac{dp}{p}\right)_{Pirani}}{\left(\frac{dp}{p}\right)_{T.C.}} \simeq \frac{p}{p'} + \frac{23}{36} \qquad \text{(A2. 11)}$$

(if the series is stopped at the second order terms in Eq. 2. 9) so that at pressures greater than $2p'/135$ the thermocouple gauge would be better. Since it is desired to operate these gauges with a minimum power input, ΔT should be kept as low as possible. In this case the thermocouple gauge will always be superior, as shown by Eq. A2. 10.

A3 DESIGN CONSIDERATIONS

In addition to this lower temperature sensitivity there are several other practical reasons for preferring the thermocouple gauge:

1. Thermocouple gauge materials are readily available in fine wire form.

2. Thermocouple materials are particularly stable. Temperature measurements can be made very precisely whereas the temperature-sensitive resistance wires are, in practice, very susceptible to random zero shift.

3. Thermocouple materials are malleable and inexpensive.

To be really useful in a low-density wind tunnel, pressure gauges must have a very small internal volume as well as being sensitive. In the end it proved possible to reduce the internal volume of the gauge to something less than one-twentieth of that of the smallest commercial gauge available. The same reduction in volume would be possible in a temperature-sensitive resistance-element gauge but for practical reasons which will be mentioned later, this approach was abandoned after some experimentation.

The success of a constant-temperature gauge depends to a very large degree on the achievement of a practical feed-back circuit. In this case it was the realization that commercially available self-balancing millivoltmeters could be readily adapted for such a duty which made these gauges a very practical reality. In fact, the same principle could be applied to a resistance-element gauge as well, as has been demonstrated commercially. An attempt was made to develop such a resistance-element feedback circuit along with the development of the thermocouple gauges but it met with only limited success. The resistance element circuit

Reproduced with permission of the copyright owner. Further reproduction prohibited without permission.

proved very prone to spurious oscillation, explainable by the non-linear response of a Wheatsone bridge using power-sensitive resistance elements. While this sort of response could be avoided by proper choice of parameters it would seem that each different gauge would therefore represent a new design problem. The objective of this research was to develop a small, sensitive type of gauge which could be used in a wide variety of conditions and sizes. It seemed particularly important that the gauge circuit operate inter-changeably for all gauges. The prospects for such a Pirani-type element seemed not too hopeful. Since, on the other hand, the thermocouple gauge circuit proved inherently stable, no further attempt was made to develop the resistance element circuit.

In the detailed design of the thermocouple gauge-head, general experience in the field (e.g. Ref. A1) dictated a few guiding principles.

1. The length of the heated wire should be great with respect to its diameter, to reduce end-conduction losses and increase low-pressure sensitivity.

2. The diameter of the wire should be as small as possible, consistent with adequate strength in order to decrease power consumption.

3. The wires should have low emissivity to decrease radiative heat transfer.

4. The alloys used should give adequate signal and make strong, reliable welds.

5. The alloys should be stable and not subject to corrosion.

6. The operating temperature of the wire should be low enough so that there will be no decomposition of organic vapours on the wire, with subsequent change in accommodation coefficient and emissivity.

A.4 EXPERIMENTAL TESTS

Because chromel-alumel thermojunctions satisfied the requirements of strength and output very well, all gauges were made of these materials.*

A4.1 O-Ring Thermocouple Gauge

Straight wires in 1/2 mil, 1 mil and 2 mil sizes were threaded through the walls of small silicone rubber o-rings, 1/4" OD,

---

* Small gauge wires used here were obtained from Sigmund Cohn Corp. 121 South Columbus Avenue, Mount Vernon, New York.

Reproduced with permission of the copyright owner. Further reproduction prohibited without permission.

1/8" I.D. to form a cross of the two dissimilar metals. The wires were spot-welded at the cross-over point.* The O-ring was then clamped between two plates to form an enclosed volume. A hole drilled in one plate wall served as pressure inlet (Fig. A1). These were calibrated in a constant current circuit to give the data of Fig. A2.

A4.2 Coiled-wire Thermocouple Gauges

A second type, using spirally wound coils instead of straight wires was tested next (Fig. A1). These spirals were sealed into crossed channels in a sheet of 1/8" silicone rubber with a drop of silicone adhesive.** This was tested as before (Fig. A3). It was decided on the basis of these tests that spirally wound wires 1 mil in diameter gave the best compromise between ruggedness, ease of manufacture and sensitivity. It was further decided that rigid-wall containers were more suitable than the rubber models tested.

Consequently, small glass-walled models were constructed, with tungsten lead-in wires sealed directly into the glass (Plate A1). These models worked quite well, but had too large an internal volume (about 2 cc lower limit) so that further design modifications were tried.

A4.3 All-Metal Gauges

In the final models the envelope was made of metal using small Kovar-glass hermetic seals as lead-throughs*** The sensing element, crossed spirals of a 0.001 inch diameter chromel and alumel were first assembled on the lead-throughs in a jig and then soldered into the gauge-head as a unit (Fig. A4).

The gauge-head body was constructed as two pieces, the main body and a cover, both machined from solid rod. The two pieces were finished smooth and soldered together to form a single cylinder. Two transverse holes were then drilled through the cylinder at right angles, intersecting to form a cross. The axes of these holes were carefully aligned to be in the plane of the soldered junction so that the drill holes formed two crossed half-cylindrical channels in the surface of each piece when the top cover was eventually unsoldered. The assembled sensing element, in its jig, was then sandwiched between these two pieces and the whole assembly soft-soldered together to form a vacuum tight enclosure. A separate small drill-hole to the junction of the cross served as the

---

* Ewald Minature Spotwelder Head No. WHD 5A
Ewald Instruments, Kent, Conn.

** Silicone A-400 Adhesive

*** No. 232 P miniature single terminal hermetic seals. Quality Hermetics Ltd. 45 Hollinger Road, Toronto 16, Ont.

Reproduced with permission of the copyright owner. Further reproduction prohibited without permission.

pressure channel.

The resulting unit, as in previous models, consisted of a cross of two dissimilar metals. Any two dissimilar arms could be utilized as a thermocouple, while the remaining two could form the heated filament whose temperature must be measured. The total gauge volume of the head was less than 0. 1 cc.

A5. POWER SUPPLY

The requirements for any power-supply for a constant temperature thermocouple gauge are rather stringent:

1. It must sense the difference in temperature between the hot junction (spot-welded crossover) and the cold-junction (essentially the gauge wall temperature) with great precision and without drift.

2. Using minute amounts of input signal power from the junction it must actuate a servo-mechanism in such a manner as to return the hot junction exactly to some pre-arranged operating condition.

3. It must do this with a minimum of hunting and yet have a reasonably fast time response (certainly less than one minute).

4. Since drift will always occur in such a complicated circuit it must include some means of checking its own calibration

5. It must be reasonably reliable, simple and foolproof.

It became apparent that all these requirements could be met quite easily by making a minor alteration to a commercially available instrument - the self-balancing, millivolt potentiometer widely used in conjunction with thermocouples for measuring temperatures.* These instruments are complex, but very reliable and sensitive. They usually have a built-in self-calibrating mechanism to take care of drift. In essence they consist of a servomechanism which adjusts the output voltage of a simple voltage divider circuit to match that of the incoming signal. This is accomplished by moving a rider on a slide wire in such a direction as to minimize the difference between the rider voltage and incoming signal voltage. This difference is determined by a very sensitive amplifier which can detect differences of a small fraction of a microvolt (Fig. A5).

---

* The particular instrument used here was a Brown "Electronik" Indicating Potentiometer (0-10 mv) made by Minneapolis-Honeywell. It will be noted that the instrument should not have a self-compensating cold junction, but rather be a true milliovoltmeter.

Reproduced with permission of the copyright owner. Further reproduction prohibited without permission.

If by changing electrical connections alone one replaced the slidewire with a fixed potentiometer set at some definite value, the servomechanism would still rotate the slide wire but the unit would no longer balance itself. The slidewire can now be connected up electrically to act as a rheostat to control the power input to the thermocouple gauge. If the phasing of the connections is right one can now connect the signal leads from the thermocouple gauge to the signal terminals of the instrument so that the unit as a whole is once more self-balancing. Now however, balance is achieved by adjusting the incoming signal to match the preselected value on the fixed potentiometer rather than by changing the voltage on the potentiometer circuit slidewire. Movement of the contact along the slidewire now changes the input power to the thermocouple gauge which changes its temperature and thus alters the signal voltage. The gauge will therefore be held at some constant temperature which will be determined by the resistance ratio in the fixed potentiometer. Because the power dissipation of the thermocouple gauges is quite low, there is no danger of damaging the slidewire. If the added potentiometer is carefully matched to the resistance of the slidewire the operation of the rest of the instrument is unaffected and the self-calibrating mechanism will still set the voltages accurately. Thus by a simple calculation one can set the gauge to any desired temperature value as accurately as one can set the resistance ratio.

Conversion to this operation is extremely simple. A 5-wire cable is made up with three wires connecting to a previously matched potentiometer and two wires connected in series with the power supply of the thermocouple gauge. The slide wire is disconnected at its terminal board and the two wires connected to the fixed terminals of the slidewire. The 3-wire group is now connected to the leads just disconnected from the slidewire (with due attention to phasing of the individual wires). A short jumper is now connected from the rider of the slidewire to one end or the other of the slidewire, transforming it into a rheostat. The particular choice of terminals here will alter the phasing of the self-balancing mechanism. When the signal leads of the gauge are connected up to the instrument in the normal fashion and phasing adjusted, the instrument is ready.

Once the phasing is correct the leads of the 5-wire cable can be permanently connected to a suitable terminal strip to match the instrument terminals. Converting between normal operation and operation as a pressure gauge is now only a matter of loosening six screws, inserting the terminal strips and retightening the screws.

Since the slide wire had a resistance of only 20 ohms in the model adapted, it was necessary to add a second larger rheostat in series, to set the instrument on scale. A resistance of 200 ohms worked quite well with a 2 volt battery. Power input was determined by measuring the voltage drop across a standard resistance of approximately an ohm. Since

Reproduced with permission of the copyright owner. Further reproduction prohibited without permission.

the heater resistance was constant, the square of the voltage drop across the standard resistance was proportional to the power input. This voltage was read with a very precise potentiometer.*

A6 SENSING ELEMENTS

The sensing elements were small enough so that work was done under a low-power microscope. The coils were hand-wound using a No. 14 beading needle (about 0.012" diameter) as a mandrel. The wire was wound in a tight spiral coil of some convenient length. The spiral was subsequently stretched to give a pitch angle of about 45° and the required length cut off (with a pair of dissecting scissors). Two coils in the middle of this section were stretched, using jewellers' tweezers, to form a straight section at the crossover point. The Kovar-glass terminals were mounted in a simple jig (Fig. A4) and aligned to fit in their corresponding grooves in the gauge body. The ends of a precut spiral were slipped over the inner ends of two opposing terminals and the spiral carefully spot-welded at the crossover point to a matching spiral of the other metal. This junction was carefully inspected and, if satisfactory, the ends of the spirals were spot-welded to the lead-throughs at several points. After a final careful inspection and alignment, the element was soldered inside the gauge-head as previously mentioned. (In a preliminary model epoxy cement was used quite successfully instead of solder.)

The spot-welding of the center crossover point was the most difficult part of this operation, in that not all welds were equally reliable. Since the time spent in actually assembling these gauges was not too great, a record of 50% success was quite acceptable.

A7 CONSTRUCTION OF PROBES

A7.1 Analysis of Relative Gauge Dimensions

The gauges were wanted for two particular functions:

1. As a gauge-head for a free-molecular pressure-probe.

2. As a gauge small enough to be embedded in a 1/8" thick flat plate.

While it is fairly obvious that the second application calls for a tiny gauge, the reason for a small internal volume in the first application may not be so apparent. In a free-molecular probe it is required that the tube diameter be a small fraction of a mean-free path, preferably 1/10. If one

---

* Brown-Rubicon self-balancing potentiometer -- 0-70 m.v. Minneapolis-Honeywell. This instrument has a least count of 2 microvolts.

Reproduced with permission of the copyright owner. Further reproduction prohibited without permission.

wants to go to higher pressures, the mean-free path is proportionately less so that the probe size must be smaller. The time required for a given volume of gas to flow through a tube is inversely proportional to the tube's internal cross-sectional area and hence, so is its response time.

The mass of gas given off by a wall (outgassing) is a function of its area so that the volume of outgassing from a gauge will be directly proportional to the internal area and inversely proportional to the pressure. For a given Knudsen number the cross-sectional area of a tube must decrease as the square of the pressure which means that for a given outgassing time the volume of outgassing must also be decreased as the pressure squared. This in turn, demands, that the internal area be inversely proportional to the pressure. *

The practical result of this is that the smaller an internal volume one can obtain, the higher is the pressure at which one can operate a free-molecule pressure probe.

In the absence of outgassing, a similar analysis shows that for a constant response time the dimensions must vary as $(p)^{-2/3}$.

In practice, outgassing times are much longer than response times and depend more on construction techniques and materials than on dimensions. However this analysis indicates that it is possible to get better performance or operate at lower pressures by decreasing gauge-head volume.

A7.2 Pressure-Pair Probe

A particular form of gauge, the pressure-pair probe was developed to measure molecular speed ratio, S, directly. This requires two separate gauge-heads at identical temperatures each connected to a separate probe. The metal gauge previously described proved ideal for this application since by putting two heads side by side in a single metal block, the gauge wall-temperature is automatically kept identical in both gauges.

---

* Assume mass of gas released from walls is $M = CA$ micron-liters (where A is the actual internal surface area of probe and gauge-head).

$\therefore$ Volume of gas evolved $= C_1 A/p$ liters.

But λ is proportional to $1/p$. If K_n is to be kept constant,

$\therefore$ d must be proportional to $1/p$

the cross-sectional area of the tube therefore varies as $1/p^2$

$\therefore$ volume of gas passed/unit time $\sim 1/p^2$

$\therefore$ To keep the response time constant, the outgassing volume must change as d changes. i.e. $\dfrac{C_1 A}{p} = C_2 \dfrac{1}{p^2}$

That is, the internal area, A, is proportional to $1/p$

(and if all dimensions scaled d is proportional to $p^{-\frac{1}{2}}$)

Reproduced with permission of the copyright owner. Further reproduction prohibited without permission.

For all sizes of probe tips down to 0.008", stainless steel hypodermic tubing proved satisfactory. Connections between the gauge-head and probe tip were made with larger gauge stainless-steel tubing.

A7.2.1 Glass Probe Tips

In recognition of the need for working at higher pressures, some time was devoted to developing techniques for producing smaller diameter probes. Below about 0.008" the hypodermic tubing becomes rather too flexible and difficult to work with. In this range the superior stiffness of glass tubing recommended itself. Glass tubing may be drawn down to any size without losing its tubular form by simple glass-blowing techniques. By proper manipulation the wall thickness can be controlled over wide ranges. The speed with which such probes can be made and their relative freedom from outgassing were further recommendations.

Glass probe-tips were made by a double-draw technique. Small-bore Pyrex glass tubing (5 mm is quite suitable) was first drawn down in an oxygen flame to a long tube about 0.020 to 0.040" O.D. or whatever diameter was desired. These draws were usually made at a relatively high temperature to give a thick wall. The resulting tube was quite strong and rather stiff. This draw was cut to a suitable length and the end then carefully re-drawn over an alcohol burner to give a final probe tip of the required diameter. These tips can be drawn as small as 0.002" if the draw is performed under a low-power microscope. For an impact probe, the tip was broken off square and carefully lapped, (under a microscope), with a fine grain sharpening stone to give a flat end which was perpendicular to the tube axis. For the static probe a very clean hole could be made in the tube wall by the following method.

A wire was threaded down the bore of the tube at least as far as the point to be perforated and the wire connected to one terminal of an adjustable high voltage power supply (0 - 5 KV). A heater wire was mounted perpendicular to the axis of the tube just below the point where the hole was desired. This heater wire was connected both to an adjustable source of power, sufficient to heat it to a dull red glow, and to the other terminal of the high-voltage power supply. (A five mil chromel wire connected across a 2.5 volt filament transformer, which in turn was controlled by a Variac, proved quite satisfactory.)

When everything was connected, the high-voltage supply was set at, say, 5 KV and the heater current cautiously raised until a spark jumped between the wires so as to pierce the glass wall. The high-voltage was immediately shut off. (Needless to say the high-voltage supply must be adequately protected against burn-out in this operation.) The heater power was then turned off and the high voltage run up again until sparking just occurs. The size of the hole punched could then be regulated by length of time this sparking was allowed to continue.

Reproduced with permission of the copyright owner. Further reproduction prohibited without permission.

The hole so obtained should be quite round with well-defined edges and straight walls. The surfaces should be perfectly smooth. Any indication of cratering or jagged edges indicated that the hole was punched at too high a voltage. The function of the heated wire was to reduce the insulating properties of the glass by raising the temperature, so that the spark jumped at a low enough voltage to avoid shattering the glass. Therefore, if signs of cratering appeared, the high voltage would be lowered and the heater temperature raised. It was found advisable that the whole operation be performed under a low-power microscope so that all phases were under visual control.

Since the glass seemed to be left in a state of strain by this procedure the tube was gently heated in this region to remove these strains. The tip of the probe was then sealed off (by a gentle draw in a flame) and the probe was completed. A large number of such probes could be made in a fairly short time and the desired size chosen by selection. While close tolerances were not easily held in the technique described, dimensions were not very critical.

The practical lower size limit of these probes is probably around 0.002 inches O.D. although such a size was never attempted. If special small flames and very thin wires were to be used, the probes might be made even smaller. However, it was felt that the outgassing times of such probes would be much too great for convenience.

This type of probe tip has been used on all-glass probes and gauge-heads with satisfactory results. No occasion arose to apply them to the all-metal gauge heads, but no problems are expected. They could readily be mounted on connecting hypodermic tubing by waxing, cementing or by a proper glass-to-metal seal.

A8 CALIBRATION OF GAUGES

The calibration of vacuum gauges is a procedure which contains many pitfalls. A considerable body of experience has been developed on the subject, most of which can be found in the literature (Ref. A1). Since not everyone in this field has made use of this information, however, it seems adviseable to describe the procedure followed in some detail.

A8.1 McLeod Gauge

The primary standard in most vacuum calibrations is the McLeod gauge. It is well known that this gauge will not measure partial pressures of condensible gases, but other features, not so well known, will bear repetition. Leck (Ref. A1) in his review of the McLeod gauge has explained that the accuracy of the gauge depends on the uncertainty in the angle of contact of the meniscus between the mercury and the glass capillary. This has the interesting result that the probable percent error

Reproduced with permission of the copyright owner. Further reproduction prohibited without permission.

of any single reading is independent of the bore-diameter of the capillary and is inversely proportional to the total cut-off volume of the gauge. Since it is not generally realized how large this error can be, a graph of this is given (Fig. A6). This is calculated on the basis of a 100 c.c. cut-off volume. Doubling the cut-off volume would simply halve the error.

Variations in surface conditions in the capillary will cause local systematic errors which can be much larger than this. Careful cleaning and use of high purity mercury will reduce this problem but not eliminate it. As an example, the readings of two McLeod gauges were plotted against each other in such a way as to produce a linear relationship (i.e. h_1 or $\sqrt{P_1}$ vs h_2 or $\sqrt{P_2}$) (Fig. A7). Both gauges had been used for some time on the tunnel but had just been carefully cleaned with nitric acid, rinsed with distilled water, than acetone and finally baked overnight in a glass blower's annealing oven. (This latter step is an excellent way of removing every trace of carbon and organic material.) Both gauges were then charged with very high purity mercury.* In spite of these precautions there were very large deviations from a straight-line plot. These points cover a pressure range from 0-50 microns, the cut-off volume of one gauge being 100 cc; the other 400 cc. The random error at any one pressure as indicated by the scatter of point is essentially that predicted by Fig. A6 but there is a large deviation of some pressure measurements from a straight line due to local systematic error as well. Obviously however, the best fit is still a straight line.

A8.2 Calibration of Thermocouple Gauges

The linear relationship between power input and pressure was made use of in the calibration of the thermocouple gauges. Both theory and experiment indicate that a plot of input power vs. pressure will give a straight line for the thermocouple gauges (at least for pressures less than 100 microns.) By calibrating the gauge at many different pressures and plotting input energy (actually $(mv)^2$) vs. pressure it was possible to fit a straight line to the calibration points. This method tended to eliminate the local systematic errors in the McLeod gauge and minimize the random errors, so that the final calibration of the thermocouple gauges was more accurate than the best possible accuracy one could get for a single-point calibration. Thereafter the thermocouple gauge sensitivity determined by this method was given more weight than single McLeod gauge readings.

The actual calibration was done by a dynamic method. The vacuum pumps were throttled back by partially closing their flap valves, to reduce backstreaming of oil vapor to a minimum. A very small flow of

---

* Cathodic Grade: guaranteed impurities less than 1 ppm
F. W Berk and Co. Inc., Woodbridge, N.J.

Reproduced with permission of the copyright owner. Further reproduction prohibited without permission.

air was admitted to the chamber to continuously purge the tunnel and so ensure an atmosphere which was truly air. The probes and gauges were then outgassed at a very low pressure ($\simeq 2 \times 10^{-4}$mm) until all evidence of outgassing had disappeared. McLeod gauge and thermocouple readings were then taken to get a zero reading. The bleed of air was then increased slightly and the tunnel allowed to equilibrate to its new pressure. McLeod and thermocouple gauge readings were then obtained at this second point. The process was repeated at suitable pressure intervals to obtain the desired calibration curve.

Caution must be observed in this form of dynamic calibration to ensure that the gauges are in stagnant air. Otherwise, ram effects can easily give systematic errors of 100 percent or more! At some pressures, the booster pumps began to perform erratically, making it difficult to get constant pressure levels. When this occurred the boosters were isolated and calibration continued using the mechanical vacuum pumps alone.

A9 PERFORMANCE

Because of the sensitivity of the power-supply circuit the gauge was a notable success. The coarse rheostat of the power circuit was first adjusted to set the instrument near the mid-point of its control range and the instrument allowed to settle down. Voltage readings, proportional to the current through the heater filaments were measured on the potentiometer to the nearest microvolt, giving five-figure precision. Because of the uncertainty in the McLeod gauge calibration the last figure could not be used, although no measurable short-term drift or jitter was apparent. The self-calibrating feature kept instrument drift to a negligible level, while the self-balancing feature automatically compensated for changes in battery voltage. At low wire-temperatures the gauge was somewhat sluggish in its response, though not to the point where it degraded its performance. The gauge was sensitive to wall temperature changes in that the change in radiative heat transfer caused a detectable zero shift. The wire temperature was inadvertently run at 150°C rather than 50°C above wall temperature for most of the experiments, so that this temperature zero shift was larger than it need have been.

When used on a speed-ratio probe, the gauge-heads were subject to large changes in temperature, in which case the zero shift was somewhat of a problem, but for a variation of a few degrees it was negligible. Because of the "clean" atmosphere and low wire-temperature there was no observable change in calibration such as sometime occurs when accommocation coefficient and emissivity change due to decomposition of vapours on the sensing element.

While the resolution of the gauge was better than 10^{-5} mm, the usable sensitivity was limited by the temperature drift. This effect

Reproduced with permission of the copyright owner. Further reproduction prohibited without permission.

can be decreased by decreasing the temperature difference between wall and heater, (e. g. Eq. A2. 7,) but it would seem that for greater precision it would be advisable to thermostat the gauge-head by some means. In this case the usable sensitivity should be in the neighbourhood of 10^{-5} mm at 10^{-2} mm Hg. There is little hope of calibrating the gauge to anything like this accuracy, but since all one usually wants is the ratio of pressures, errors will tend to cancel. In this case it might be possible to utilize the full sensitivity of the gauge.

A10 RESULTS

Because of limitations on the upper range of the McLeod gauge no attempt was made to extend calibration to the upper limit of the thermocouple gauge' range. A semi-log plot of P vs. millivolts (proportional to current input to gauge) is shown in Fig. A8. At the highest reading, (1. 2 mm), there was no indication of a drop in sensitivity. From the performance of other hot-wire gauges it seems likely that the upper limit might be one to two orders of magnitude higher .

The change in zero reading due to wall temperature changes is shown for one of the gauges in Fig. A9. In this experiment the change in wall temperature was quite extreme. Figure A10 gives the calibration curve p vs. mv^2 for this gauge. This particular gauge was embedded in a glass plate 1/8" thick and had an estimated internal volume of 0. 04 cc. It had a somewhat lower sensitivity than the larger gauges and relatively high radiation loss. It therefore could be expected to have a very high zero shift for a given temperature rise. From the slope of Figure A9 it is possible to calculate that the shift is approximately 0. 07 microns/degree C.

Figure A11 gives a p vs. mv^2 calibration curve for the two gauges in a pressure-pair probe. It is estimated that the temperature shift would be about 0. 01 microns/degree C in these gauges.

A11 CONCLUSIONS

The use of a thermocouple vacuum gauge in the constant-temperature mode has proved to result in a very sensitive, yet stable and rugged gauge, one that can be constructed in the laboratory from readily available materials and by simple techniques. This allows the experimentalist to build his own gauges to suit his particular application. The use of a modified self-balancing millivoltmeter greatly simplifies the operation of this gauge and enhances it precision. While these instruments are rather expensive they are common equipment in many laboratories. The modification is so easily and quickly accomplished that the unit can be converted from one use to the other at will.

The data presented here indicate that the accuracy of these gauges will always be limited by the accuracy of the calibrating

Reproduced with permission of the copyright owner. Further reproduction prohibited without permission.

standard. The range of the gauge should be several orders of magnitude greater than commercially available equipment. While the usable sensitivity is limited by a small zero shift due to changes in wall temperature, a crude form of temperature regulation would probably give them a sensitivity of say 10^{-5} mm at 10^{-2} mm.

No indication of a change in sensitivity of the gauge was found during more than a month's constant use. The gauge seemed to be entirely free from the random zero shift that plagues the Pirani gauge, although this particular fault might have been missed if it were smaller than 10^{-4} mm.

The development of small, sensitive, pressure-gauges and small probe tips has increased the pressure at which free-molecule probes may be used. Experiments already conducted have been carried out a full decade above pressures previously possible and the technique can certainly be extended by another decade.

A further application of this circuit could be made to the free-molecule heat-transfer gauge (Ref. A2). By employing crossed thermocouple wires instead of a heated tungsten wire (i.e. thermocouple vs. Pirani gauge) the use of this instrument could probably be greatly simplified.

REFERENCES*

1. Leck, J.H. Pressure Measurements in Vacuum Systems, Institute of Physics, London, 1957.

2. Laurmann, J.A. Ipsen, D.C. Use of a Free Molecule Probe in High Speed Rarefied Gas Flow Studies, Oct. 1957, WADC Tech. Rep. 57-440.

---

* Also in main list.

Reproduced with permission of the copyright owner. Further reproduction prohibited without permission.

TABLE OF CONTENTS

APPENDIX B

		Page
B1.	INTRODUCTION	B1
B2.	MATHEMATICAL DEVELOPMENT OF DISTRIBUTION FUNCTION	B2
B3.	DETERMINATION OF FLOW PROPERTIES	B6
	B3.1 Density Near the Leading Edge	B7
	B3.2 Tangential Velocity Near the Leading Edge	B9
	B3.3 Vertical Velocity Near the Leading Edge	B10
	B3.4 Temperature Near the Leading Edge	B10
	B3.5 Speed Ratio Near the Leading Edge	B12
B4.	DISCUSSION	B13
	B4.1 Maxwell Slip Conditions	B13
	B4.2 Basic Assumptions	B14
B5	CONCLUSIONS	B15

Reproduced with permission of the copyright owner. Further reproduction prohibited without permission.

NOTATION

APPENDIX B

dA	infinitesimal area
c_m	most probable speed of molecules $= \sqrt{2RT}$
$\overline{c^2}$	average value of c^2
c_i	component of random velocity of a molecule in the x_i plane
ζ_i	non-dimensional random velocity components
$\operatorname{erf}\lambda$	$\frac{2}{\sqrt{\pi}} \int_0^{\lambda} e^{-\zeta^2} d\zeta$ error function
f	distribution function
k	proportionality constant used in the Rayleigh analogy to convert time to distance from the leading edge of a flat plate ($kx = Ut$)
L	symbol for the Laplace Transform
m	mass of molecule
n	number density of molecules in the gas (number/unit volume)
p	pressure, in particular, static pressure
R	gas constant (per unit mass)
s	molecular speed ratio $s = U/c_m$
s	transformed variable of the Laplace transformation
t	time
T	temperature
T'	$\sqrt{T_o \cdot T_w}$
J	nondimensional temperature jump $2 \cdot \frac{T_w - T_{(x,o)}}{T - T'}$
U	free-stream velocity
$u, v, w,$ u_1, u_2, u_3	alternate designators of the directed velocity components of the gas in cartesian coordinates

Reproduced with permission of the copyright owner. Further reproduction prohibited without permission.

x, y, z x_1, x_2, x_3	alternate designators of the cartesian coordinates
α	accommodation coefficient $\equiv \frac{T_{in} - T_{out}}{T_{in} - T_w}$
β	constant used in the modified Boltzman equation, proportional to collision frequency
ρ	density = nm
η_o	$\frac{yu}{KX\ cmo}$
η_w	$\frac{yu}{kx\ cm}$
λ	mean free path
μ_o	$2 \cdot \frac{V(x,y)}{\lambda m_o} - \eta_o$
μ_w	$2 \cdot \frac{V(x,y)}{\lambda m_w} - \eta_w$
ξ, η, ζ	running variables for velocities in the three cartesian coordinate plane
φ_o	$1 + 2/3 \left(\frac{U - U(x,y)}{\lambda m_o} \right)^2 + 2/3 \left(\frac{V(x,y)}{\lambda m_o} \right)^2$
φ_w	$1 + 2/3 \left(\frac{U(x,y)}{\lambda m_w} \right)^2 + 2/3 \left(\frac{V(x,y)}{\lambda m_w} \right)^2$

Subscripts and Superscripts

o	designating conditions at time $t \neq 0$ (free stream conditions)
eq	designating conditions at time $t = \infty$ (wall conditions)
w	designating wall conditions
(-)	related to the negative (incoming) part of a two-stream distribution function
(+)	related to the positive (outgoing) part of a two-stream distribution function
'	designating a system of coordinates with free stream velocity
''	designating a system of coordinates fixed with respect to the wall
·	designates the Laplace transform of a function

Reproduced with permission of the copyright owner. Further reproduction prohibited without permission.

APPENDIX B

A Kinetic Theory Solution for Flow Near the Leading Edge of a Flat Plate

B1. INTRODUCTION

The historic Blasius solution for boundary-layer growth along a flat plate fails for small Reynolds number and therefore leaves uncertain the situation at and near the leading edge of the plate. Many attempts have been made to extend the theory to lower Reynolds number, or to produce a new solution which would hold at the leading edge, but progress has been hampered to a large extent by the lack of experimental data to verify theory. For an infinite plate in continuum flow there is no obvious characteristic dimension, so that changing the scaling factor must not change the form of the solution. It was this fact that allowed Blasius to postulate a one-parameter type of solution for this problem. As one increases the "magnification" it must eventually occur that the individual motion of the gas particle will become apparent and at this stage an obvious characteristic dimension has appeared - the mean-free path of the molecules. It is thus no longer possible to postulate a single-parameter solution for this region. As the pressure of a gas is decreased the mean-free path increases so that in a given system the distance from the leading edge at which the Blasius solution fails will also increase. In the U. T. I. A. S. Low-Density wind tunnel it is possible to decrease the pressure to the point where flow in this region may be investigated experimentally with sufficient spatial resolution to separate out the desired information.

Since experimental data could be obtained, a theoretical solution against which they might be tested was also desirable. In this region the usual boundary-layer assumptions, particularly that of a thin boundary layer, are quite untenable, so that extrapolations from boundary-layer theory seemed unsatisfactory. Similarly, no reliable set of boundary conditions seemed available to match with the Navier-Stokes equations, so that such an approach seemed of doubtful value.*

Some attempts have been made to solve the Rayleigh problem (an infinite flat plate started impulsively from rest) by means of the Maxwell-Boltzmann equations, rather than the Navier-Stokes equations. Any solution obtained can be related to flow around the leading edge of a flat plate by assuming the distance along the plate in the latter case as being related to time elapsed in the former by the relation $x = kUt$ where U is flow velocity. In general the mathematics have been too involved to allow an explicit solution (Ref. B1) so that approximate methods are

---

* Reference B3 gives an adequate discussion of various attempted solutions

Reproduced with permission of the copyright owner. Further reproduction prohibited without permission.

usually resorted to. Yang and Lees (Ref. B2 and 3) have tried a linearized treatment using Grad's 13-moment equation (Ref. B4) but were forced to use approximate assymptotic solutions for long and short times because of mathematical difficulties. As an alternative method they dropped the collision terms in the Maxwell-Boltzmann equations and got a "zero-order" solution of a very simple form (Ref. B3). In this case however, the solutions are independent of time (or distance along the plate) at the plate surface, a rather unconvincing result.

The question arises, whether or not a slightly more meaningful approximation to the Maxwell-Boltzmann equations is possible, which will still yield explicit solutions to the Rayleigh problem. The so-called "Modified Boltzmann Equation" or "Single Relaxation-Time Boltzmann Equation" (Ref. B5) as introduced by Krook (Ref. B6) has a very simplified form of the collision parameter and has been successfully exploited to get solutions in closed form which resemble solutions of the true Maxwell-Boltzmann equations except for the values of various constants. Since an idea of the functional relationship was all that was required in this instance this model was investigated more fully. It became apparent that a solution of a somewhat restricted nature was possible.

B2. MATHEMATICAL DEVELOPMENT

The Boltzmann equation can be written:

$$\frac{\partial f}{\partial t} + \xi \frac{\partial f}{\partial x} + \eta \frac{\partial f}{\partial y} + \zeta \frac{\partial f}{\partial z} = \iint n' (f_1' f_2' - f_1 f_2) \cdot \sigma^2 \Omega \cos\psi \, d\chi \, d\omega_2 \qquad \text{(B2.1)}$$

where the meaning of the symbols are defined in many standard texts (e.g. Ref. B7). For the one-dimensional time-variant case the left-hand side becomes:

$$\frac{\partial f}{\partial t} + \eta \frac{\partial f}{\partial y}$$

For the modified Boltzmann equation it is usual to write (for one-dimensional time-variant case):

$$\frac{\partial f}{\partial t} + \eta \frac{\partial f}{\partial y} = \beta (f_{eq} - f) \qquad \text{(B2.2)}$$

where η is the velocity in the y direction, f is the distribution function at any given point, f_{eq} is the local drifting Maxwellian distribution function which yields values for density, mean momentum and mean energy equal to those for the distribution function f and β is a function of collision frequency (considered constant). This equation expresses, in a particularly simple form, the strong tendency of a gas to assume the equilibrium value.

Reproduced with permission of the copyright owner. Further reproduction prohibited without permission.

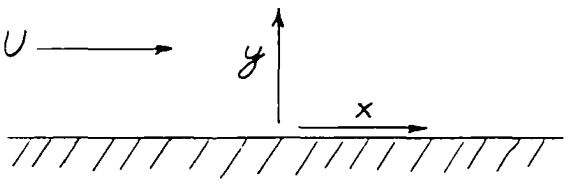

Let us assume an infinite plate, in equilibrium with its surroundings, as being impulsively brought to rest at t = 0 from an original velocity U. Assume that the gas has a Maxwellian distribution of random velocities at temperature T_o and is traveling at mass velocity U i. e.

$$f_o = \frac{n_o e^{-c_i^2}}{\pi^{3/2} c_{m_o}^3} \qquad \text{(B2. 3)}$$

Assume the plate takes on a temperature of T_w at $t > 0$. Another equilibrium distribution will be attained at time $t = \infty$, at which time the temperature will be T_w and the gas will have zero velocity i. e.

$$f_{eq} = \frac{n_{eq} e^{-c_i^2}}{\pi^{3/2} c_{m_w}^3} \qquad \text{(B2. 4)}$$

where $c_i = \frac{c_i}{c_m} \equiv \frac{\text{ith component of random velocity}}{\sqrt{2RT}}$

To render the equations soluble, f_{eq} in Eq. B2. 2 will be replaced by f_{eq} of Eq. B2. 4. Admittedly, this is a very drastic simplification of the problem, because the local tendency for the distribution function to approach a Maxwellian is now replaced by a tendency to approach the final steady-state solution with the same time constant at each instant and position. It is also clear that this simplified form violates the condition that number, momentum and energy are conserved in binary collisions. In view of this serious shortcoming no rigorous conclusions can be drawn from the results. Nevertheless, the calculations were made in the hope that some overall features of the phenomenon would be brought out explicitly by the theory.

Since β is assumed constant the equation can be solved simply by Laplace transformations (Ref. B8).

$$\alpha \frac{\partial f}{\partial t} = s\bar{f} - f[o] \qquad \text{(B2. 3)}$$

Reproduced with permission of the copyright owner. Further reproduction prohibited without permission.

where $f_{[o]} \equiv$ free-stream value of f(f at $t < o$)

$$\therefore \; s\bar{f} + \eta \frac{d\bar{f}}{dy} + \beta \bar{f} = \frac{\beta f_{eq}}{s} + f_0 \qquad \text{(B2.5)}$$

$$\frac{d\bar{f}}{dy} = -\frac{s+\beta}{\eta}\left(\bar{f} + c_1\right) \qquad \text{(B2.6)}$$

where

$$c_1 = -\frac{\beta/s\, f_{eq} + f_0}{s+\beta} \qquad \text{(B2.7)}$$

i.e. $\log(\bar{f} + c_1) = -\frac{s+\beta}{\eta} y + \text{Const.}$

$$\therefore \; \bar{f} = -c_1 + c_2 e^{-\frac{s+\beta}{\eta} y} \qquad \text{(B2.8)}$$

From physical conditions the solution can be considered in two parts as η is assumed positive or negative, that is, as a two-stream function. The form of the two streams need not be identical at y = 0 but must approach symmetry as $y \to \infty$ due to molecular collision (i.e. they must be two halves of a Maxwellian distribution). This is the first boundary condition, i.e. $f_+ \to f_{(-)}$ at $y \to \infty$.

If one assumes perfect accommodation at the wall ($\alpha = 1$) then the outgoing stream will be the positive portion of f_{eq} ($\equiv f_w$).

Thus

$$f_{+(y=0)} = f_w \qquad \text{for } \eta > 0 \qquad \text{(B2.9)}$$

i.e. $$\left(\bar{f}_+\right)_0 \equiv \frac{f_w}{s} = \frac{\beta f_w + s f_0}{s(s+\beta)} + c_{2+} \qquad \text{(B2.10)}$$

from Eq. B2.8

$$\therefore \; c_{2+} = \frac{f_w - f_0}{s+\beta} \qquad \text{(B2.11)}$$

Reproduced with permission of the copyright owner. Further reproduction prohibited without permission.

so that $$\bar{f}_+ = \frac{f_w}{s} - \frac{f_w}{s+\beta} + \frac{f_0}{s+\beta} + \frac{f_w - f_0}{s+\beta} \cdot e^{-\frac{s+\beta}{\eta} y}$$

thus $$f_t = f_w - (f_w - f_0)\, e^{-\beta t} \qquad t < y/\eta$$
$$= f_w \qquad t \geq y/\eta \quad (\eta + \infty) \qquad \text{(B2.12)}$$

as $y \to \infty$ $\quad f_+ = f_-$ and therefore $\bar{f}_+ = \bar{f}_{(-)}$

so that at $y \to \infty$

$$c_{2+} \cdot e^{-\frac{s+\beta}{|\eta|} y} = c_{2-}\, e^{+\frac{s+\beta}{|\eta|} y}$$

$$\therefore c_{2-} = c_{2+}\, e^{-\frac{2(s+\beta)}{|\eta|} y} = 0 \qquad \text{(B2.13)}$$

$$\therefore \bar{f}_- = \frac{f_w}{s} + \frac{f_0 - f_w}{s+\beta}$$

so that $$f_- = f_w - (f_w - f_0)\, e^{-\beta t} \qquad \text{(B2.14)}$$

where $$\eta < 0$$

Combining B2.14 and B2.12 gives:

$$f = f_w + (f_0 - f_w)\, e^{-\beta t} \qquad \eta < y/t$$
$$= f_w \qquad \eta \geq y/t \qquad \text{(B2.15)}$$

The distribution function of the stream varies with distance above the plate in a rather striking way and the shape of the η component of this distribution function itself is not too hard to visualize. At any point $\eta < y/t$ the probability of a particle having a velocity η assumes a mean value between that for f_0 (the incoming wave) and f_w (the outgoing wave) where the mean is weighted by the factor $e^{-\beta t}$. For $\eta > y/t$ the probability is given by f_w alone. At fixed time, t, the shape of the distribution function can be thought of as a fixed contour which is independent of y upon which is superposed a step-function moving so that it always appears at the point $\eta = y/t$. The amplitude of this step-function is such that for velocities above this value the distribution is that of the final state f_w.

The fixed contour itself changes with time, having the shape of a Maxwellian distribution (fo) at t = 0 and decaying to that of fw expon-

Reproduced with permission of the copyright owner. Further reproduction prohibited without permission.

entially as $t \rightarrow \infty$. The size of the step function that converts the "fixed" contour to fw thus varies with t and y. The ξ and ζ components of the distribution function are more difficult to visualize in that they depend on the value of the η component with which they are associated and obey either $fw + (fo - fw)e^{-\beta t}$ if $\eta < y/t$ or f_w if $\eta \geq y/t$

By the analogy $kx = Ut$ one can transform the impulsive motion of an infinite flat plate into flow around the leading edge of a thin flat plate, where x is the distance from the leading edge, U is plate velocity at $t < 0$ and k is a proportionality constant, (probably close to 1).

We thus get:

$$f = f_w + (f_0 - f_w)\, e^{-\frac{\beta k x}{U}} \quad \text{for } \eta < \frac{yU}{kx}$$
$$= f_w \quad \text{for } \eta \geq \frac{yU}{kx} \qquad \text{(B2.16)}$$

By comparison with the Yang and Lees solution (Ref. 3), it can be seen that step-functions represent the contribution from the transport terms of the Boltzmann equation, while the exponential term represents the modification due to inter-molecular collision. For the true Boltzmann equation one might expect a more complicated expression, so that it should not be too surprising that this simple analysis itself does not lead to the Navier-Stokes solution for the case of $x \rightarrow \infty$.

B3. DETERMINATION OF FLOW PROPERTIES

Knowing f it is possible to calculate all significant flow parameters by means of the Maxwell transfer equations (Ref. 1).

Thus $$\rho(x,y) = \overline{m\, n_{xy}} = m \int_{-\infty}^{\infty}\int_{-\infty}^{\infty}\int_{-\infty}^{\infty} f \, d\xi_1 \, d\xi_2 \, d\xi_3 \qquad \text{(B3.1)}$$

where $\xi_i = U_i + c_i$ (U_i is directed motion and c_i is random motion)

where we write:

$$f_w = \frac{n_w\, e^{-c_i''^2}}{\pi^{\frac{3}{2}} c m_w^3}$$

$$f_0 = \frac{n_0\, e^{-c_i'^2}}{\pi^{\frac{3}{2}} c m_0^3}$$

$$\xi_1 = c_1'' = c_1' + U = c_1 + U_1 \qquad \text{(B3.2)}$$
$$\xi_2 = c_2'' = c_2' = c_2 + U_2$$
$$\xi_3 = c_3'' = c_3' = c_3 + U_3$$

Reproduced with permission of the copyright owner. Further reproduction prohibited without permission.

Here the primed coordinates are used with the free-stream distribution function f_o, and the double primed are used with the wall distribution function, f_w. Let unprimed values refer to any general system of coordinates.

B3.1 Density Near Leading Edge of Flat Plate

$$\rho(x,y) = m \int_{-\infty}^{\infty}\int_{-\infty}^{\infty}\int_{-\infty}^{\infty} f \, d\xi_1 \, d\xi_2 \, d\xi_3$$

but from Eq. B2.16 we can write this:

$$\overline{m n_{(x,y)}} = m \int\int\int_{-\infty}^{\infty} (f_o - f_w) \, d\xi_1 \, d\xi_2 \, d\xi_3 + m e^{-\frac{\beta R x}{U}} \int\int\int_{-\infty}^{\infty} (f_o - f_w) \, d\xi_1 \, d\xi_2 \, d\xi_3 \tag{B3.3}$$

$$\therefore \overline{n}_{(x,y)} = \int\int\int_{-\infty}^{\infty} \left[f_w + (f_o - f_w) e^{-\frac{\beta R x}{U}} \right] d\xi_1 \, d\xi_2 \, d\xi_3 - e^{-\frac{\beta R x}{U}} \int\int\int_{-\infty}^{\infty} (f_o - f_w) \, d\xi_1 \, d\xi_2 \, d\xi_3 \tag{B3.4}$$

By Eq. B3.2 change variables to

$$c_1' = \frac{c_1'}{c_{m_o}} \qquad c_1'' = \frac{c_1'}{c_{m_w}} \quad \text{etc.}$$

With new limits of integration

$$\eta_o \equiv \frac{yU}{RxC_{m_o}} \text{ and } \eta_w \equiv \frac{yU}{RxC_{m_w}} \tag{B3.5}$$

$$\therefore \bar{n}_{(x,y)} = n_w + e^{-\frac{\beta R x}{U}} \left[n_o \operatorname{erf} \eta_o - n_w \operatorname{erf} \eta_w \right] \tag{B3.6}$$

$\therefore \bar{n}_{(x,y)} = n_w$ for y/x small

$= n_o$ for y/x large

For x = y $\quad \bar{n} = n_w + e^{-\frac{\beta R x}{U}} \left[n_o \operatorname{erf} \frac{U}{RC_{m_o}} - n_w \operatorname{erf} \frac{U}{RC_{m_w}} \right]$

$$\bar{n}_{(y,y)} = n_w + \left[n_o \operatorname{erf} \frac{U}{RC_{m_o}} - n_w \operatorname{erf} \frac{U}{RC_{m_w}} \right]$$

Assuming a perfect gas ($p = \rho RT$)

$$\frac{p_o}{p_w} = \frac{n_o T_o}{n_w T_w} \tag{B3.7}$$

Reproduced with permission of the copyright owner. Further reproduction prohibited without permission.

for a closed system. Since the number of molecules striking the wall must equal the number leaving the wall, a second identity can be established to relate n and T. To do this one must calculate the transport of molecules across a surface dA parallel to the flow.

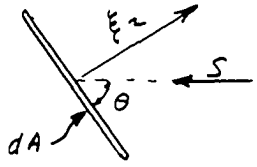

$$dn = \int_{-\infty}^{\infty}\int_{-\infty}^{\infty}\int_{-\infty}^{\infty} f \xi_2 \, d\xi_1 \, d\xi_2 \, d\xi_3 \qquad \text{(B3.8)}$$

at the wall $\frac{\partial U}{\partial RX} = 0$

$$\therefore \; f = f_w + (f_0 - f_w)\, e^{-\frac{\beta RX}{U}}$$ for all incoming particles

and $f = f_w$ for all reflected particles

$$\therefore \; dn = \frac{1}{\pi^2}\left\{\int_{-\infty}^{\infty}\int_{-\infty}^{\infty}\int_{-\infty}^{0} c_{m_w}^4 f_w \, \zeta_2'' \, d\zeta_1'' \, d\zeta_2'' \, d\zeta_3'' \right.$$

$$+ e^{-\frac{\beta RX}{U}}\left[\int_{-\infty}^{\infty}\int_{-\infty}^{\infty}\int_{-\infty}^{0} c_{m_0}^4 f_0 \, \zeta_2' \, d\zeta_1' \, d\zeta_2' \, d\zeta_3' \right.$$

$$\left.\left. - \int_{-\infty}^{\infty}\int_{-\infty}^{\infty}\int_{-\infty}^{0} c_{m_w}^4 f_w \, \zeta_1'' \, d\zeta_1'' \, d\zeta_2'' \, d\zeta_3'' \right] \right\}$$

$$= \frac{c_{mw}}{2\sqrt{\pi}} n_w + e^{-\frac{\beta RX}{U}}\left(\frac{n_0 c_{m_0}}{2\sqrt{\pi}} - \frac{n_w c_{mw}}{2\sqrt{\pi}}\right) \qquad \text{(B3.9)}$$

Similarly the number leaving the surface ($f = f_w$) is

$$dn' = \frac{n_w c_{mw}}{2\sqrt{\pi}} \qquad \text{(B3.10)}$$

but $dn = dn'$

$$\therefore \; \frac{n_w c_{mw}}{2\sqrt{\pi}} = \frac{n_w c_{mw}}{2\sqrt{\pi}} + e^{-\frac{\beta RX}{U}}\left(\frac{n_0 c_{m_0}}{2\sqrt{\pi}} - \frac{n_w c_{mw}}{2\sqrt{\pi}}\right)$$

or $$\frac{n_0}{n_w} = \frac{c_{mw}}{c_{m_0}} \qquad \text{(B3.11)}$$

combining Eq. 3.7 and 3.11 and recalling $\frac{c_{m_0}}{c_{mw}} = \sqrt{\frac{T_0}{T_w}}$ one gets:

Reproduced with permission of the copyright owner. Further reproduction prohibited without permission.

$$\frac{\rho_0}{\rho_w} = \sqrt{\frac{T_0}{T_w}} = \frac{c_{m_0}}{c_{m_w}} = \frac{n_w}{n_0}$$

$$n_0 \rho_0 = n_w \rho_w$$

$$n_w = n_0 \frac{c_{m_0}}{c_{m_w}}$$

$$n_0 - n_w = n_0 \frac{c_{m_w} - c_{m_0}}{c_{m_w}} \qquad \text{(B3.12)}$$

$$= n_w \frac{c_{m_w} - c_{m_0}}{c_{m_0}}$$

From B3.6 we get:

$$\bar{n}_{(x,y)} = n_w \left[1 + e^{-\frac{\beta^* x}{U}} \left(\frac{c_{m_w}}{c_{m_0}} \operatorname{erf} \eta_0 - \operatorname{erf} \eta_w \right) \right] \qquad \text{(B3.13)}$$

at the wall, (y = 0)

$$\bar{n}(x,0) = n_w = n_0 \frac{c_{m_0}}{c_{m_w}} \qquad \text{(B3.14)}$$

B3.2 Tangential Velocity Near the Leading Edge of a Flat Plate

We may write:

$$\bar{n}\,\bar{U}_{(x,y)} = \int_{-\infty}^{\infty}\int_{-\infty}^{\infty}\int_{-\infty}^{\infty} \xi_1 f \, d\xi_1 \, d\xi_2 \, d\xi_3 \qquad \text{(B3.15)}$$

If this equation is manipulated as in Eq. 3.2:

$$\bar{n}\,U_{(x,y)} = \frac{n_0 U}{2} \left(1 + \operatorname{erf} \eta_0 \right) e^{-\frac{\beta^* x}{U}} \qquad \text{(B3.16)}$$

from Eq. B3.14 we get

$$U_{(x,y)} = \frac{U}{2} \frac{c_{m_w}}{c_{m_0}} e^{-\frac{\beta^* x}{U}} \frac{1 + \operatorname{erf} \eta_0}{1 + e^{-\frac{\beta^* x}{U}} \left[\frac{c_{m_w}}{c_{m_0}} \operatorname{erf} \eta_0 - \operatorname{erf} \eta_w \right]} \qquad \text{(B3.17)}$$

$$\therefore \quad U_{(x,0)} = \frac{U}{2} \frac{c_{m_w}}{c_{m_0}} e^{-\frac{\beta^* x}{U}} \qquad \text{(B3.18)}$$

Reproduced with permission of the copyright owner. Further reproduction prohibited without permission.

B3.3 Vertical Velocity Near the Leading Edge of a Flat Plate

Write:

$$\overline{n_{(x,y)}}\ \overline{V_{(x,y)}} = \int_{-\infty}^{\infty}\int_{-\infty}^{\infty}\int_{-\infty}^{\infty} \xi_2 f \, d\xi_1 \, d\xi_2 \, d\xi_3 \tag{B3.19}$$

Treating as Eq. B3.2 one gets:

$$\overline{n_{(x,y)}}\ \overline{U_{(x,y)}} = \frac{n_w c_{mw}}{2\sqrt{\pi}} e^{-\frac{\beta k x}{U}} \left(e^{-\eta_w^2} - e^{-\eta_0^2} \right) \tag{B3.20}$$

$$\overline{U_{(x,y)}} = \frac{c_{mw}}{2\sqrt{\pi}} e^{-\frac{\beta k x}{U}} \frac{e^{-\eta_w^2} - e^{-\eta_0^2}}{1 + e^{-\frac{\beta k x}{U}} \left(\frac{c_{mw}}{c_{m0}} \operatorname{erf}\eta_0 - \operatorname{erf}\eta_w \right)} \tag{B3.21}$$

$$\therefore V_{(x,0)} = 0 \qquad \text{as expected} \tag{B3.22}$$

B3.4 Temperature Near the Leading Edge of a Flat Plate

If we define the temperature as:

$$\overline{c^2} = 3RT$$

we may write:

$$3RT_{(x,y)} \cdot \overline{n}_{(x,y)} = \int_{-\infty}^{\infty}\int_{-\infty}^{\infty}\int_{-\infty}^{\infty} (c_1^2 + c_2^2 + c_3^2) f \, d\xi_1 \, d\xi_2 \, d\xi_3 \tag{B3.23}$$

but $c_i = \xi_i - U_i$ (B3.2)

$$\therefore \quad c_1 = c_1' + (U - u_i) = c_1'' - u_1$$
$$c_2 = c_2' - u_2 = c_2' - u_2 \tag{B3.24}$$
$$c_3 = c_3' = c_3''$$

where $u_1 = U_{(x,y)}$ $u_1 = V_{x,y}$

by using Eqs. B3.24 and B2.16, Eq. B3.23 can be expanded and treated as in previous sections to give

Reproduced with permission of the copyright owner. Further reproduction prohibited without permission.

$$T_{(x,y)} = \frac{T_w \cdot \zeta_w + \sqrt{T_w \cdot T_0}\, e^{-\frac{\beta R x}{U}}\left(\zeta_0 \frac{1+\operatorname{erf}\eta_0}{2} + \frac{2}{3}\mu_0 \frac{e^{-\eta_0^2}}{2\sqrt{\pi}}\right)}{} $$

$$\frac{- T_w\, e^{-\frac{\beta R x}{U}}\left(\zeta_w \frac{1+\operatorname{erf}\eta_w}{2} + \frac{2}{3}\mu_w \frac{e^{-\eta_w^2}}{2\sqrt{\pi}}\right)}{1 + e^{-\frac{\beta R x}{U}}\left(\sqrt{T_w/T_0}\operatorname{erf}\eta_0 - \operatorname{erf}\eta_w\right)} \qquad \text{(B3.25)}$$

where

$$\zeta_0 = 1 + \frac{2}{3}\left(\frac{U - U_{(x,y)}}{c_{m_0}}\right)^2 + \frac{2}{3}\left(\frac{U_{(x,y)}}{c_{m_0}}\right)^2$$

$$\zeta_w = 1 + \frac{2}{3}\left(\frac{U_{(x,y)}}{c_{m_w}}\right)^2 + \frac{2}{3}\left(\frac{U_{(x,y)}}{c_{m_w}}\right)^2$$

$$\mu_0 = 2\frac{U_{(x,y)}}{c_{m_0}} - \eta_0$$

$$\mu_w = 2\frac{U_{(x,y)}}{c_{m_w}} - \eta_w$$

at $y = 0 \quad v \to 0 \quad \mu \to 0 \quad \eta \to \operatorname{erf}\eta \to 0$

$$\therefore T_{(x,0)} = T_w\left[1 + \frac{2}{3}\left(\frac{U_{(x,0)}}{c_{m_w}}\right)^2\right] + \sqrt{T_w \cdot T_0}\, e^{-\frac{\beta R x}{U}}\left[1 + \frac{2}{3}\left(\frac{U - U_{(x,0)}}{c_{m_0}}\right)^2\right]$$

$$- T_w\, e^{-\frac{\beta R x}{U}}\left[1 + \frac{2}{3}\left(\frac{U_{(x,0)}}{c_{m_w}}\right)^2\right] \qquad \text{(B3.26)}$$

$$\therefore T_{(x,0)} = T_w + e^{-\frac{\beta R x}{U}}\frac{\sqrt{T_0 \cdot T_w} - T_w}{2} + \frac{2U_{(x,0)}^2 + e^{-\frac{\beta R x}{U}}\left[\sqrt{\frac{T_w}{T_0}}\left(U - U_{(x,0)}\right)^2 - U_{(x,0)}^2\right]}{6R}$$

Reproduced with permission of the copyright owner. Further reproduction prohibited without permission.

This can be reduced to:

$$T_{(x,o)} = T_w + \frac{e^{-\frac{\beta k x}{U}}}{2}\left\{\left(\sqrt{T_o \cdot T_w} - T_w\right) + \left[\frac{U^2}{3R}\sqrt{\frac{T_w}{T_o}}\right]\cdot\left[1 - \sqrt{\frac{T_w}{T_o}}\cdot\frac{e^{-\frac{\beta k x}{U}}}{2}\left(1 - \frac{e^{-\frac{\beta k x}{U}}}{2}\,\frac{\sqrt{T_w}-\sqrt{T_o}}{\sqrt{T_o}}\right)\right]\right\}$$

$$= T_w + T_w e^{-\frac{\beta k x}{U}}\left\{\frac{\sqrt{T_o}-\sqrt{T_w}}{\sqrt{T_w}} + \frac{S'}{3}\left[1 - \left(\sqrt{\frac{T_w}{T_o}}\,\frac{e^{-\frac{\beta k x}{U}}}{2}\right)\left(1 - \frac{e^{-\frac{\beta k x}{U}}}{2}\,\frac{\sqrt{T_w}-\sqrt{T_o}}{\sqrt{T_o}}\right)\right]\right\} \qquad \text{(B3.26)}$$

where $S' \equiv U/(2R\sqrt{T_o \cdot T_w})^{\frac{1}{2}}$

$$T_{(x,o)} = T_w + \frac{\sqrt{T_o \cdot T_w} - T_w}{2}\, e^{-\frac{\beta k x}{U}}\left\{1 + \frac{U^2}{3R}\,\frac{1}{T_o - \sqrt{T_o \cdot T_w}}\left[1 - \left(\frac{e^{-\frac{\beta k x}{U}}}{2}\sqrt{\frac{T_w}{T_o}}\right)\left(1 - \frac{e^{-\frac{\beta k x}{U}}}{2}\,\frac{\sqrt{T_w}-\sqrt{T_o}}{\sqrt{T_o}}\right)\right]\right\} \qquad \text{(B3.27)}$$

If one writes $T' = \sqrt{T_o \cdot T_w}$

$$\therefore T_{(x,o)} - T_w = \frac{T'-T_w}{2}\, e^{-\frac{\beta k x}{U}}\left\{1 + \frac{U^2}{3R}\,\frac{1}{T_o - T'}\left[1 - \frac{T'}{T_o}\, e^{-\frac{\beta k x}{U}}\left(1 - e^{-\frac{\beta k x}{U}}\,\frac{T'-T_o}{T_o}\right)\right]\right\} \qquad \text{(B3.28)}$$

Suppose $T_w > T_o$ and set $J = \frac{T_w - T_{(x,o)}}{T_w - T'}\cdot 2 \equiv$ normalized temperature jump

$$J = \left\{1 - \frac{U^2}{3R(T'-T_o)}\left[1 - \frac{T'}{T_o}\, e^{-\frac{\beta k x}{U}}\left(1 - e^{-\frac{\beta k x}{U}}\,\frac{T'-T_o}{T_o}\right)\right]\right\} e^{-\frac{\beta k x}{U}} \qquad \text{(B3.29)}$$

B3.5 Speed Ratio Near the Leading Edge of a Flat Plate

If one assumes $c_m \equiv \sqrt{2\,RT}$ it is possible to write an expression for S(x, o)

$$S(x,o) = \frac{U(x,o)}{c_m(x,o)}$$

$$S(x,o) = \frac{\frac{1}{2}\, U_\infty \cdot c_{m_w}/c_{m_o}\; e^{-\frac{\beta k x}{U}}}{\sqrt{2RT_w}\left\{1 + e^{-\frac{\beta k x}{U}}\left[\frac{T'-T_w}{T_w} + S'^2\left\{1 - \frac{T'}{T_o}\, e^{-\frac{\beta k x}{U}}\left(1 - e^{-\frac{\beta k x}{U}}\,\frac{T'-T_o}{T}\right)\right\}\right]\right\}}$$

$$\approx \frac{U_\infty}{2c_{m_o}}\, e^{-\frac{\beta k x}{U}}\left\{1 - \frac{e^{-\frac{\beta k x}{U}}}{4}\left[\quad\right] + \cdots\cdots\right\} \qquad \text{(B3.30)}$$

Reproduced with permission of the copyright owner. Further reproduction prohibited without permission.

where

$$[\quad] \equiv \frac{T'-T_w}{T_w} + \frac{S'^2}{3}\left[1 - \frac{T'}{T_0}\frac{e^{-\frac{\beta\rho x}{U}}}{2}\left(1 - e^{-\frac{\beta\rho x}{U}\frac{T'-T_0}{T}}\right)\right]$$

$$\therefore S_{(x,o)} = \frac{S_\infty}{2} e^{-\frac{\beta\rho x}{U}} - \frac{S_\infty}{8} e^{-2\frac{\beta\rho x}{U}}[\quad] + \frac{3}{32} S_\infty e^{-3\frac{\beta\rho x}{U}}[\quad]^2 + \quad \text{(B3.31)}$$

if $T_w = 500^oK$ $T_o = 300^oK$ $S_\infty = 0.5$

then at the leading edge,

$$S_\infty = \frac{S_\infty}{2}\ (1 + .045 + .008 + \ldots\ )$$

This means the slip speed-ratio will fall off exponentially from the leading edge approximately as

$$S_{(x,o)} = \frac{S_\infty}{2}\ e^{-\frac{\beta\rho x}{U}}$$ with an error of 5% under worst conditions

where $S_\infty = \frac{U_\infty}{\lambda_{m_o}}$ i.e. free-stream value.

B4. DISCUSSION

B4.1 Maxwell Slip Conditions

The Maxwell slip conditions are usually postulated as:

$$U_{(x,o)} = K\lambda\left(\frac{\partial U}{\partial y}\right)_{x,o}$$

The theory given here can be used to check this assumption

Since $$\frac{\frac{\partial U}{\partial y}}{U_{(x,o)}} = \frac{1}{K\lambda}$$ and should be independent of x

according to the Maxwell theory.

But we have $U_{(x,y)} = \frac{U_\infty}{2}\frac{\lambda_{mw}}{\lambda_{mo}}\frac{e^{-\frac{\beta\rho x}{U}}(1+\text{erf}\,\eta_o)}{1+e^{-\frac{\beta\rho x}{U}}\left[\frac{\lambda_{mw}}{\lambda_{mo}}\text{erf}\,\eta_o - \text{erf}\,\eta_w\right]}$

Reproduced with permission of the copyright owner. Further reproduction prohibited without permission.

from Eq. B3.17 where

$$\eta_0 = \frac{\rho U_\infty}{RX} / c_{m_0} \qquad \eta_w = \frac{\rho U_\infty}{RX} / c_{m_w}$$

$$\therefore \left(\frac{\partial U}{\partial \eta}\right)_0 = \frac{2}{\sqrt{\pi}} \frac{U_\infty}{RX} \frac{1}{c_{m_0}} e^{-\frac{\beta RX}{U}} \left[1 - e^{-\frac{\beta RX}{U}} \frac{T_w - T_0}{T'}\right]$$

$$\therefore \frac{\left(\frac{\partial U}{\partial \eta}\right)_0}{U_{(x,0)}} = \frac{2 S_\infty}{\sqrt{\pi} RX} \left[1 - \frac{T_w - T_0}{T'} e^{-\frac{\beta RX}{U}}\right]$$

and is inversely proportional to x even for $T_w = T_0$.

Hence the Maxwell slip conditions do not apply near the leading edge of a flat plate, in this theoretical simplified model. This may be an indication of the limitations of the basic simplified assumption that was made in the writing of the Krook equation.

B4.2 Basic Assumptions

The basic theoretical shortcoming of the particular, simplified version of the simple vibration time model of the Boltzmann equation was indicated in Sec. B2.

This solution of the flow about the leading edge of a flat plate furthermore assumes that the Rayleigh analogy holds (i.e. $X = \frac{Ut}{k}$), even at the leading edge. However it is easily demonstrated that the analogy cannot hold at this point (i.e. where t = 0) since it requires that at negative values of t, (i.e. ahead of the leading edge), the flow be undisturbed. From kinetic theory we know that a certain portion of the molecules striking the leading-edge of an actual plate must be reflected in an upstream direction and therefore must disturb the flow several mean-free paths ahead of the leading edge. This means that the Rayleigh analogy cannot hold at the leading-edge of a flat plate, so that this solution is of limited usefulness. On the other hand, downstream of the leading edge the solution should approximate the behaviour of the flow, so that the analogy should have some value in suggesting functional relationships of the flow parameters in the region between the leading edge and that section where no-slip conditions occur.

This development completely ignores the effect of imperfect accommodation at the walls and is in that way rather unrealistic. On the other hand, so little is known about accommodation that there would be no real gain in rigour even if some form could be devised for allowing for this

Reproduced with permission of the copyright owner. Further reproduction prohibited without permission.

factor. Because of the relatively simple form of the incoming distribution function it might be possible to introduce a process of iteration to account for imperfect energy exchange and modify the reflected wave in the usual fashion (Ref. B2) but it seems that this would defeat the original purpose of producing a simple, explicit solution.

B5. CONCLUSIONS

The relationships developed here have been tested experimentally in the U. T. I. A. S. tunnel and an exponential decay for slip velocity and temperature jump was found as predicted. It seems reasonable to assume that the form of the general predictions made by this theory have some validity in the immediate neighborhood of the leading edge.

REFERENCES*

1. Gross, E. P. Jackson, A. E. — Kinetic Theory of the Impulsive Motion of an Infinite Plane, Phys. of Fluids 1, No. 4, p. 318, (1958).

2. Yang, H. T. Lees, L. — Rayleighs Problem at Low Mach Number According to the Kinetic Theory of Gases, J. Math and Phys. 35, No. 3, (Oct. 1956).

3. Yang, H. T. Lees, L. — Rayleighs Problem at Low Reynolds Number According to the Kinetic Theory of Gases, Rarefied Gas Dynamics, Proceedings F. M. Devienne, Ed., Pergamon Press, 1960.

4. Grad, H. — On the Kinetic Theory of Rarefied Gases, Comm. Pure Appl. Math Vol. 2, No. 4, p. 331, 1949.

5. Gross, E. P., Jackson, A. E. Ziering, S. — Boundary Value Problems in Kinetic Theory of Gases, Am. Phys. 1, (1957).

6. Krook, M — Dynamics of Rarefied Gases, Phys, Rev. 99, 1896 (1955).

7. Patterson, G. N — Molecular Flow of Gases, J. Wiley and Sons, 1956.

8. Churchill, R. — Modern Operational Mathematics in Engineering, McGraw-Hill, 1944.

* Also in main list.

Reproduced with permission of the copyright owner. Further reproduction prohibited without permission.

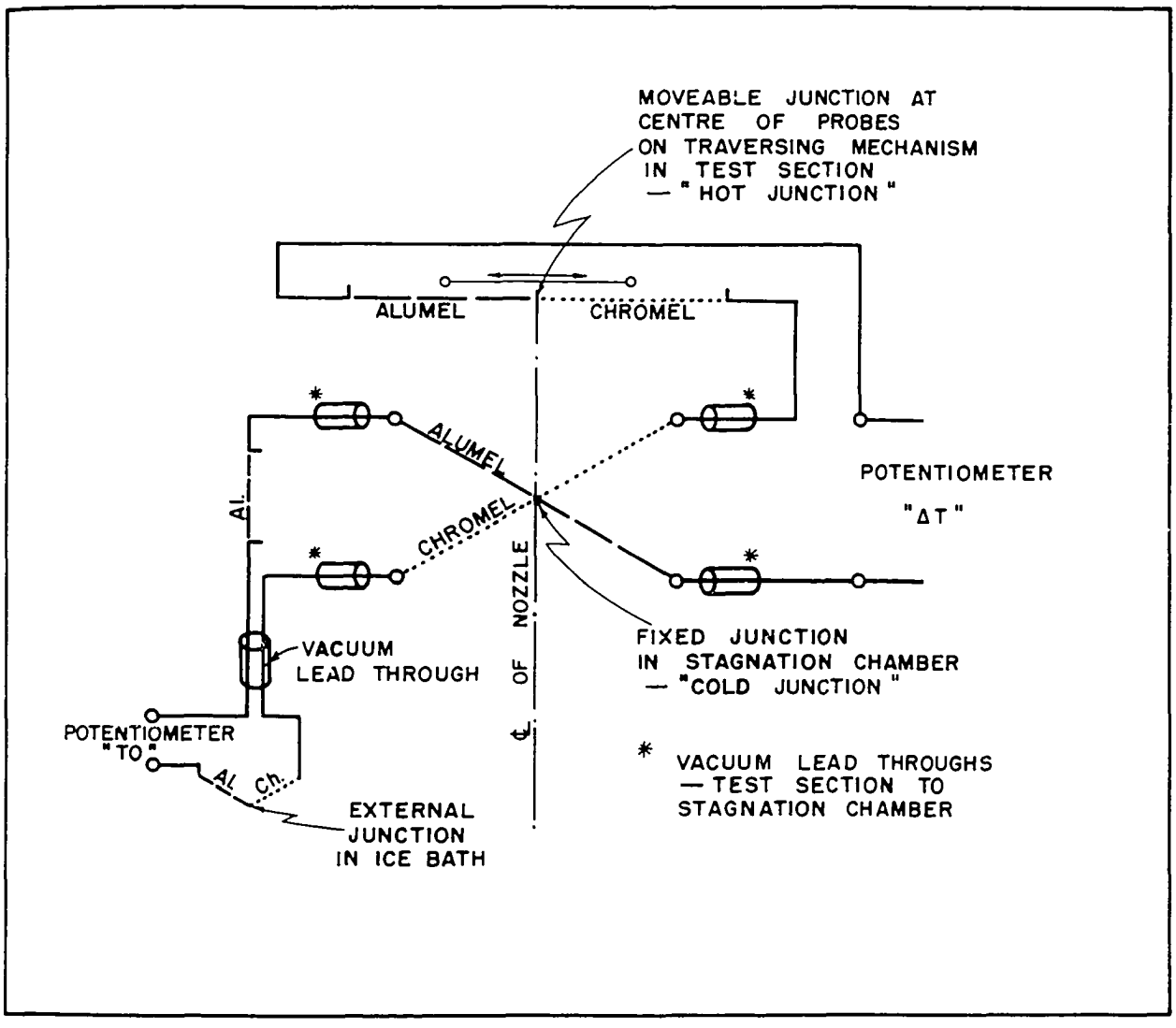

FIG. 1 SCHEMATIC OF UTIAS EQUILIBRIUM TEMPERATURE PROBE SETUP

Reproduced with permission of the copyright owner. Further reproduction prohibited without permission.

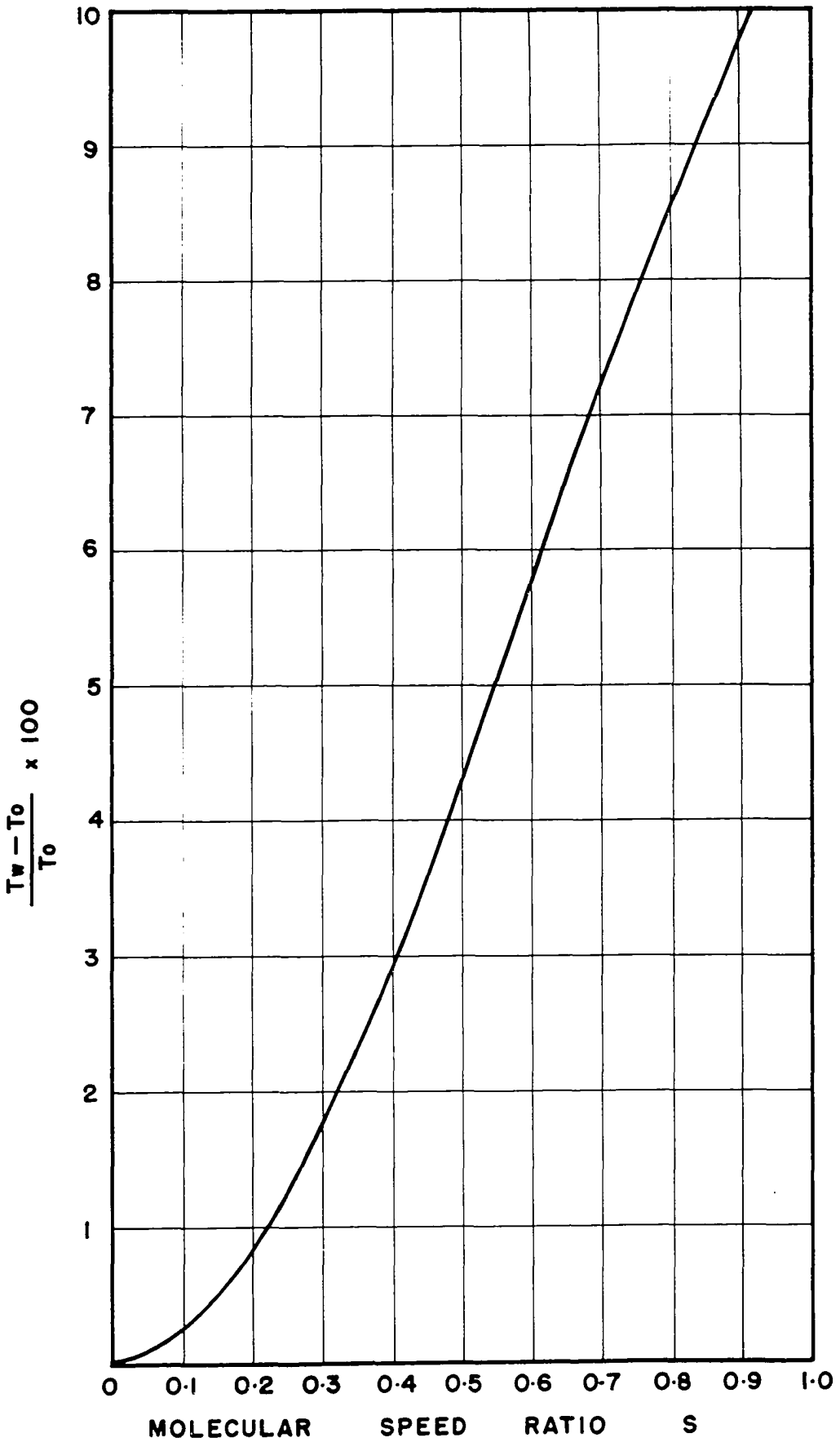

FIG. 2 THEORETICAL RESPONSE OF EQUILIBRIUM TEMPERATURE PROBE IN TERMS OF TOTAL TEMPERATURE

Reproduced with permission of the copyright owner. Further reproduction prohibited without permission.

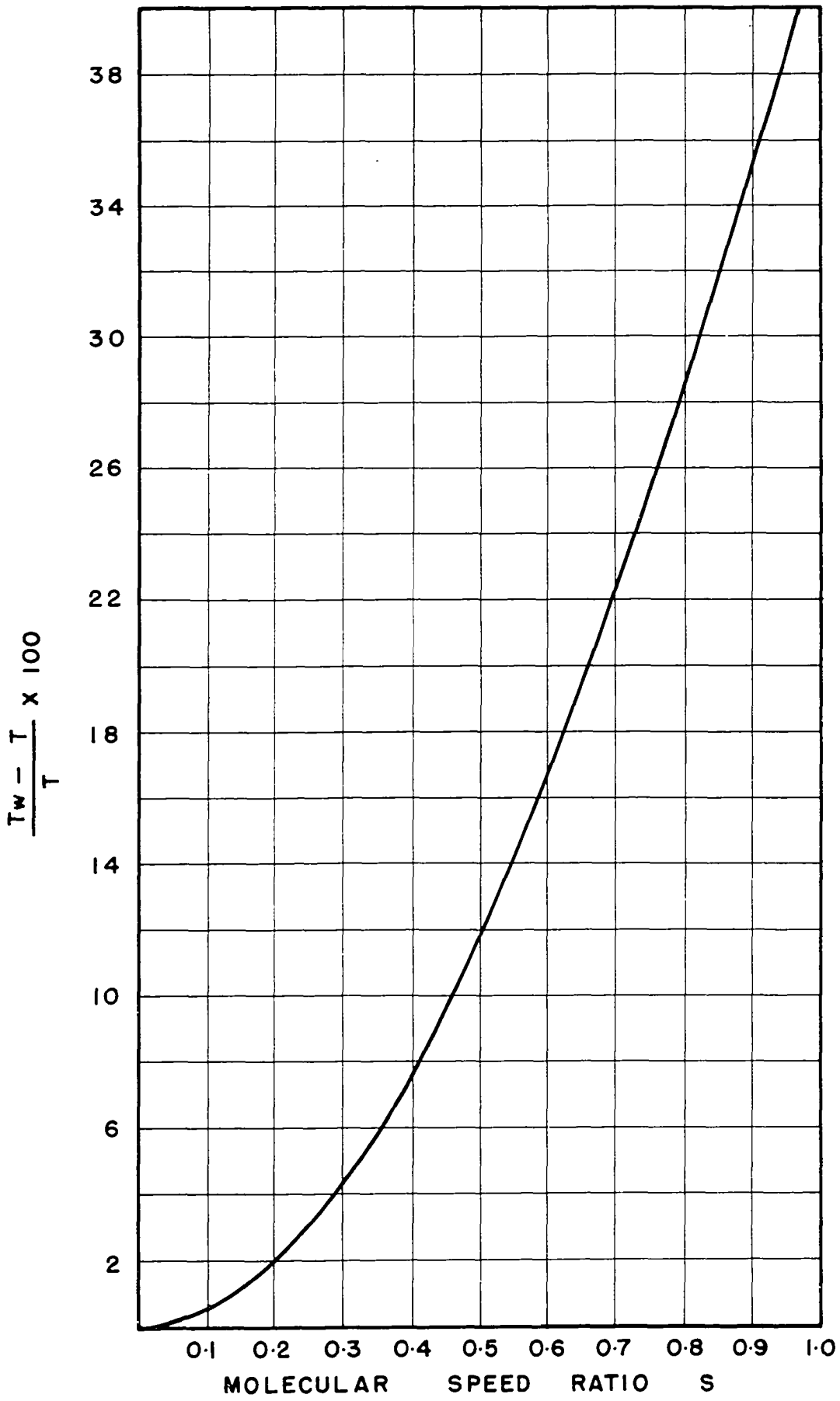

FIG. 3 THEORETICAL RESPONSE OF EQUILIBRIUM TEMPERATURE PROBE IN TERMS OF STATIC TEMPERATURE

Reproduced with permission of the copyright owner. Further reproduction prohibited without permission.

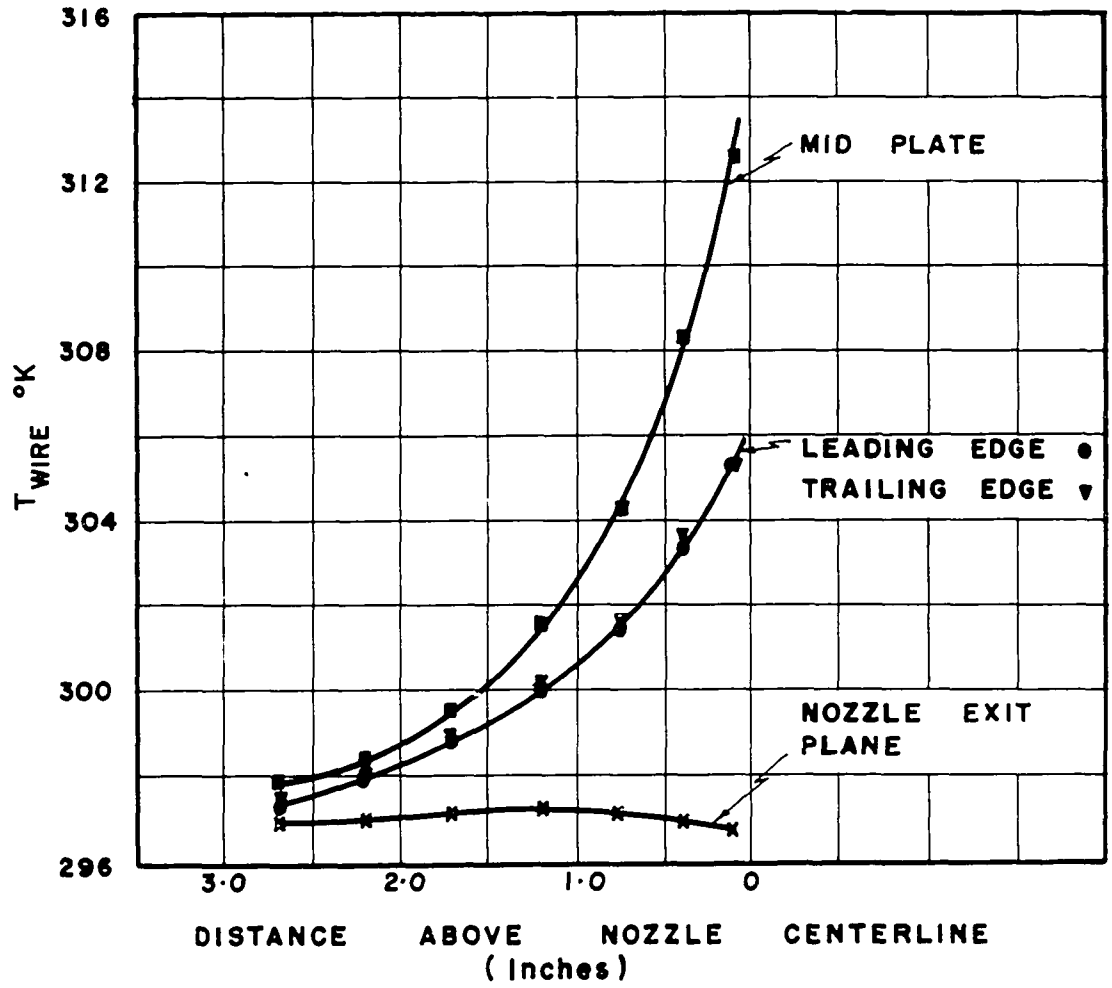

FIG. 4 WIRE TEMPERATURE OVER 100°C PLATE IN STILL AIR (10^{-4} mm)

Reproduced with permission of the copyright owner. Further reproduction prohibited without permission.

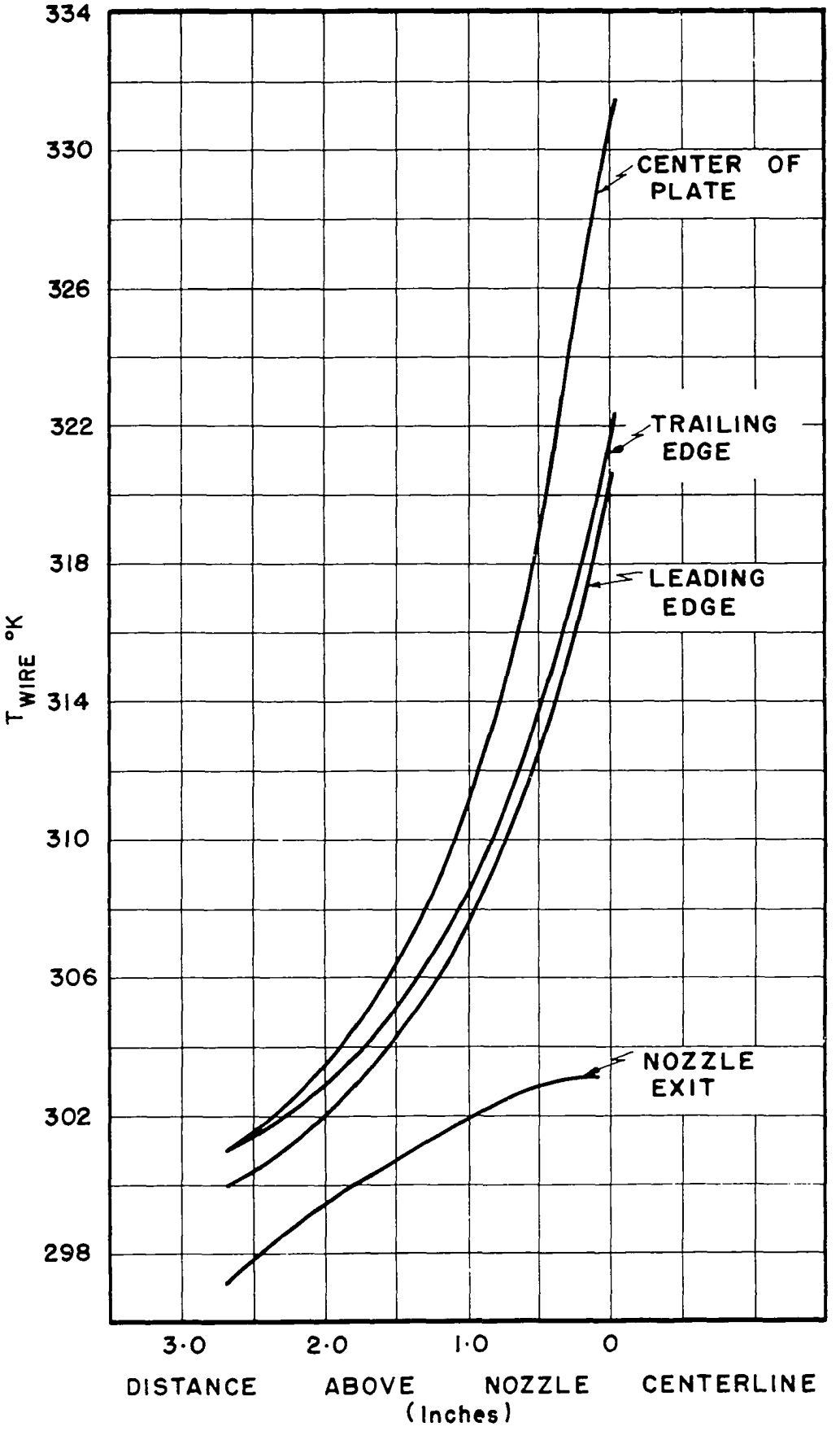

FIG. 5 WIRE TEMPERATURE OVER 100°C PLATE IN STILL AIR (20 microns)

Reproduced with permission of the copyright owner. Further reproduction prohibited without permission.

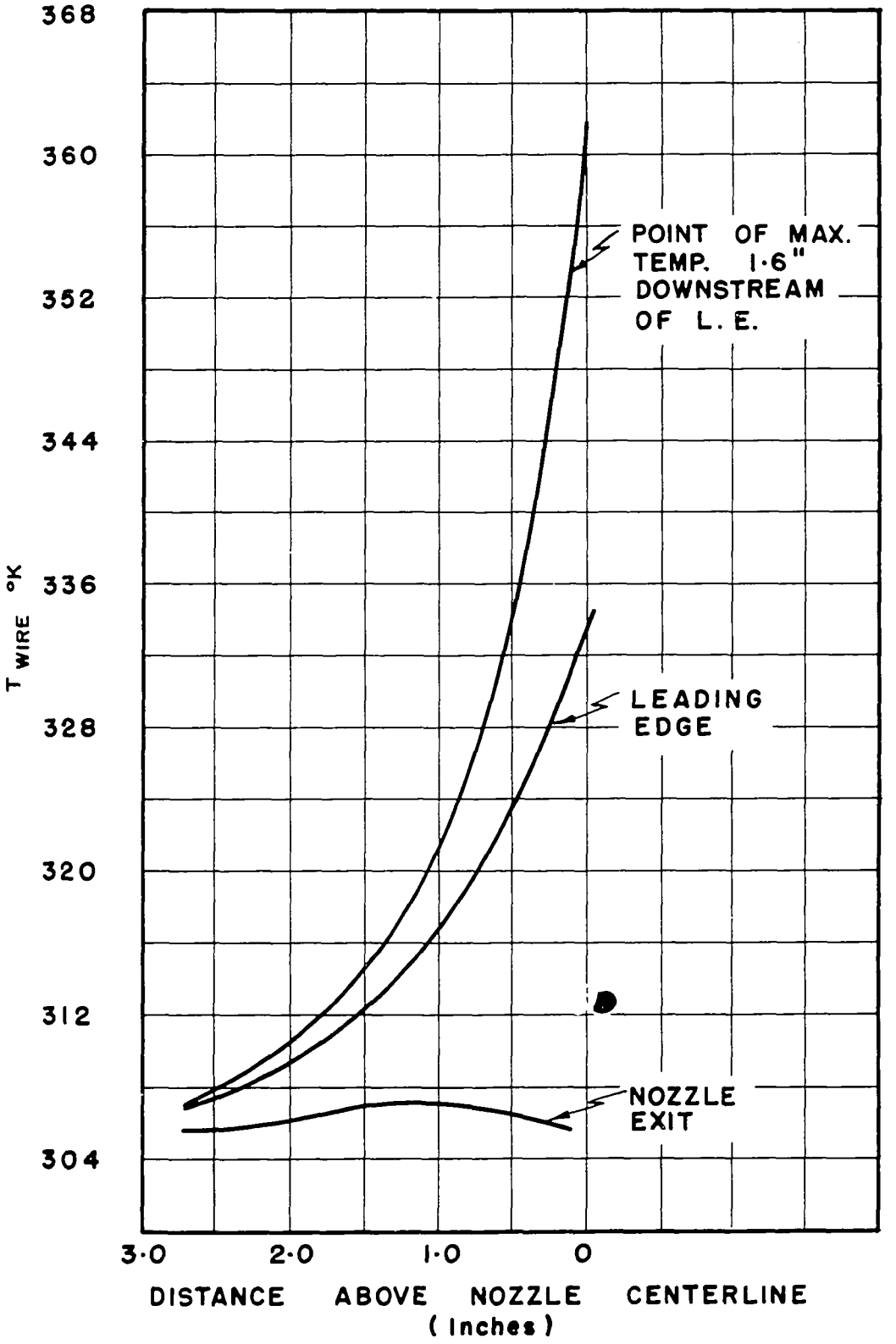

FIG. 6 WIRE TEMPERATURE OVER 200°C PLATE IN STILL AIR (10^{-4} mm)

Reproduced with permission of the copyright owner. Further reproduction prohibited without permission.

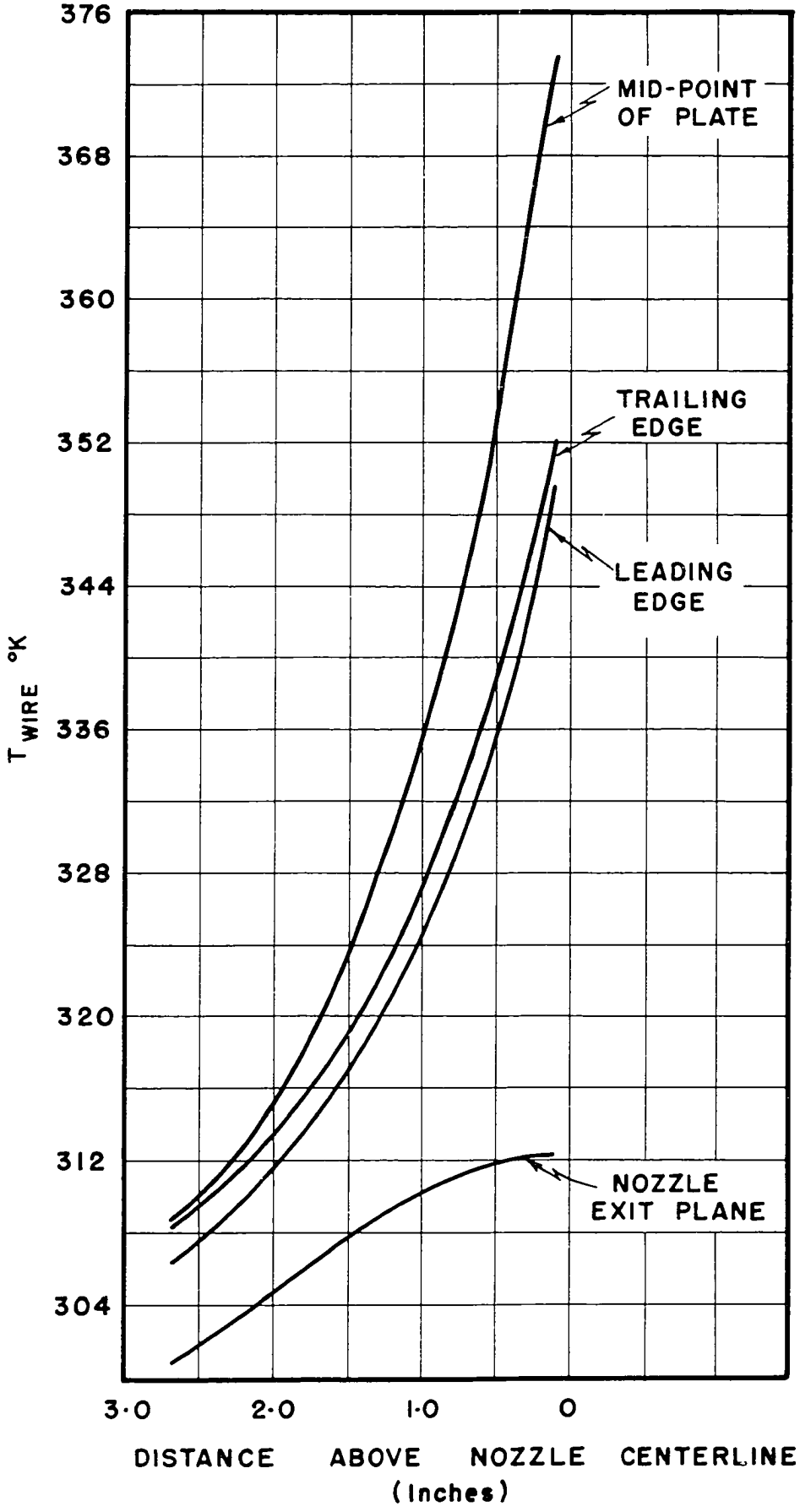

FIG. 7 WIRE TEMPERATURE OVER 200°C PLATE IN STILL AIR (20 microns)

Reproduced with permission of the copyright owner. Further reproduction prohibited without permission.

Reproduced with permission of the copyright owner. Further reproduction prohibited without permission.

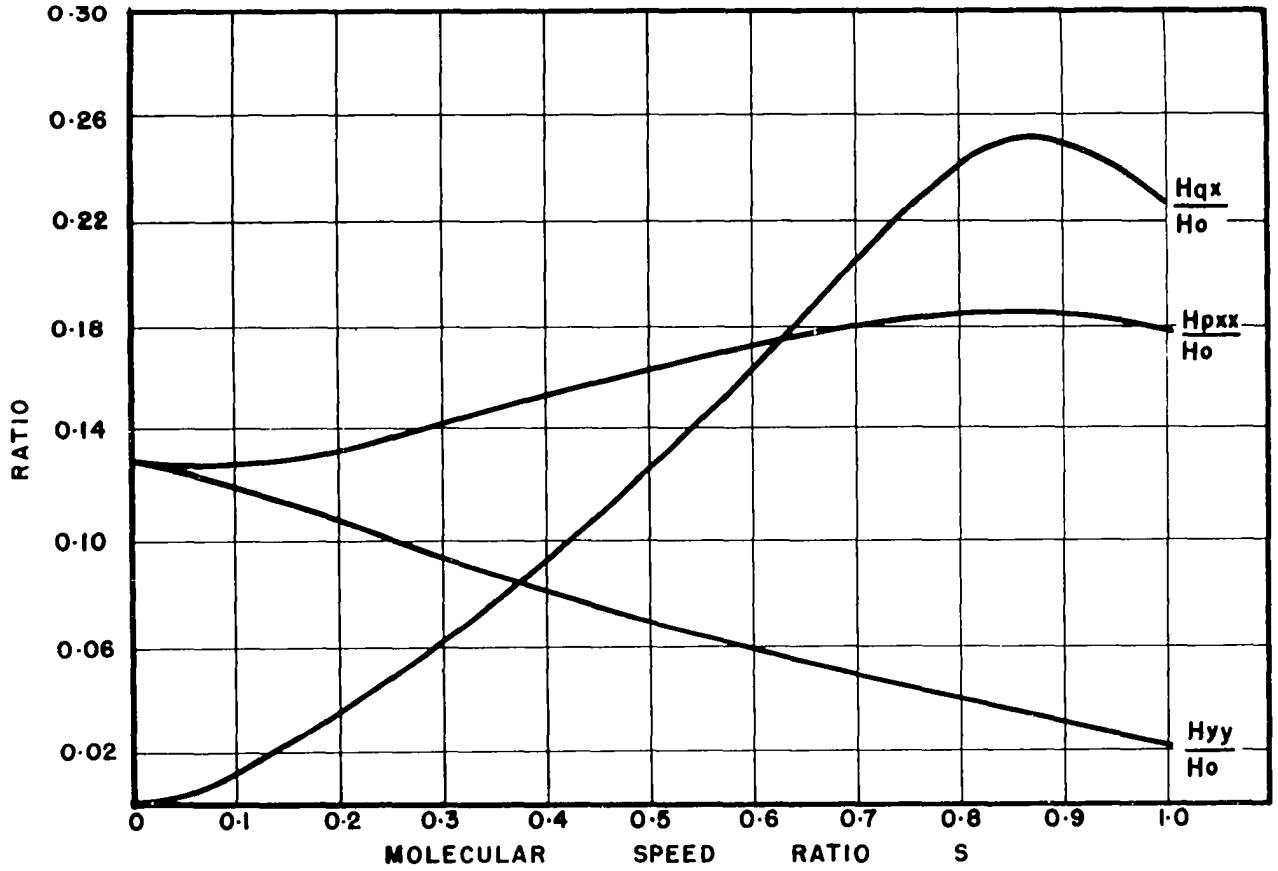

FIG. 8 NON-ISENTROPIC FLOW TERMS FOR EQUILIBRIUM TEMPERATURE PROBE

$$\text{Reading} = \text{isentropic value} \times \left[1 + \frac{p_{xx}}{p} \cdot \frac{H_{p_{xx}}}{H_o} + \frac{p_{yy}}{p} \cdot \frac{H_{p_{yy}}}{H_o} + \frac{q_x}{pU} \cdot \frac{H_{q_x}}{H_o} \right]$$

where

$$\frac{p_{xx}}{p} = -\frac{4}{3} \frac{\mu}{p} \frac{\partial U}{\partial x} \simeq -5 \times 10^{-6} \frac{\partial U}{\partial x} \quad \frac{\text{sec}}{\text{cm}}$$

$$\frac{p_{yy}}{p} = -\frac{4}{3} \frac{\mu}{p} \frac{\partial U}{\partial y} \simeq -5 \times 10^{-6} \frac{\partial U}{\partial y} \quad \frac{\text{sec}}{\text{cm}}$$

$$\frac{q_x}{pU} = -\frac{\lambda}{pU} \frac{\partial T}{\partial x} \simeq 1.5 \times 10^{-2} \frac{\partial T}{\partial x} \quad \frac{\text{cm}}{^\circ\text{C}}$$

for these experiments

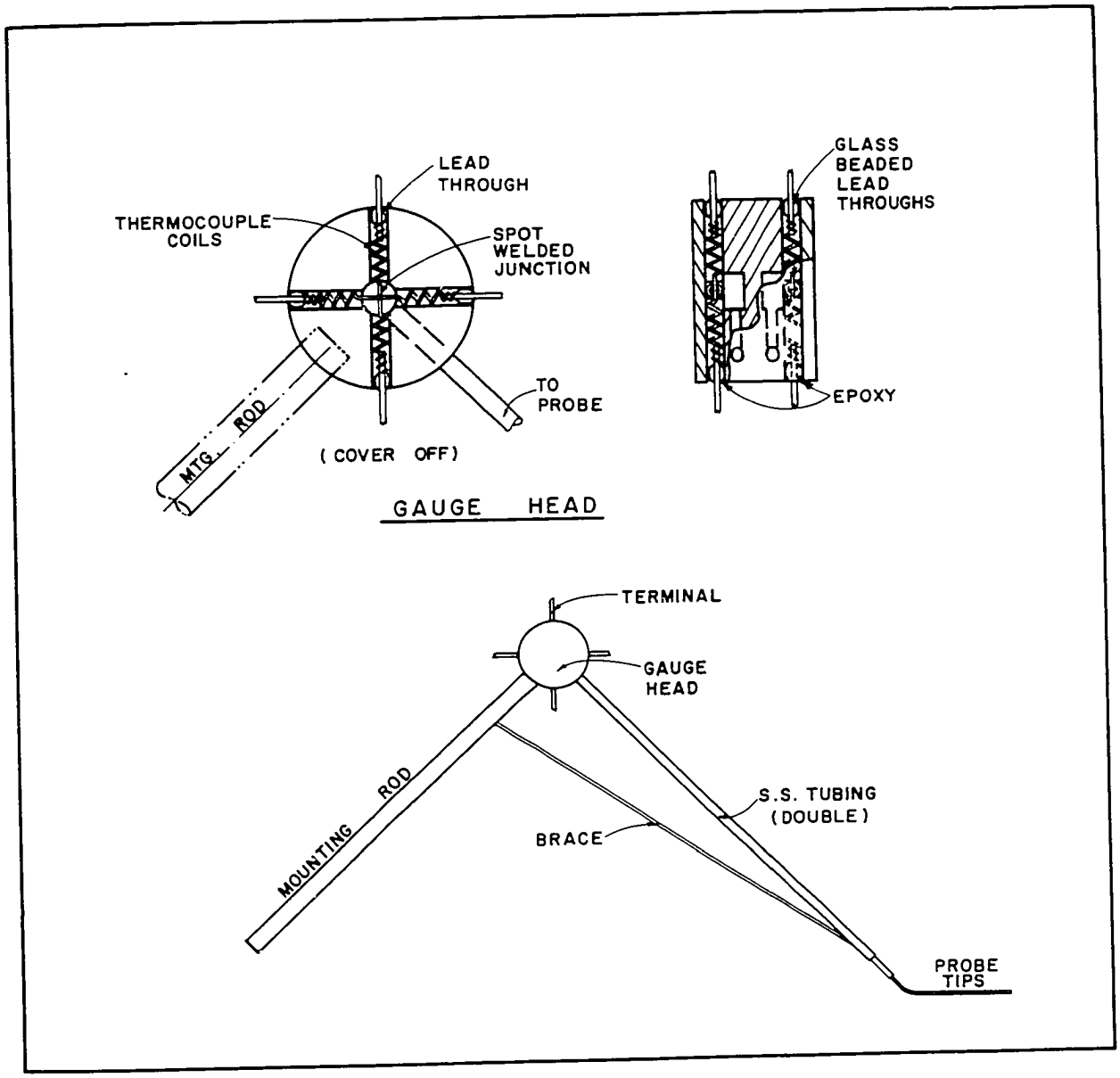

FIG. 9 UTIAS PRESSURE PAIR PROBE

Reproduced with permission of the copyright owner. Further reproduction prohibited without permission.

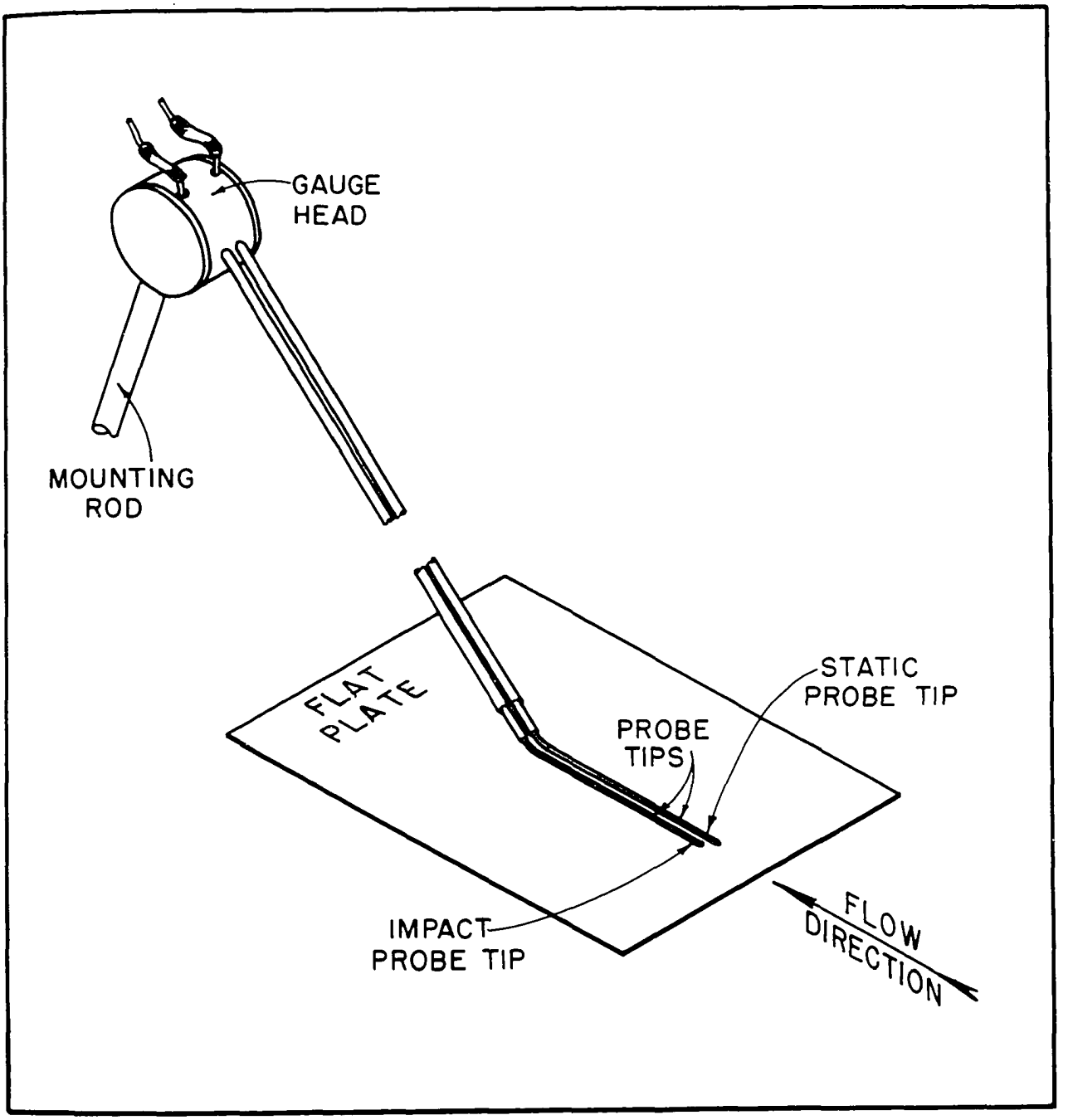

FIG. 10 CONFIGURATION OF PRESSURE PAIR PROBE

Reproduced with permission of the copyright owner. Further reproduction prohibited without permission.

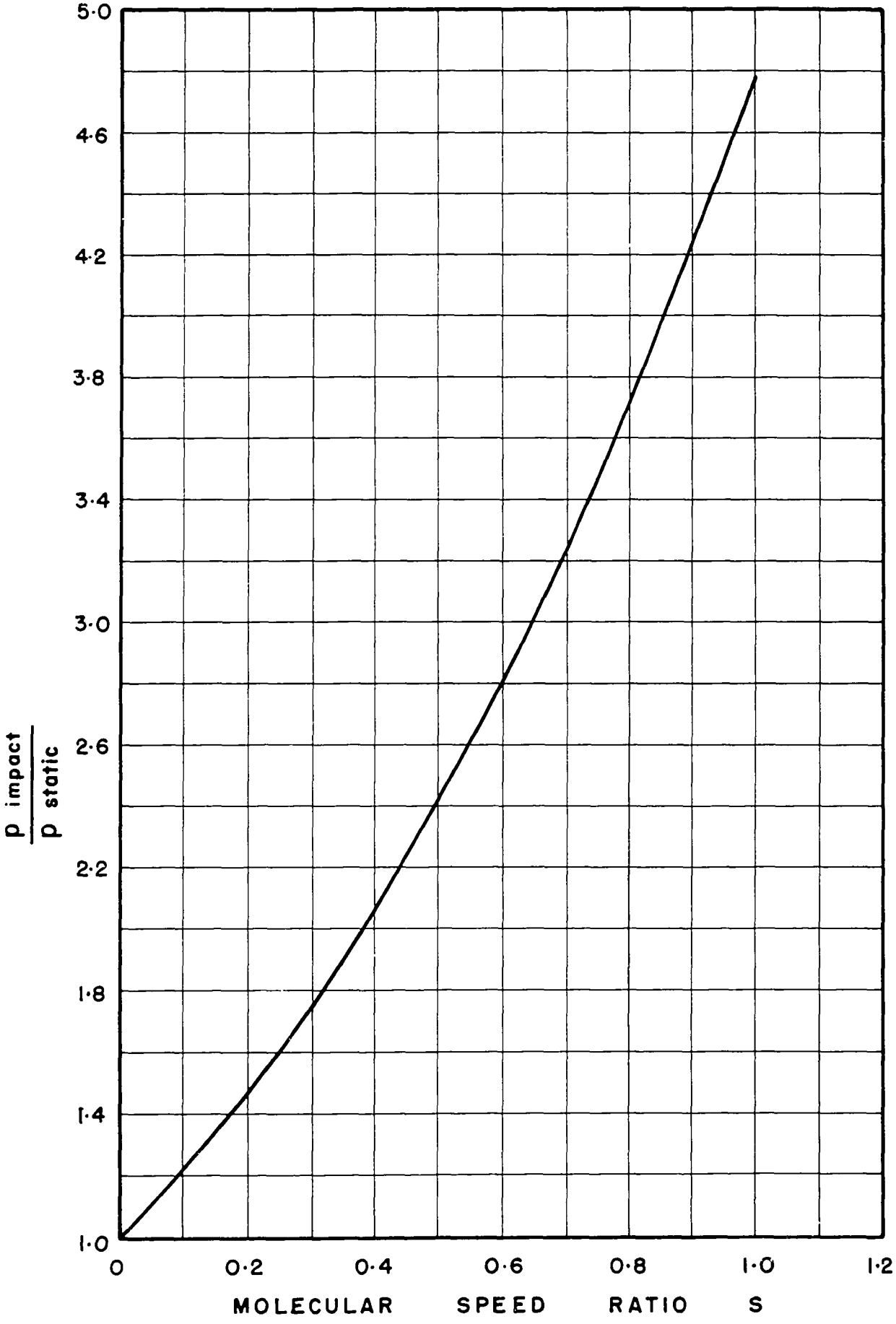

FIG. 11 THEORETICAL RESPONSE OF A LONG-TUBE IMPACT PROBE IN FREE MOLECULE FLOW

Reproduced with permission of the copyright owner. Further reproduction prohibited without permission.

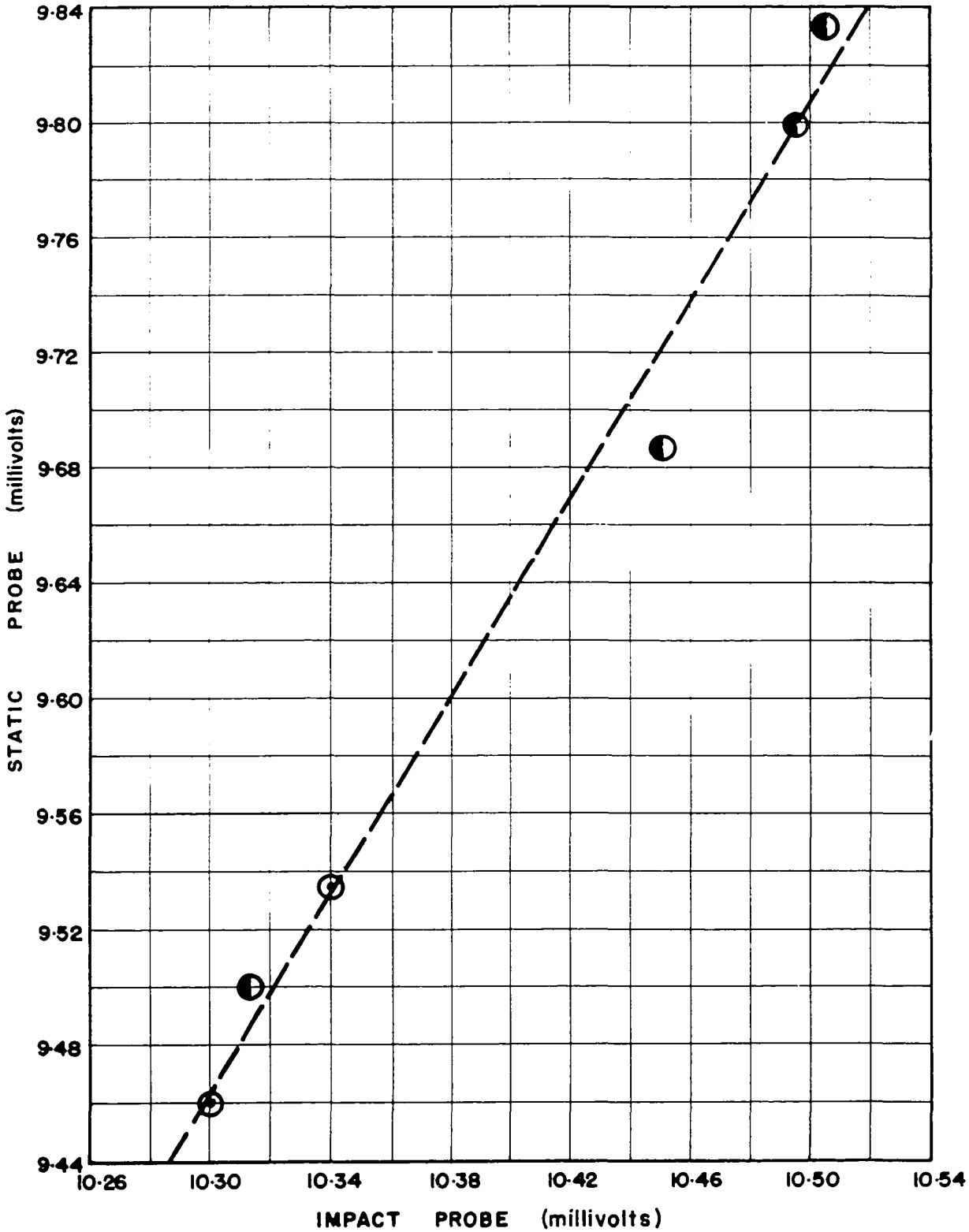

FIG. 12 RELATIVE CHANGE IN RESPONSE OF IMPACT AND STATIC PROBES DUE TO ZERO SHIFT AT 20 MICRONS AS GAUGE HEAD TEMPERATURE VARIED IN STILL AIR

Reproduced with permission of the copyright owner. Further reproduction prohibited without permission.

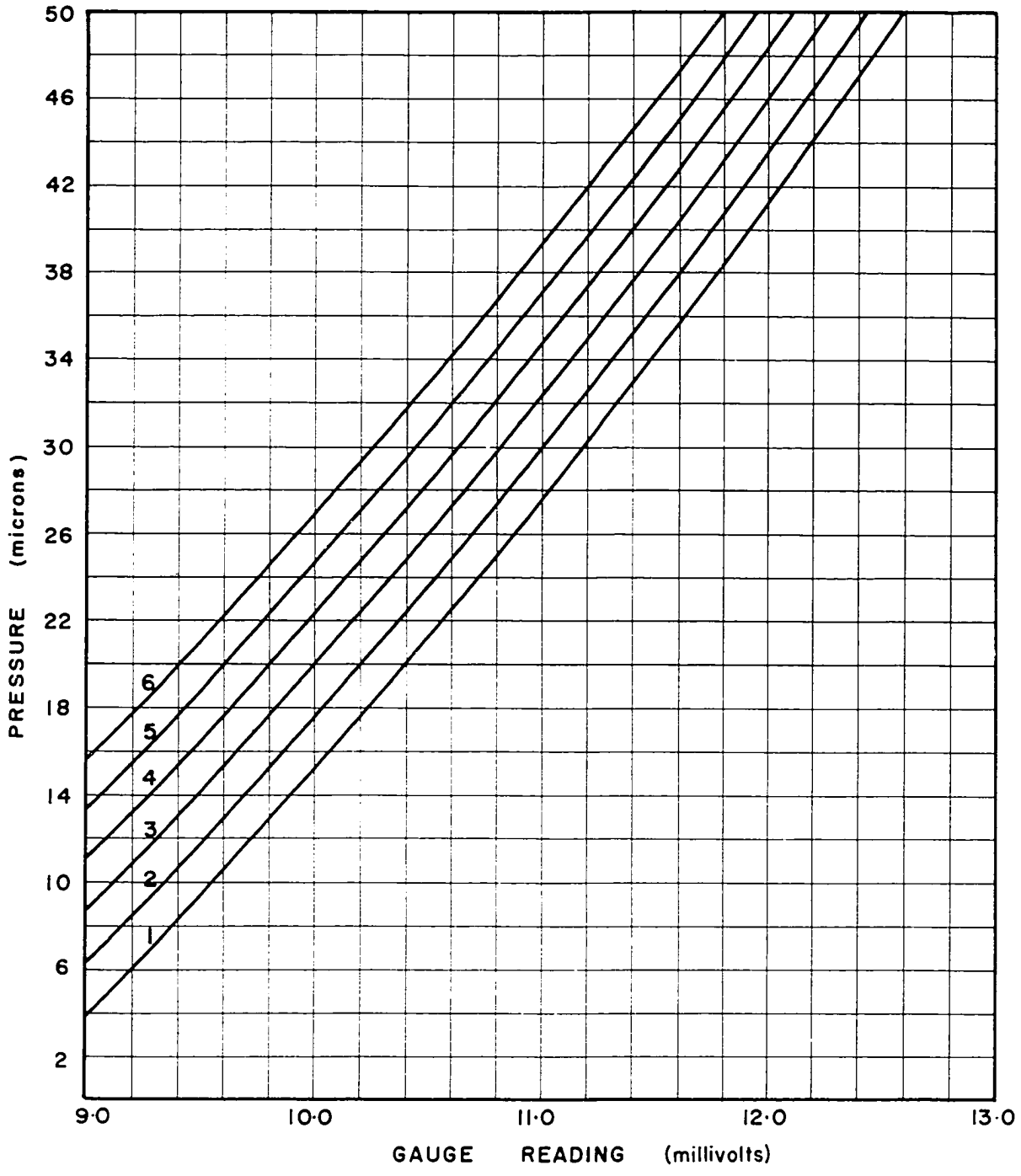

FIG. 13 STATIC PRESSURE PROBE CALIBRATION FAMILY

Reproduced with permission of the copyright owner. Further reproduction prohibited without permission.

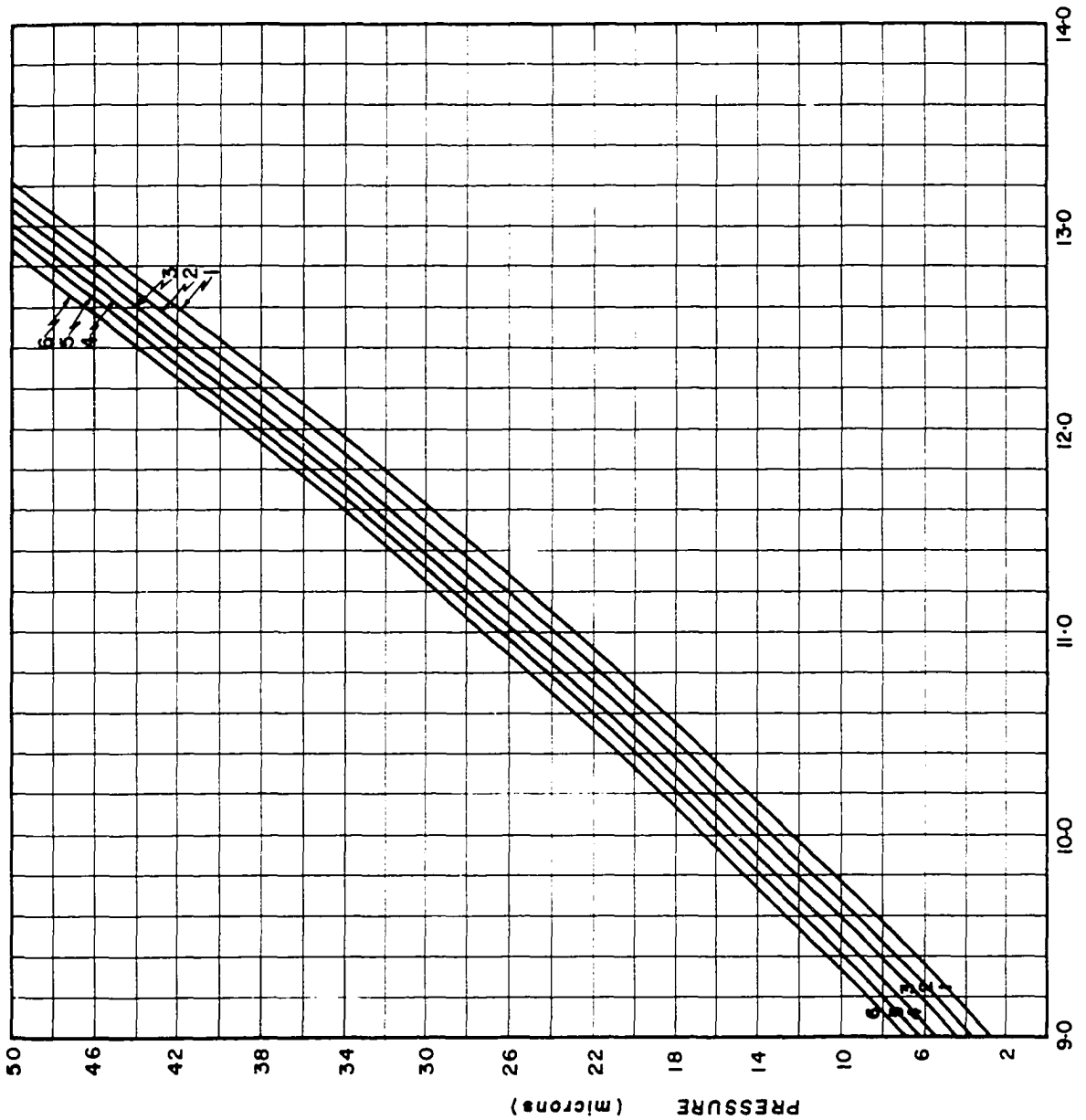

FIG. 14 IMPACT PRESSURE PROBE CALIBRATION FAMILY

Reproduced with permission of the copyright owner. Further reproduction prohibited without permission.

Reproduced with permission of the copyright owner. Further reproduction prohibited without permission.

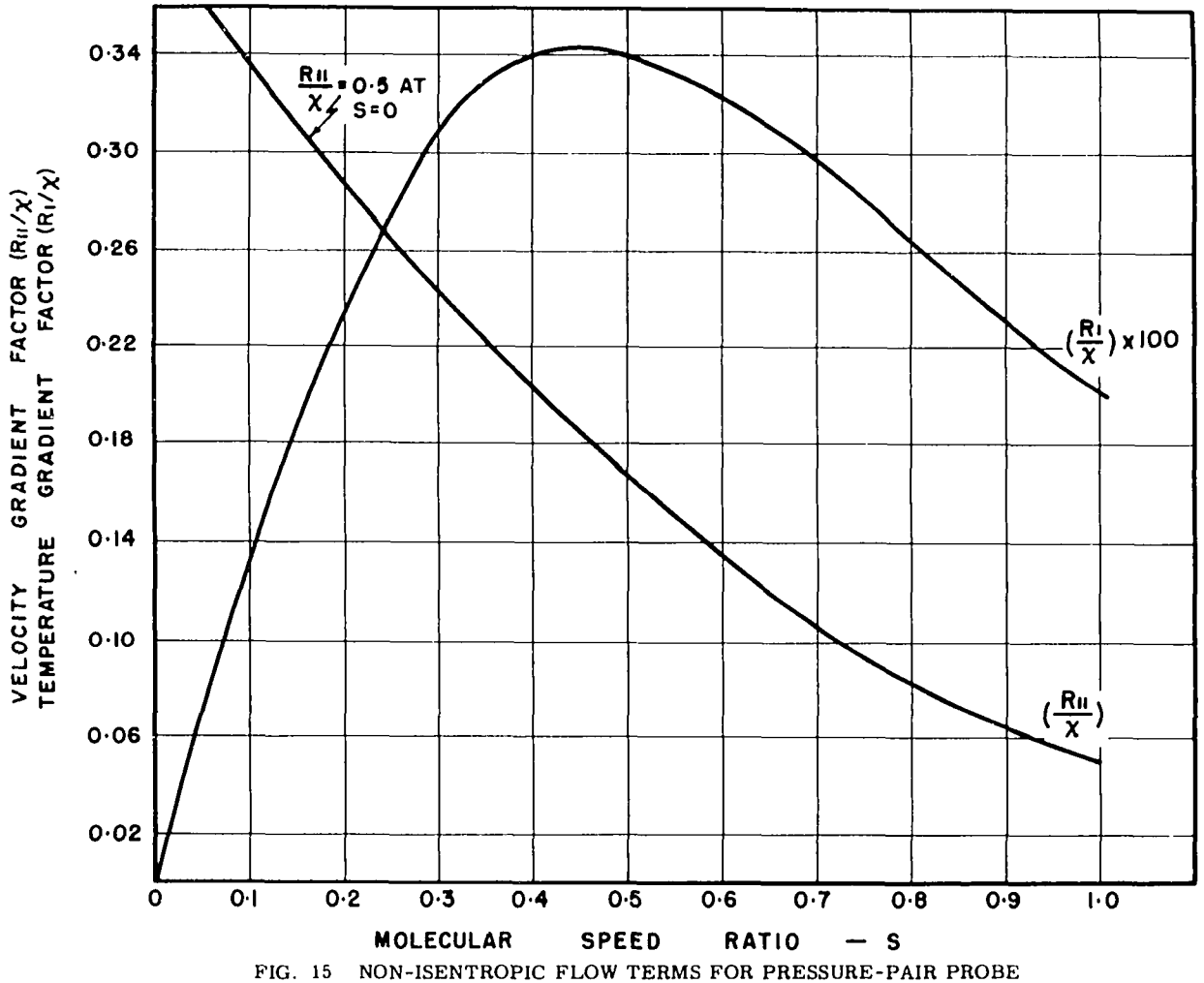

FIG. 15 NON-ISENTROPIC FLOW TERMS FOR PRESSURE-PAIR PROBE

$$\text{Reading} = \text{isentropic value} \times \left[1 + \frac{R_1}{\chi}\left(\frac{\lambda}{p}\frac{2}{C_m}\right)\frac{\partial T}{\partial x} - \frac{R_{11}}{\chi}\frac{4}{3}\frac{\mu}{p}\frac{\partial U}{\partial x}\right]$$

where $\frac{\lambda}{p}\frac{2}{C_m} \simeq 10^{-6}$

$\frac{4}{3}\frac{\mu}{p} \simeq 5\times10^{-6}$ for these experiments

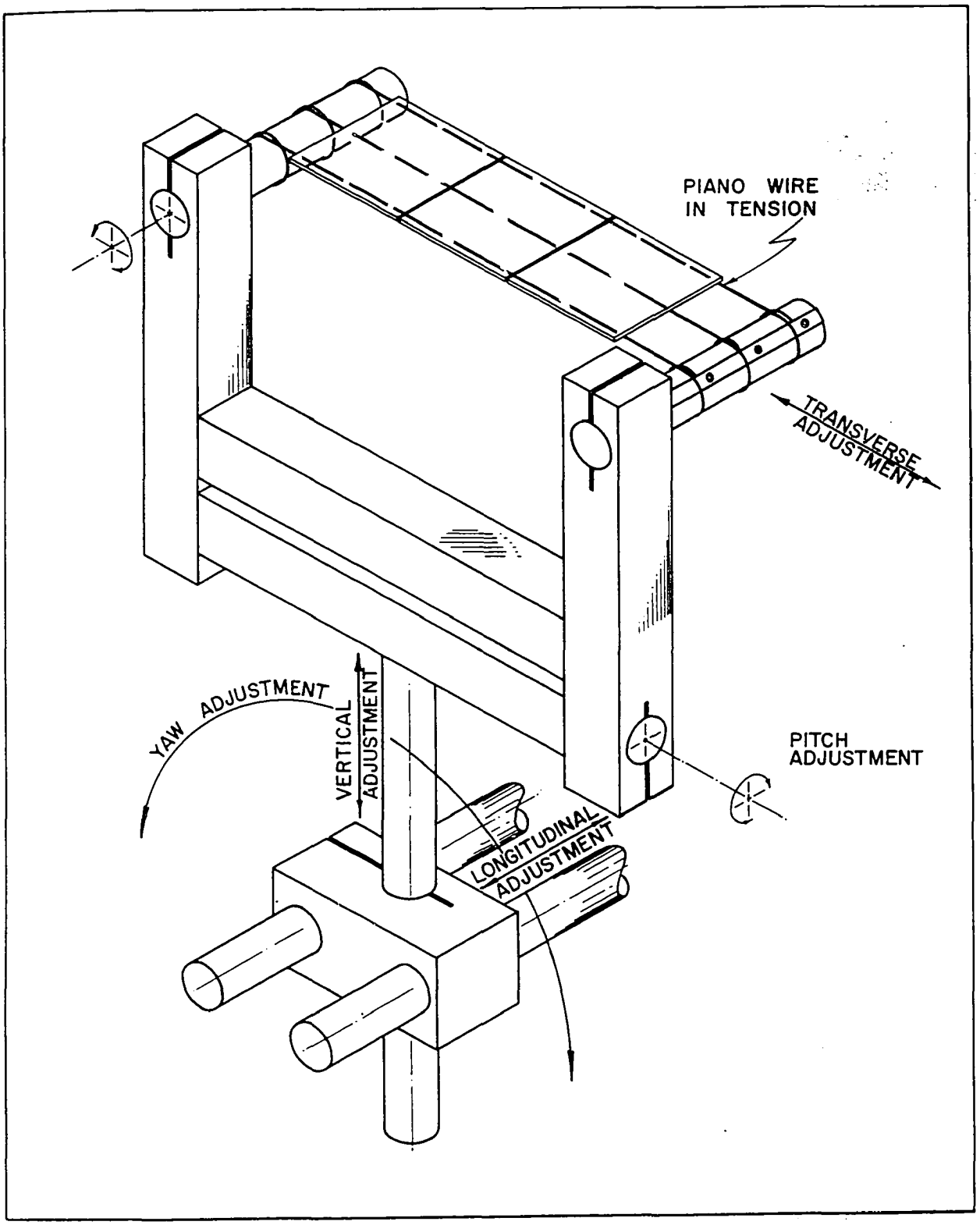

FIG. 16 FLAT PLATE AND HOLDER

Reproduced with permission of the copyright owner. Further reproduction prohibited without permission.

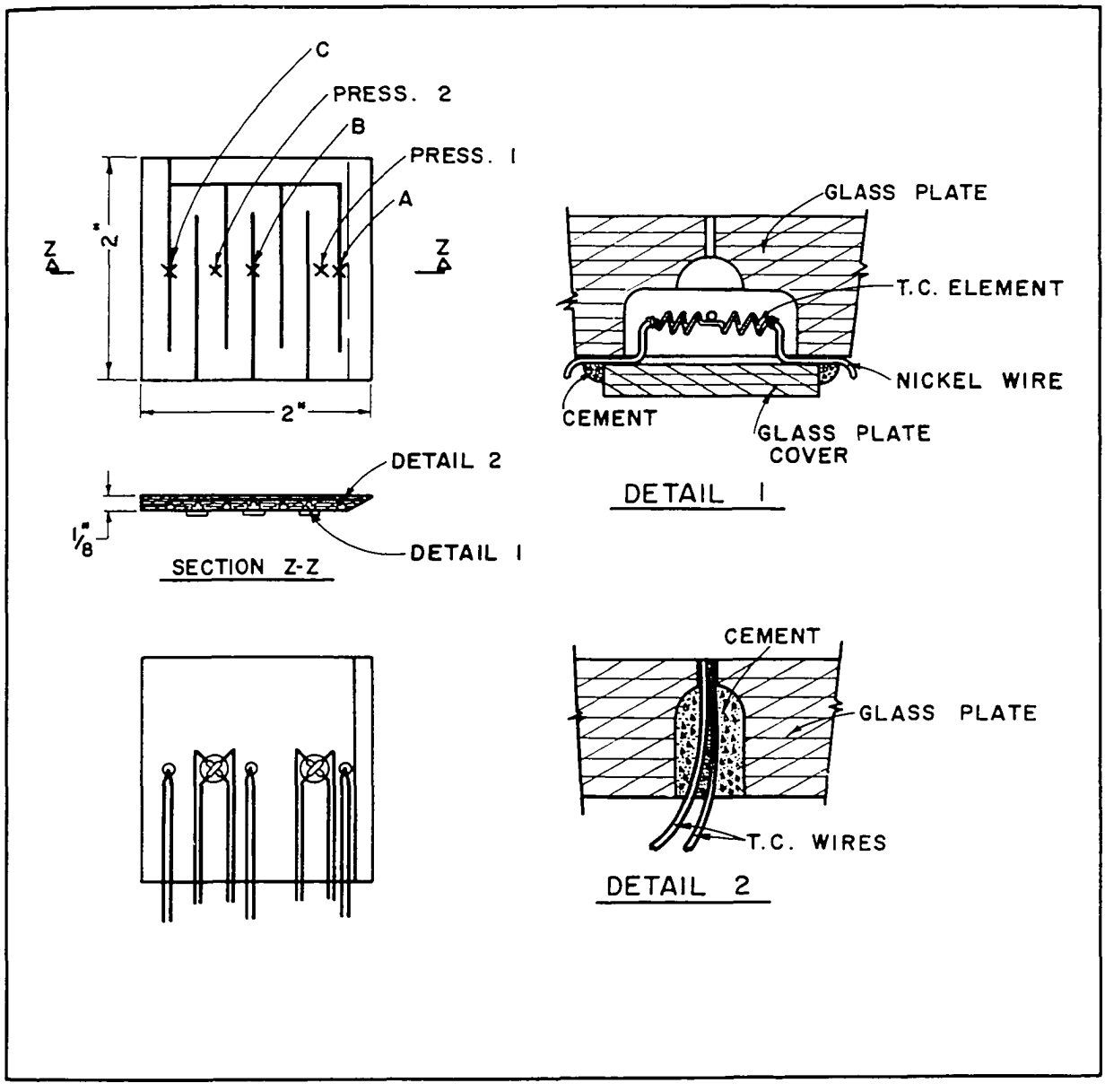

FIG. 17 DETAIL DRAWING OF THE FULLY INSTRUMENTED FLAT PLATE MODEL

Reproduced with permission of the copyright owner. Further reproduction prohibited without permission.

Reproduced with permission of the copyright owner. Further reproduction prohibited without permission.

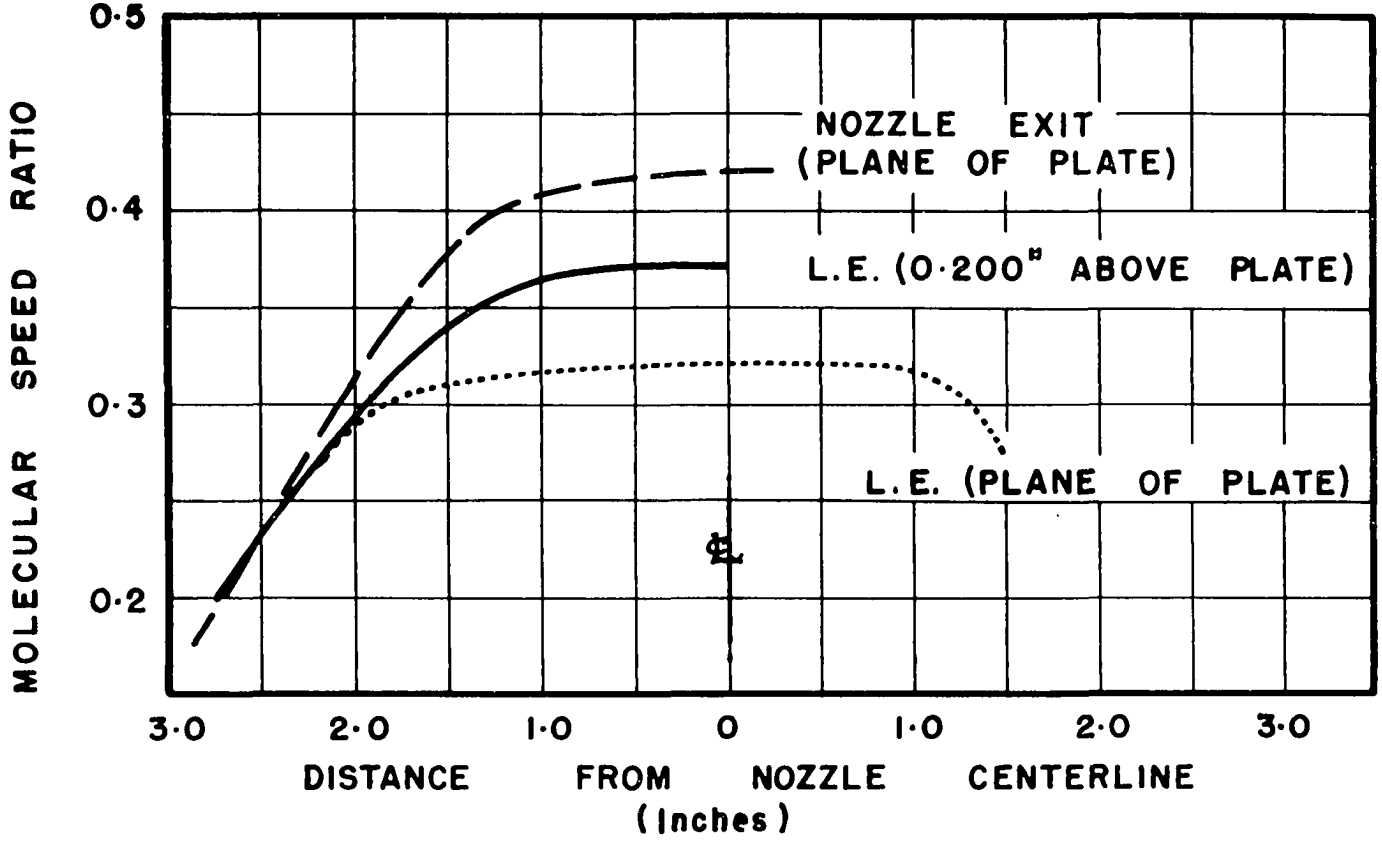

FIG. 18 TRANSVERSE TRAVERSE BY EQUILIBRIUM TEMPERATURE PROBE OVER ROOM TEMPERATURE PLATE AT MACH 0.5

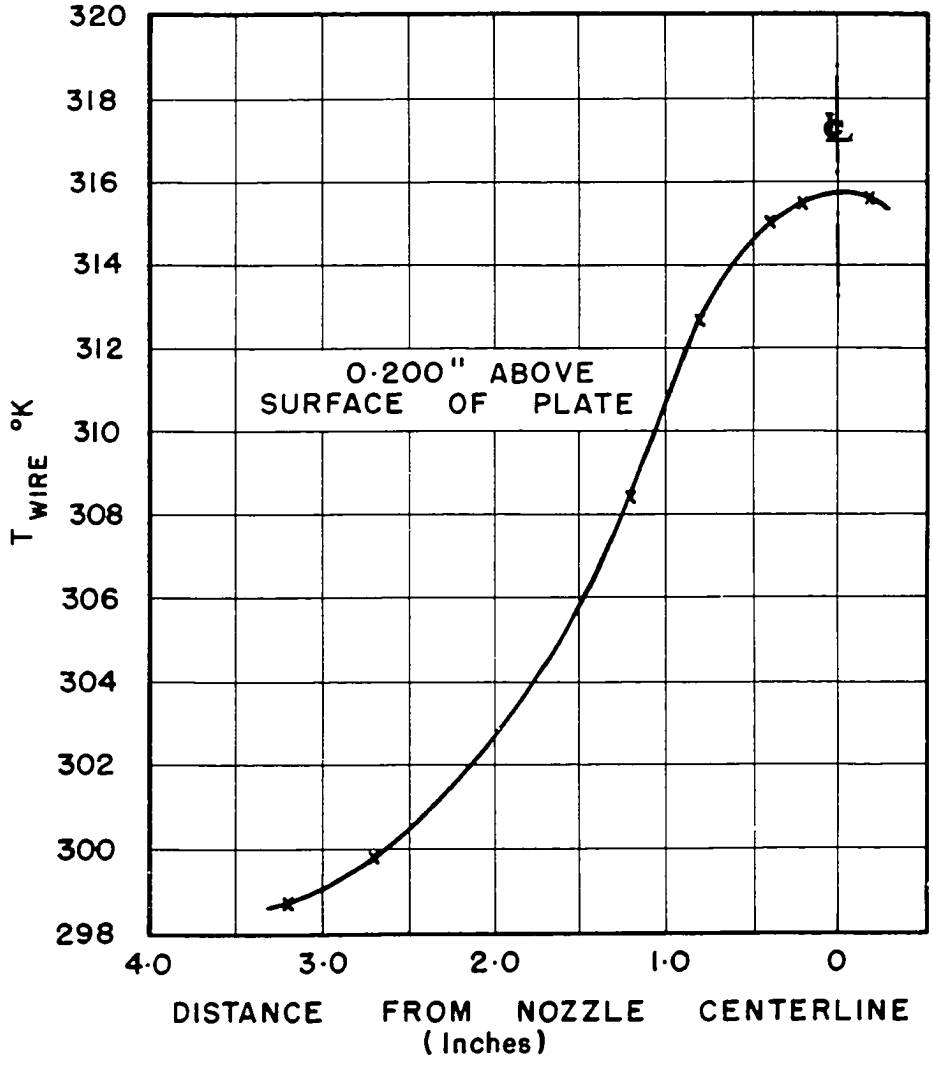

FIG. 19 TRANSVERSE TRAVERSE BY EQUILIBRIUM TEMPERATURE PROBE OVER 100°C PLATE AT MACH 0.5

Reproduced with permission of the copyright owner. Further reproduction prohibited without permission.

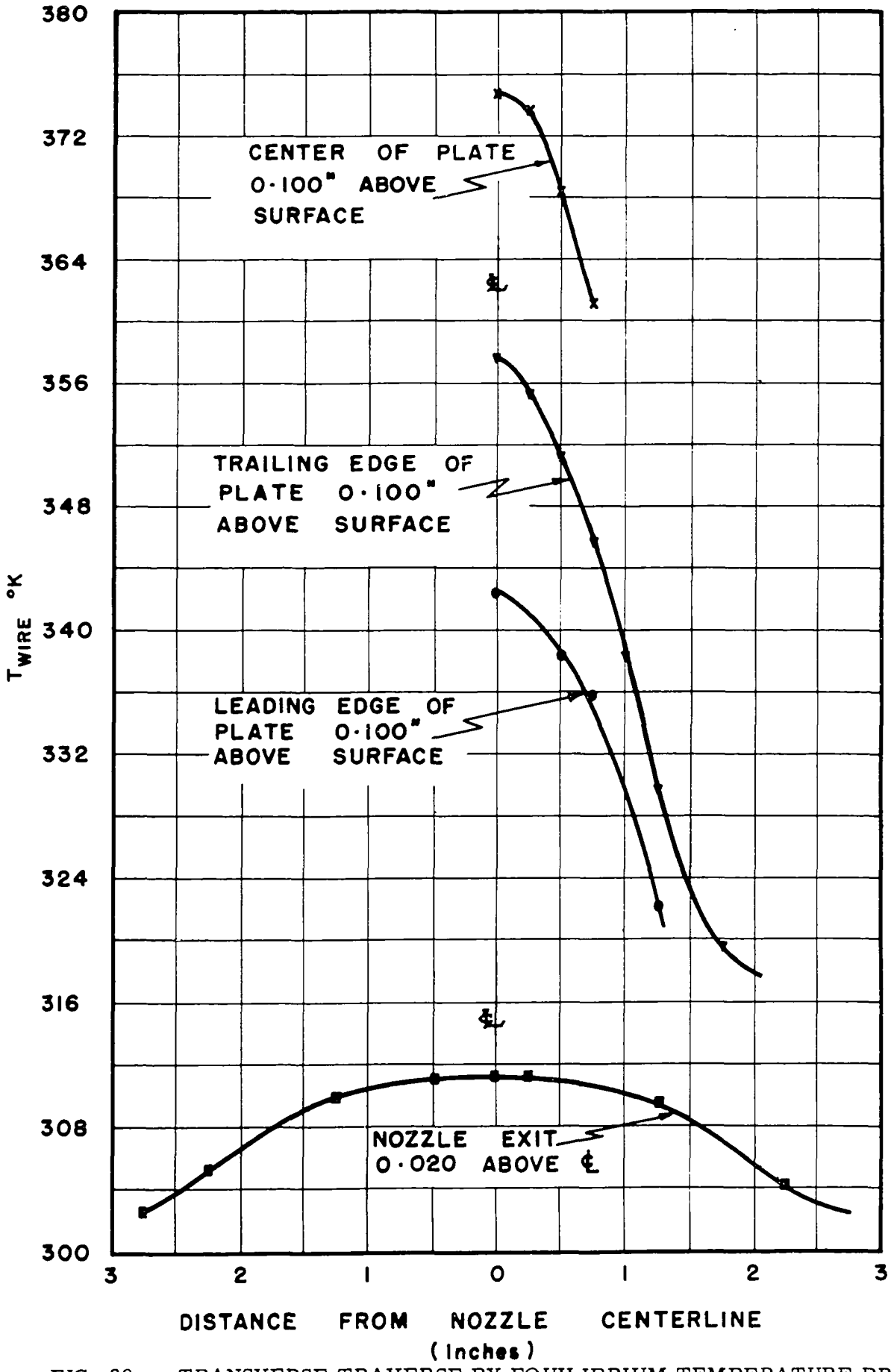

FIG. 20 TRANSVERSE TRAVERSE BY EQUILIBRIUM TEMPERATURE PROBE OVER 200°C PLATE AT MACH 0.5

Reproduced with permission of the copyright owner. Further reproduction prohibited without permission.

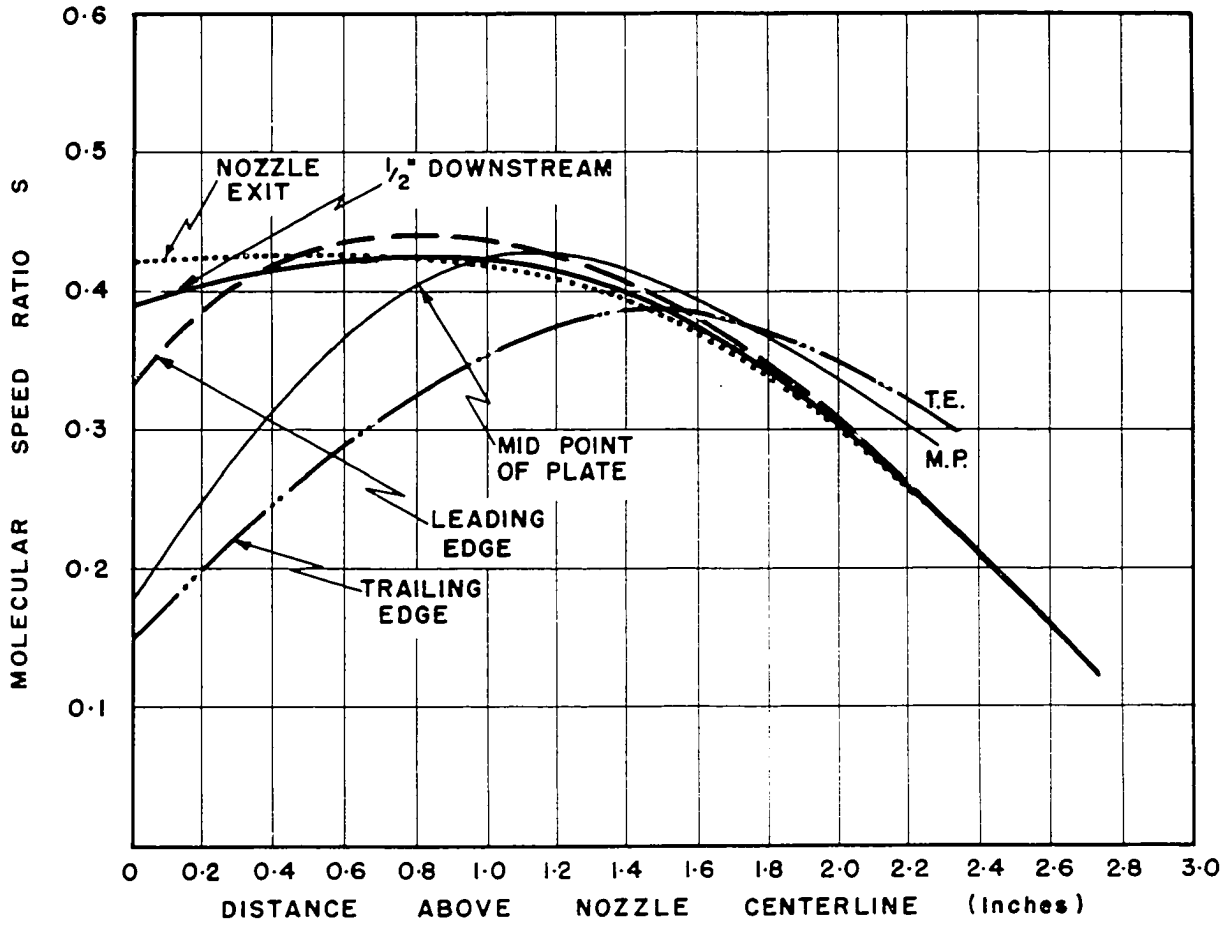

FIG. 21 MOLECULAR SPEED RATIO ABOVE THE ROOM TEMPERATURE PLATE AS OBTAINED BY VERTICAL TRAVERSES WITH THE EQUILIBRIUM TEMPERATURE PROBE

Reproduced with permission of the copyright owner. Further reproduction prohibited without permission.

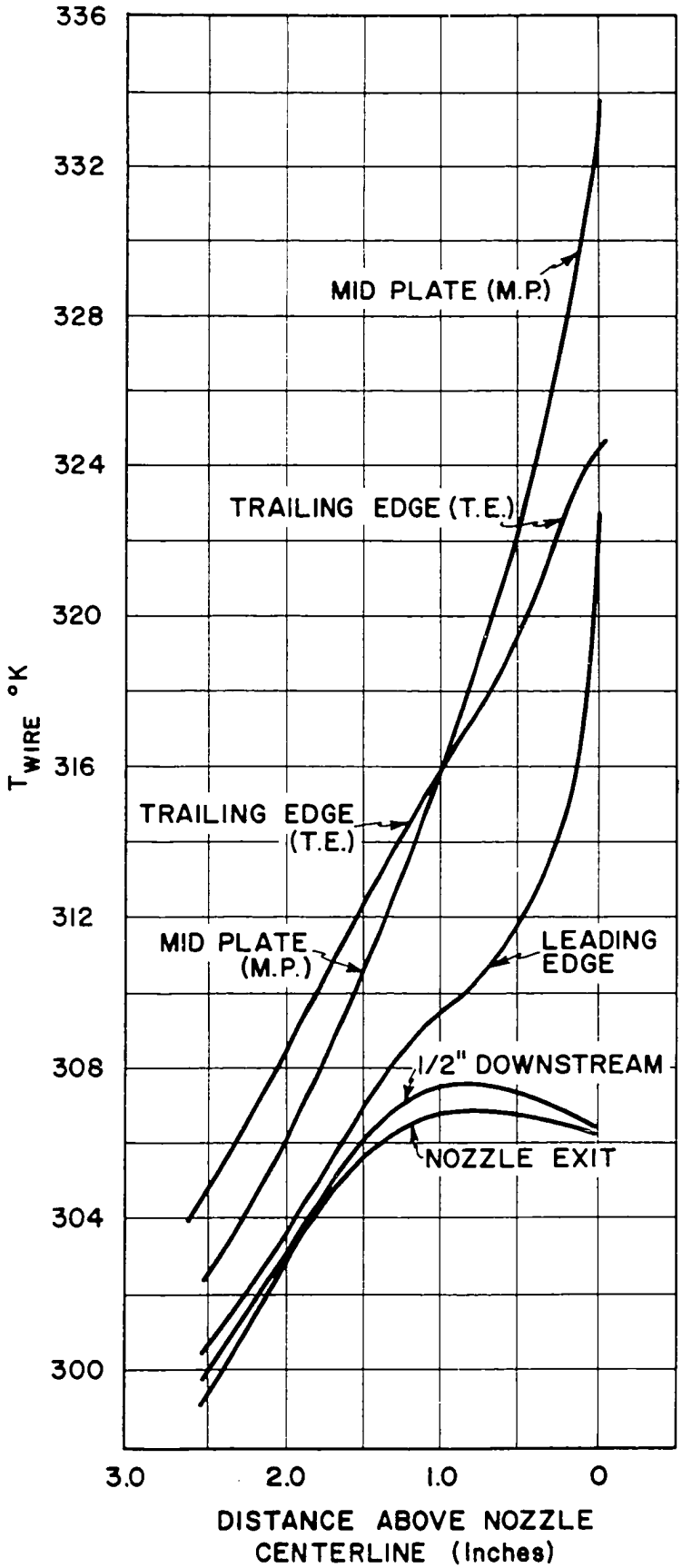

FIG. 22 EQUILIBRIUM TEMPERATURES ABOVE THE 100°C PLATE AS OBTAINED BY VERTICAL TRAVERSES

Reproduced with permission of the copyright owner. Further reproduction prohibited without permission.

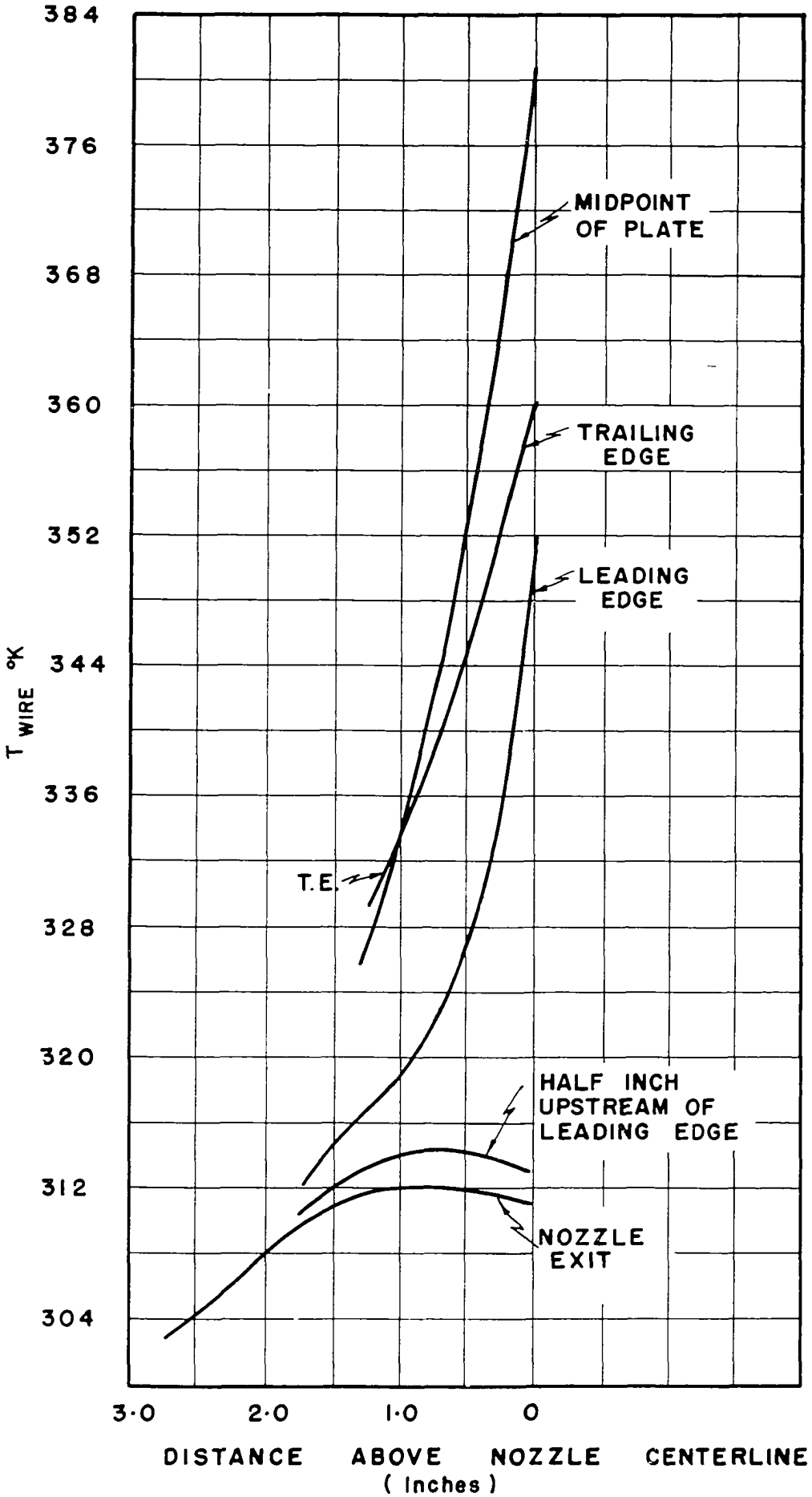

FIG. 23 EQUILIBRIUM TEMPERATURES ABOVE THE 200°C PLATE AS OBTAINED BY VERTICAL TRAVERSES

Reproduced with permission of the copyright owner. Further reproduction prohibited without permission.

Reproduced with permission of the copyright owner. Further reproduction prohibited without permission.

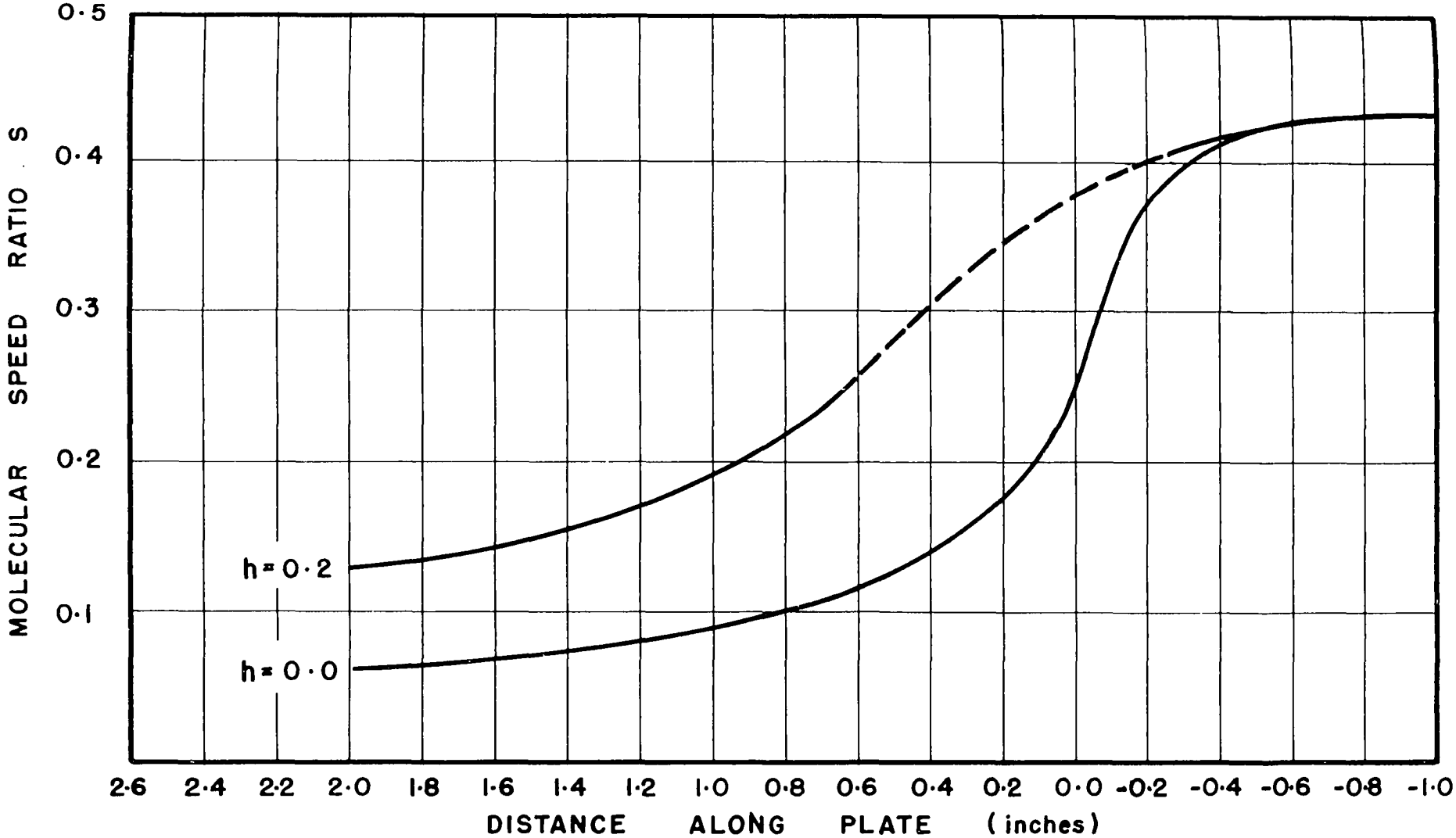

FIG. 24 CORRECTED MOLECULAR SPEED RATIOS ABOVE THE ROOM TEMPERATURE PLATE AS OBTAINED BY THE PRESSURE PAIR PROBE

Reproduced with permission of the copyright owner. Further reproduction prohibited without permission.

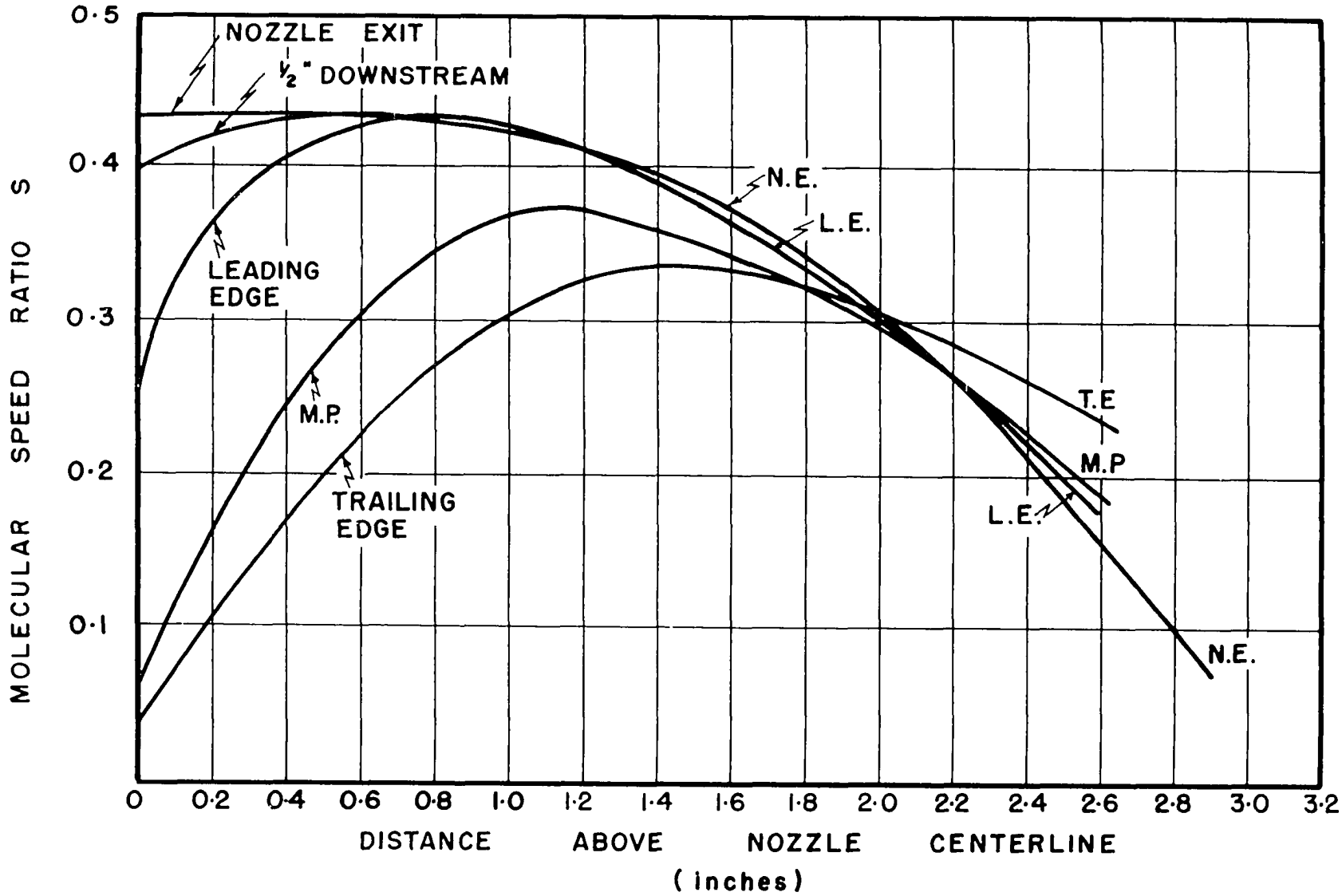

FIG. 25 CORRECTED MOLECULAR SPEED RATIOS ABOVE THE 100°C PLATE AS OBTAINED BY THE PRESSURE PAIR PROBE

Reproduced with permission of the copyright owner. Further reproduction prohibited without permission.

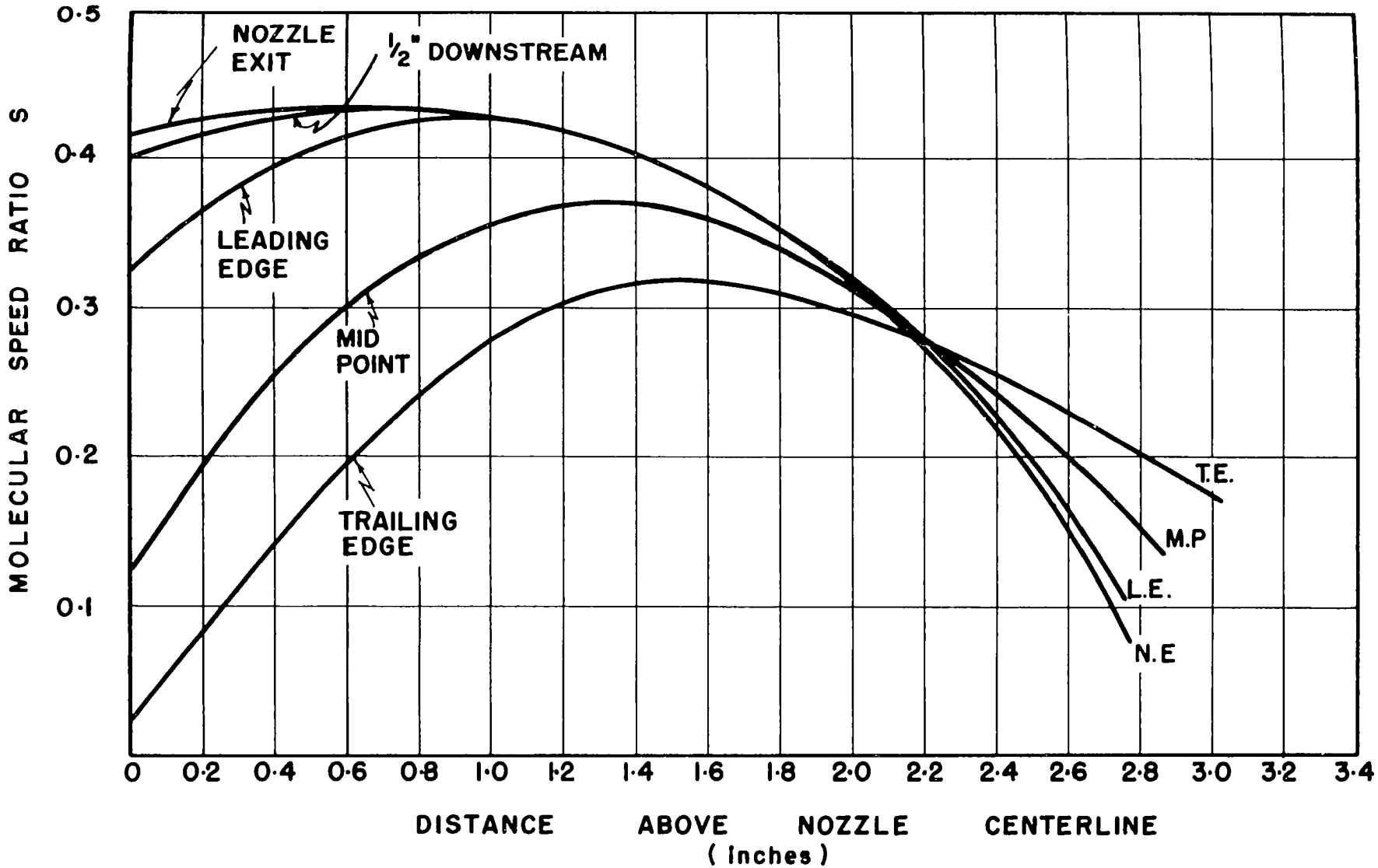

FIG. 26 CORRECTED MOLECULAR SPEED RATIOS ABOVE THE 200°C PLATE AS OBTAINED BY THE PRESSURE PAIR PROBE

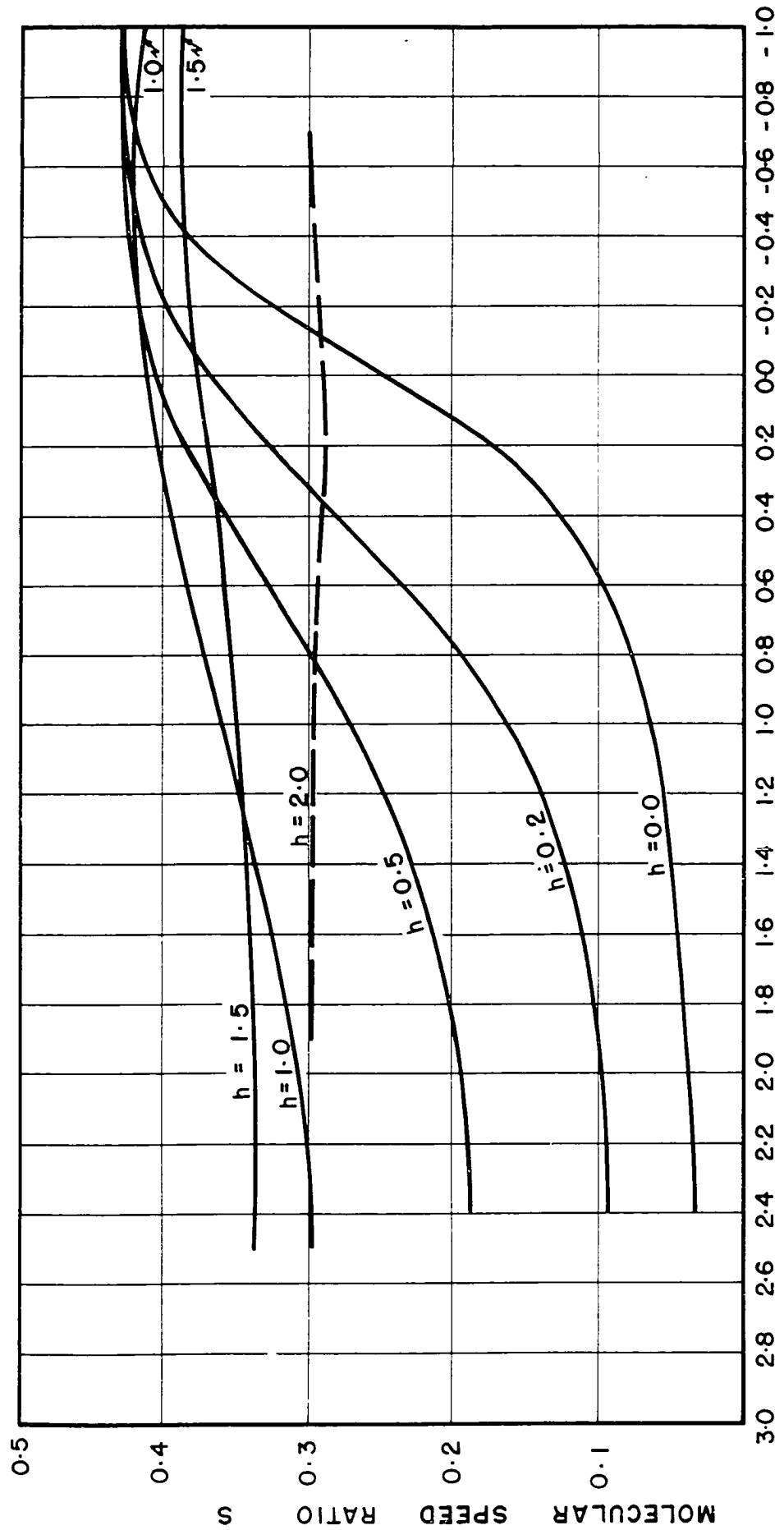

FIG. 27 CROSS PLOT OF PRESSURE PAIR PROBE DATA TAKEN OVER 100°C PLATE

Reproduced with permission of the copyright owner. Further reproduction prohibited without permission.

Reproduced with permission of the copyright owner. Further reproduction prohibited without permission.

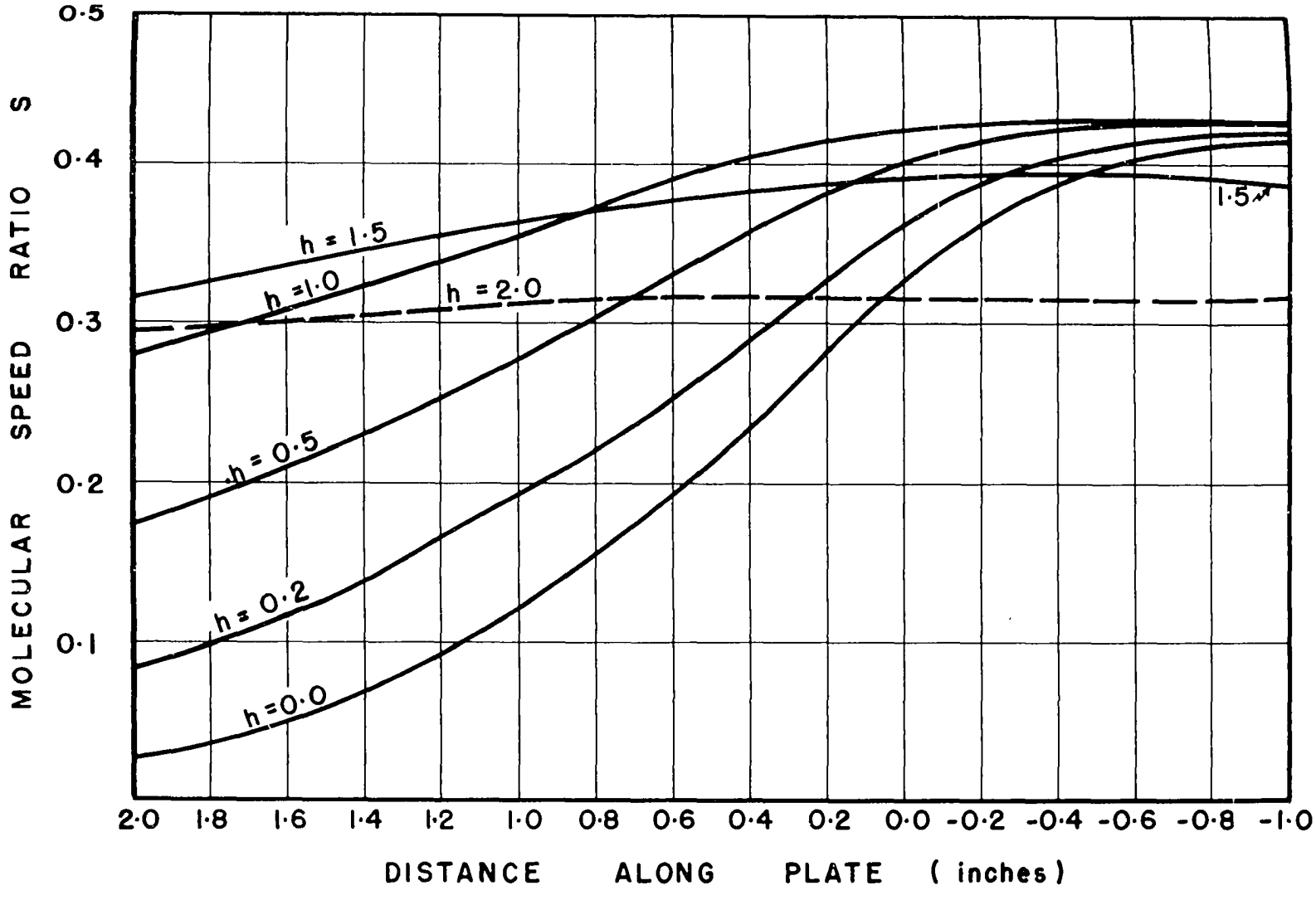

FIG. 28 CROSS PLOT OF PRESSURE PAIR PROBE DATA TAKEN OVER 200°C PLATE

Reproduced with permission of the copyright owner. Further reproduction prohibited without permission.

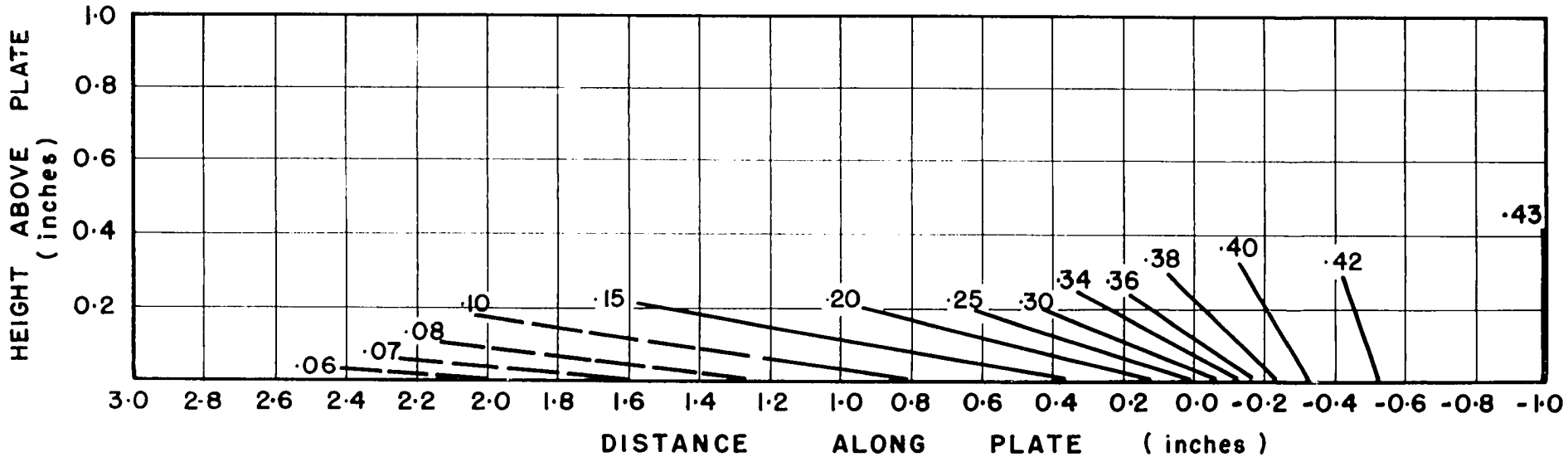

FIG. 29 LINES OF CONSTANT MOLECULAR SPEED RATIO IN THE FLOW FIELD ABOVE THE ROOM TEMPERATURE PLATE

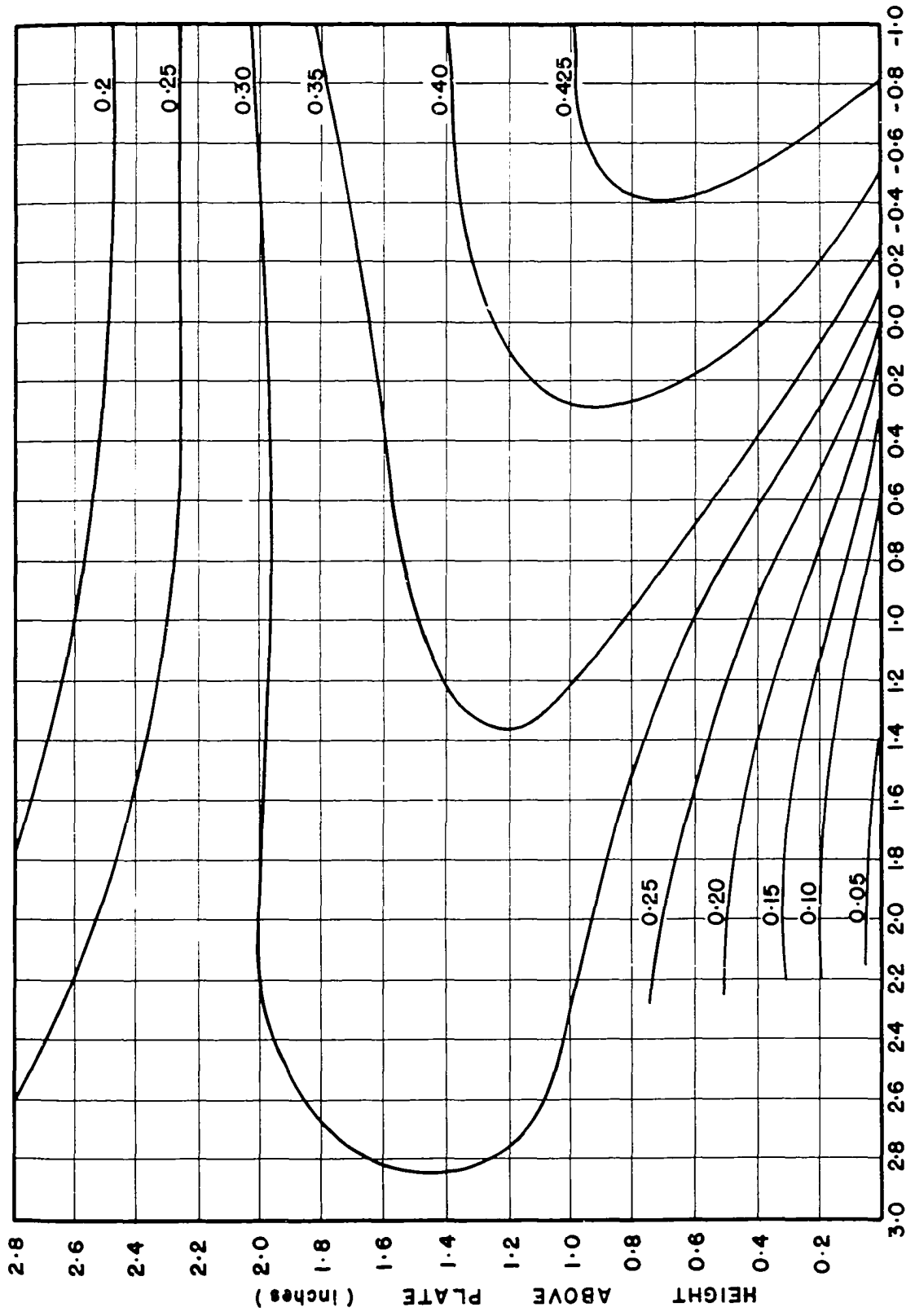

FIG. 30 LINES OF CONSTANT MOLECULAR SPEED RATIO IN THE FLOW FIELD ABOVE THE 100°C PLATE

Reproduced with permission of the copyright owner. Further reproduction prohibited without permission.

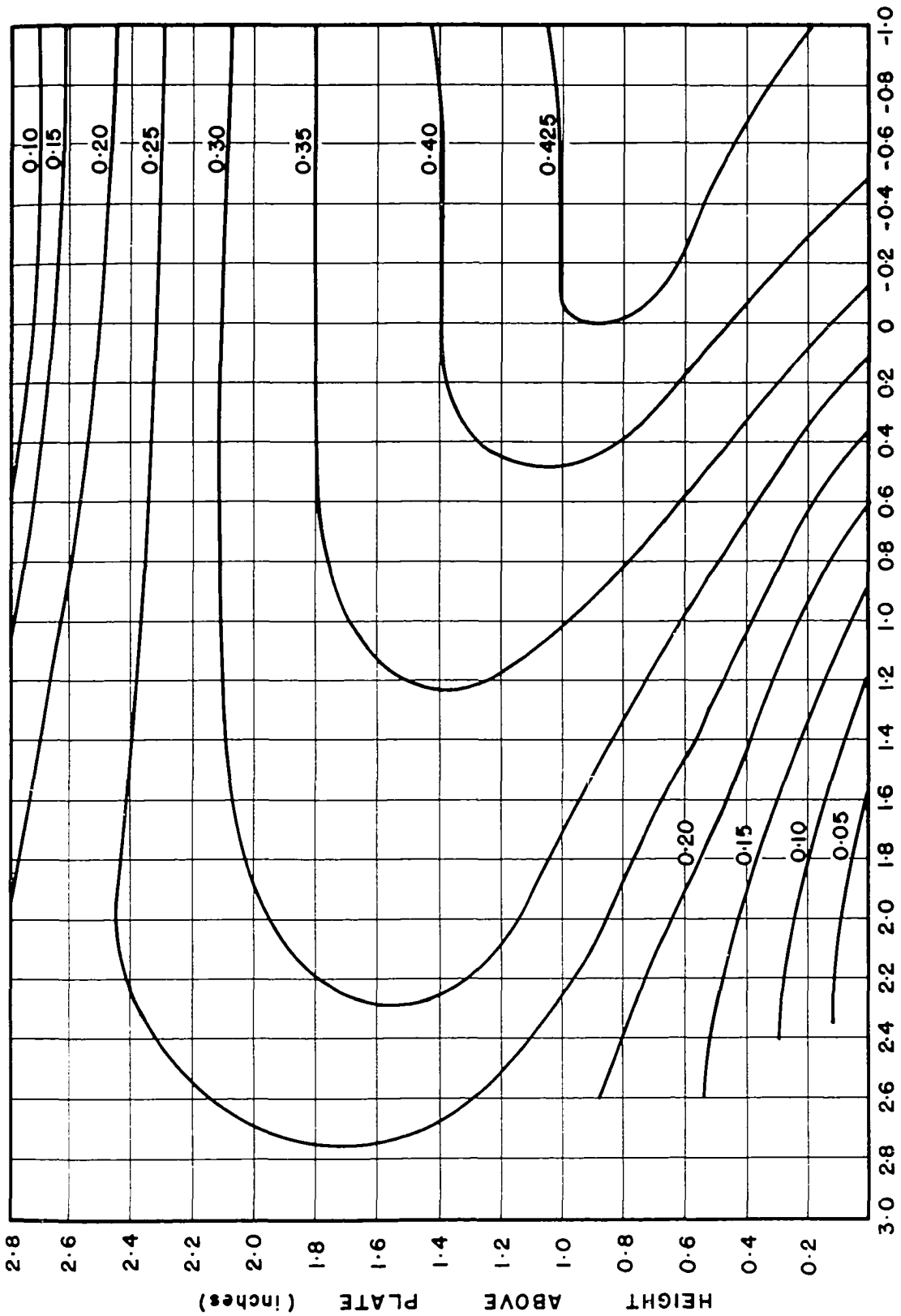

FIG. 31 LINES OF CONSTANT MOLECULAR SPEED RATIO IN THE FLOW FIELD ABOVE THE 200°C PLATE

Reproduced with permission of the copyright owner. Further reproduction prohibited without permission.

Reproduced with permission of the copyright owner. Further reproduction prohibited without permission.

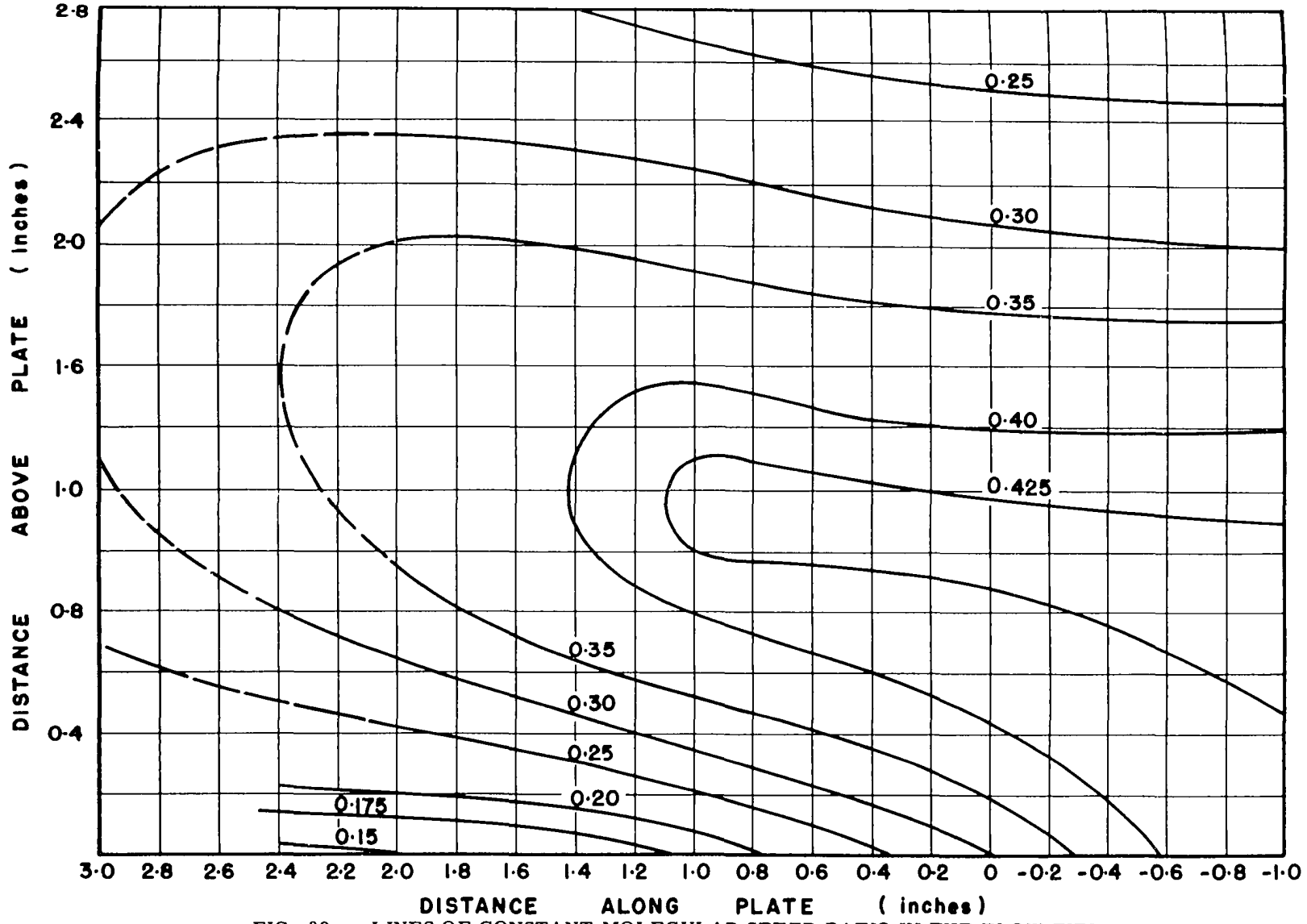

FIG. 32 LINES OF CONSTANT MOLECULAR SPEED RATIO IN THE FLOW FIELD ABOVE THE ROOM TEMPERATURE PLATE AS GIVEN BY THE EQUILIBRIUM TEMPERATURE PROBE

Reproduced with permission of the copyright owner. Further reproduction prohibited without permission.

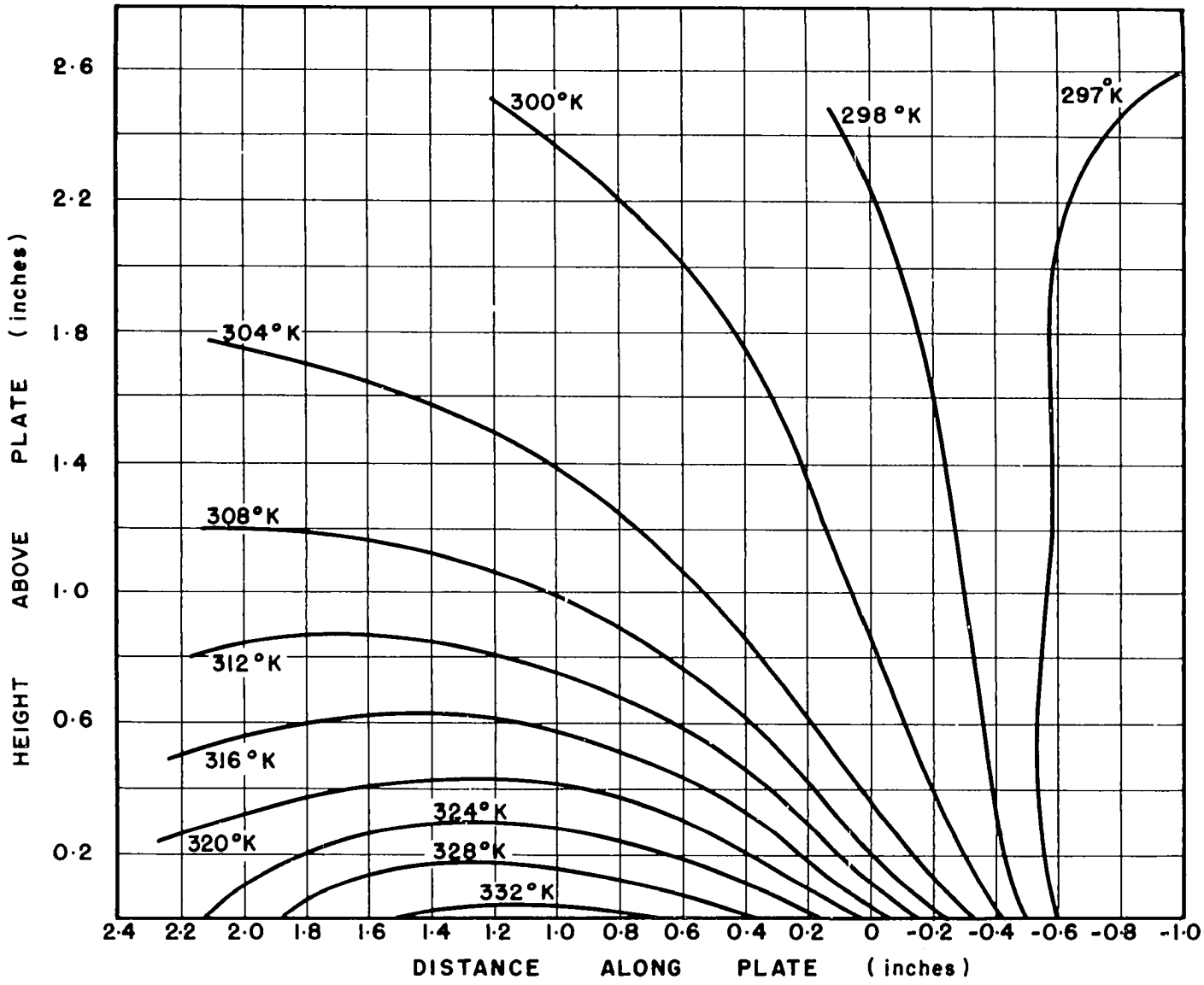

FIG. 33 LINES OF CONSTANT TOTAL TEMPERATURE IN THE FLOW FIELD ABOVE THE 100°C PLATE

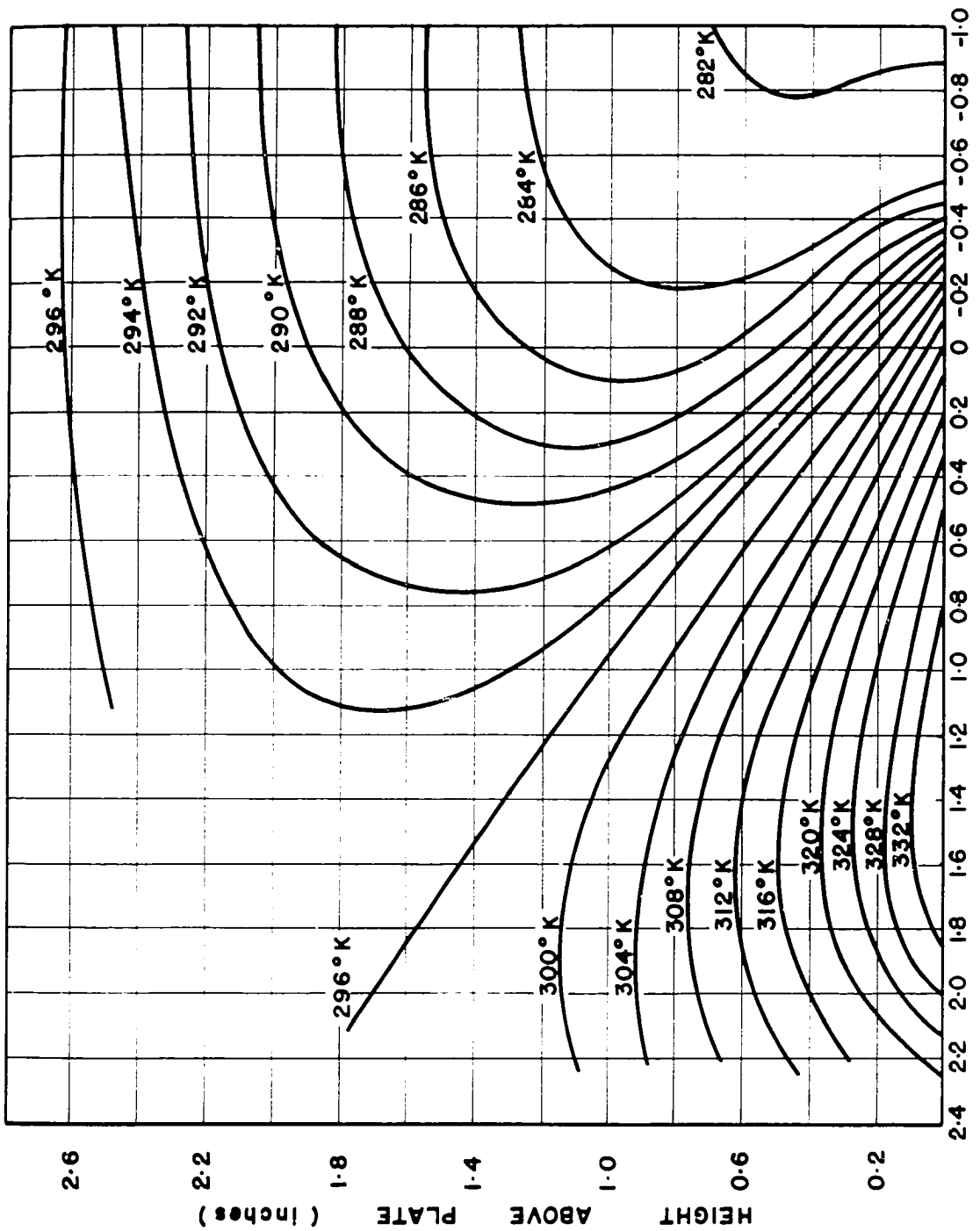

FIG. 34 LINES OF CONSTANT STATIC TEMPERATURE IN THE FLOW FIELD ABOVE THE 100°C PLATE

Reproduced with permission of the copyright owner. Further reproduction prohibited without permission.

Reproduced with permission of the copyright owner. Further reproduction prohibited without permission.

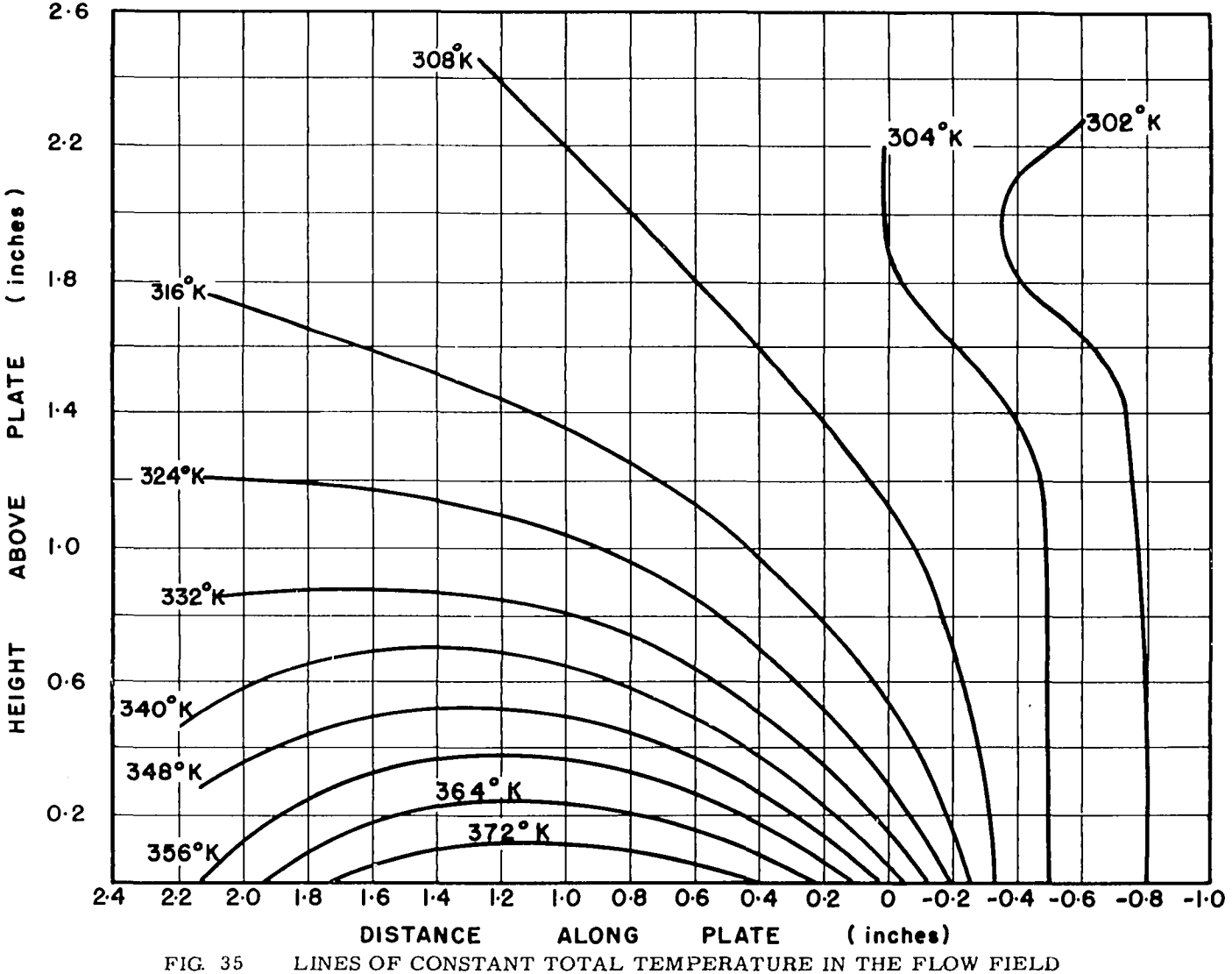

FIG. 35 LINES OF CONSTANT TOTAL TEMPERATURE IN THE FLOW FIELD ABOVE THE 200°C PLATE

Reproduced with permission of the copyright owner. Further reproduction prohibited without permission.

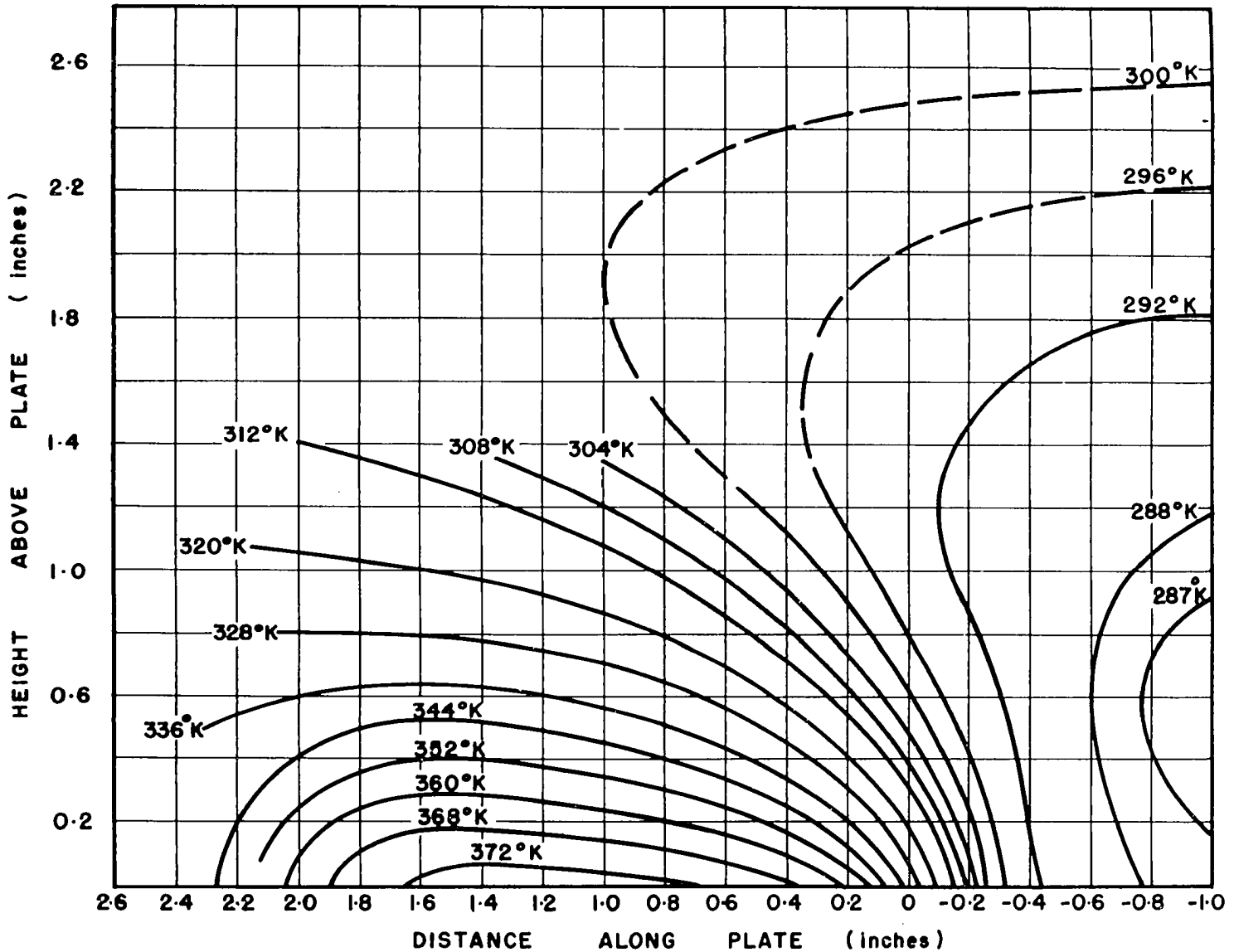

FIG. 36 LINES OF CONSTANT STATIC TEMPERATURE IN THE FLOW FIELD ABOVE THE 200°C PLATE

Reproduced with permission of the copyright owner. Further reproduction prohibited without permission.

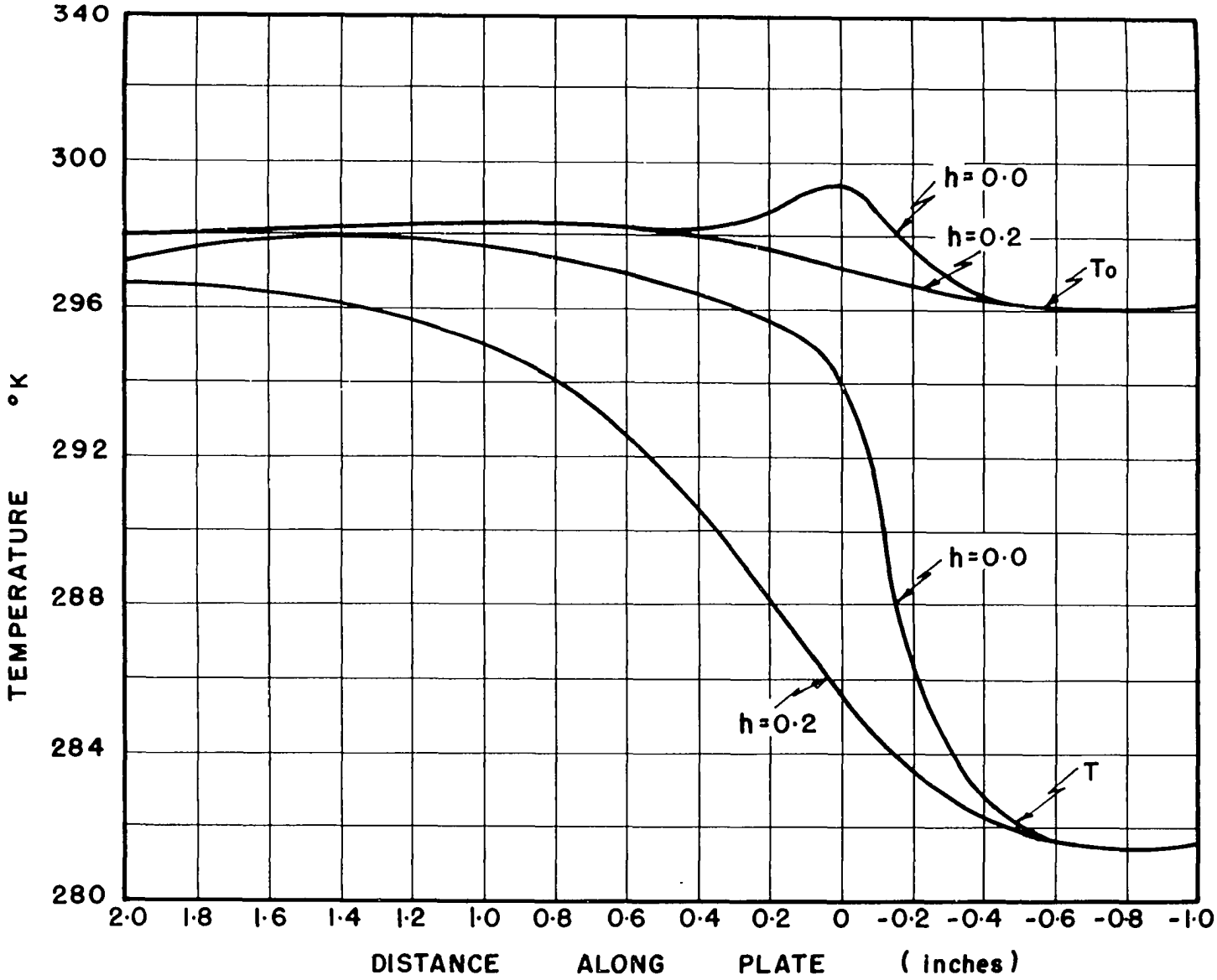

FIG. 37 STATIC AND TOTAL TEMPERATURE IN THE FLOW FIELD ABOVE THE ROOM TEMPERATURF PLATE

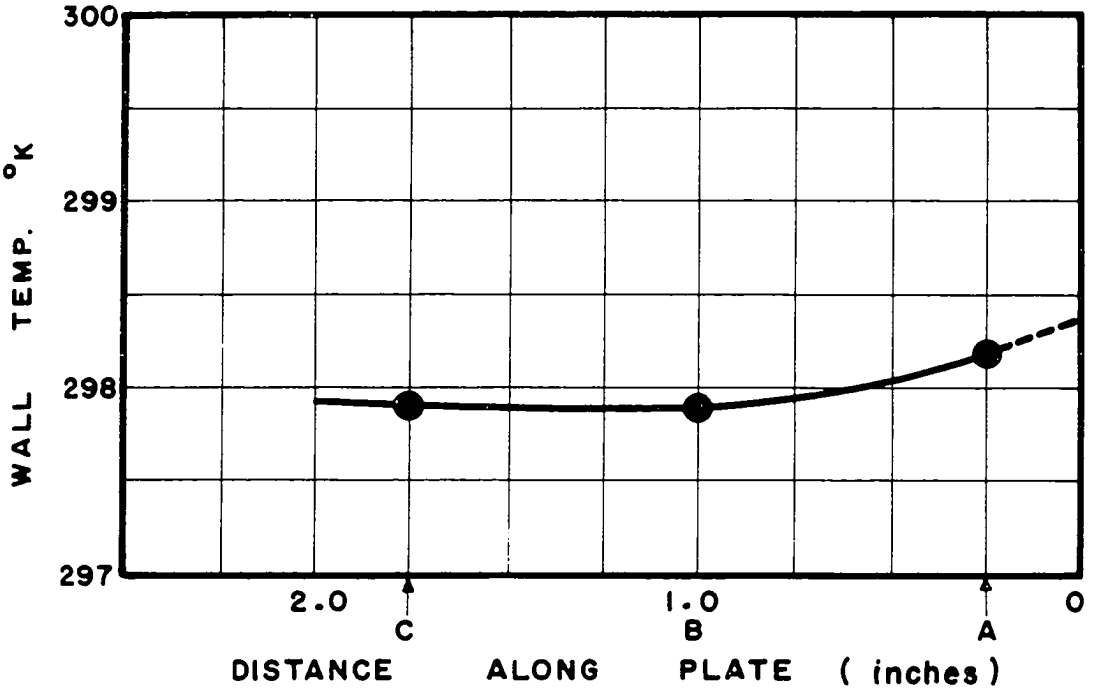

FIG. 38 ACTUAL WALL TEMPERATURE ON THE ROOM TEMPERATURE FLAT PLATE

Reproduced with permission of the copyright owner. Further reproduction prohibited without permission.

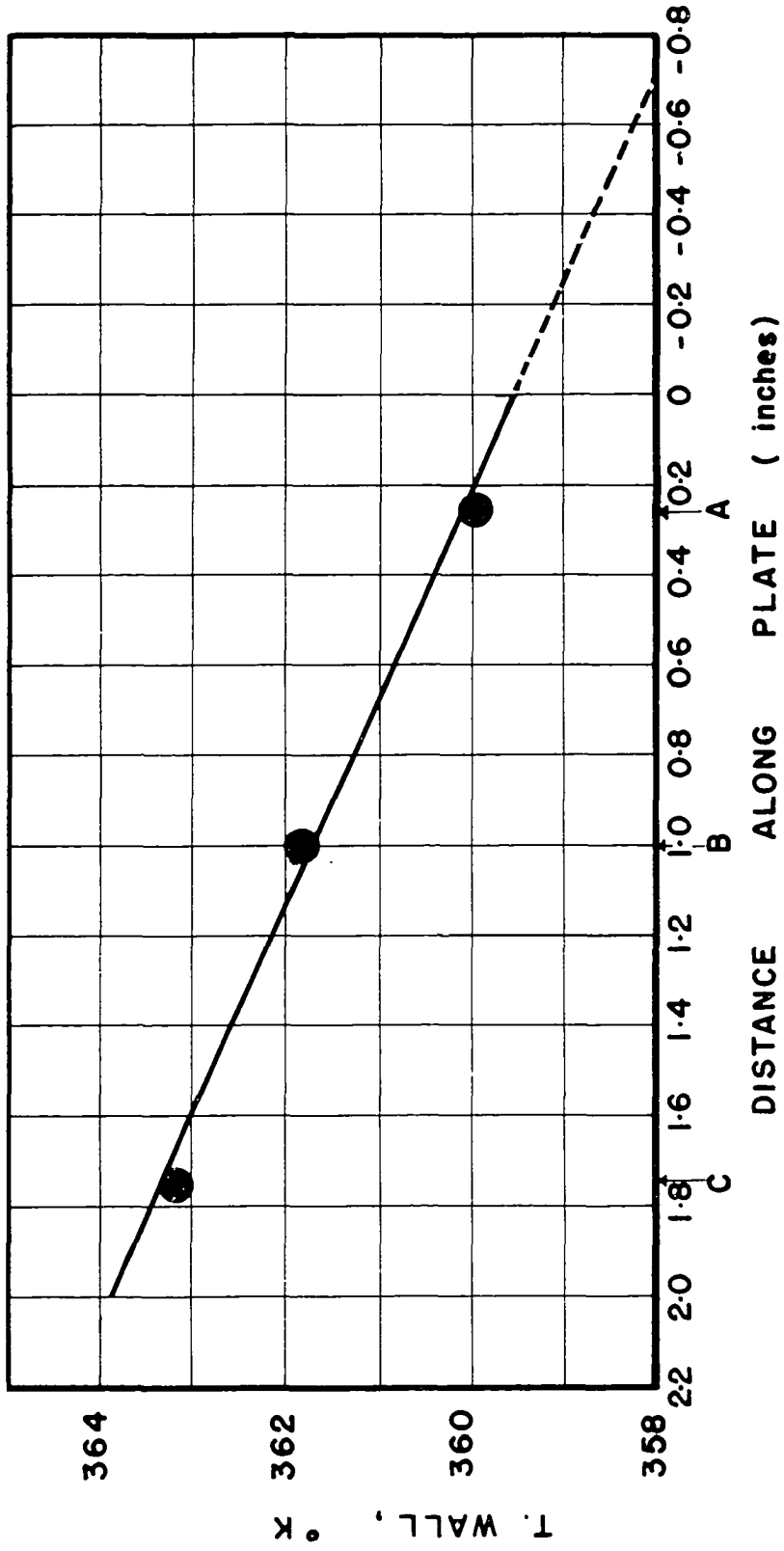

FIG. 39 ACTUAL WALL TEMPERATURE ON THE 100°C FLAT PLATE

Reproduced with permission of the copyright owner. Further reproduction prohibited without permission.

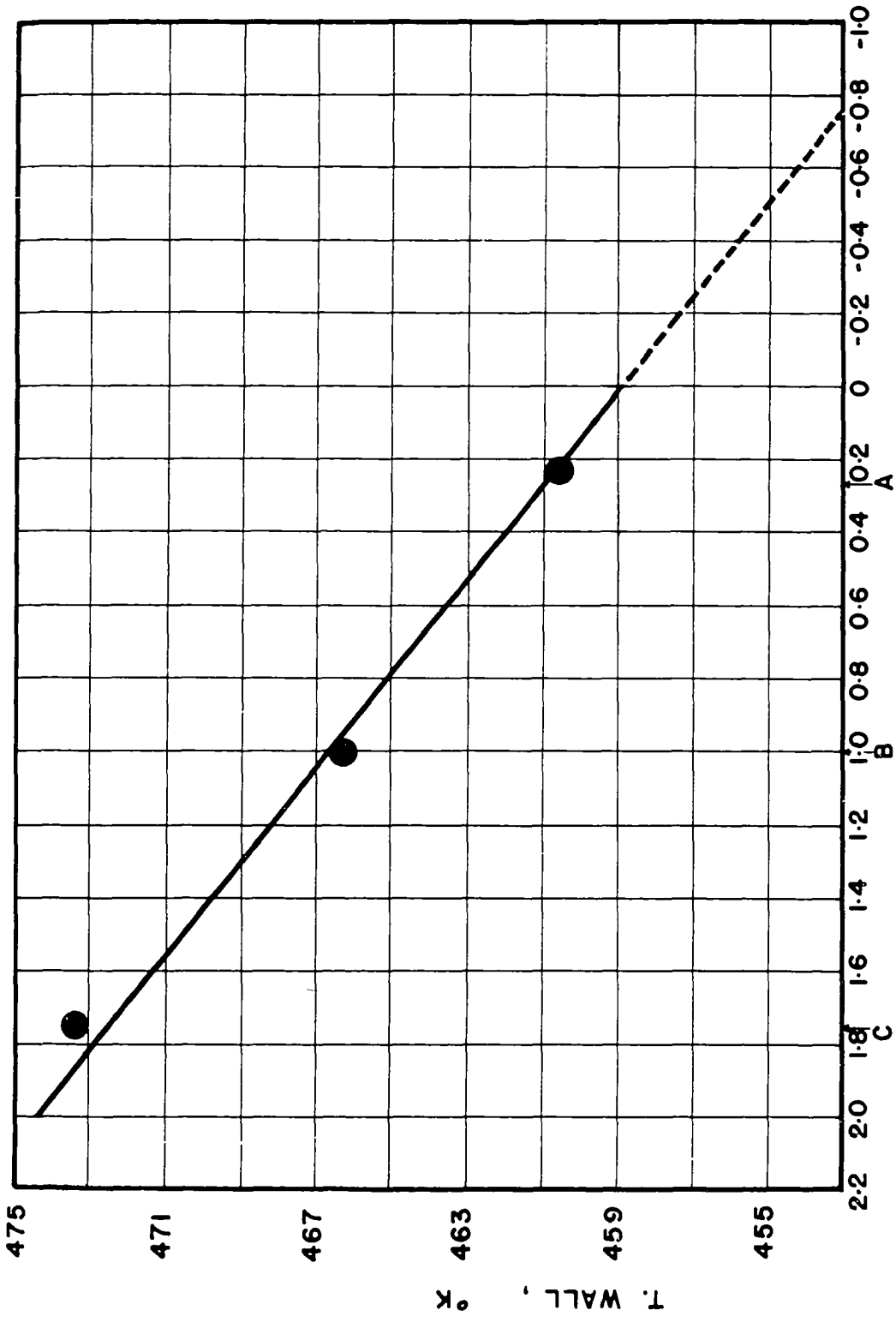

FIG. 40 ACTUAL WALL TEMPERATURE ON THE 200°C FLAT PLATE

Reproduced with permission of the copyright owner. Further reproduction prohibited without permission.

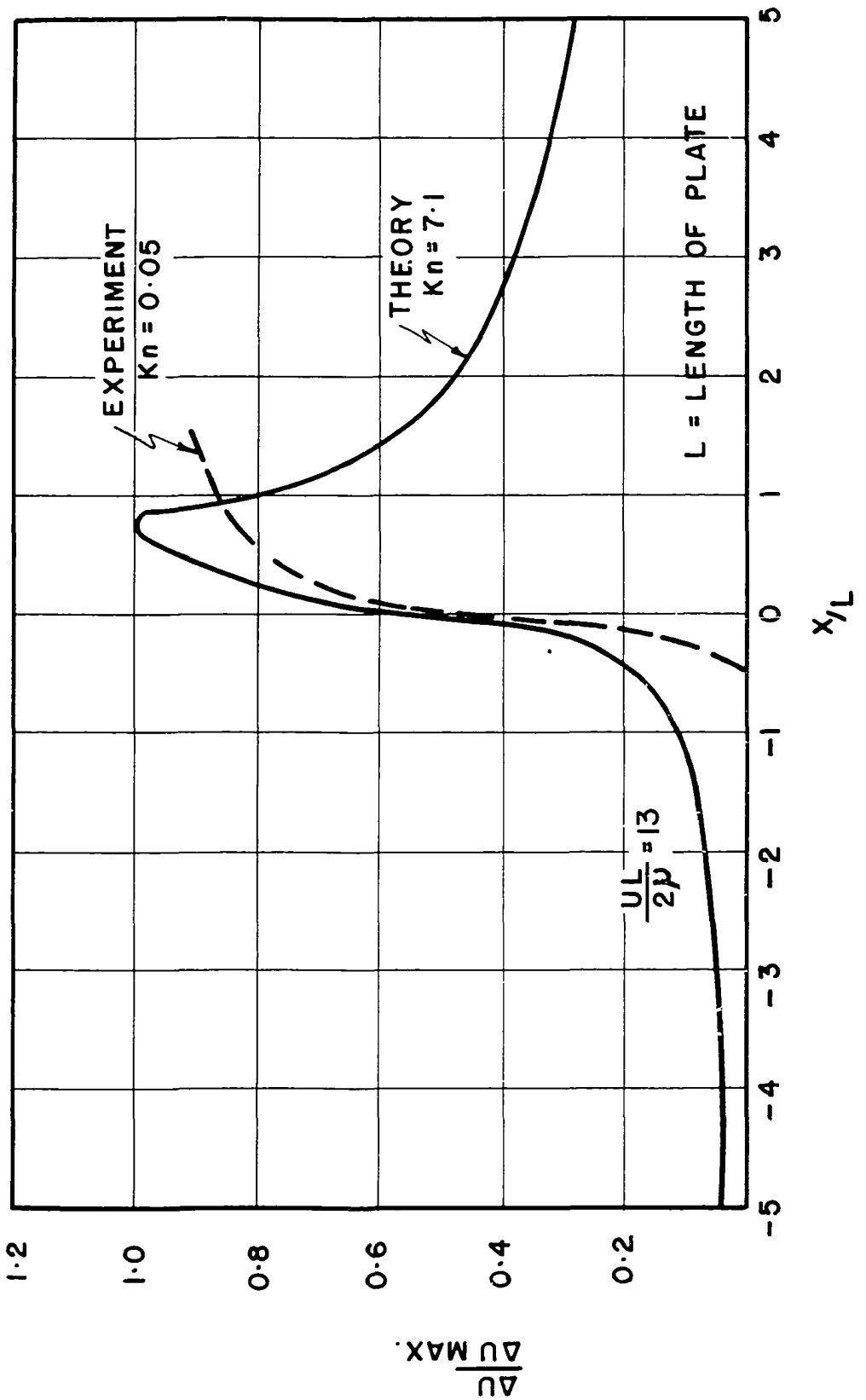

FIG. 41 COMPARISON OF EXPERIMENTAL SLIP VELOCITY WITH THEORY OF LAURMANN

Reproduced with permission of the copyright owner. Further reproduction prohibited without permission.

Reproduced with permission of the copyright owner. Further reproduction prohibited without permission.

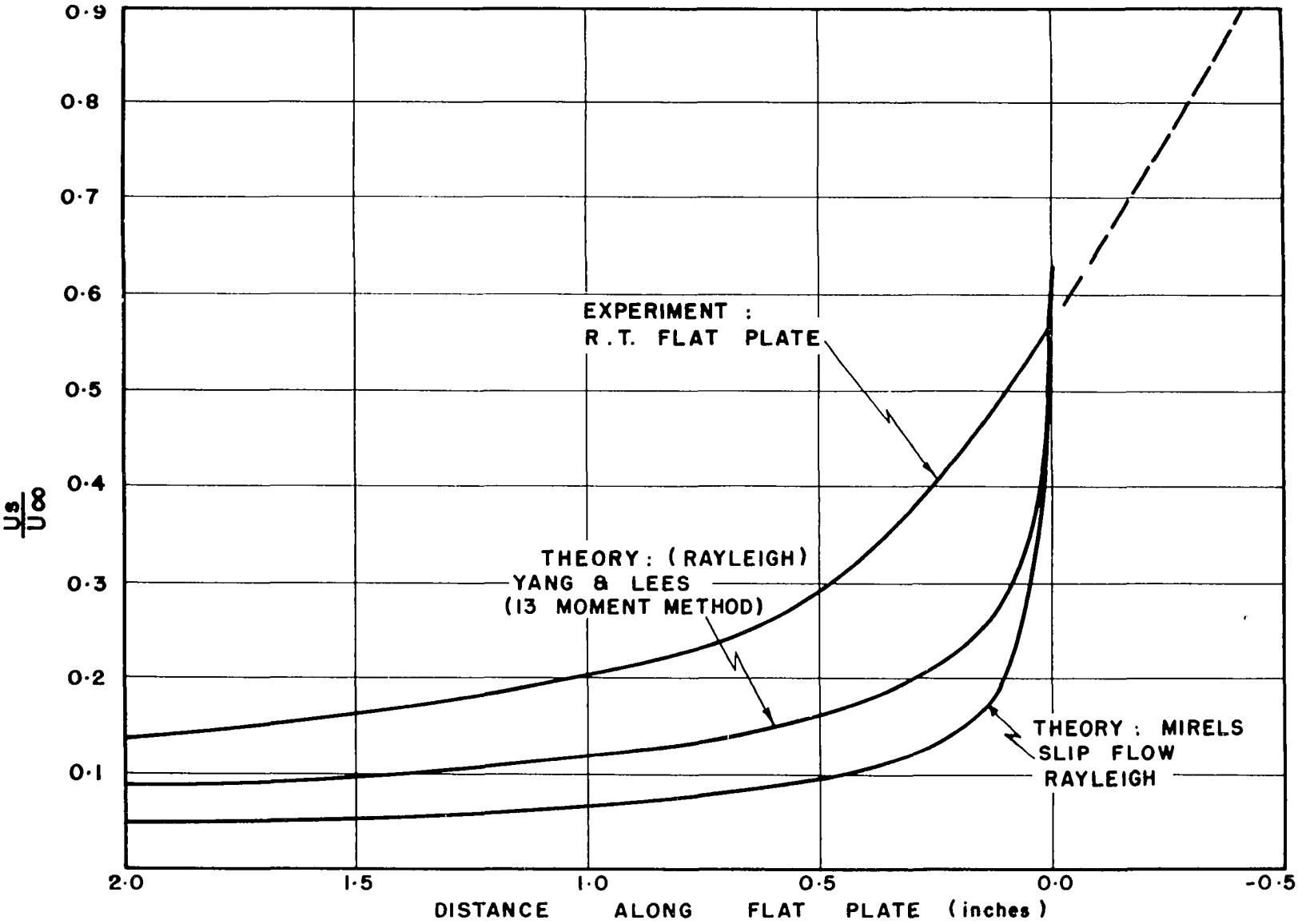

FIG. 42 COMPARISON OF EXPERIMENTAL SLIP VELOCITY WITH VARIOUS THEORETICAL SOLUTIONS

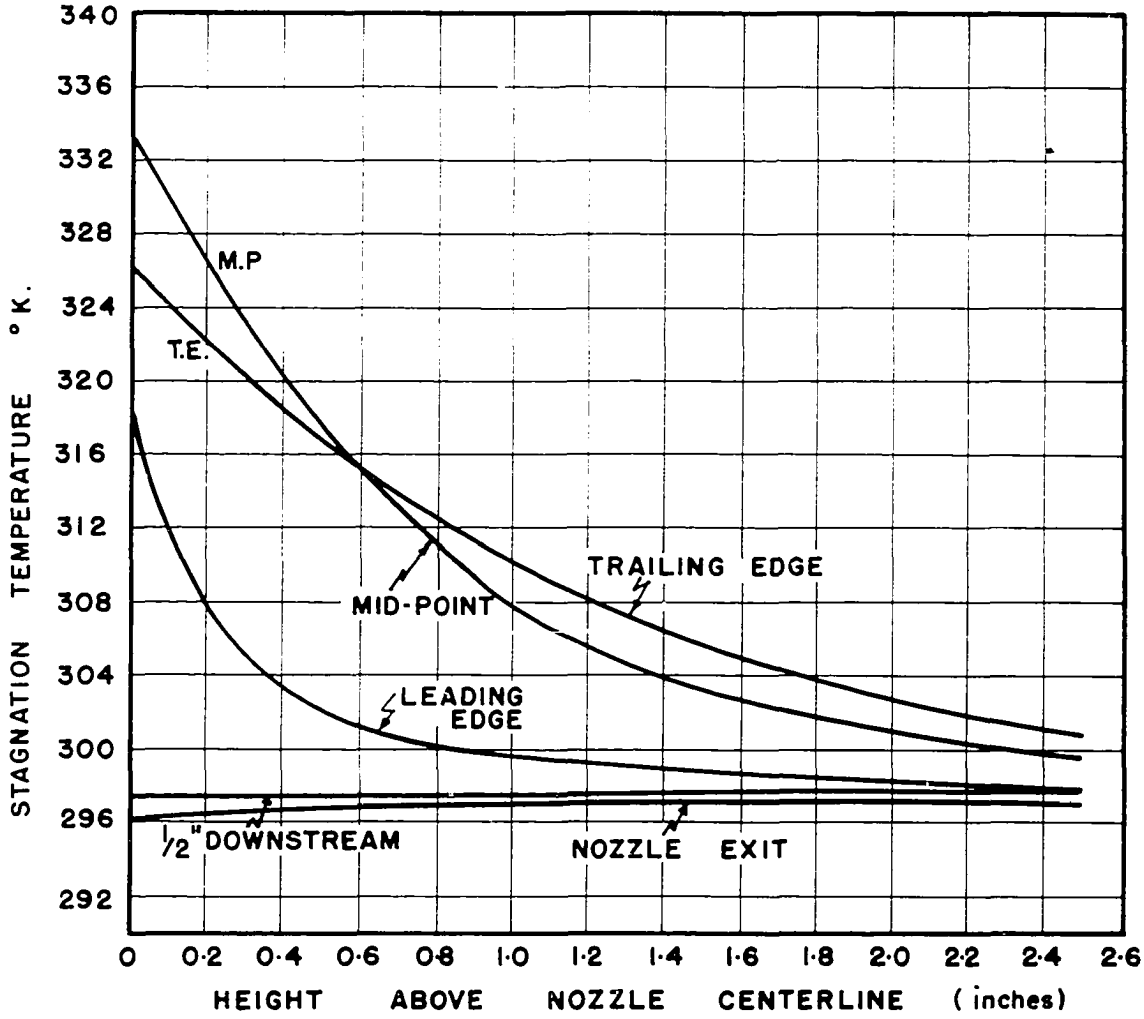

FIG. 43 PLOTS OF VARIATION OF TOTAL TEMPERATURE ABOVE 100°C PLATE

Reproduced with permission of the copyright owner. Further reproduction prohibited without permission.

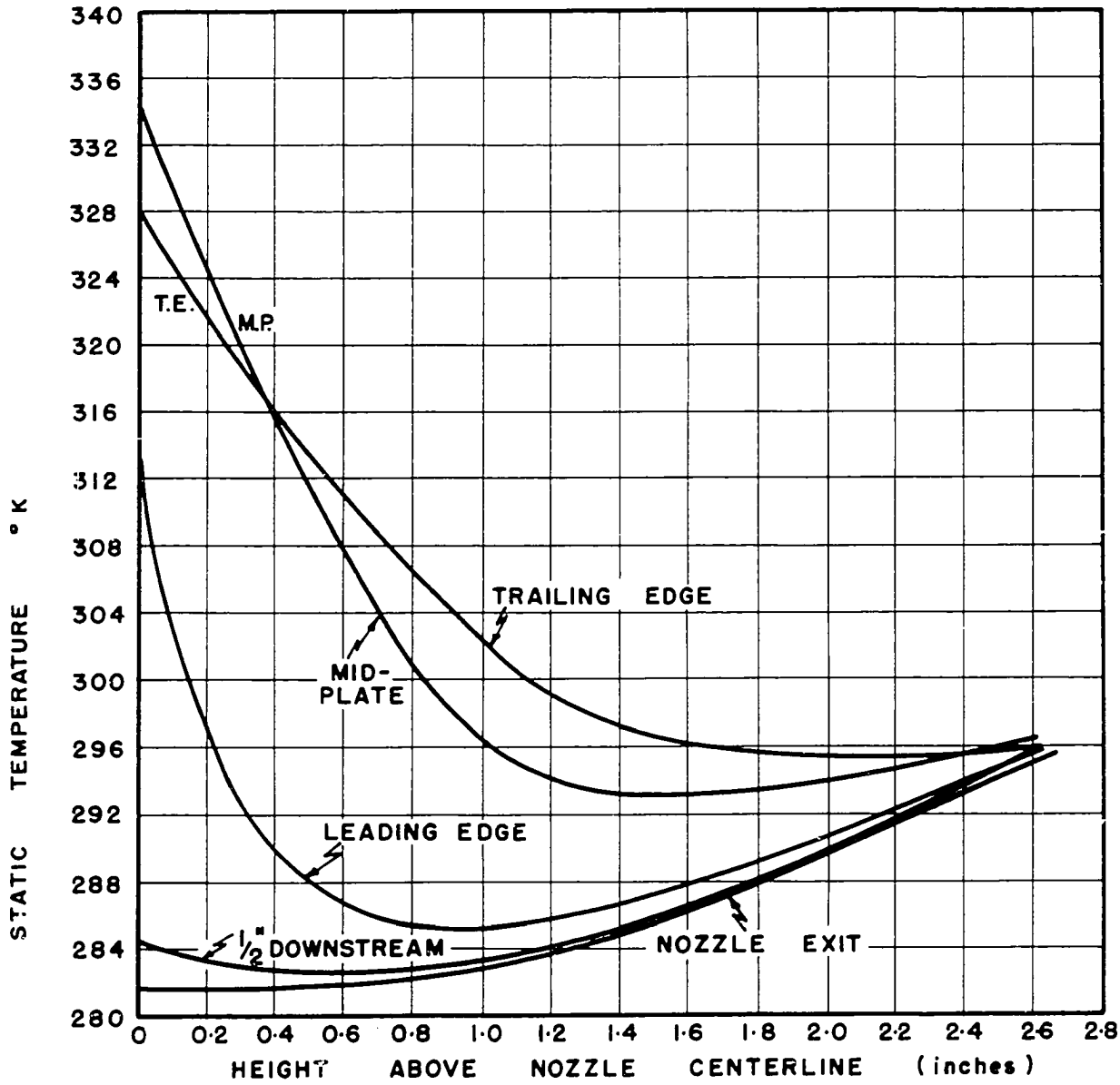

FIG. 44 PLOTS OF VARIATION OF STATIC TEMPERATURE ABOVE 100°C PLATE

Reproduced with permission of the copyright owner. Further reproduction prohibited without permission.

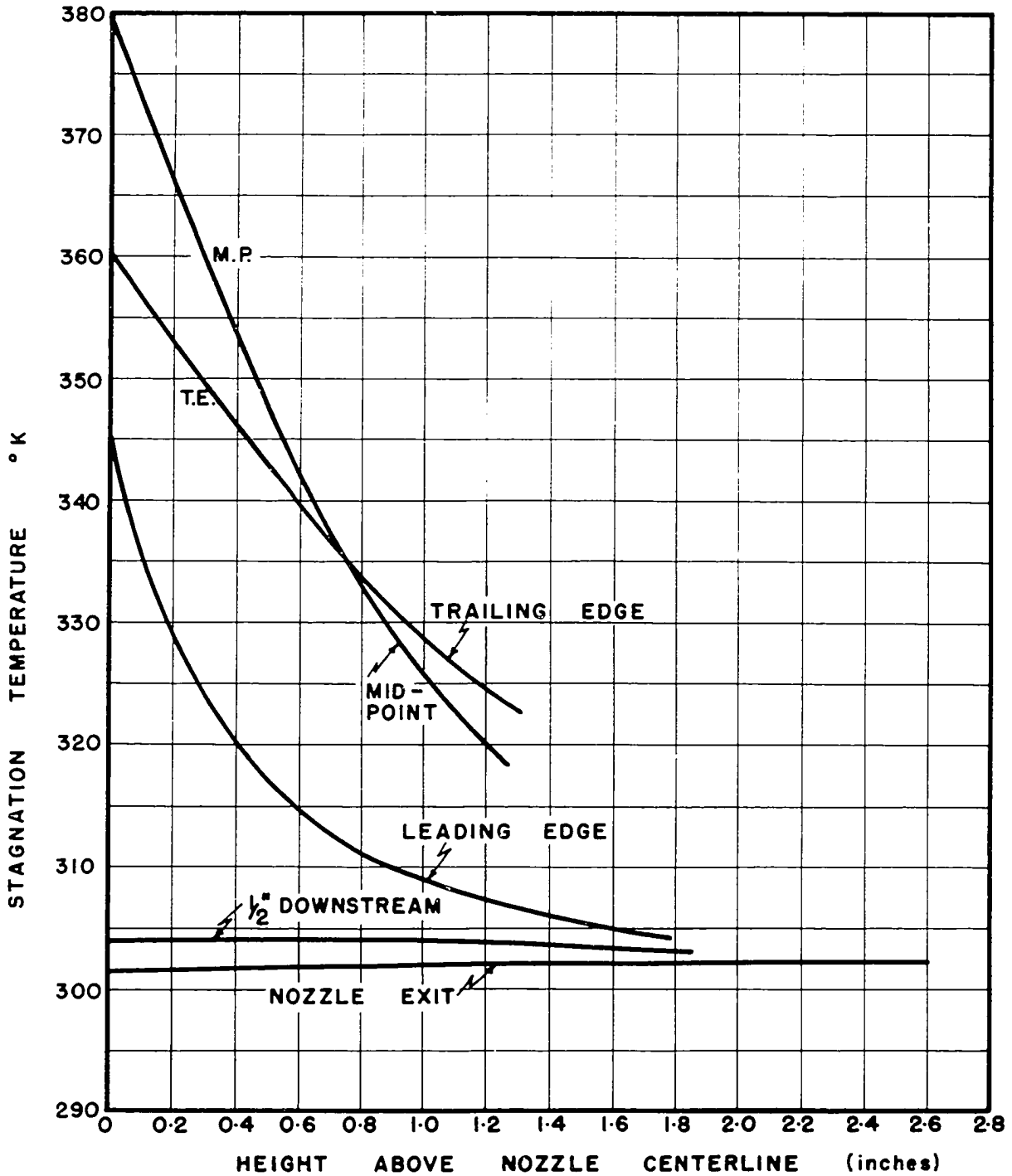

FIG. 45 PLOTS OF VARIATION OF TOTAL TEMPERATURE ABOVE 200°C PLATE

Reproduced with permission of the copyright owner. Further reproduction prohibited without permission.

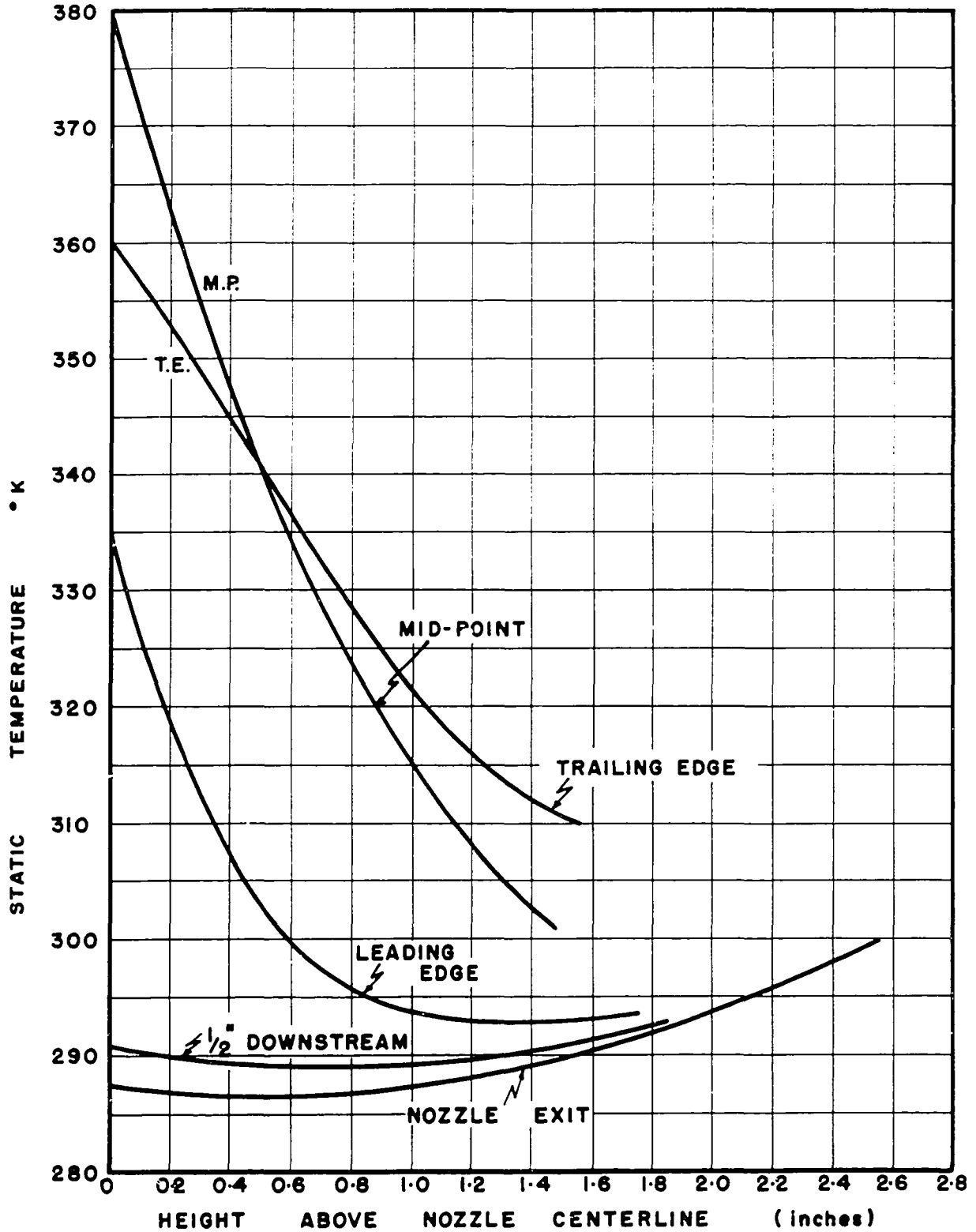

FIG. 46 PLOTS OF VARIATION OF STATIC TEMPERATURE ABOVE 200°C PLATE

Reproduced with permission of the copyright owner. Further reproduction prohibited without permission.

Reproduced with permission of the copyright owner. Further reproduction prohibited without permission.

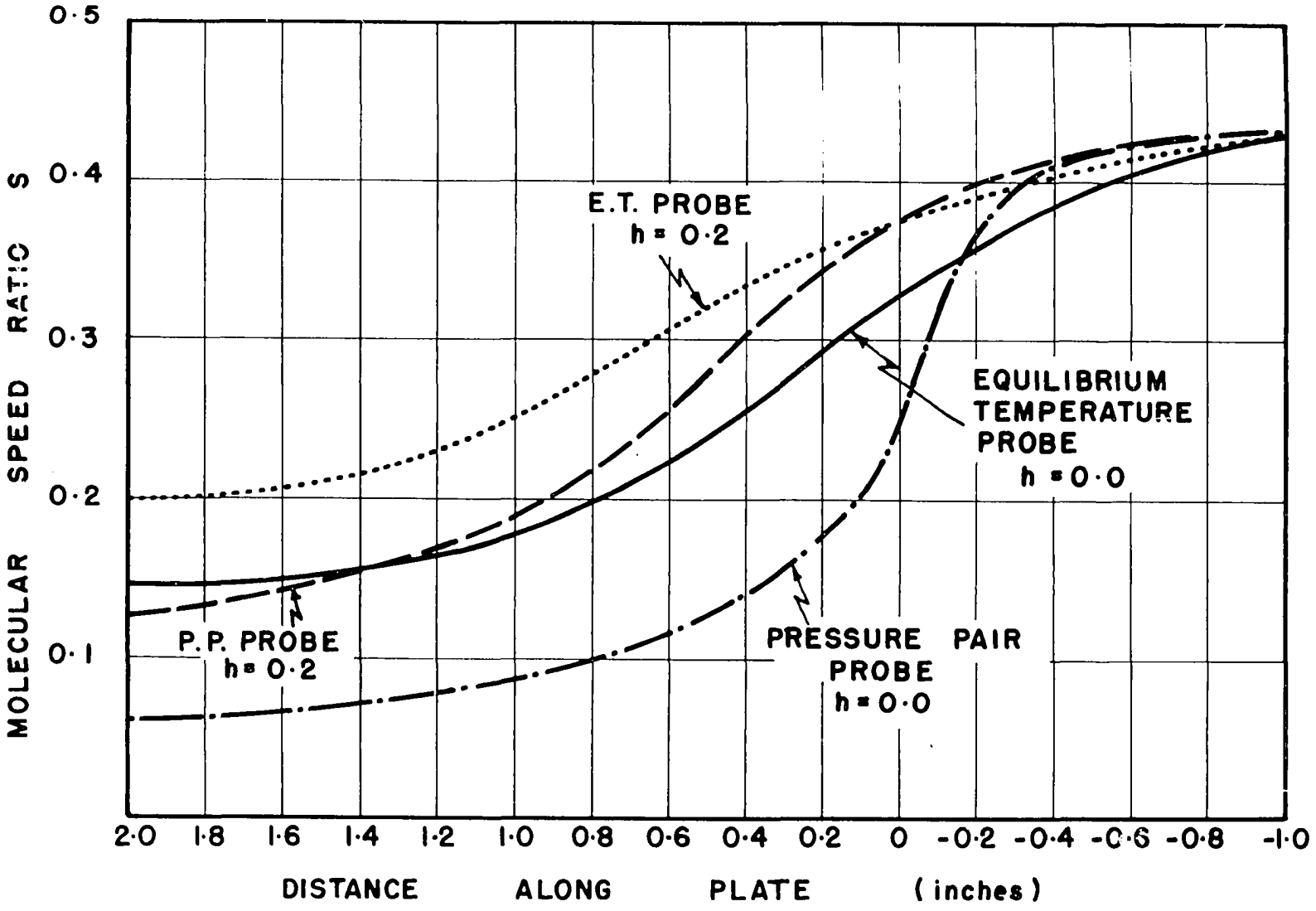

FIG. 47 COMPARISON OF SPEED RATIOS AS OBTAINED BY THE EQUILIBRIUM TEMPERATURE PROBE AND THE PRESSURE PAIR PROBE FOR THE ROOM TEMPERATURE PLATE

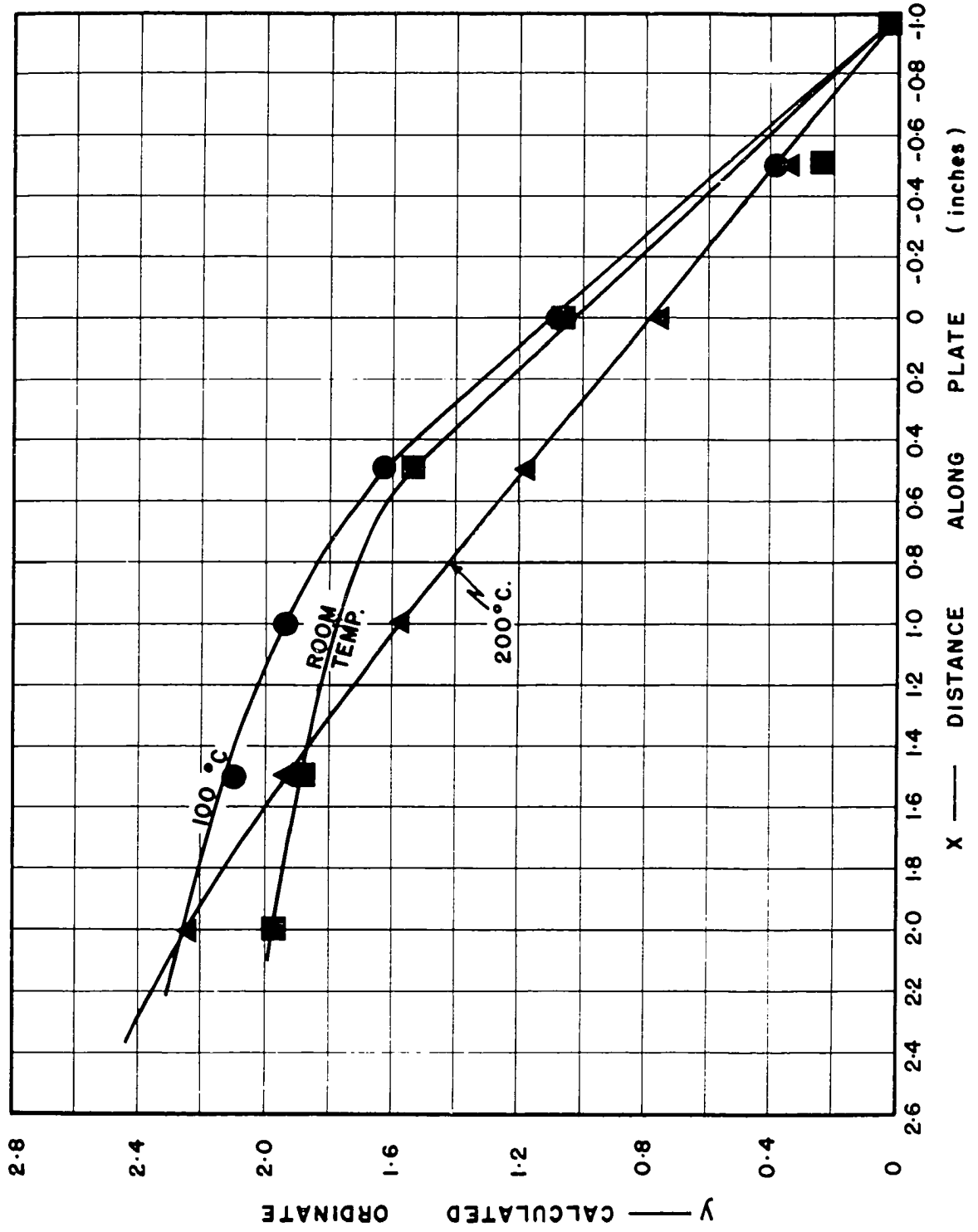

FIG. 48 GAUSSIAN ERROR CURVE PLOTS OF SLIP VELOCITY

Reproduced with permission of the copyright owner. Further reproduction prohibited without permission.

Reproduced with permission of the copyright owner. Further reproduction prohibited without permission.

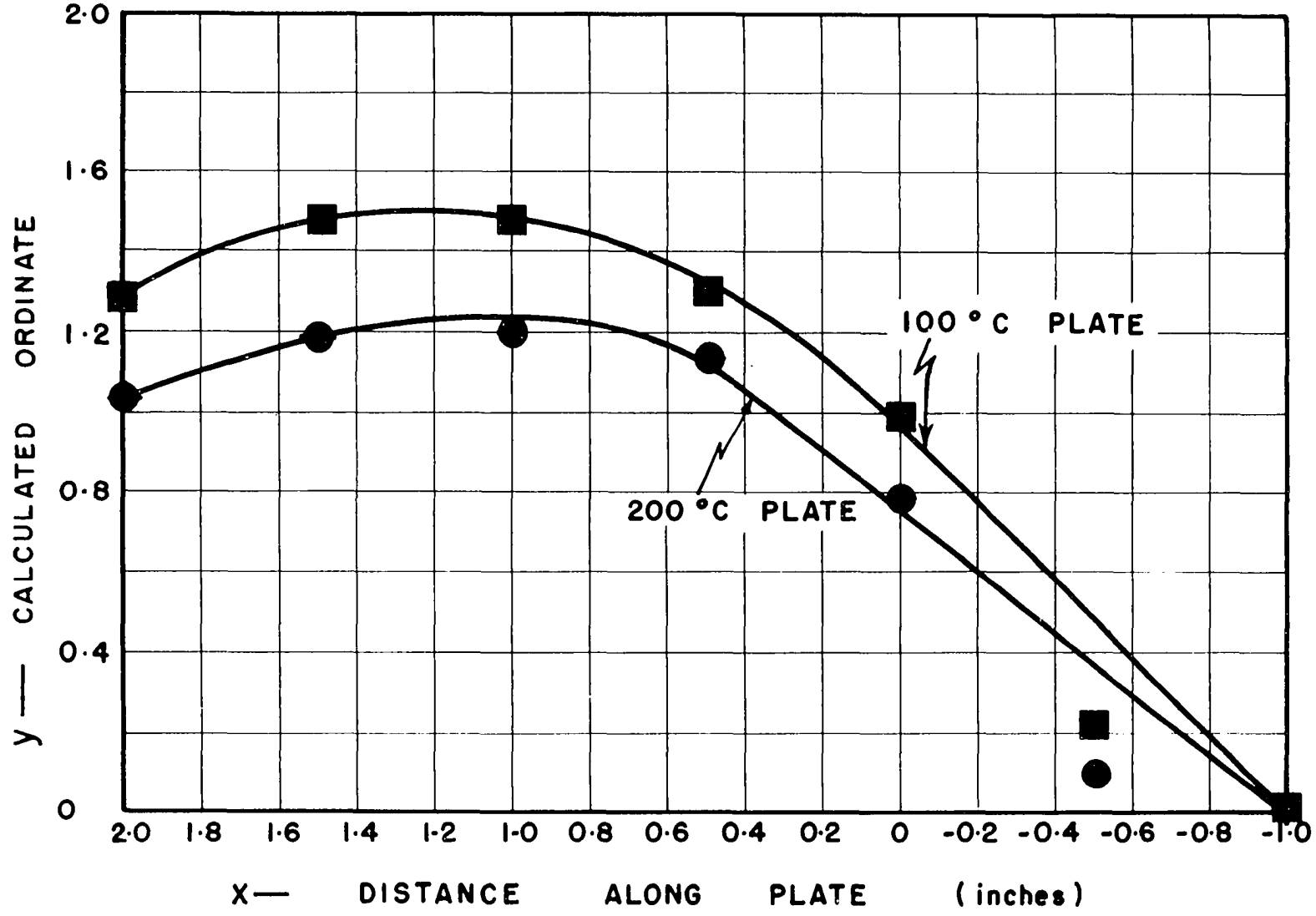

FIG. 49 GAUSSIAN ERROR CURVE PLOTS OF TEMPERATURE JUMP

Reproduced with permission of the copyright owner. Further reproduction prohibited without permission.

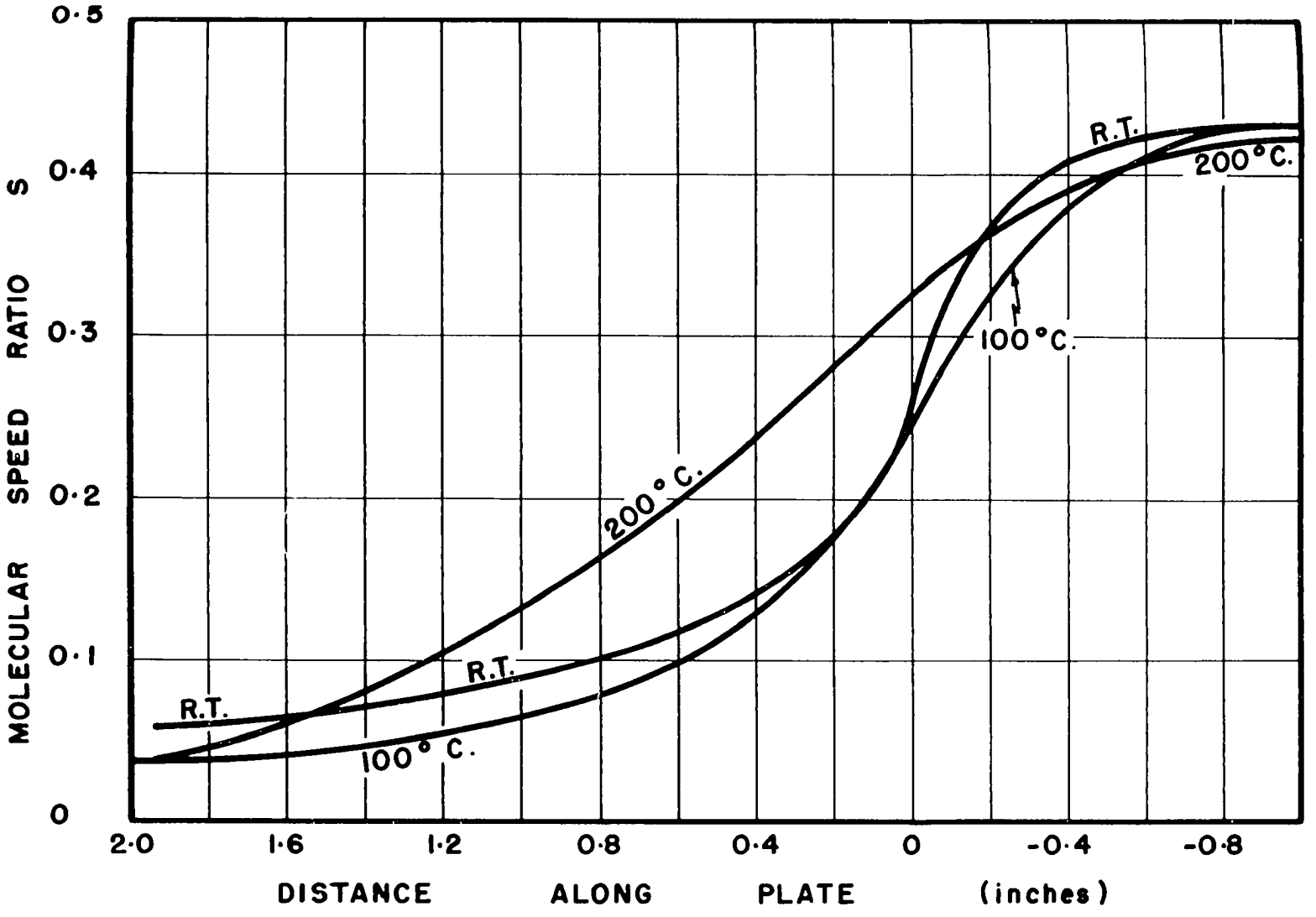

FIG. 50 EXPERIMENTAL VALUES OF MOLECULAR SPEED RATIO ON THE NOZZLE AXIS

Reproduced with permission of the copyright owner. Further reproduction prohibited without permission.

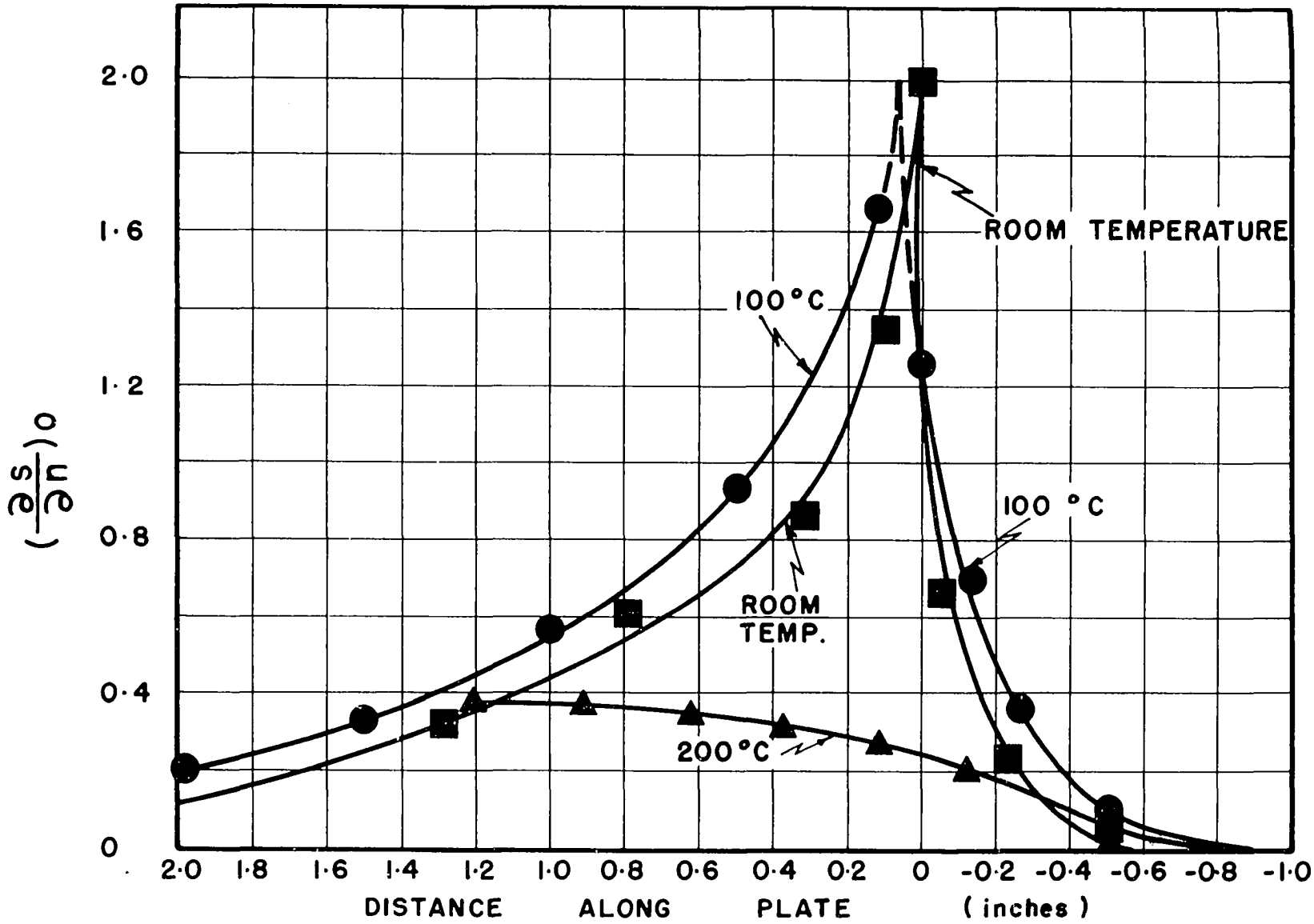

FIG. 51 RATE OF CHANGE OF MOLECULAR SPEED RATIO ON A FLAT PLATE WITH DISTANCE FROM LEADING EDGE.

Reproduced with permission of the copyright owner. Further reproduction prohibited without permission.

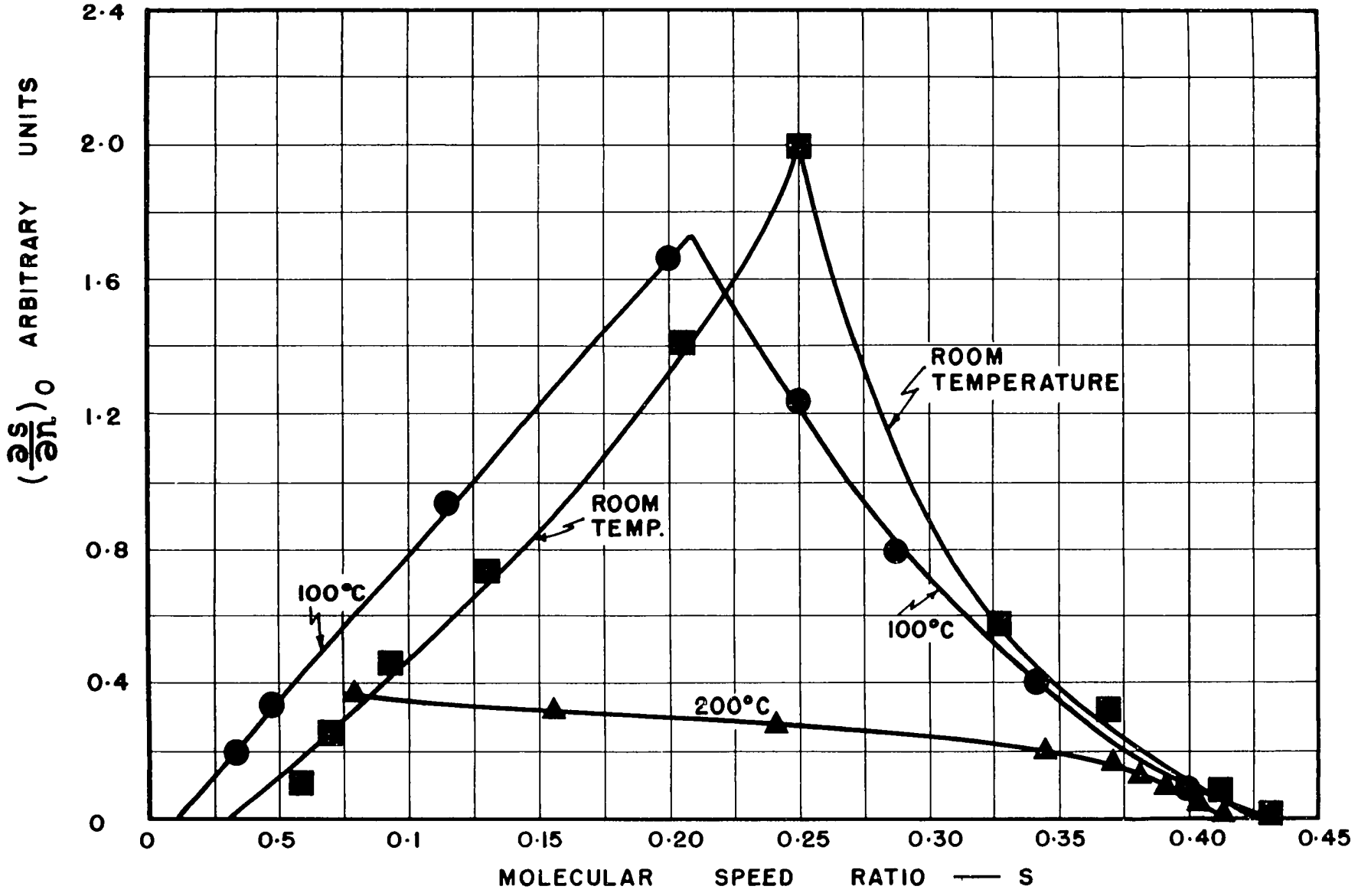

FIG. 52 RATE OF CHANGE OF MOLECULAR SPEED RATIO OVER A FLAT PLATE IN TERMS OF MOLECULAR SPEED RATIO, S

Reproduced with permission of the copyright owner. Further reproduction prohibited without permission.

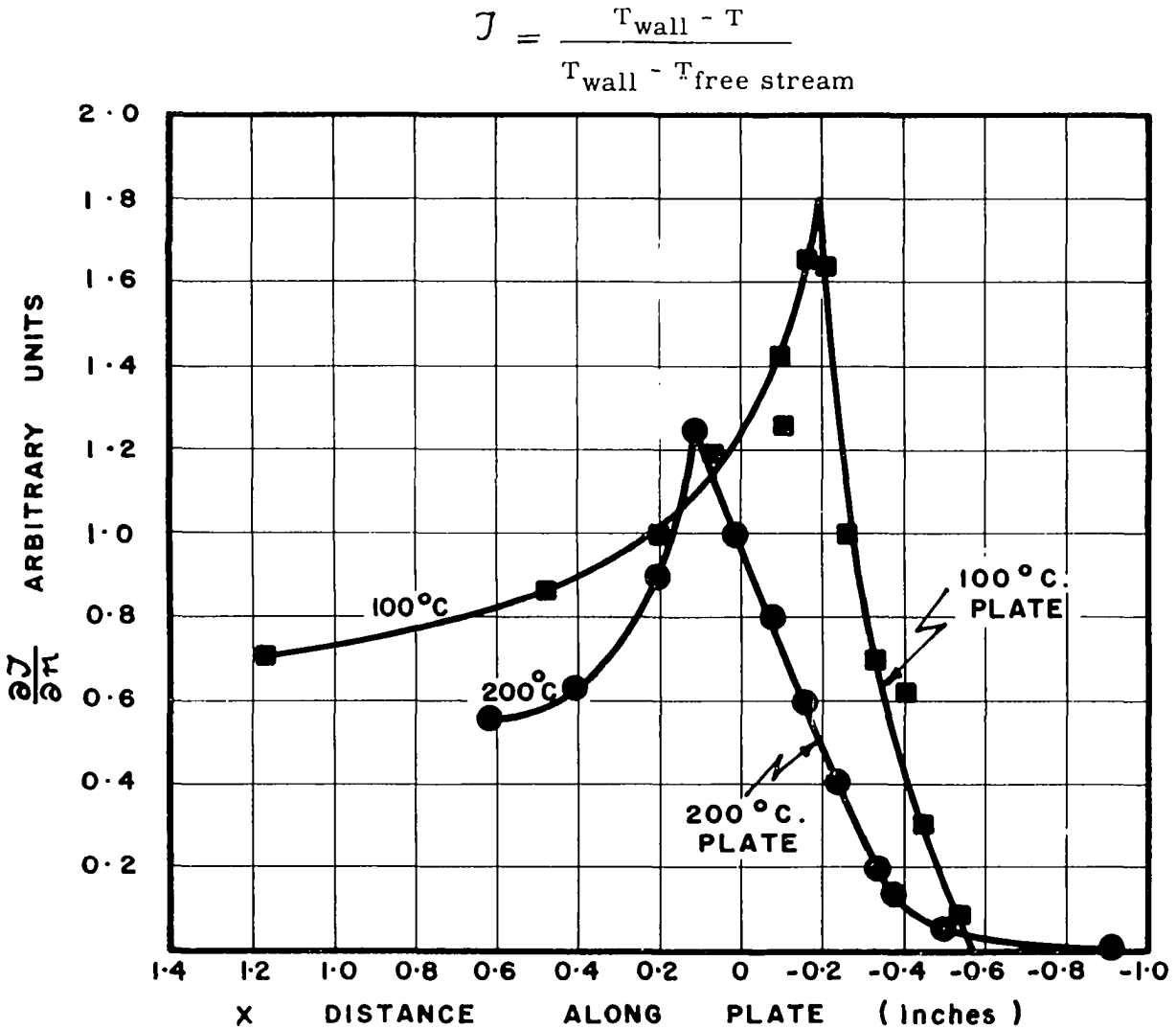

FIG. 53 RATE OF CHANGE OF TEMPERATURE JUMP WITH DISTANCE FROM LEADING EDGE OF A FLAT PLATE

Reproduced with permission of the copyright owner. Further reproduction prohibited without permission.

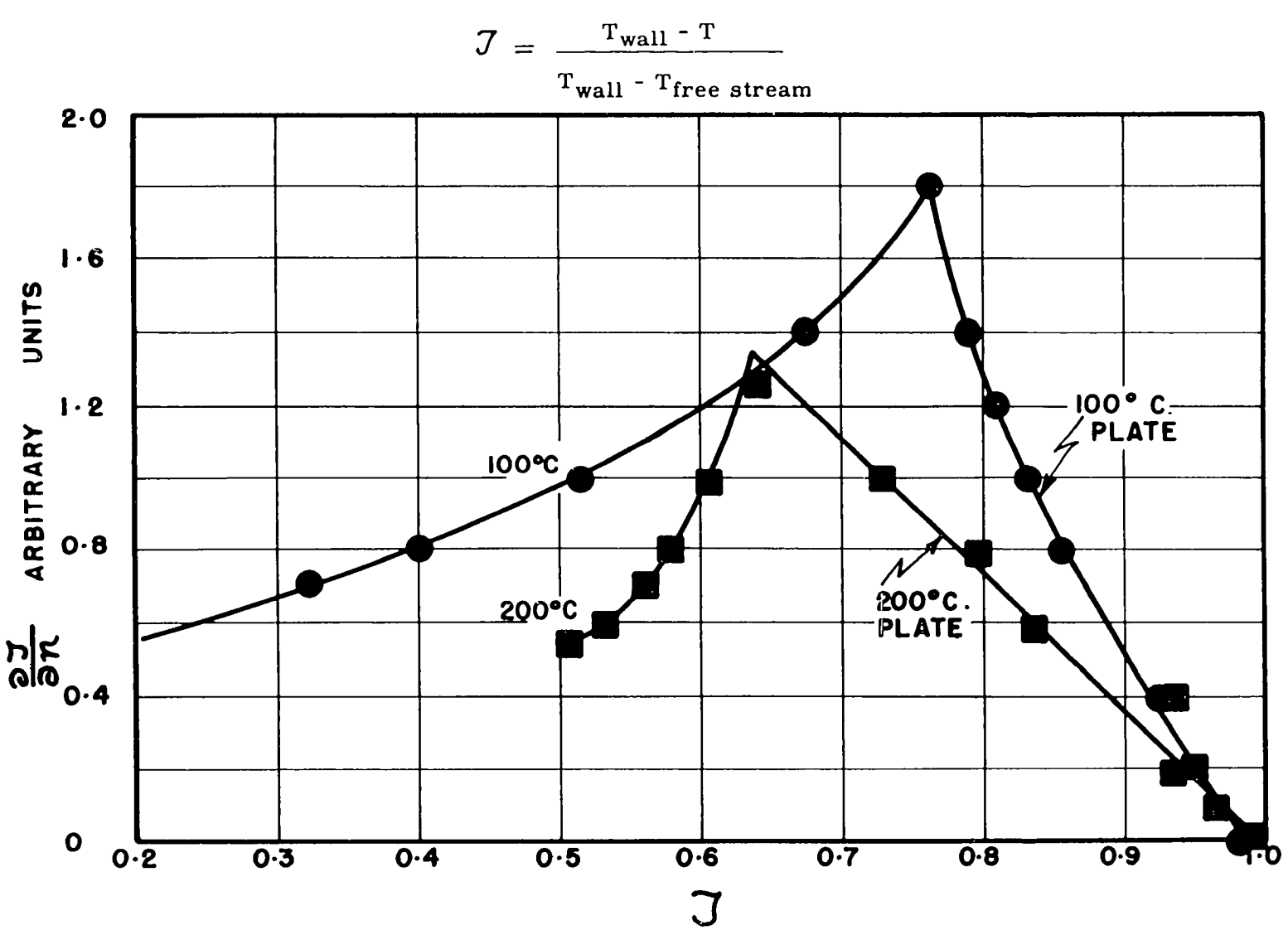

FIG. 54 RATE OF CHANGE OF TEMPERATURE JUMP WITH TEMPERATURE

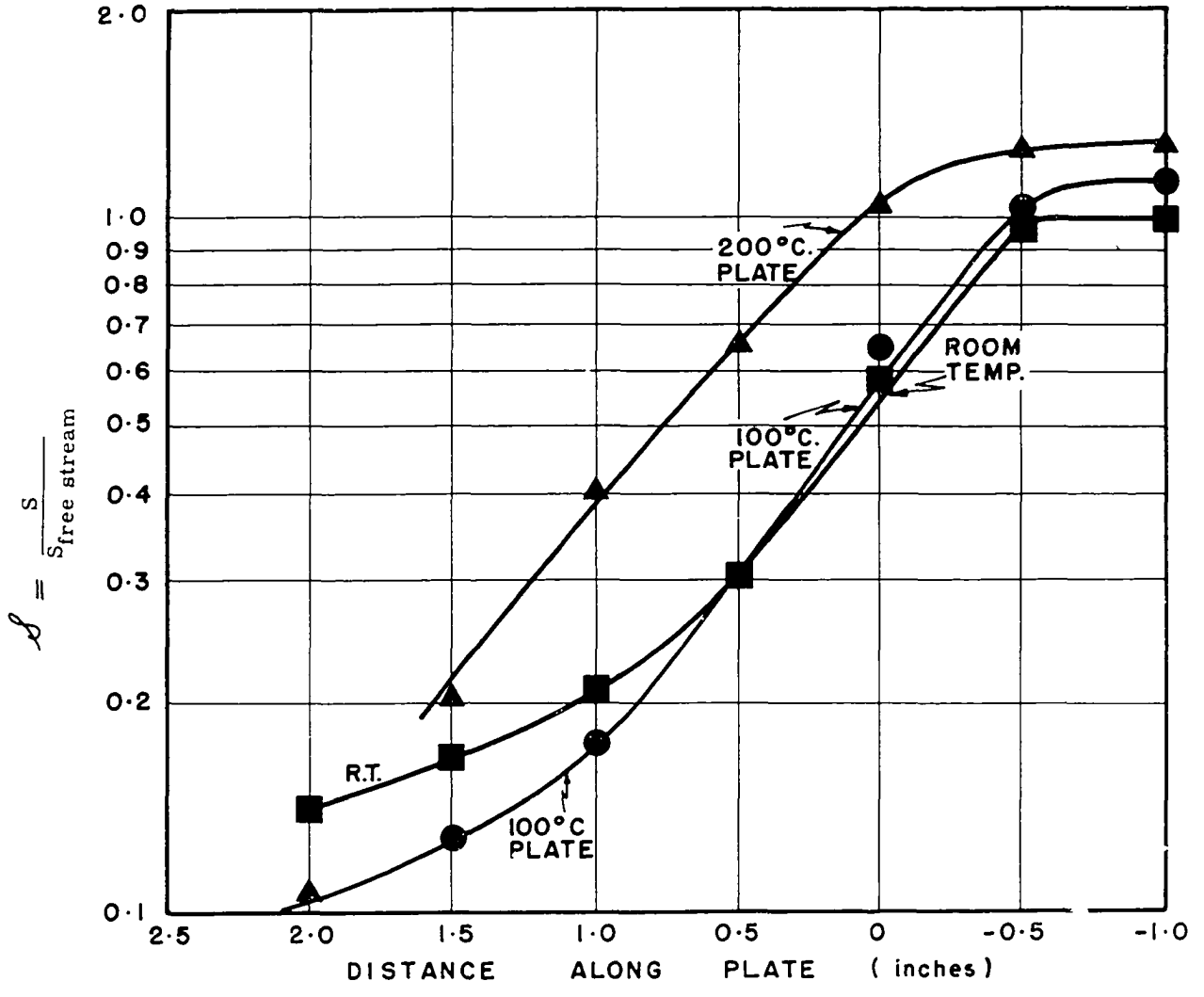

FIG. 55 NORMALIZED MOLECULAR SPEED RATIO ALONG THE FLAT PLATE

Reproduced with permission of the copyright owner. Further reproduction prohibited without permission.

Reproduced with permission of the copyright owner. Further reproduction prohibited without permission.

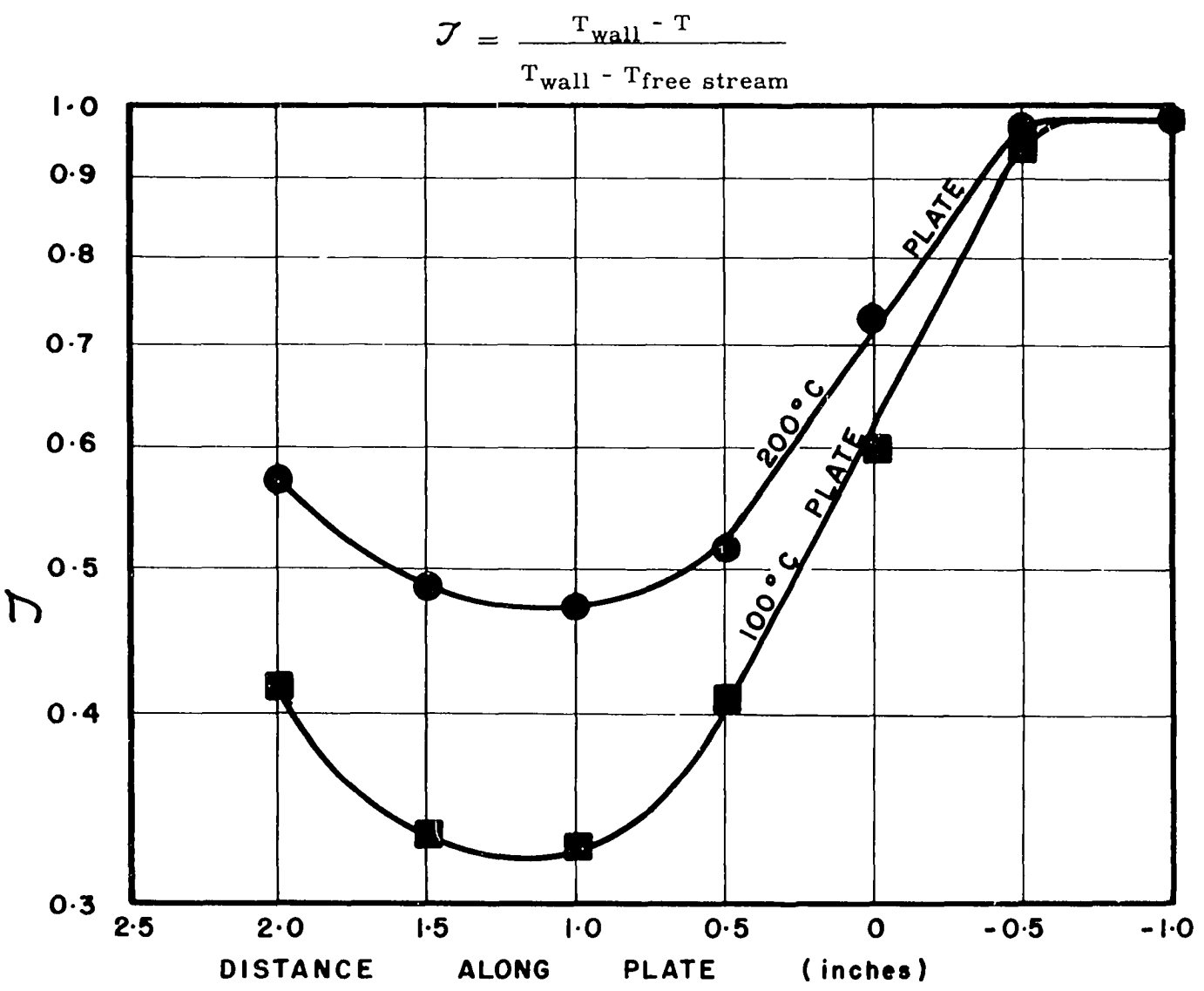

FIG. 56 NORMALIZED TEMPERATURE JUMP ALONG THE FLAT PLATE

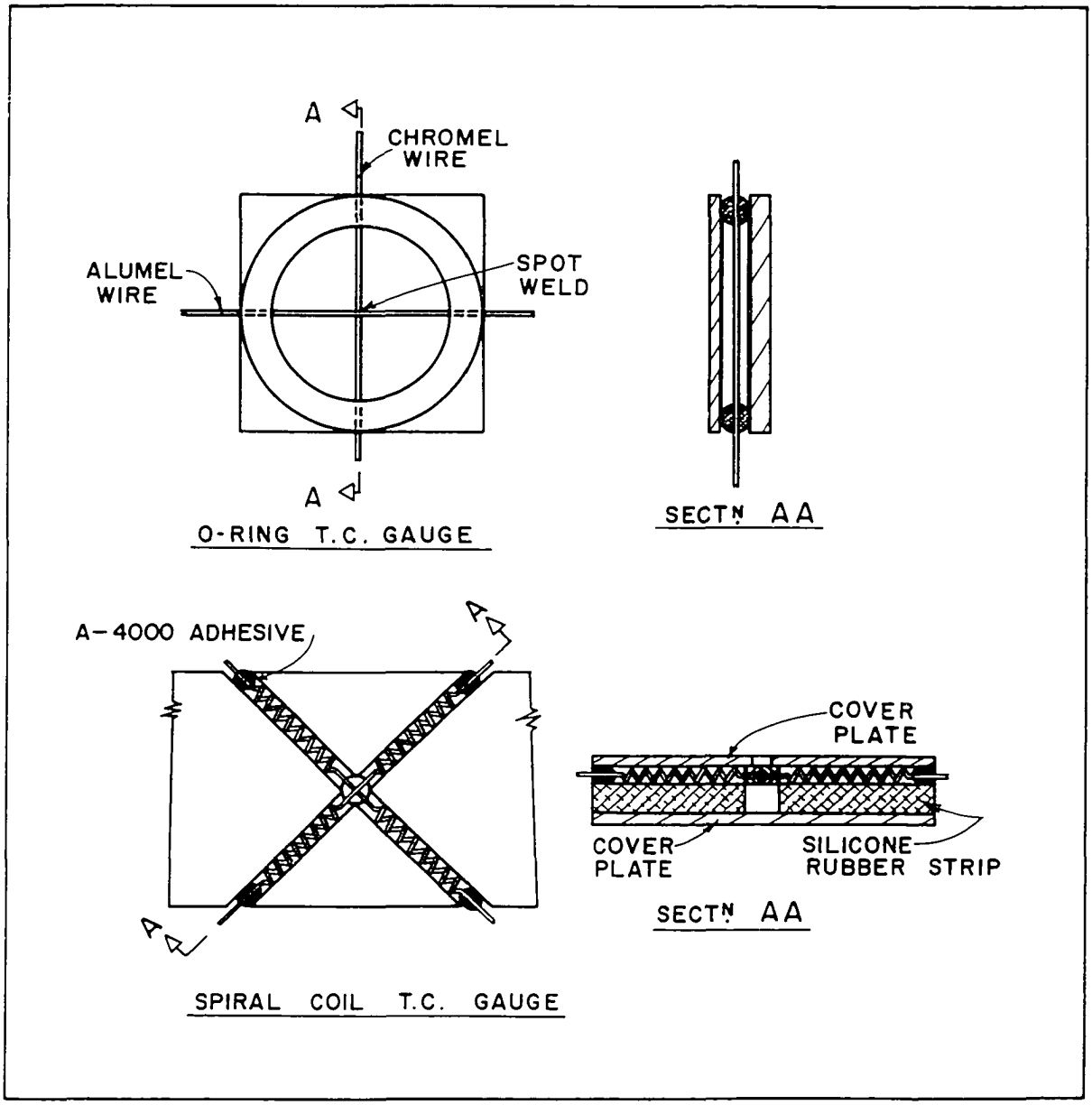

FIG. A.1 EARLY MODELS OF THERMOCOUPLE GAUGES

Reproduced with permission of the copyright owner. Further reproduction prohibited without permission.

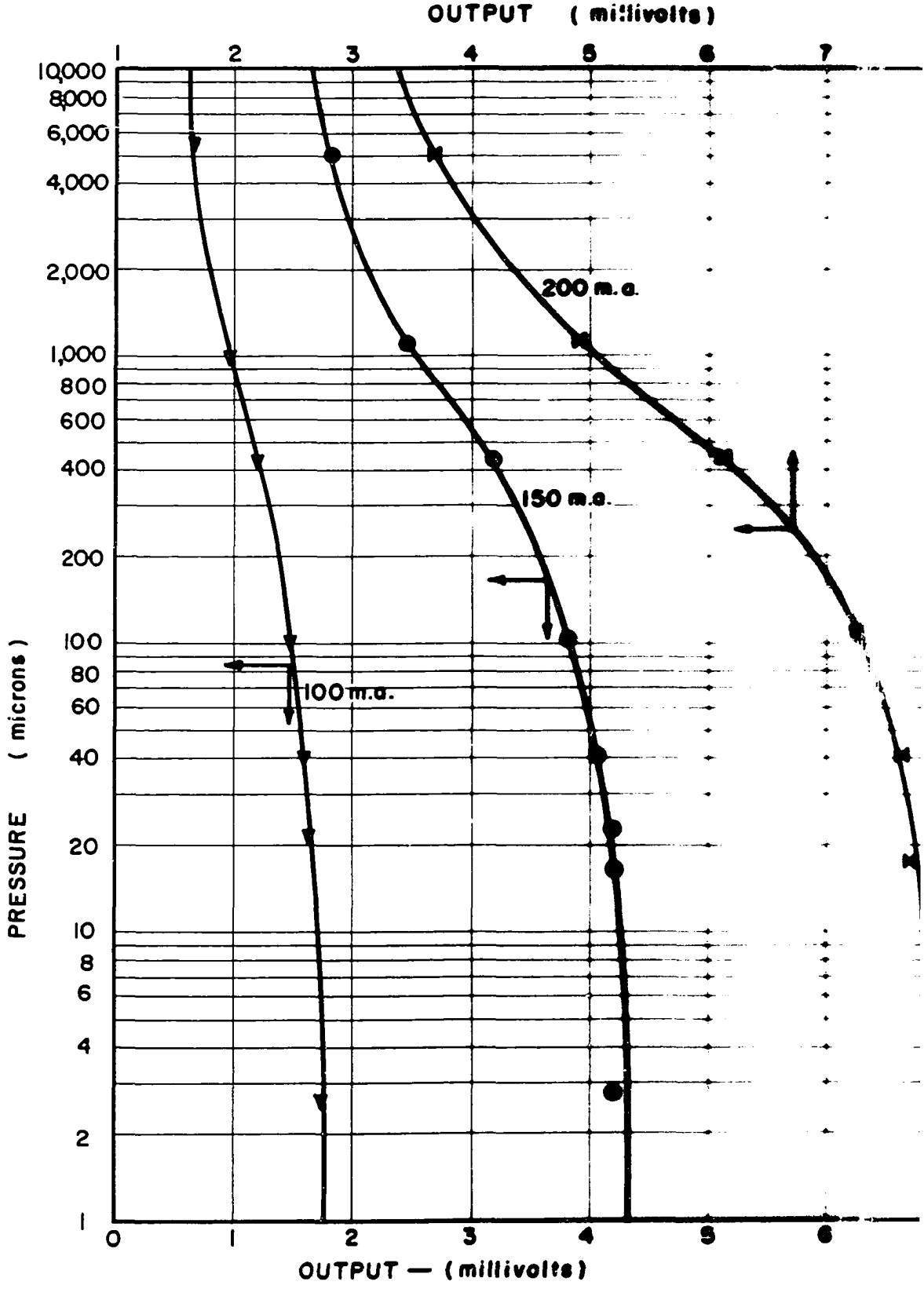

FIG. A. 2 CALIBRATION CURVE OF THE O-RING TYPE THERMOCOUPLE GAUGE

Reproduced with permission of the copyright owner. Further reproduction prohibited without permission.

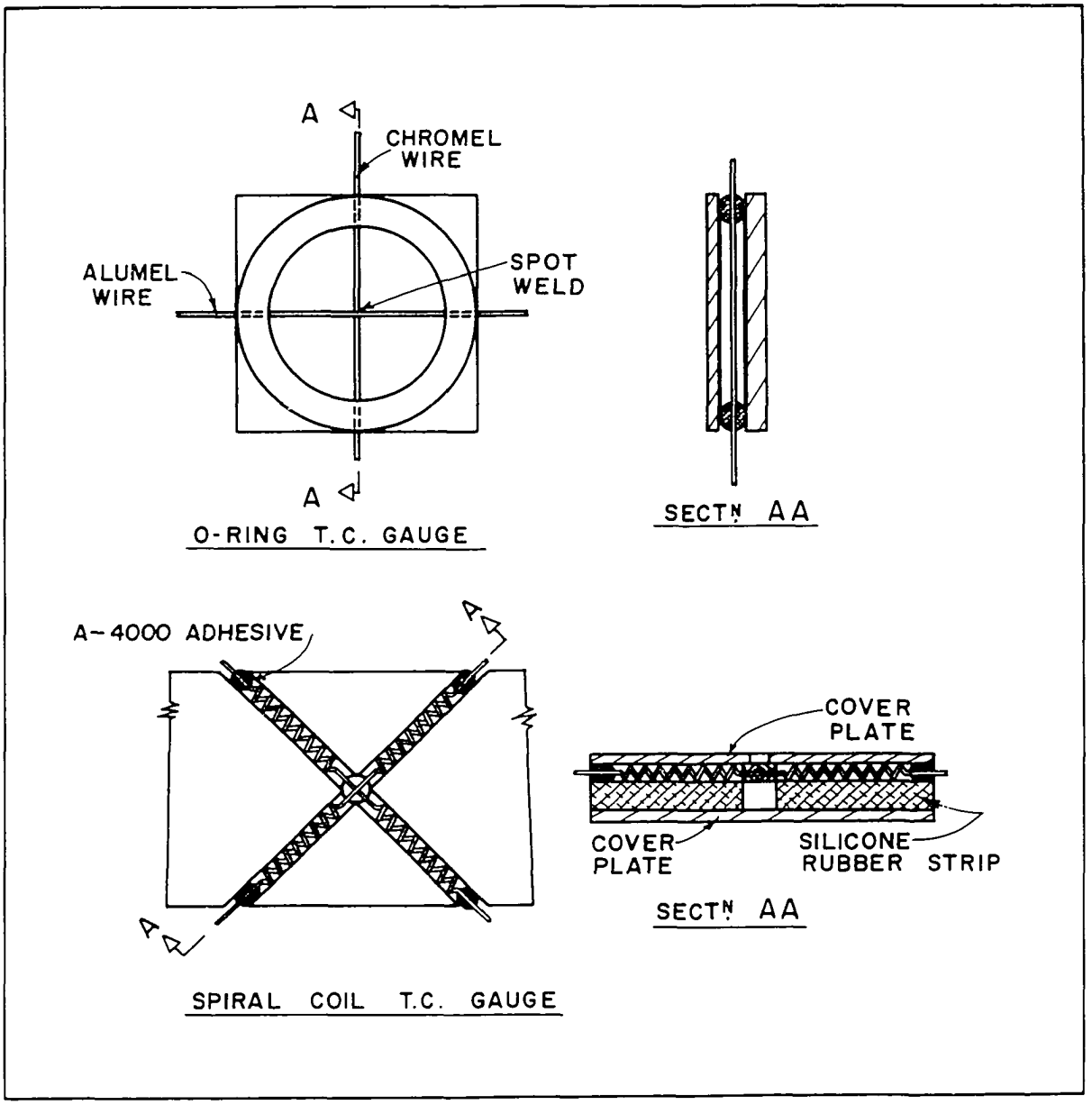

FIG. A.1 EARLY MODELS OF THERMOCOUPLE GAUGES

Reproduced with permission of the copyright owner. Further reproduction prohibited without permission.

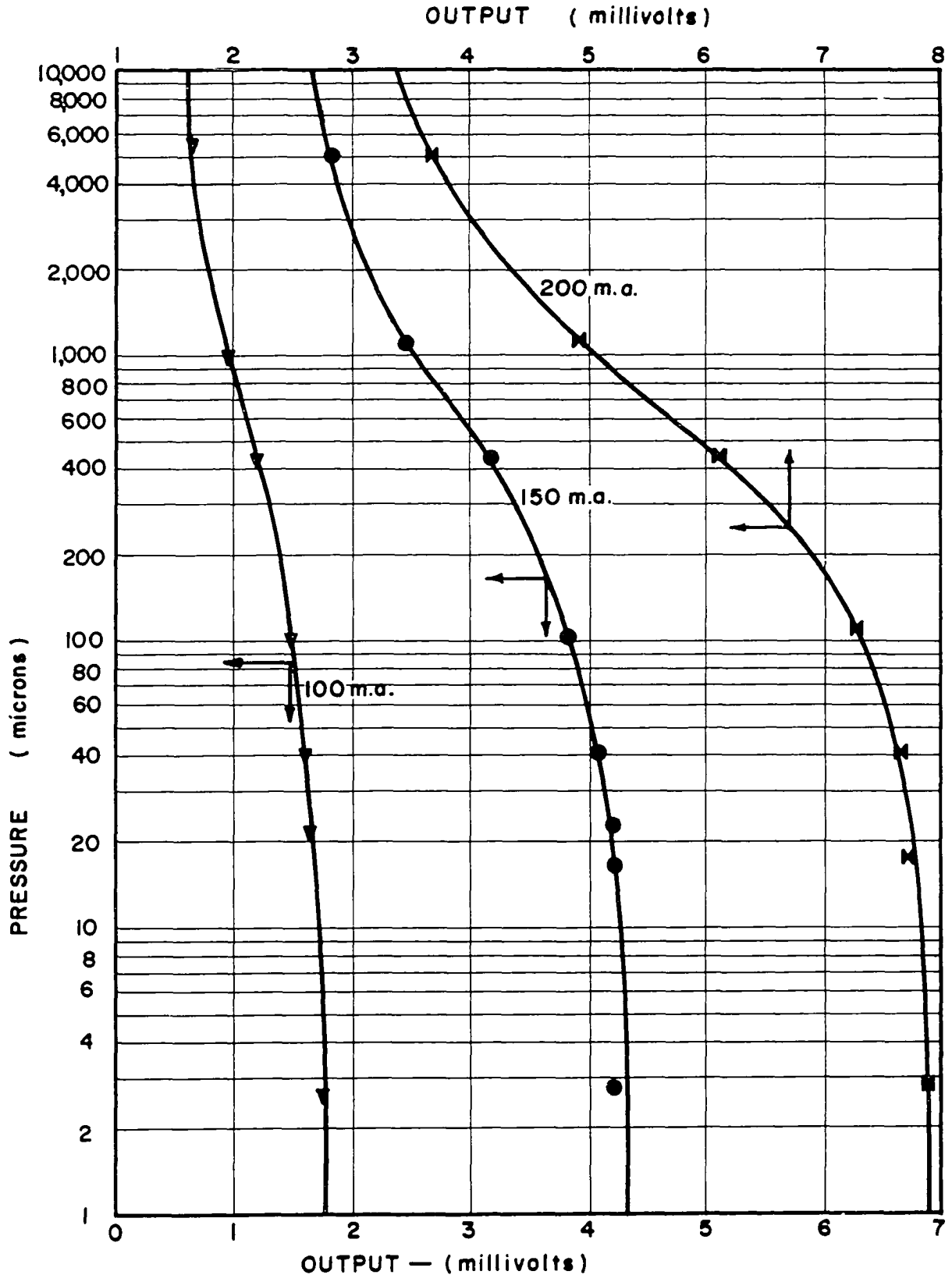

FIG. A. 2 CALIBRATION CURVE OF THE O-RING TYPE THERMOCOUPLE GAUGE

Reproduced with permission of the copyright owner. Further reproduction prohibited without permission.

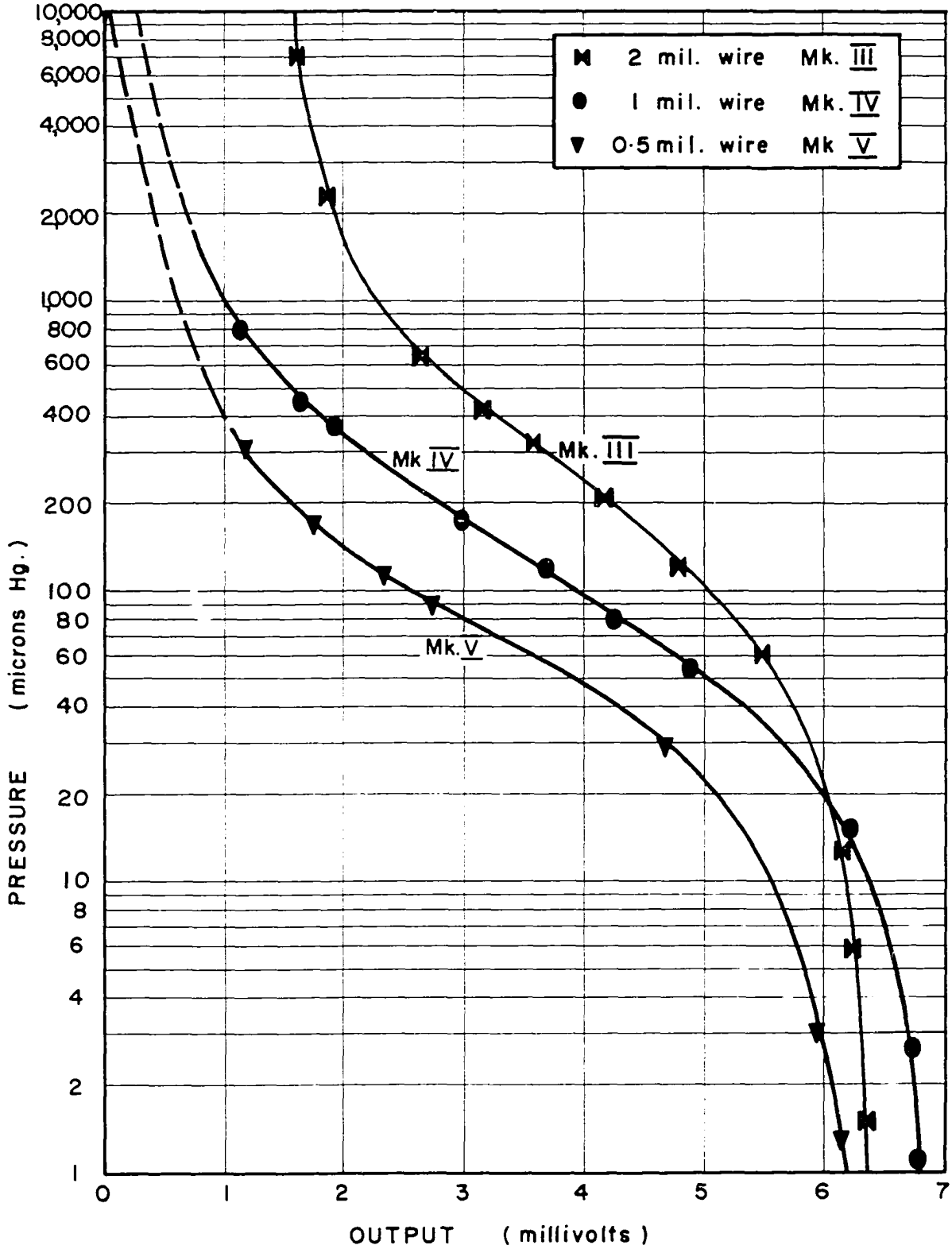

FIG. A. 3 CALIBRATION CURVE OF THE FLAT-STRIP TYPE THERMOCOUPLE GAUGE

Reproduced with permission of the copyright owner. Further reproduction prohibited without permission.

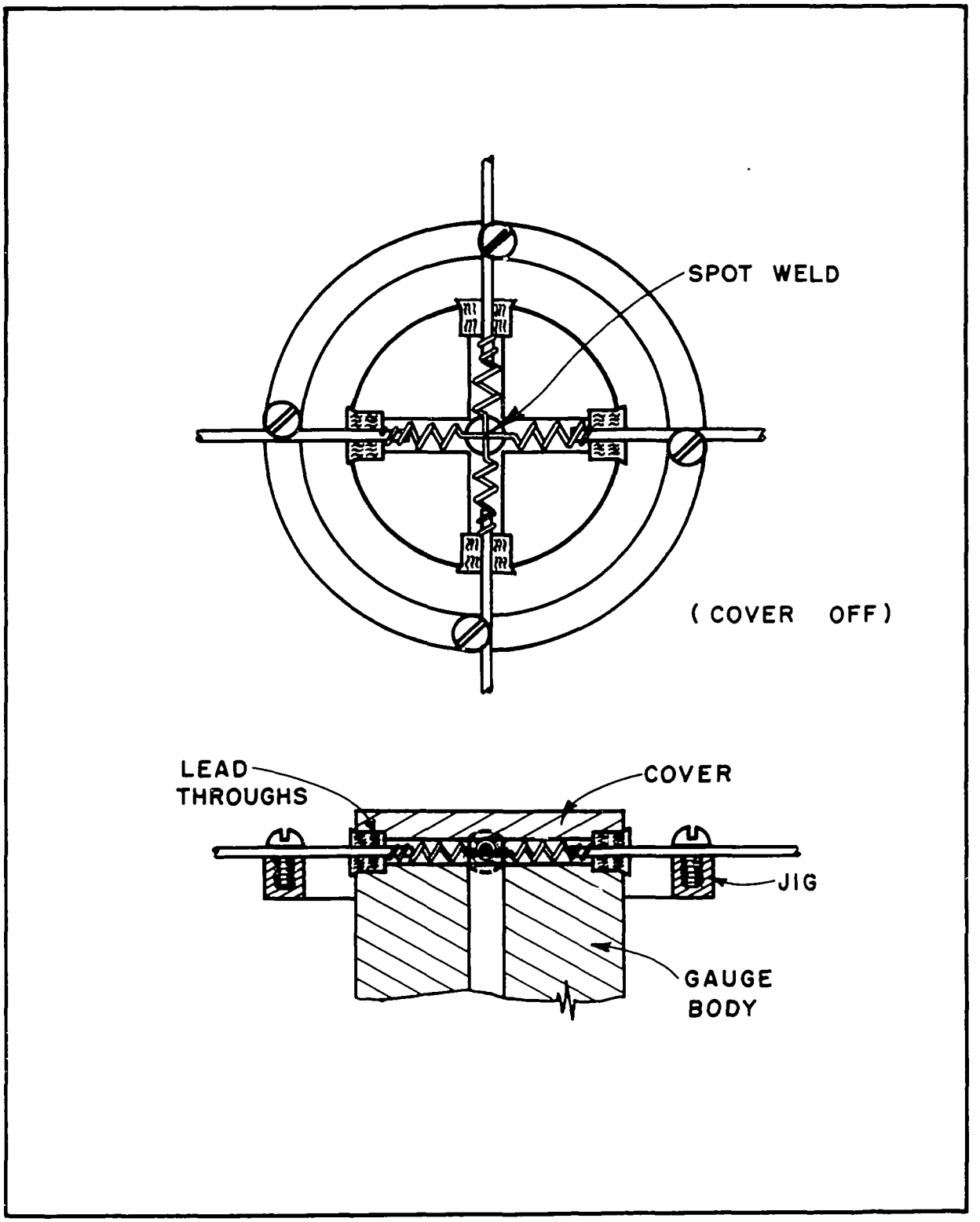

FIG. A. 4 CONSTRUCTION OF THE METAL GAUGE HEAD

Reproduced with permission of the copyright owner. Further reproduction prohibited without permission.

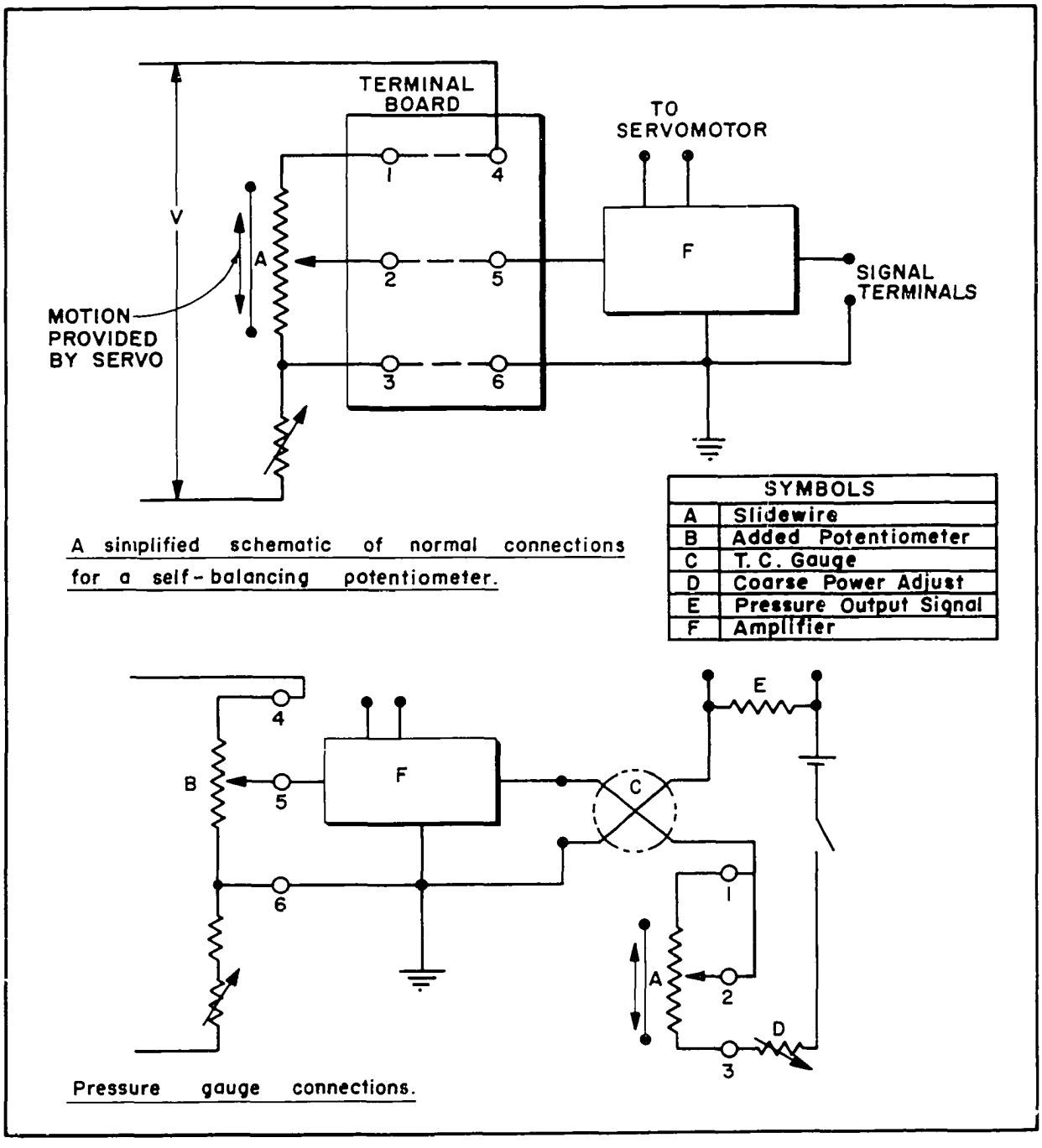

FIG. A. 5 SCHEMATIC WIRING DIAGRAM OF SELF-BALANCING POTENTIOMETER BEFORE AND AFTER MODIFICATION

Reproduced with permission of the copyright owner. Further reproduction prohibited without permission.

Reproduced with permission of the copyright owner. Further reproduction prohibited without permission.

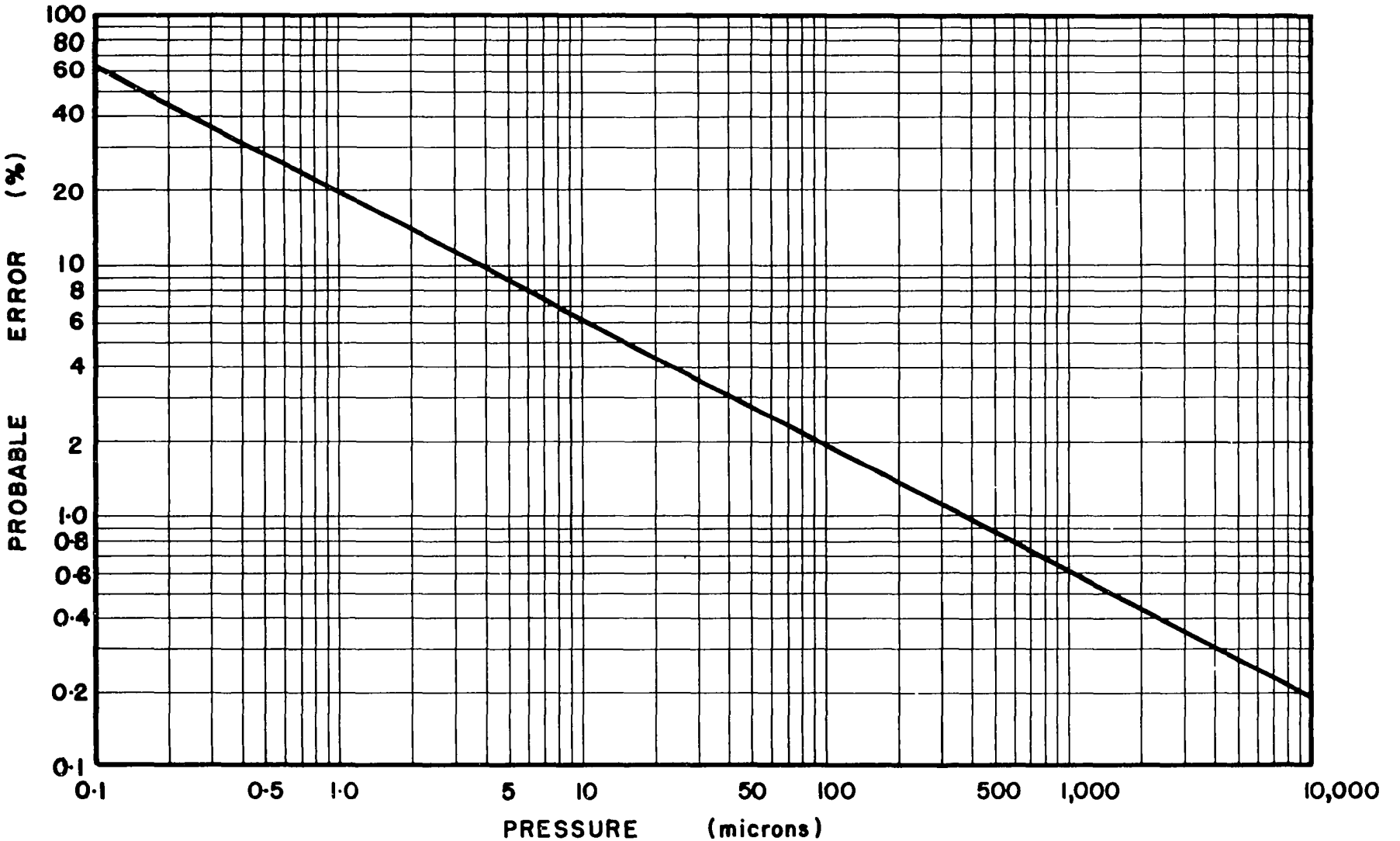

FIG. A. 6 RANDOM ERROR PREDICTED FOR A McLEOD GAUGE WITH 100 cc CUT-OFF VOLUME

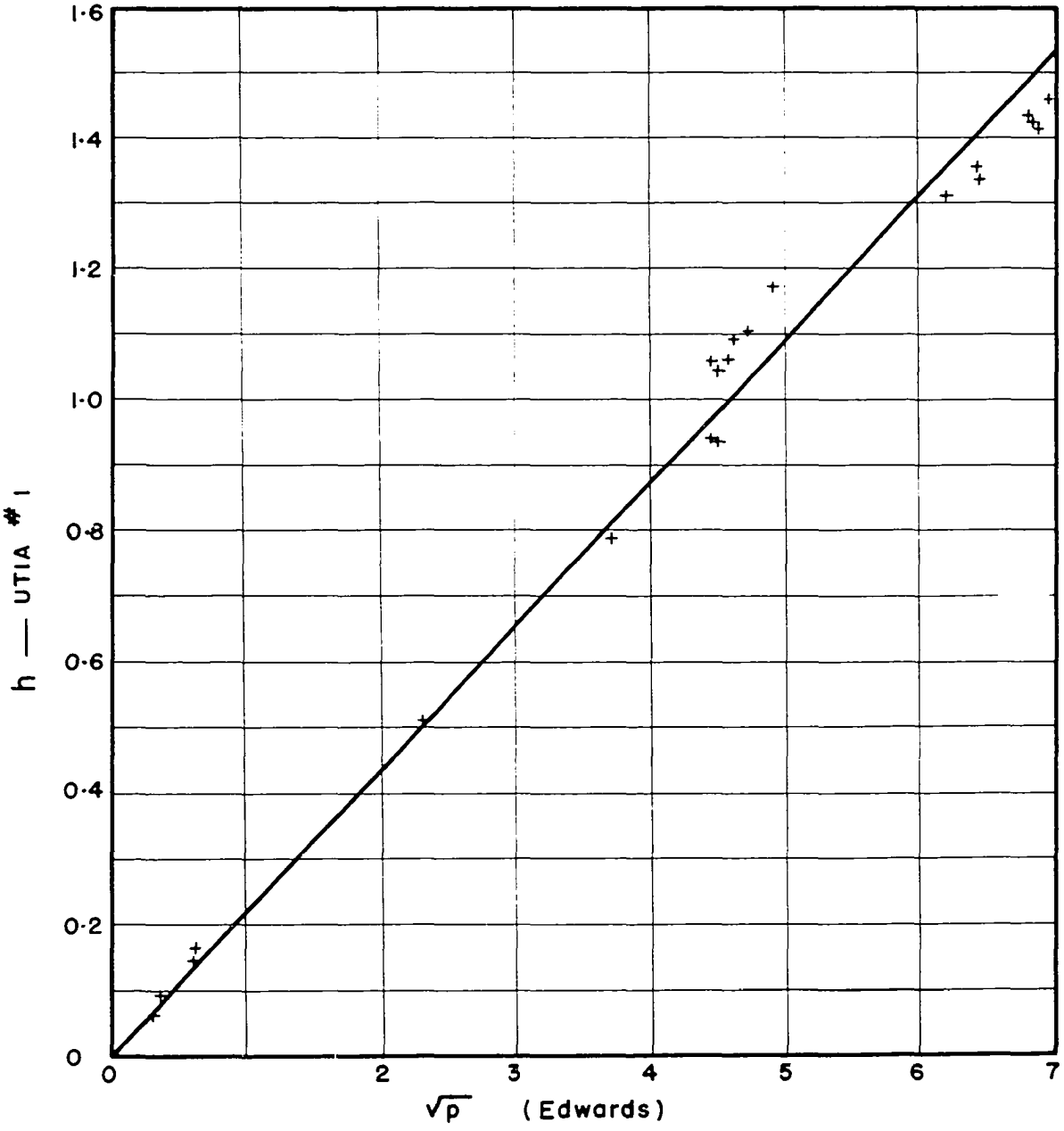

FIG. A. 7 COMPARATIVE HEIGHT OF MERCURY COLUMNS OF TWO McLEOD GAUGES READING THE SAME PRESSURES

Reproduced with permission of the copyright owner. Further reproduction prohibited without permission.

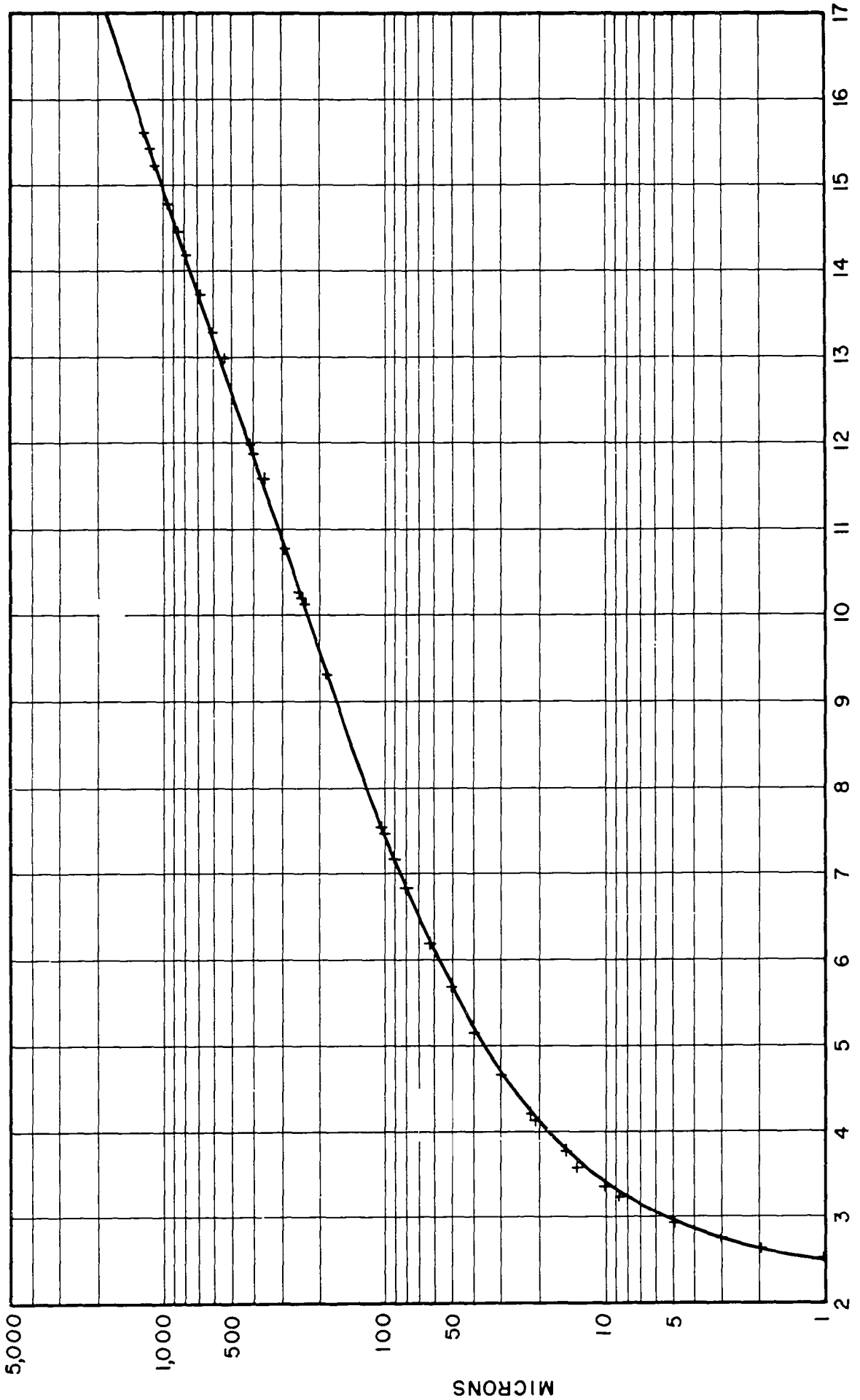

FIG. A.8 CALIBRATION CURVE OF A THERMOCOUPLE GAUGE

Reproduced with permission of the copyright owner. Further reproduction prohibited without permission.

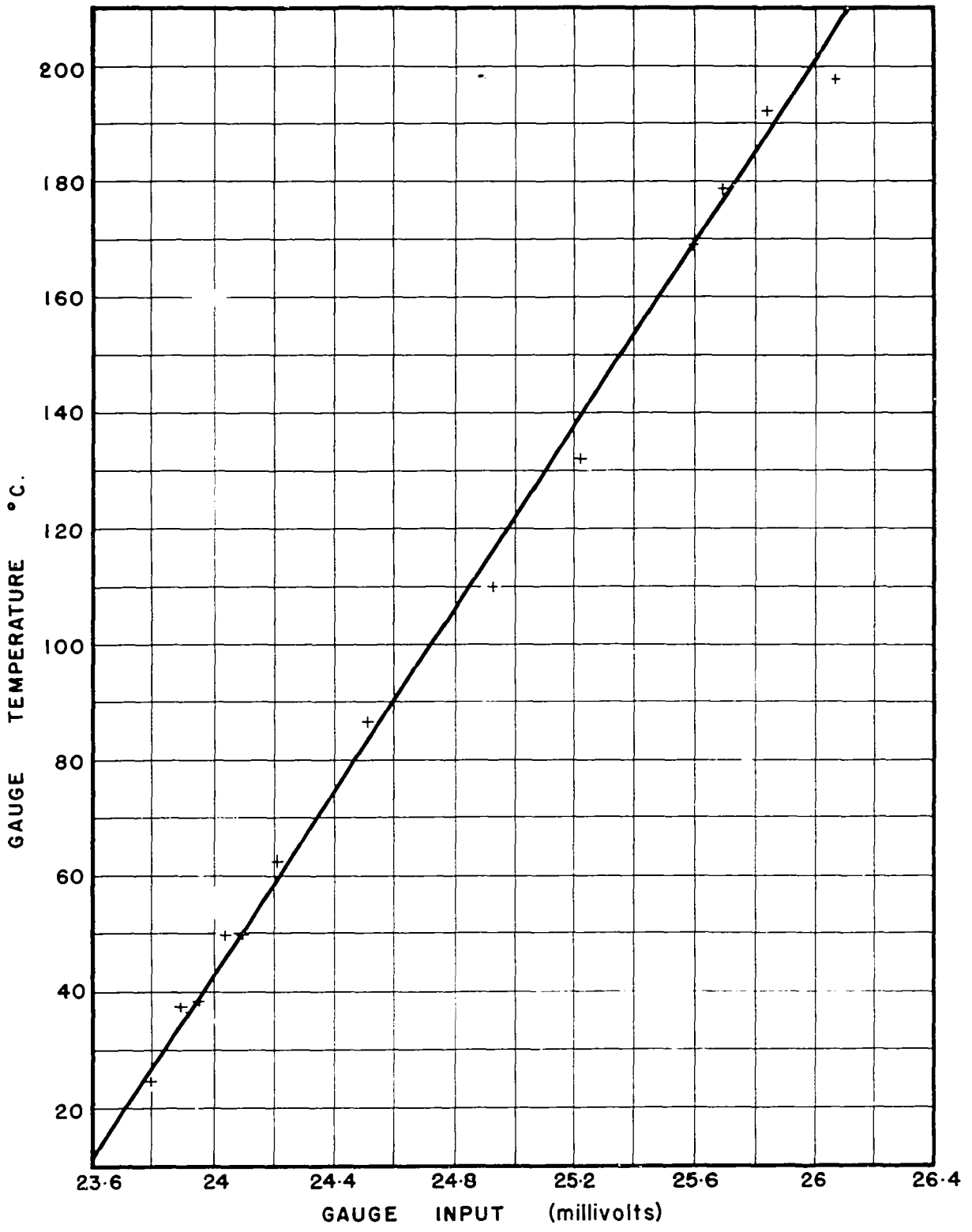

FIG. A. 9 EFFECT OF GAUGE HEAD TEMPERATURE ON THERMOCOUPLE GAUGE RESPONSE AT 20 MICRONS

Reproduced with permission of the copyright owner. Further reproduction prohibited without permission.

FIG. A. 10 CALIBRATION OF THERMOCOUPLE GAUGE (PRESSURE VERSUS RELATIVE POWER INPUT)

Reproduced with permission of the copyright owner. Further reproduction prohibited without permission.

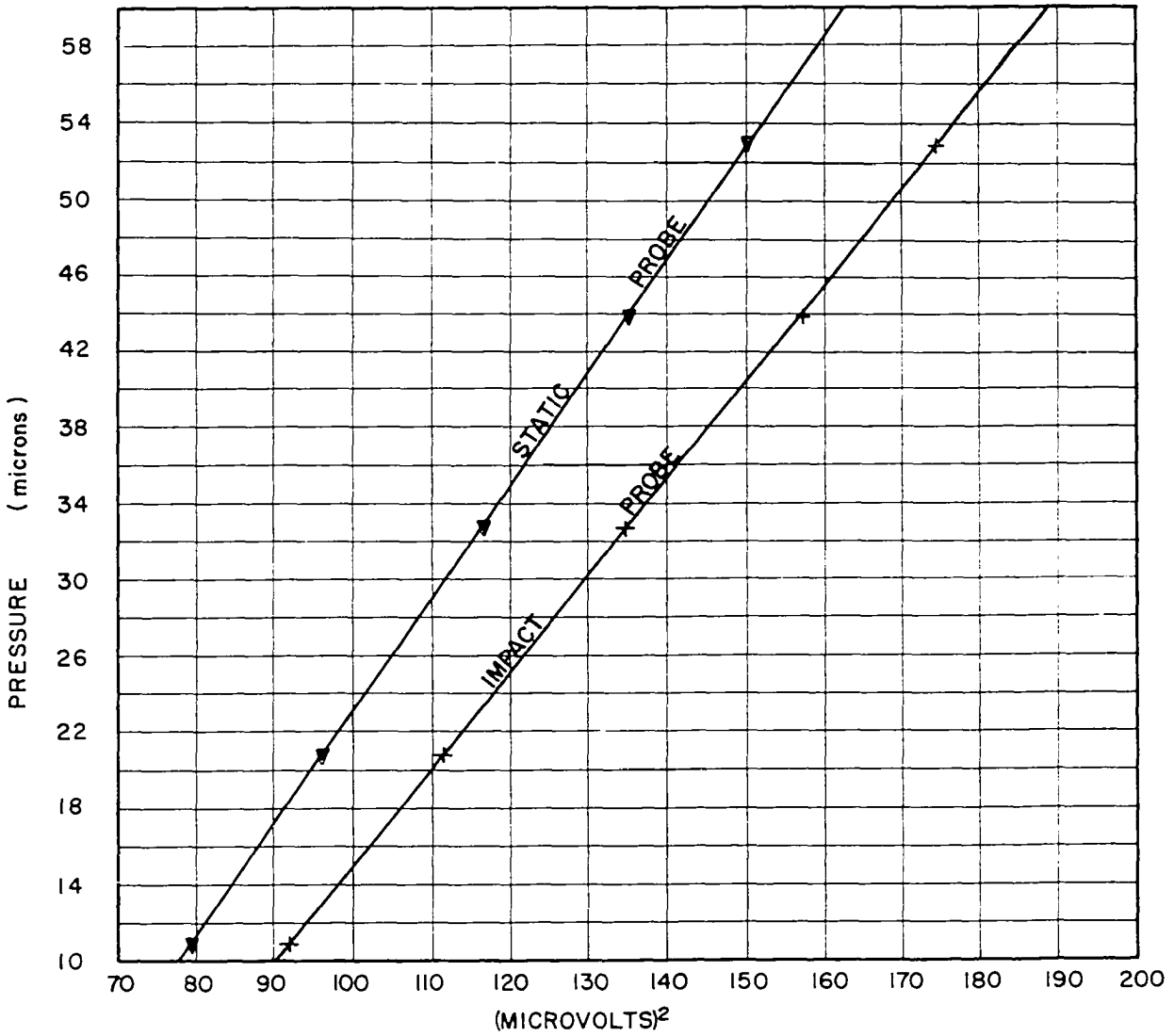

FIG. A. 11 CALIBRATION OF A THERMOCOUPLE GAUGE (PRESSURE VERSUS RELATIVE POWER INPUT)

Reproduced with permission of the copyright owner. Further reproduction prohibited without permission.

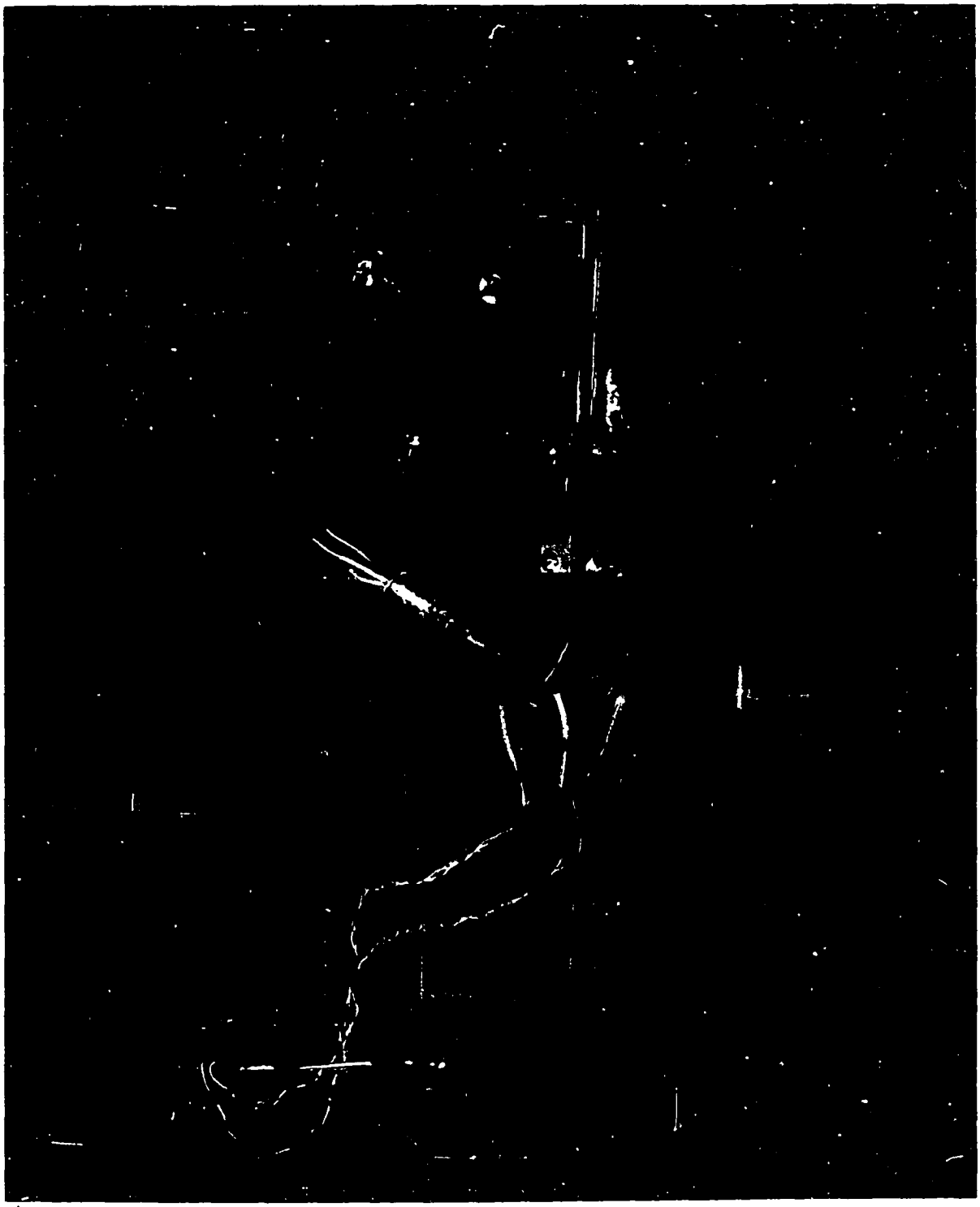

PLATE A. 1 SEVERAL MODELS OF GLASS THERMOCOUPLE GAUGES AND AN ASSEMBLED PRESSURE-PAIR PROBE WITH GLASS PROBE TIPS

Reproduced with permission of the copyright owner. Further reproduction prohibited without permission.

Reproduced with permission of the copyright owner. Further reproduction prohibited without permission.

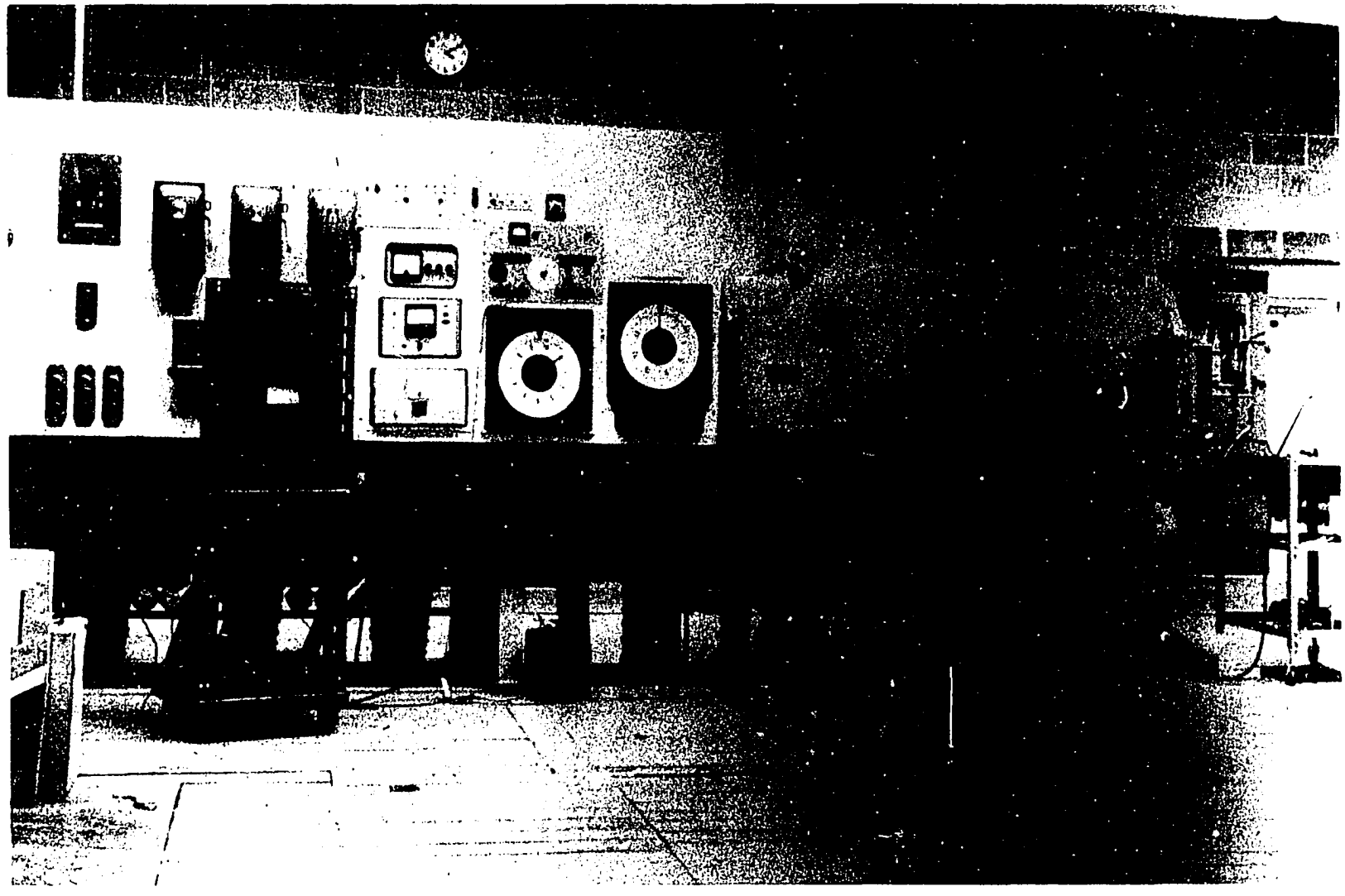

PLATE 1 UTIA LOW DENSITY WIND TUNNEL

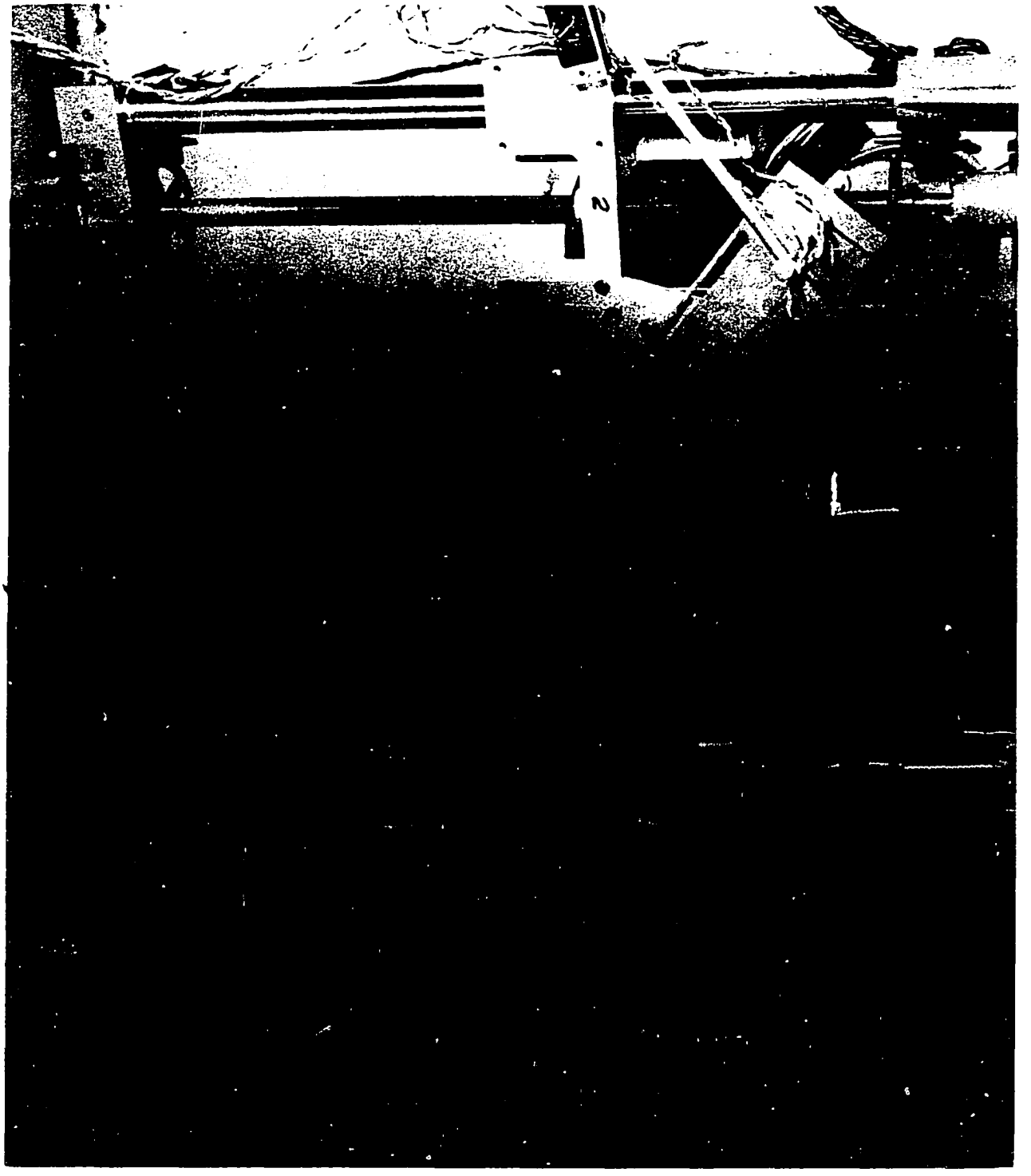

PLATE 2 VIEW OF TEST SECTION SHOWING (1) NOZZLE (2) TRAVERSING MECHANISM (3) FLAT PLATE MODEL AND MODEL HOLDER, (4) EQUILIBRIUM TEMPERATURE (5) PRESSURE PAIR PROBE

Reproduced with permission of the copyright owner. Further reproduction prohibited without permission.